中国科学院
紫金山天文台

Research Annual Report

2014

科研工作年度报告

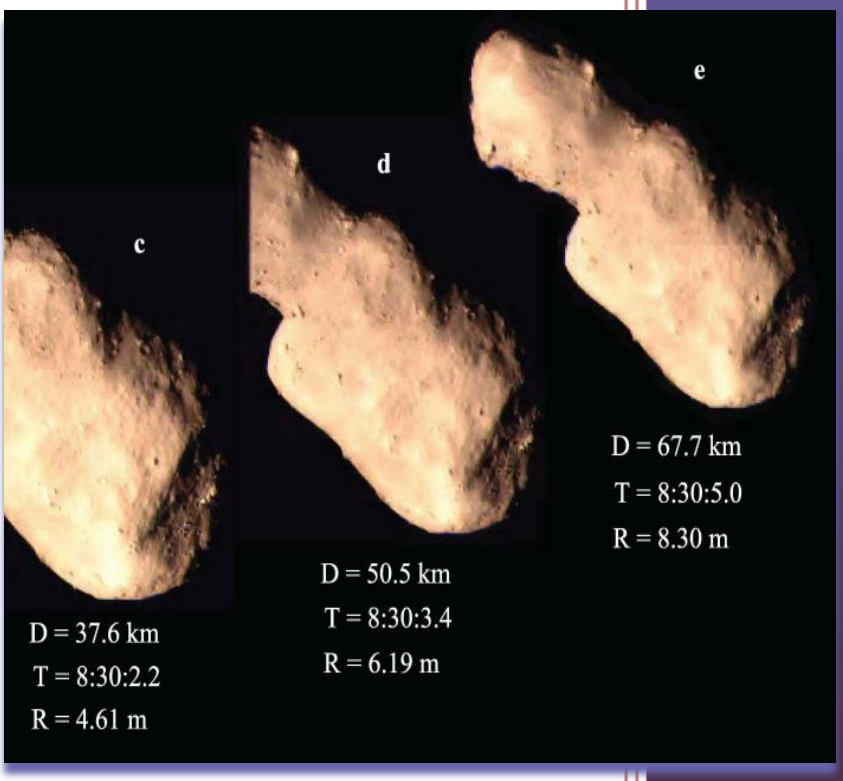

Purple Mountain Observatory CAS

中国科学院紫金山天文台

2014科研工作年度报告

中国科学院紫金山天文台科技处

2015年4月

Cover: The Ginger-shaped Asteroid 4179 Toutatis: New Observations from a Successful Flyby of Chang'e-2
(from Scientific Reports , see also page 113)

封面：嫦娥二号在飞越时对图塔蒂斯小行星成像结果（取自 Scientific Reports , 具体参见 112 页）

目录

注：目录中文章作者只列排名最前本单位人员，作者名后带*为第一作者文章，未带星号者为非第一作者文章。

中国科学院紫金山天文台
科技处

地 址：南京市北京西路 2 号
邮 编：210008
电 话：+86-25-8333-2288, 2018
传 真：+86-25-8333-2288
电 邮：pmokjc@pmo.ac.cn
http://www.pmo.cas.cn

Purple Mountain Observatory
Chinese Academy of Sciences

ADD :2 West Beijing Road,
Nanjing 210008, China
TEL : +86-25-83332288
FAX : +86-25-83332288
Email :pmokjc@pmo.ac.cn
http://www.pmo.cas.cn

2014 年度科研工作总结

一、 科研工作总体情况

1. 概述

2014 年，紫台共有在研项目 260 项（包括新增项目 109 项）。其中，主持国家重点基础研究发展计划（973）项目 3 项和子项 7 项；主持（或承担）中国高技术研究发展计划（863）项目 17 项（新增 6 项）；主持（或承担）国家其他项目 16 项；主持（或承担）国家自然科学基金项目 130 项（新增 30 项），其中重大项目 1 项、重点项目 6 项（新增 2 项）、面上项目 28 项（新增 7 项）、杰出青年基金 1 项，主持（或承担）国家自然科学基金重大科研仪器研制项目 2 项；承担中科院战略先导科技专项课题 7 项和子课题 10 项，主持（或承担）中科院知识创新工程重要方向项目 3 项，"百人计划"项目 3 项；承担江苏省自然科学基金 9 项；横向项目 11 项（新增 5 项）。

2014 年，紫台共发表科技论文 222 篇，其中国际合作论文 72 篇。SCI 论文 157 篇，影响因子 3.0 以上的 108 篇；申请专利 9 件，其中发明专利 9 件；申请软件著作权 3 件；专利授权数 4 件，均为发明专利。共获省部级科技奖励 7 项，其中第一单位一等奖 1 项。

2. 重要进展和重大成果

1）3 个重大突破进展

院"空间科学"战略性先导科技专项（A 类）项目"暗物质粒子探测卫星（DAMPE）"于 2014 年 9 月底成功转入正样研制阶段，并完成欧洲核子中心（CERN）束流实验。

南极天文中心组织参加第 31 次南极科考，AST3-2 运往南极冰穹 A。继续深入开展南极天文台相关的关键技术攻关。南极相关的 973 项目"利用南极巡天望远镜在超新星宇宙学及太阳系外行星方面的前沿研究"、国家自然科学基金重大项目"极端台址环境下的天文望远镜关键技术方法研究"和重大科研仪器设备研制项目"太赫兹超导阵列成像系统"进展顺利，完成了中期目标，在时域天文、极端环境下的望远镜与探测系统关键技术、太赫兹成像阵列等方面取得阶段性重要进展。

空间目标与碎片观测系统建设取得重要阶段性进展。二代光电阵正式投入运行，大幅度提高了全网的探测能力。相关成果获省部级一等奖（第一单位），并成功推广至国内其他部门。代表国家航天局参加"欧空局 GOCE 卫星"陨落期 IADC 国际联测试验，预报精度列 11 个主要联测国家之首，为国家争得荣誉。

2）5 个重点培育方向进展

973 项目"日地空间天气预报的物理基础与模式研究"取得重要进展。青年 973 项目"暗物质粒子探测卫星的相关科学研究"取得重要进展，通过中期检查。成功预言了 AMS-02 观测到的原初电子宇宙射线能谱超出；提出快变射电暴有望成为高效的宇宙暗能量新探针。

中科院战略性先导科技专项（B 类）"宇宙结构起源——从银河系的精细刻画到深场宇宙的统计描述"项目于 2014 年立项，紫台负责课题 3 项，承担合作课题 10 项。

"银河画卷"计划 2014 年度完成了 1030 个单元的观测，目前已完成整个观测计划的 25%。

"农历的编算和颁行"国家标准成功立项。

3）重要研究成果

在国际上率先提出：如果将来快变射电暴的红移被直接测定，那么它们有望成为高效的宇宙暗能量新探针。该研究成果的想法被列为国际大科学工程"平方公里阵（SKA）"最重要的科学目标之一。

成功预言了 AMS-02 观测到的原初电子宇宙射线能谱超出，并指出该超出的来源最可能是邻近的中等寿命的超新星遗迹。

详细研究了双中子星并合引力波事件的电磁辐射的光变曲线，成功解释了近期发现的一类新的宇宙学相对论源。该成果对未来时域天文领域关于这类暂现源的巡天具有指导意义。

宇宙原初气体可能无法有效形成恒星。通过对两个低金属元素含量的近邻恒星形成星系的多波段红外观测，结合恒星形成率的测量，在《自然》杂志联合发表研究论文，指出 130 亿年前的宇宙原初气体可能无法有效形成恒星。

“银河画卷”计划利用德令哈 13.7 米毫米波望远镜，在银河系第二象限最遥远的区域发现了一段新分子气体旋臂，这是迄今探测到离银河系中心最远的旋臂。该发现更新了人们对银河系结构的认识，并将对整个银河系的分子云与恒星的形成等方面的研究产生重要的引导作用。

成功研制 1.4 THz 频段国际上最高灵敏度的超导 HEB 热电子混频器、850 微米波段 8×8 像元超导 MKIDs 探测器阵列、和 350 微米波段 32×32 像元超导 MKIDs 探测器阵列芯片。

针对太阳射电爆发现象，提出了由激波和快电子束直接放大射电辐射的新机制。

二、 研究活动进展

I. 暗物质和空间天文研究部

宇宙学、暗物质及高能天体物理研究

本年度在暗能量性质、宇宙微波背景、暴涨宇宙学、量子宇宙学、相对论流体及其在宇宙学和高能天体物理中的运用等方面进行了较深入的研究，取得了一些成果。

1）暗能量性质方面的研究。在去年工作的基础上继续分析了 Ia 型超新星、伽玛暴、重子声学振荡等观测数据在限制暗能量性质时所产生的偏差。随着研究的深入，需要更大强度的数值计算，原来编写的程序在运行速度上已经不能满足相应的要求，将其中的大部分进行了改写和优化，并进行了扩充，包括了更多的参数化暗能量的方案。运用新编写的程序进行了相应的数据分析和模拟计算，尝试了各种不同的数据组合和参数化暗能量的方案，初步明确确定了近年来一直在关注的暗能量性质演化的一个问题的答案。计划将该工作总结为两篇论文，其中第一篇已经基本成文，第二篇相关的内容正在进行数值模拟计算。

2）宇宙微波背景、暴涨宇宙学及相关问题。近期对宇宙微波背景(CMB)的精确观测(WMAP 及 Planck)表明 CMB 的各向异性功率谱在大尺度上有非平庸的结构。其中 CMB 功率谱在 10 到 50 附近的反常波动行为，无法从标准ΛCDM 模型和标准暴涨模型中获得，原初扰动可能伴有奇异过程(singular processes)。我们通过引入粒子的共振产生，干扰标准暴涨的慢滚过程，从而在原初扰动谱中得到一个标度依赖的特征震荡。这一原初震荡将演化为 CMB 功率谱上的特征行为，从而较自然地解释了观测中的反常行为。相关的工作已完成，已投 Phys. Rev. D. (Sun Zhang and Yi-Qiao Dong, submitted to PRD)

3）量子宇宙学相关问题。一般而言，宇宙是个经典的观测客体，其在量子层次上的演化特性要体现在准经典近似极限下，从而可以被观测到。按 Hartle 定则（Hartle criterion），宇宙经典极限下的行为体现在宇宙波函数的震荡行为（e 指数为虚数）。我们运用 Noether 途径，研究了具有标量场和矢量场的最小耦合宇宙模型，通过对称性的切入，解出 Wheeler-De Witt (WDW)方程，找到了相应的宇宙经典波函数，讨论了其演化行为。我们的结果修正了前人研究中的错误，给出了正确的对称性和途径。在我们讨论的模型下，我们认为这个问题已经解决。相关的工作已完成，已投 Phys. Lett. B. (Sun Zhang, submitted to PLB)

4）相对论流体及其在宇宙学和高能天体物理中的运用。相对论流体既关系到宇宙学的流体动力学描述，又关系到致密天体的内部结构、伽玛暴的动力学过程等，相关问题涵盖面很广。我们着重研究其在宇宙学及高能天体物理中的运用。现在的阶段，我们着重研究了相对论超流体的最重要的性质：声速和激波演化，确定了基本的图像，为进一步运用于宇宙学和致密天体内部结构创造了条件。已发表论文两篇，已投稿一篇。(Sun Zhang, PLB 729 (2014) 136；Sun Zhang, Yi-Qiao Dong, CTP 62 (2014) 729； Sun Zhang, Yi-Qiao Dong, submitted to MPLB.)

宇宙伽马暴、中子星及相关物理研究

继续在高能天体物理方面进行研究，主要围绕宇宙伽玛射线暴、X 射线双星等高能辐射现象，另外我们也根据国际上的最新发展及时调整研究计划。去年国际上确认发现了一类新的射电爆发现象—快变射电暴，我们及时给予了关注和研究，讨论了它可能的宇宙学应用，工作得到了国际同行的关注。

1）伽玛暴中心引擎究竟是物质为主还是磁场为

主一直没有定论 ,我们对伽玛暴 GRB120308A 的研究有助于解决这个问题。GRB120308A 是 Swift 卫星观测到的一个长暴，它的一个显著特征是在它的早期光学余辉中发现有较强的偏振，并且偏振度随时间逐渐下降。这暗示了在早期余辉的辐射区域中应存在着规则的磁场。在正反激波模型的框架下，我们拟合了这个暴的光学和 X 射线余辉性质 ,发现反向激波区域的磁场比正向激波区域的磁场要强约 10 倍，这表明从中心能源出来的外流体是中等磁化的。考虑到外流体在加速和瞬时辐射阶段会有一部分磁能耗散，因此我们的工作表明至少对部分伽玛暴其中心引擎释放的能量中坡印廷流占了相当的比例。

2） Fermi 卫星观测到不少伽玛暴都有大于 100MeV 的高能辐射，其起源目前尚不清楚。我们研究了 GRB130821A 和 GRB131231A 的大于 100MeV 的高能辐射。对 GRB130821A，我们发现这个暴的周围介质应是均匀介质，并且外流体的洛伦兹因子是几百，并且它的 GeV 辐射极可能来自于正向激波的同步辐射。而对 GRB131231A，其大于 100MeV 的高能余辉辐射的谱指数约是 0.54，探测到的最高能量的光子是 62GeV。我们发现，无论是电子还是质子的同步辐射都不能很好的解释观测事实，而被外激波加速的电子的同步自康普顿散射可以较好地解释这个暴高能辐射的光变和能谱性质。因此伽玛暴的 GeV 辐射可能来自不同成分，有的主要来自正向激波的同步辐射，而另一些主要来自逆康普顿散射。

3）分析了 Be/X 射线双星 X Per 自 1999 到 2013 年的分光数据，结合该源公开的测光数据，我们发现了系统的光学亮度和 Halpha 以及 HeI 6678 发射线强度之间存在几处反相关变化关系，我们把这个现象解释为 Be 星物质喷发的结果。由于 Be 星物质以粘滞时标向外扩散，那么 Be 星的活动性和致密星的 X 射线辐射存在一个时间延迟，我们利用中子星作为探针来限制 Be 星星周盘中物质的运动，估算了不同时期 X Per 星周盘中粘滞系数的大小，结果表明 X Per 不可能观测到 I 型 X 射线爆发。这一研究结果发表在 2014 年 12 月 1 日的 AJ 上。

4）快变射电暴是 2013 年里得以确认的一类持续时间只有毫秒量级、流量可达 1Jy 的单脉冲型射电爆发事件，探测率可高达 10000/天。它们的物理起源尚不清楚，但所测得的色散量远远超过银河系星际介质的贡献，所以一般认为最可能来自于宇宙深处的致密星表面。我们指出色散量中包含着光子传播距离的信息，如果将来快变射电暴的红移被直接测定，那么它们有望成为高效的宇宙学暗物质、暗能量新探针。我们这个想法被射电天文学家 Jean-Pierre Macquart 列入 SKA 项目“killer science”的主要科学目标之一。我们还讨论了快变射电暴对观测到的甚高能宇宙线的贡献。我们发现，如果快变射电暴起源于大质量中子星塌缩成黑洞或者是双中子星并和过程，那么由于期间释放的能量很大以及快变射电暴很高的爆发率，我们观测到的甚高能宇宙线中将有相当部分来自快变射电暴的贡献。相反，如果快变射电暴来自双白矮星的碰撞或者是磁星的耀发，则对甚高能宇宙线的贡献都很小。因此我们提出通过对甚高能宇宙线来源的分析可以区分不同的快变射电暴的起源模型。

在苏州组织举办了一次关于伽玛射线暴研究的小型研讨会，来自紫金山天文台、南京大学、广西大学、国家天文台、华中科技大学、河北师范大学等七十余人参加了会议。

太阳高能及相关物理过程研究

本年度开展工作：“先进天基太阳天文台”（ASO-S)背景型号研究在先导专项经费没有到位的情况下，多方筹集资金，按计划推进，年内获得基金委重大仪器专项补充支持；团组成员与实验室联合提出的“大面积太阳伽马射线谱仪”（LASGA)年内通过多轮竞争，入选国家空间站首批项目指南；团组成员继续推进地基两维太阳光谱诊断日冕仪; 有 4 个空间卫星项目（3 个负责，1 个参与）正在准备正式提案，以响应 ESA-CAS 合作卫星提案征集；另有一与欧洲合作卫星计划正在尝试申请 ESA 的 M4 机会。在太阳高能物理研究方面 ,主要在粒子事件、太阳磁龙卷风、活动区磁拓扑结构、CME 特性、以及基于 RHESSI 观测的耀斑研究等方面取得进展。国际合作活跃，邀请包括院爱因斯坦讲习教授 Jokipii 在内的多名知名专家来访 ,组织了两个国际会议，其中 ASO-S Forum: Exploring Solar Eruptions and their Origins，对 ASO-S 起到很好推进作用。

1）太阳空间探测项目全面推进

太阳空间探测是推动太阳物理研究进展的主要手段。目前国内开展的太阳物理研究大都基于国际上的太阳卫星观测数据。尽快研制和发射我国自己的太

阳探测卫星，是当务之急。本团组成员作为首席科学家承担的先进天基太阳天文台(ASO-S)背景型号研究，2014 年取得实质性进展：初步完成了卫星方案设计，完成三大载荷初步方案设计，完成部分关键技术攻关，启动了火箭系统、发射场系统、测控系统、地面支撑系统、科学应用系统的需求分析。就 ASO-S 的推进专门召开了国际论坛，邀请来自 7 个国家的 30 余位国际顶尖同行对 ASO-S 进行国际评估，其“一磁两暴”先进的科学目标得到国际同行的广泛认可。此外，针对我国将于 2020 年发射空间站的机遇，团组成员和实验室一起提出“大面积太阳伽马射线谱仪（LASGA)”搭载的提案，年内经过反复论证，于年末正式入选空间站载荷项目指南。如果一切顺利，2015 年将立项，之后将于 2020 年发射入轨，LASGA 有望在太阳活动 25 周峰年期间发挥巨大作用。此外，团组成员或作为负责人或作为参加者，积极介入多个中欧合作太阳探测卫星计划的遴选。

2）太阳粒子事件及磁拓扑结构研究取得进展

团组博士后 Firoz et al. (2014, ApJS)研究了太阳活动 24 周第一个 GLE 事件，主要是检验 CME 激波加速粒子是否起主导作用。利用太阳射电 II 型暴观测，并结合日冕不同高度粒子密度的时间演化，推求激波的高度和速度。结果表明，一方面耀斑对激波加速过程有贡献，另一方面 CME 驱动的激波可以产生该高能粒子事件。此外，Firoz et al. (2014, ApSS)还利用不同中子观测站的数据，综合研究了 GLE17 事件，核心是辨别该事件到底起因于耀斑还是 CME 的爆发。结果支持 GLE71 很可能是激波加速产生的，之前的耀斑可能加强了激波的作用。

在活动区磁拓扑结构研究方面，我们使用 SDO 卫星的矢量磁场数据，对活动区 11158 的磁场拓扑结构进行了研究。使用更加接近观测结果的非线性无力场外推的方法，得到了活动区的三维磁场。在此基础上计算了该活动区的磁力线压缩因子，发现在耀斑事件发生前后，活动区的大尺度磁场结构基本保持稳定；通过压缩因子，还确定了磁绳在 X2.2 级耀斑中的重要作用，并且支持日冕物质抛射与磁绳的爆发相关。该工作已经在 ApJ 发表。

太阳活动的多波段观测研究

在本年度我们利用高分辨率观测在极紫外喷流、小尺度活动、耀斑的粒子行为和耀斑环的整体行为方面取得了一些进展。

1）研究了 2011 年 10 月 15 日 SDO/AIA 观测到的极紫外喷流。发现喷流在极紫外波段表现出暗化现象。通过对比极紫外图像和 Ha 图像，发现极紫外喷流暗化正好对应于 Ha 日浪。喷流的极紫外暗化可能是因为热的辐射被冷的日浪物质吸收导致。另外，我们还研究了 2011 年 7 月 22 日 SDO/AIA 观测到的重复性极紫外喷流。该喷流亮度、高度随时间减小，暗示能量的逐步释放，随若干次等离子体团的出流。研究发现这些等离子体团呈现多温特性，且可能是新浮磁流与日冕已有磁场发生重联的电流片的撕裂模不稳定性产生的。

2）研究了 2009 年 8 月 23 日靠近太阳极区冕洞的一个日冕亮点。提出了一个唯象模型来解释亮点中往复式重联和增亮现象。利用高分辨率资料，可能发现了太阳米粒之间的磁场重联过程。高时间分辨观测发现，在这个亮点中不断地有亮结构从亮点的中心向两侧运动。沿着这些亮点结构运动的方向，画出一条狭缝，得到这个狭缝的时空演化图。显示这些出流具有同时、同速、对称和准周期性，完全符合磁场重联的标准模型。

3）继续研究太阳耀斑中软 X 射线振荡和辐射源在环中运动的观测侧研究以及太阳活动爆发中磁场重联双向流的观测研究。分析了 2002 年 12 月 26 日的一个 C 级耀斑。观测发现这个耀斑沿着磁环有三个源，他们都在 3-6keV 能段有两分钟的振荡周期，其中两个源的振荡几乎同相位，但与另一个源几乎反相位。这些振荡可能与源在磁环中运动有关，具体的软 X 射线物理振荡机制需要更多的观测现象研究。

4）利用紫外和 X 射线的成像观测研究了发生在 2011 年 2 月 24 日的一个 M6.6 级极边缘耀斑，非常详细地得出了该耀斑在能量释放时日冕源、耀斑环、旁边宁静环以及磁绳所表现出的一些运动学特征：磁绳的缓慢上升和迅速爆发；磁绳之上宁静环的缓慢上升和迅速爆发；旁边宁静环的缓慢下降和迅速下降；EUV 耀斑环的收缩和膨胀；X 射线日冕源的 U 形运动轨迹等。得到如下结论：磁绳的爆发在太阳活动区造成了低压区，该低压区以阿尔芬速度(快模磁声波)往外传播，造成了旁边宁静环的缓慢下降和迅速下降；X 射线日冕源的运动方向沿着磁绳爆发的方向；耀斑上升期的能量释放过程与下降期的能量释放过程不

一样，上升期的能量可能来自磁绳内部的重联过程。

合作完成一本专著《耀斑环物理》。

暗物质与空间天文实验室

本年度主要进行暗物质粒子探测卫星有效载荷的研制工作，负责有效载荷总体即对有效载荷五个分系统的研制协调及工作部署监督、中子探测器的研制、BGO 量能器结构部分的研制工作 ;完成分系统验收测试、集成测试及卫星力学试验；暗物质粒子探测卫星工程于 2014 年 9 月底，顺利转入初样阶段。2014 年 11 月，完成有效载荷第一阶段束流工作。

1）暗物质粒子探测卫星研制进展

战略性先导专项暗物质粒子探测卫星，目前已经完成卫星研制的方案阶段（包括方案设计、电性件、结构件)和初样研制阶段(鉴定件)的研制 ,截止 2014 年 12 月 1 日，经过载荷电性件及初样件的桌面联试和束流试验、力学振动试验等验证，表明机、电、热接口符合预定设计，相关指标符合预期要求，圆满完成方案阶段所有研制任务。鉴定件阶段，有效载荷总体于 2014 年 4 月底完成载荷各单机的环境试验,包括力学环境试验、温度环境试验、老练试验、电磁测试以及载荷桌面电性能联合测试等多项试验及测试，之后于 2014 年 8 月结合卫星平台完成各项整星试验，按照工程总体所制定的转正样阶段工作要求，暗物质粒子探测卫星工程于 2014 年 9 月底成功转入正样研制阶段。

2014 年 10~11 月 ,探测器初样件在欧洲核子中心进行了三周的束流试验，主要对探测器以下性能进行测试：能量线性、能量分辨（主要针对电子） 、粒子的能量重建（能量泄露）、以及探测器能量的绝对定标（dE/dx)；触发效率的测试；探测器点扩散函数（PSF, point spread function)；粒子的反冲特性（Back splash determination)；探测器有效面积（Effective Area)；探测器粒子分辨能力，如 e/p 分辨能力。实验结果表明：DAMPE 工作正常，电性能、探测器性能稳定；DAMPE 对电子的响应和预期相符；DAMPE 对光子的响应和预期相符。

卫星工程自 2014 年 9 月底转入正样研制阶段以来 ,各项工作正紧锣密鼓展开 ,力争 2015 年底发射。

2）暗物质粒子探测卫星在紫台的科学组的研究进展

（1)AMS-02 数据中原初电子宇宙射线能谱超出（变硬）的预言及邻近电子宇宙射线源的证认：在 AMS-02 正式公开首批数据前 1 个月，我们推测原初的电子宇宙射线可能在高能段有变硬行为，这将使得正电子宇宙射线占正负电子宇宙射线的比例随能量的上升趋势变平或甚至出现下降(Feng, et al. 2014 PLB; arXiv:1303.0530V1)。对 AMS-02 及 Fermi-LAT 等的电子数据的联合分析的确支持“高能电子能谱变硬”这一观点 (e.g., Linden & Profumo 2013; Yuan & Bi 2013) ,在暗物质模型参数拟合时需加以考虑. 我们的工作在 2014.9.18 丁肇中先生在 CERN 的新闻发布会报告引用，并被随后在 PRL 上发表的 2 篇 AMS-02 论文引用。基于最新的 AMS-02 的正电子、负电子宇宙射线能谱数据，我们严格证明：只要宇宙射线正电子超出的辐射源所产生的高能段负电子不比正电子多，现有的 AMS-02 数据中强烈需要一个负电子原初能谱的超出，而该超出的来源最可能是邻近的中等寿命的超新星遗迹，尤其是 Monogem (Li, Shen & Lu et al. 2014 arXiv:1412.1550).

（2）我们还密切关注一些相关领域尤其是快变射电暴的进展，并积极探讨可能的宇宙学应用前景。快变射电暴(fast radio bursts)是 2013 年里得以确认的一类持续毫秒量级、流量强达~1Jy 的单脉冲型射电爆发事件，全天区的探测率原则上高达~10000/天。它们的物理起源尚不清楚，但所测得的色散量远远超过银河系星际介质的贡献，所以一般认为最可能来自于宇宙深处的致密星表面。目前国际上对快变射电暴的研究尤其是其物理起源研究进行得如火如荼，已迅速形成一个重要的科学前沿领域。我们指出色散量中包含着独立的光子传播距离的信息，如果将来快变射电暴的红移被直接测定，那么它们有望成为高效的宇宙学暗物质、暗能量新探针(Zhou et al. 2014 PRD; arXiv:1401.2927；见图 2)。我们比国际上其他合作组的类似工作领先一个月完成(arXiv:1402.2498)。射电天文学家 Jean-Pierre Macquart 把我们提出的这种可能列为耗资数十亿美元的平方公里射电阵 SKA 项目“killer science”的主要目标之一(https://indico.skatelescope.org/getFile.py/access?contribId=2&resId=0&materialId=slides&confId=275). 最近入选中国“SKA 组白皮书”。

电离气体研究团队与其合作者们首次将电荷交换光谱模型应用到星暴星系 M82 的高分辨率 X 射线

光谱中去（M82 星系是超级风研究中研究得最多，最为经典的例子），成功的拟合了整条 X 射线光谱包括 O VII 禁线。通过限制这个新的物理成分，研究者们用简单的模型自洽地解释了超级风物理特征和外流性质。结果表明，电荷交换过程（人们所知道的彗星 X 射线发射机制）在这里极大地增强了原子跃迁线的禁线辐射，并在整个波段贡献的流量占到四分之一。即四分之三的软 X 射线辐射来自于充满空间的热气体外流，而四分之一的辐射来自于冷热交界面的较小空间，与此前观测到的冷气体边界增强现象相符。研究者们也首次得以推断冷热气体的相互作用面积，要比超级风的几何截面大上一个量级，表明了两相气体之间的充分混合。这一碰撞混合过程使得更多冷气体被加载到热气体外流中，每年将有多达十几个太阳质量的物质流出星暴星系 M82。这个简单模型一致地解释了距离星系中心 11 kpc 的区域的软 X 射线辐射，并给出了超级风所能到达的距离下限。该工作表明，电荷交换过程可以对于来自星暴星系的 X 射线辐射起到很重要的贡献，并为天体物理中相互作用面的研究领域提供了一个非常有价值的工具。（iopscience.iop.org/0004-637X/794/1/61）

II. 南极天文和射电天文研究部

恒星结构、演化与脉动研究

本年度的研究工作围绕以下三个问题开展：1）湍动对流的非各向同性对恒星脉动稳定性的影响；2）低光度的主序和亚巨星以及红巨星中的 g 模振荡；3）变星脉动稳定性对金属丰度的依赖性。研究工作取得了如下阶段性成果：

完成了在非局部和非各向同性对流理论下恒星径向和非径向脉动理论计算程序的编制工作，并计算了质量 M=0.6 - 3.0 M⊙恒星从 ZAMS 到 RG 演化模型的线性非绝热脉动的理论计算，得到一个与观测大致相符的理论的δScuti 和γDoradus Stars 变星脉动不稳定区。

研究了δScuti 和γDoradus Stars 的脉动激发机制，提出了一个与传统理论不同的理论观点：δScuti 和γDoradus Stars 型变星的激发机制并无实质上的差异。他们很可能同属 Cepheid instability strip 底部的同一类脉动变星，只不过δScuti 是 P-mode 脉动的亚群，而γDoradus 是 g-mode 脉动的子群。δScuti - γDoradus 脉动不稳定区内大部分的脉动星很能可能是 p-mode 和 g-mode 同时激发的。δScuti / γDoradus hybrids, 他们之间的关系非常类似于 RR Lyrae 型变星中 RRc,RRab 和 RRd 这间的关系。

南极天文中心

南极天文中心组织参加第 31 次南极科考，AST3-2 和改造后的 CSTAR 结束漠河测试和试运行，运往南极冰穹 A。AST3-2 在漠河越冬测试过程中发现 CCD 发热导致镜筒内视宁度较低等问题，采取了特别设计的循环制冷，试观测效果良好，发现超新星一颗。CSTAR 升级改造，加装了赤道仪，实现全自动观测，完成了漠河越冬测试，主要科学目标是进行系外行星的搜索。能源平台升级方面，加入了太阳能与风能发电系统清洁能源方案，并已经完成高原风力发电测试和风能的设计方案；对平台的仪器仓和发电仓都进行了轻量化设计，通讯采用最新的 PILOT II。

继续深入开展南极天文台相关的关键技术攻关。973 项目“利用南极巡天望远镜在超新星宇宙学及太阳系外行星方面的前沿研究”通过中期检查。承担中科院先导 B 项目“宇宙结构起源-从银河系的精细刻画到深场宇宙的统计描述”中相关课题研究，进展顺利。组织了“2014 International Collaboration Meeting on Antarctic Survey Telescopes”国际会议。

紫台、南大、国台等多家单位开展南极天文合作，利用 CSTAR 于 2008 年在南极冰穹 A 观测得到的数据，在寻找系外行星方面取得重要进展（Wang et al. 2014, ApJS, 211, 26）。基于 CSTAR 2008 年的观测数据（包括 i 波段每 20 秒一幅图共计 29 万多幅有效的观测图片），利用掩星方法和可靠的探测手段，首次在南极利用中国自己的望远镜发现了 10 颗系外行星候选者，并且利用随后的光谱观测证认其中 4 颗可能是巨行星（气态的类木行星）。

吴雪峰及其合作者开展了伽玛暴系列研究工作：

（1）中心引擎方面：对 GRB 121027A 中的突然 X 射线剧烈增亮进行了时变分析，得到一个周期约为 86 秒的光变成分，并提出这样的周期光变可能是该暴中心黑洞和吸积盘进动造成的（Hou et al. 2014, MNRAS, 441, 2375）。对 GRB 130925A 中的 X 射线耀发时标演化也进行了数据分析，得到耀发时标随时间

的演化，他们提出这样的耀发时标演化也可能是由于中心黑洞进动形成的（Hou et al. 2014, ApJL, 781, L19）。对存在后期能量注入情形下的晚期余辉进行了详细研究，特别是利用星风环境下的能量注入模型成功解释了伽玛暴 GRB 120326A 的 X 射线和光学余辉平台阶段辐射和随后的增亮现象（Hou et al., 2014, ApJ, 785, 113）。（2）暴周环境方面：吴雪峰及其合作者对可能在伽马暴暴周存在密度跳变的成因问题进行了重新考虑，在他们的这个最近工作中（Geng, Wu, Li, Huang & Dai, 2014, ApJ, 792, 31），他们处理的正反激波过程满足整体能量守恒，并作了严格的数值计算。该工作表明，密度跳变一般情况下会使得伽玛暴余辉光变曲线产生小幅度的增亮。（3）双中子星并合（短时标伽玛暴起源的主流模型）引力波事件的电磁辐射行为。如果并合产物是大质量强磁场中子星而非国际上传统认为的黑洞，那么这类引力波暴的电磁辐射将非常强，他们在理论上首次详细得研究了该类电磁辐射的光变曲线。他们近期成功应用此模型解释了美国加州理工学院帕洛玛暂现源工厂近期发现的一类新的宇宙学相对论源 PTF11agg（Wu et al. 2014, ApJL, 781, L10）。他们在并合产物是大质量毫秒自转磁星的框架下提出的双中子星并合电磁辐射模型，对未来时域天文领域对这类暂现源的巡天具有重要的指导意义。（4）利用最新的伽玛暴红移样本对宇宙恒星形成和金属丰度演化进行了研究（Wei, Wu, Melia, Feng, & Wei, 2014, MNRAS, 439, 3329）。他们的样本包括了具有已知红移（红移低于 4）、主暴阶段平均光度超过 1.8 1051 erg/s 的 118 个 Swift 发现的伽玛暴。根据他们的最新样本，伽玛暴爆发率和恒星形成率的差异可以以红移 z 来参数化，即(1+z)^δ。在这个工作中，他们发现指数δ=0.80。这样的维像参数化结果，如果假设是由伽玛暴爆发率依赖于金属丰度所造成的，那么对应的截断金属丰度为 0.52 倍的太阳金属丰度。最后，他们利用高红移伽玛暴样本（红移大于 4，最高达 9.4）对高红移恒星形成率进行了限制，得到的恒星形成率正比于(1+z)^(-2.41+1.87/-2.09)。（5）还用类星体引力透镜成像不同像的时间延迟，对宇宙学模型及其参数进行了限制（Wei, Wu & Melia 2014, ApJ, 788, 190）。目前能用的样本有 12 个，对标准宇宙学模型（Lambda CDM）参数的限制结果如下：哈勃常数 H0 =87+17/-16 km/s/Mpc，宇宙物质密度参数Ωm=0.48+0.25/-0.37。我们基于目前的样本进行了模拟，未来如果这样的样本增加到 150 个左右，则对标准宇宙学模型参数的限制结果可达到 H0 =71+/-2.1 km/s/Mpc, Ωm=0.34+0.20/-0.18。（6）利用 ROTSE-III 自动光学暂现源搜寻望远镜观测到的 58 个伽玛暴光学样本，对伽玛暴光学光度函数进行了限制（Cui et al. 2014, ApJ, 795, 103）。该 58 个样本其中有 18 个是探测到光学辐射，另外 40 个则是辐射上限。该光学光度函数定义在光学 R 波段以及爆后 100 秒的时刻。该研究结果表明，单幂率光度函数与观测样本不符，可以在较高置信度区域被排除；而指数上升、幂律下降的光度函数，拐折双幂律光度函数，Schechter 光度函数则与目前观测一致，暂时不能被排除或者得到很好的限制。（7）一般认为不同尺度的黑洞喷流系统其物理本质可能是相同的，且伽玛暴喷流也与射电平谱类星体喷流类似，是高磁化高辐射效率的。吴雪峰及其合作者进一步发现（Lyu et al. 2014, ApJ, 793, 36），伽玛暴与射电平谱类星体有相似的辐射机制，却有不同的谱能关系，其原因可能为伽玛暴是快冷却机制主导，而 Blazar 属于慢冷却机制主导，进一步分析发现伽玛暴喷流和射电平谱类星体喷流都是磁能主导、主导辐射机制为电子同步辐射。该研究结果给出了不同尺度相对论性喷流物理规律相似性的证据。

李国亮开展的研究工作主要包括：（1）在多球面大天区引力透镜效应模拟，为巡天观测模拟做准备。在面密度计算和强引力区增强算法上做了改进。(2）初步建立了一套新的图像叠加算法，亮点是消除了像素化卷积效应，合理重建采样不足的图像。（3）在 PCA 的基础上，发展了 EMPCA 算法，提高了点扩散函数重建的可信度。

张雪光完成了光学选、乏宽线区活动星系核物理性质研究方面的工作（Zhang, MNRAS, 438, 557）。他从斯隆巡天数据库(SDSS Stripe82 Database)中对乏宽线区活动星系核进行了系统搜寻，最终得到 281 个比较可靠的乏宽线区活动星系核候选体。这比目前已知的乏宽线区活动星系核样本至少大 4 倍。

蒙克来等在 HOD 框架下计算星系三点相关函数方面取得了进展。

星系宇宙学和暗能量研究

本年度成功举办第十届中德星系宇宙学国际会议，参会者为 160 人左右。负责 5 个培育项目之一（"观测宇宙学"），并开展如下研究：研究宇宙大尺度结构，

完成程序编写；研究椭圆星系的金属丰度梯度演化，已基本完成，正成文；研究冷暗物质模型下的暗物质晕吸积历史，已基本完成并正在成文；研究星系形成模型，正进行。本年度新引进 2 名外籍博士后。

研究了星系的 2 点相关函数，解决了半解析模型中星系的成团性过高的问题。研究了星系空间分布，首次利用流体数值模拟解释了星系空间分布与中央星系形状直接的相关性。基本完成了弱引力透镜的全天成图。

星系中的恒星形成研究

本年度在星系中的恒星形成，星系形态结构演化等方面取得了显著的进展。7 月举办了主题包括近邻星系研究、巡天计划、星系环境和星系团、高红移星系、宇宙学、暗物质研究、高能物理、活动星系核与黑洞等的 130 多人参加的学术研讨会。10 月在南京举办了 50 人左右的学术讨论会，讨论 JCMT(James Clerk Maxwell Telescope)望远镜的科学，观测等讨论会。协助上海天文台在 9 月份举办了第一次关于 JCMT 的交接管理，科学等方面的讨论会。团组在 2014 年共邀请了国内外专家 12 位来紫台访问，进行学术交流。

郑宪忠等成功将 FTS 仪器改造升级并运送至阿里狮泉河站址，获得连续 2 个月的观测数据，取得初步分析结果。

施勇与高煜，王均智，张智昱等合作研究发现宇宙原初气体可能无法有效地形成新恒星。宇宙大爆炸后气体随着宇宙膨胀而渐渐冷却，在大约 130 亿年前，开始坍缩形成宇宙第一代和第二代恒星。其内部剧烈的核聚变反应把氢和氦合成其他更重的元素，如碳和氧等，部分重元素通过恒星风和超新星爆发返回到气体中，使气体中的重元素含量逐渐增加。恒星在富含金属元素气体中形成是科学家们在邻近宇宙，包括银河系中发现的新恒星诞生的主要途径。各种理论模型在缺乏金属元素以及由这些金属元素组成的分子和尘埃颗粒情况下，恒星形成的效率会降低，即单位质量气体在单位时间内只有较少一部分才能转化成恒星，然而这些理论预测一直缺乏有效的天文观测来证实。研究团队通过对两个低金属元素含量的近邻的恒星形成星系 Sextans A 和 ESO 146-G14 的多波段红外观测，结合恒星形成率的测量，发现这些恒星形成区域恒星形成效率远低于类银河系星系的观测结果，虽然研究指出此时分子氢仍大量存在。暗示了 130 亿年前宇宙原初气体可能无法有效地形成新恒星。

恒星形成定律无论在观测还是理论天体物理中都是非常重要的。张智昱和高煜等利用 APEX 12 m 望远镜对 20 个近邻恒星形成星系观测了 HCN J = 4 → 3, HCO+ J = 4 → 3, 和 CS J = 7 → 6 三条谱线发射，结合文献中的数据，研究了目前为止最稠密(密度~106 cm-3)的分子气体光度和红外光度之间的关系。发现 LCS, J=7-6 -LIR and LHCN, J=4-3 -LIR, 呈线性相关，LHCO+, J=4-3-LIR 呈超线性相关。LCS, J=7-6 -LIR 相关性跨越了 8 个量级的光度，并延伸到银河系分子云核的尺度。这样的线性关系似乎在所有密度大于 104 cm-3 的区域都成立，说明恒星形成率并不与稠密分子气体的自由下落时标相关。

闻璋正和郑宪忠等发展出一套能够自动测定星系形态的新方法，尤其适于证认具有潮汐不对称结构的并合星系。这一方法的核心是把一个星系分成等亮度的内部和外围两部分，对星系外围部分测定其不对称度 Ao 和其“质心”相对内部区域“质心”的偏离度 Do 两个形态参数；星系形态越不规则，其 Do 和 Ao 两参数越大，因而可以将具有不同形态的星系区分开。与已有的 CAS 和 Gini-M20 方法相比，此方法避开星系中心高面亮度区域的影响，对探测低面亮度的纤细子结构更为敏感。如图所示，基于 GEMS 巡天的哈勃空间望远镜高分辨图像数据对 764 个红移 $0.35<z<0.9$ 的星系组成的完备样本测定形态参数，证实样本星系在 Do-Ao 参数空间分布成单一序列：统计而言，椭球星系和盘星系等形态规则星系与并合星系等形态不规则星系分布在此序列不同位置上。与国际上的同类方法比较，这一方法在证认并合星系，特别是有潮汐尾等特殊不对称结构的星系方面最为有效。新方法是面向国际上的欧几里得（EUCLID）计划和大型综合巡天望远镜计划（LSST），和国内已列入规划的南极昆仑站暗宇宙巡天望远镜计划（KDUST）等巡天计划的大数据，可以开展超大样本的星系形态测量，探索星系结构的起源。
(http://iopscience.iop.org/0004-637X/787/2/130)

安芳霞，郑宪忠与其合作者们利用位于世界最好的地面天文观测台址之一的美国夏威夷的 3.6 米口径 CFHT 望远镜近 3 晚的观测时间，成功获得南天一个深场观测天区的近 400 平方角分最深的窄带观测。研究者们利用这一独有观测，结合其他观测数据，可以

从图像探测到数以万计的各类天体中，精确证认出红移 z=2.24(100 亿年前)正在大规模形成恒星的星系，并系统研究它们的能谱分布、形态、Hα发射线等多方面特征。研究发现，这些强 Hα发射线星系与通常颜色选的恒星形成星系类似，质量介于约十亿至千亿太阳质量范围，呈现恒星形成率与星系质量的相关关系和消光与星系质量相关关系。而哈勃空间望远镜的高分辨率、高灵敏度成像观测揭示这些 100 亿年前发射线星系具有多样性的形态。

赵应与高煜和与吕南姚、徐聪、严琳研究员以及其他欧美合作者就赫歇尔空间望远镜科研项目《对近邻亮红外星系中暖分子气体的光谱巡天观测》/《WISE 挑选红外亮 QSOs 的 PACS 分光观测》进行合作，1）利用 ALMA 观测了临近亮红外星系 NGC 34 核区，CO (6-5) 的动力学和形态分布都表明星系核区存在一个尺度约 200pc 的致密旋转盘结构。而且，在核区半径约 100pc 以内气体柱密度很高($>10^4$ $M_\odot$ pc^{-2})。2）利用 Herschel SPIRE/FTS 对 GOALS 子样本的早期 65 个亮红外星系（LIRGs）的光谱观测数据，获得了 CO 从 J = 4 到 13 的谱线能量分布（SLED）。结果表明中-J CO 谱线发射之和与总红外光度之比基本上与 c(60/100)无关；恒星形成主导的星系的中值为-4.13 dex。

王均智与高煜等研究人员合作利用位于西班牙的 IRAM 30 米毫米波望远镜在近邻的活动星系 NGC1068 中测到了氧化硅(SiO)以及甲醇(CH3OH)分子的超脉泽发射。分析表明，氧化硅脉泽来自非常靠近星系中心黑洞的高温气体盘，而甲醇脉泽来自喷流区域。该发现不仅使得超脉泽家族的数目由三个变成了五个，而且为利用这些新的脉泽发射研究近邻星系中核区的气体性质、中心黑洞以及活动星系核对宿主星系的反馈打开了一个新的窗口。该工作发表在《Nature Communications》杂志（10.1038/NCOMMS6449）。

毛业伟和郑宪忠等通过观测分析和理论模拟相结合发现消光曲线的线性背景斜率和其中的近紫外驼峰特征会显著影响 IRX-UV 关系，它们的变化是导致 IRX-UV 关系产生弥散的又一个原因。这个结果解释了毛业伟前一项工作中星族年龄效应无法解释的观测现象。消光曲线对星系观测性质的影响也曾被一些理论模型所预期，而论文细致地解析消光曲线中不同成分在星系观测性质中的不同表现，同时在实际观测中检查消光曲线的变化，这还是第一次。工作中还讨论了尽管消光曲线对星系观测性质的影响相当可观，但是在观测中确定消光曲线却是非常困难的，原因包括消光曲线的线性背景斜率和近紫外驼峰特征在星系观测性质中有耦合效应，它们的观测表现相互影响、相互掩盖；同时，消光曲线的特征只有在年轻富尘埃的系统中才能显露；另外，确定消光曲线需要对不同波段尘埃消光进行准确估计，这一点也非常困难。正因为在观测中消光曲线的形式不容易被确定，所以它对观测结果的影响也往往被忽略，尽管这种影响很可能相当严重。

分子云与恒星形成研究

2014 年度本团组在银河画卷计划—CO 分子巡天、系外行星大气、年轻星外流活动、极小质量恒星和褐矮星的星周盘结构和演化等研究方向进行了研究。中科院先导 B 项目“银河系气体分布及恒星形成”和国家基金委重点项目“银河画卷计划—CO 分子巡天”项目实施顺利；继续参加国家基金委重大科研仪器设备研制专项“太赫兹超导阵列成像系统”项目。在第四届“中智天文研讨会”等双边和国际大会上进行了广泛深入的交流；通过多渠道加强了的人员交流和国际合作。

1）“银河画卷计划-CO 分子巡天”进展顺利

完成对 M17 区附近的分子云 L=（12.0，16.5）&B=（-1.5，0.5）形态及物理性质的分析，其分子谱线展示出多个成分，对应银河系不同的旋臂，它们的形态及物理特征均不相同，发现了大量处于早期的分子云核及泡状分子云结构；对 M16 区附近分子云 L=(15.0,18.5),B=(-0.5,2.0)的分析已经完成，发现了一个与 M16 中心的年轻星星团成协的巨大双极型泡状结构，可能是星团形成的产物。子天区-Rosette 天区的观测和研究取得进展。完成了该天区主要分子云 Rosette 的结果分析，新发现一批新的分子云，论文草稿已经完成。在 2014 年度完成了该天区 27 个天区单元（6.75 平方度）的观测、数据检查和归档。

2）系外热木星大气研究取得系列成果

为了研究白昼大气的性质，使用 ESO 2.2m 望远镜的 GROND 成像设备同时在 g′ r′ i′ z′ JHK 这七个光学到近红外的波段对 3 颗热木星 WASP-5b、WASP-43b 和 WASP-46b 进行了成像观测，均成功探

测到白昼大气热发射信号，并得出 WASP-5b 大气没有逆温层,其化学组成可能是富碳的；WASP-46b 大气热再分布效率非常低,几何反照率较高 ,大气中可能存在反射云层；WASP-43b 大气中可能存在高层反射云霾。综合我们的结果可以得出（1）近红外波段(JHK）所诊断的深层行星大气呈等温状态；（2）观测证据支持较热的热木星普遍处于低效的热再分布状态的假说；（3）观测证据支持主星活动抑制热木星大气中的逆温层的假说。在 A&A 发表论文 3 篇。利用透射光谱研究热木星大气成分的工作，已经完成了结果分析，相关论文也已经完成了初稿。

3）外流搜寻、激发源证认和外流性质统计研究取得重要成果

对典型恒星形成区 Vela C 分子云进行了大视场（2 平方度）[SII] λλ6717/6731 谱线发射的深度成像观测，新发现 18 个光学外流天体（HH 天体），即 HH1090-1107。使用 WISE 数据和我们所发展的证认方法，在该分子云中新发现了 11 个中红外外流天体(EGO)。同时对该分子云中的年轻星天体(YSO)进行了普查，证认出 56 个年轻星天体。在此基础上分析得出了 12 个 HH 天体和 5 个 EGO 的激发源。对该分子云中外流的统计性质进行了研究，得出该分子云中外流长度的中值是 0.35 pc，外流方向是随机的。论文已在 AJ 发表。

使用 VLT 及附属设备 NACO、SINFONI 和 VISIR 对大质量恒星形成区 M17 的 UC1 和 IRS5 区进行了近中红外分光与成像观测研究，在它们周围发现了双极反射云，暗示祝这两个系统存在质量外流，其中的 IRS5 实际是一个多星系统 ,可能至少存在 4 颗年轻星，而 IRS5A 是一个大质量年轻星 ,其质量吸积阶段已经结束；UC1 也是个大质量年轻恒星系统，偏振观测暗示可能存在星周盘，但同样结束了吸积阶段。这项工作已投 A&A，目前进入二审阶段。

4）极小质量恒星和褐矮星星周盘研究取得重要成果

为了解极小质量恒星和褐矮星星周盘的物理特性，使用 Herschel/PACS 对年轻星协 TW Hya 中的 5 个极小质量恒星和褐矮星进行了观测，在 70 微米和 100 微米波段均探测到这些天体，在 160 微米波段探测到其中的 3 个天体。这些探测结合这些天体的 2MASS、WISE 和 SCUBA-2 的数据，可以构建这些天体宽波段的能谱分布。使用我们发展的辐射转移模型，得出了星周盘的物理特性：与较大质量恒星的星周盘相比，这些极小质量恒星和褐矮星星周盘的几何形态较为平坦，盘的质量要小很多，但盘的标高却很接近。论文已在 A&A 发表。

5）河外星系中的分子气体研究

通过对一个高红移原星系团中四个 Lyman alpha 团块射电和远红外数据的分析,发现一半的 Lyman alpha 团块与射电和远红外源成协。通过红外源的连续谱能谱分析,其红移与 Lyman alpha 星系的红移是一致,证实两者在物理上是成协的。进一步的分析证明,射电和远红外很可能都来自恒星形成,从而揭示了部分 Lyman alpha 团块的加热机制是恒星形成。这个成果已经完成论文撰写,并已投稿到 A&A 杂志。利用 IRAM 30m 望远镜,对近邻星系 NGC253 和超亮红外星系 Mrk 231 进行 CN,13CN 以及 CO 谱线观测。对于 NGC 253,12C/13C 的丰度比为 40+/-10,这个比值大于银河系 CMZ 区域的对应值，表明在 NGC 253 中有更高的气体进入星系中心。而在 Mrk 231 中,12C/13C 的丰度比为 100,这个结果与 Arp220 星系中是一致的。

毫米波与亚毫米波技术实验室

本年度工作主要包括：1）针对铝制反射面和碳纤维反射面两个 5m 太赫兹天线概念设计方案，开展了极端台址环境下望远镜性能仿真研究、太赫兹碳纤维原型面板试制与测试、太赫兹铝制原型面板环境实验，开展了高精度面板促动器工业调研与试制，以及望远镜近场全息测量实验研究；2）国家重大科研仪器设备研制专项“太赫兹超导阵列成像系统”和“多波段多大气成分主被动综合探测系统-太赫兹辐射波谱仪”，研制进展顺利，并通过基金委的中期检查和中科院的年度监理；3）“太赫兹超导探测器研制平台一期”，转入常规运行阶段，成功制备出第一批全制程超导隧道结芯片；4）太赫兹频段超导相干和非相干探测技术研究及应用，包括多波束接收机技术研究、太赫兹超导混频器温度及频率相关性研究、超宽带太赫兹超导探测器研制以及太赫兹测量平台构建等。

主要进展包括：

1）国家重大科研仪器设备研制专项“太赫兹超导阵列成像系统”关键技术取得突破，顺利通过基金委的中期检查和中科院的年度监理。该项目在 2014

年度进展顺利，完成了针对两种探测器阵列的低温光学系统设计，以及 POST 望远镜与 0.3K 杜瓦间集成方案设计；研制了基于 Nb 和 TiN 两种超导薄膜的 8×8 像元超导动态电感探测器（MKIDs）阵列，以及基于 TiN 超导薄膜的 1024 像元超导动态电感探测器阵列，实现 MKIDs 探测器阵列芯片的制备与亚 K 温区低温特性初步表征，以及 MKIDs 频域读出复用单元的初步研制和测试；实现单像元超导 TES 探测器特性表征，灵敏度达到预期目标，并完成了 8×8 像元超导 TES 探测器阵列芯片和时域读出复用单元方案的初步设计等。

2）南极 5 米太赫兹望远镜关键技术研究。完成南极 5 米太赫兹望远镜（DATE5）系统和分系统的方案设计；完成了 H350 波段超导隧道结混频器的设计以及芯片和基座制备，并对制备完成的超导隧道结芯片进行了初步的直流特性表征；完成了 H200 波段超导 HEB 混频器单元原理芯片的研制，性能处于国际前沿水平；完成了 2GHz 带宽 FFTS 宽带高分辨率数字频谱仪的研制。另外，太赫兹本振源和 4K 低温制冷等关键单元的试制进展顺利。

极端台址环境下太赫兹望远镜性能仿真研究。针对极端台址环境下两个 5m 太赫兹天线（铝制反射面和碳纤维反射面）概念设计方案，开展了重力、温度场和风载荷条件下望远镜面形和指向误差分析，特别是以典型极端台址实测气象数据作为输入条件，模拟包括均匀温变、温度梯度、局部热载荷以及随机温度分布在内的各种热载荷对望远镜天线性能的影响，从而了解太赫兹望远镜在极端台址条件下的整体工作性能。此外，还对碳纤维反射面方案中的天线外罩与天线机箱内部温度控制方案进行了仿真计算和设计优化，从仿真计算的结果可以知道，利用压缩机等机器产生的废热，通过设计/调节各项几何物理参数（进风口面积和进风速度、出风口位置/面积/数量、风扇的位置/数量/速度等），基本上可以达到我们温控预期要求。

太赫兹碳纤维原型面板试制与测试。与上海复合材料科技有限公司合作，共同开展面向南极 5m 太赫兹望远镜应用的碳纤维原型面板试制和测试评估，完成了面形精度 1.4 微米的殷钢模具，并制作了第一个碳纤维原型面板，精度达 5.2 微米，接近技术指标要求。

太赫兹铝制原型面板环境实验。利用已加工好的铝质原型面板开展了极端台址环境模拟实验，实验围绕以下重点关心的问题展开：1）铝质原型面板在低温环境下的面形精度；2）铝质面板表面结霜特性，以及相应防霜方案的实验验证和方案优化；3）可能由防霜系统引起的表面形变化等。实验在租用的环境模拟实验舱中进行，模拟了从室温至-60℃的温度变化范围。

太赫兹面板促动器工业调研与试制。联合哈尔滨工业大学精密工程研究所开展了面向极端台址条件的太赫兹面板促动器原型试制。原型促动器的设计要求是在行程±1 mm 条件下，实现单向 1 微米的位移精度。促动器机械结构设计时考虑了两种方案，即差动丝杆驱动方式和精密丝杆直接驱动方式。目前已分别完成上述两种促动器方案的原型样件试制，正在进行相关力学性能的实验室测试。

望远镜近场全息测量实验研究。完成了近场全息测量实验系统的研制，该实验系统主要由 3mm 波段双通道相关接收机和发射源、测试天线、系统控制与数据采集等部分构成。测试天线是一个口径 1.45m、焦比 0.35 的碳纤维铝蜂窝结构抛物面天线，面形精度优于 0.2mm，采用主焦馈源照明。利用研制的实验系统开展了近场全息测量实验，测量结果表明，目前系统重复测量精度达到 4.7 微米，接近技术要求，还将继续开展研究进一步提高测量精度。

3）太赫兹频段超导相干和非相干探测技术研究及应用。开展了 NbN 太赫兹超导 SIS 隧道结直流与探测器特性的温度相关性研究，太赫兹超导 HEB 混频器频率与温度相关性研究，均取得原创性结果；实现超宽带太赫兹超导探测器研制，成功应用于太赫兹测量平台构建及波束特性近场测量等；基于太赫兹 TDS 和 VNA 测量技术，实现硅基材料介质特性的宽带测量，开展了多波束超导 SIS 接收机关键技术研究。

4）在"大规模像元超导混频阵列"关键技术研究方面取得了以下进展：（1）推进了基于 NbTiN 高能隙超导材料微带线的超导参量放大器的制备工艺研究，获取了超导微带线的微波损耗特性与制备参数之间的可靠关系；（2）利用 GeSi 异质结三极管设计并制备了单级和双极微波放大器。在 0-5GHz 频段达到了噪声温度小于 10K 的结果；（3）完成了传输线型式串联结阵列分布混频器的理论研究工作。这种新型的混频器电路能够同时拓展超导隧道结混频器的射频带宽和中频带宽。在一个完整波导单模带宽内实现均

匀的变频效率，同时可使中频带宽从 2GHz 拓展到 20GHz（4）研制成功 4K 温区 4-8GHz 铁氧体环形器，与同济大学合作进行了 YFeO 铁氧体的烧结工艺研究。

5）“太赫兹超导探测器研制平台一期”成功转入常规运行阶段，为实验室太赫兹超导探测器技术研究提供有力支撑。“太赫兹超导探测器研制平台一期”共包含三台主设备，分别为超导及金属薄膜磁控溅射系统、绝缘层磁控溅射系统和掩膜对准光刻系统。运行迄今，实验室已经可以自主溅镀包括 Nb、Al、Ti 和 SiO2 在内的单层或多层金属及绝缘层薄膜，重点制备的 Nb 膜溅射速率可以通过改变直流电流或者射频功率进行良好控制。2014 年度，实验室利用研制平台，成功制备全制程超导隧道结芯片，质量因子高达 12 以上。利用该系列设备，实验室还自主制备了国家重大科研仪器设备研制专项“太赫兹超导阵列成像系统”项目中 TES 超导探测器的 Ti 超导薄膜，制备了基于 Al 膜的周期结构等器件。

6）中科院先导专项 B 项目顺利进行；成功完成 973 项目的结题验收；并按时间、按指标完成中科院创新方向性项目和江苏省重点基金项目的有关工作，按节点要求完成项目结题验收汇报。

青海观测站

运行情况：13.7 米望远镜全年开机运行 294 天，其中对外开放课题观测 294 天。2014 年度新受理课题观测申请 12 件，安排国内外申请的课题观测 14 件，完成 CO、HCO+、CH3OH 等分子谱线的课题观测。2014 年度望远镜平均每天扫描 1.5 平方度的天区。2014 年度无论在设备运转、开放课题观测时间，还是在设备稳定运行、数据产出量方面，继续保持历史高位，数据质量则有更大提高。2014-2015 观测季节的开放课题观测从 2014 年 9 月 11 日开始。

主要工作进展包括：

为降低副反射面热形变导致的测量误差，由中国电子科技集团公司第五十四研究所研制，望远镜副反射面成功更换为碳纤维材料。增加斩波轮调制装置，实现波束调制功能，进而可实施连续谱的调制观测，拓展望远镜研究方向；更换了超导成像频谱仪系统的部分像元的 HEMT 放大器、在杜瓦内部 50K 冷级金属罩贴防热辐射薄膜，改善接收机的稳定性，确保“银河画卷计划”工作顺利进行。

2014 年度，“银河画卷计划”共计完成 972 个巡天单元（每个单元 30′×30′大小）。截止到 2014 年底，“银河画卷计划”巡天工作 831 平方度的天区观测，包括 M17, Aqualia Rift, Cygnus X, W3/W4/W5, GEM OB1, Monoceros Nebula, Maddalena Cloud, 和 Califirnia Cloud 等比较有名的天体目标，对其中的分子云演化和恒星形成过程进行了研究，数据质量完全符合科学家的要求，彰显了“超导成像频谱仪系统+OTF 观测模式”的强大威力。

孙燕等在银河系第二象限最遥远的区域新发现了一段分子气体旋臂，这段分子旋臂位于银河系已知的“外旋臂”之外更远的位置上，距离银河系中心 4.5-6 万光年，在垂直于银盘方向的厚度约 1-2 千光年。这是至今为止探测到的离银河系中心最远的旋臂。研究组利用位于青海的 13.7 米毫米波望远镜探测来自星际空间的一氧化碳分子的谱线发射，在对银河系的巡天观测中新发现了 72 个远距离的星际分子云，这些分子云的空间分布勾画出了银河系的这段新旋臂。新发现的分子云质量都超过 100 倍太阳质量，一些分子云甚至超过了 1 万倍太阳质量。人民日报介绍了这项科研成果。

国家天文台研究者利用紫金山天文台青海德令哈观测基地 13.7 米望远镜对 H II 区 G53.54-0.01（N115）进行了 CO 分子谱线的观测，三个云核中探测到被 HII 区 G53.54-0.01 膨胀堆积的气体，另一个云核中没有探测到被堆积的气体，而是探测到了分子外向流，通过计算，存在分子外向流的云核具有大的质量，进而说明该大质量恒星可能是被 H II 区 G53.54-0.01 通过 collect and collapse 过程触发形成的。

紫台研究人员用基地的 13.7 米毫米波望远镜对超新星遗迹 IC 443 进行了 CO 三条分子谱线的观测，观测覆盖了 2.25 平方度的天区，首次揭示了环绕这个超新星遗迹北部的连续分子壳层结构和遗迹东侧的离散分布的分子云团块结构，发现了 62 个年轻星候选体聚集在 IC 443 的视场内，这些年轻星候选体主要集中在超新星遗迹的射电辐射边缘，很可能是被遗迹的前身星的剧烈活动（例如紫外辐射，星风等）触发的。

围绕 13.7 米毫米波射电望远镜的建设、技术创新，成就出一批活跃在国际学科前沿的有影响的科研骨干。他们在使用基地望远镜的同时，积极申请其他国际一流望远镜，如德国 Effelsberg100m，日本

Nobeyama45m 美国的VLA、VLBA以及欧洲的EVN、IRAM30m等的观测，做出了许多国际一流工作。

2014年12月底，宋项目基建工程已经全部完工；宋1米光学望远镜，正在进行望远镜系统调试。50Bin望远镜正在进行实验性观测。

作为青海省爱国主义和科普教育基地，继续承担着爱国主义教育和科普宣传的任务，配合当地政府开展一系列天文科普宣传工作。由海西州政府与紫金山天文台共建的"德令哈天文科普馆"项目布展工作已全部完成，相关工作已移交给海西州文化场馆管理有限公司。

在院修缮专项资金的支持下，对基地锅炉、发电机、深井泵、圆堡风机等设备进行了改造；对科研与辅助房屋进行了修缮，解决了漏雨等问题；安装了全站安全监控系统，为科研工作提供了安全保障；对站区部分道路、围墙进行了修缮，改善了工作环境。为望远镜运行和来访观测人员提供了良好的工作和生活条件。提高了青海观测站的竞争实力，实现了青海观测站科研平台基础能力的提升，为观测站承担高水平的研究提供了基础支撑的保障。

为了星地量子科学实验卫星一体化实验的顺利实施，2014年基本完成了1.2米量子通信科学实验专用望远镜观测楼工程土建工程，圆顶已基本安装完工。

III. 应用天体力学和空间目标与碎片研究部

空间目标与碎片观测研究中心

本年度在科研、重大设备研制、完成国家任务以及观测网的持续运行等各方面开展了大量工作，主要有：（1）院观测网持续运行，目标管理能力持续增长，圆满完成多项国家任务；（2）30厘米完成了南山子阵的外场检测、全系统入网试验及评估工作；GDZ设备经专家鉴定为"这是一项原创性的成果，总体设计先进，技术创新突出，达到同领域国际领先水平"，获得军队科技进步一等奖1项；（3）GDZ设备成功推广至国内其他部门，并已立项实施；（4）完成了90厘米望远镜和捆绑望远镜的验收；（5）院配套基建项目顺利进行，完成了项目的财务审计、档案和验收材料准备工作；（6）完成了院修购项目"观测网升级改造"、"洪河一期升级改造"的验收；（7）继续开展空间目标运动理论与应用研究，在特殊轨道动力学特征及其长期演化规律研究、编目技术、陨落期预报方法、天文定位、识别方法、大气模型改进、碰撞预警、空间碎片测光方法、暗弱目标探测方法以及空间碎片精确定位研究，并初步拓展到卫星姿态动力学领域。

主要成果和进展如下：

1）2014年中心参加了多项国家任务，并得到了各方好评。主要有：①委内瑞拉"遥感1号"卫星碰撞预警任务；②俄罗斯发射一箭七星应急监测任务；③我国"遥感3号"卫星与意大利SKYMED1卫星碰撞预警任务；④俄罗斯COSMOS1939卫星陨落期IADC国际联测试验；⑤低轨道火箭体光度IADC国际联测试验；⑥我国火箭发射减缓辅助评估。特别地：从2014年2月公布的IADC报告获知，在中心代表国家航天局参加的欧空局GOCE卫星陨落期IADC国际联测试验（2013年11月）中，中心所作的预报结果在参加联测的11个主要航天国家组织中预报精度名列第一，为我国争得了荣誉。

2）2014年度完成了15项课题的结题与验收。承担了国家自然科学基金，863课题、国防科工局空间碎片专题以及院修购专项等相关课题的研究工作。设备研制项目进展顺利：90厘米项目于2014年5月完成了项目验收；捆绑式望远镜于2014年5月完成项目验收工作；30厘米完成年度合同验收；院观测系统配套基建项目已完成全部内容及财务审计工作；望远镜升级项目完成外场安装工作。

3）课题进展情况：继续深入开展人造天体的一些特殊轨道的长期演化规律、空间碎片的观测方法、空间碎片非质点旋转运动特征提取及分析等方面的工作。

以中国北斗导航系统中IGSO（倾斜同步轨道）卫星为背景，研究了倾斜同步轨道的长期动力学演化，指出在日月共振作用下，高倾角倾斜同步轨道的偏心率在长期演化过程中会达到很高的值，不再保持近圆特征，并据此提出了这类卫星的减缓策略：通过选择合适的发射时间（即初始升交点经度）可以使任务结束的高倾角倾斜同步轨道卫星的在轨寿命显著减少。该工作受邀做国际会议报告1次，论文在ASR期刊审稿中。

从理论上探讨了Molniya型轨道的长期演化特征。给出了考虑地球非球形引力摄动时，Molniya轨道中等周期运动的近似分析解。并进一步阐明了平运动共

振对长周期运动的贡献。相关工作已于 2014 年发表于《Advances in Space Research》。研究了日月共振对 Molniya 轨道长周期运动的影响，利用单共振模型和共振重叠模型，给出了 Molniya 轨道在长周期运动中偏心率和倾角的变化范围，并利用半分析方法初步探讨了月球升交点共振的影响。

研究了小行星同步静止轨道航天器姿态稳定性问题。考虑小行星的二阶非球形引力场，研究了四阶重力梯度力矩作用下航天器的姿态稳定性。采用模态离散化方法，得到了航天器离散化的姿态动力学方程，进而探讨了航天器在轨道坐标系中相对平衡的稳定性，推导出稳定性的充分条件；以太阳系大多数小行星为背景，小行星同步静止轨道航天器存在三类可能的姿态稳定区域。该工作已于 2014 年发表于《Astrophysics andSpace Science》。

从绕非主轴旋转的单轴模型在轨旋转运动的微分方程出发，结合轨道性质，将方程分解为可探测的初级函数形式，得到本体极迹频率和进动频率的演化规律表达式，随后建立模型目标在轨道上旋转运动的漫反射光变的数值模拟，对得到的表达式进行数值验证. 结果表明，两者间的误差小于 1%. 利用理论表达式和数值结果，可以反解出刚体任意时刻动量矩方向和其对称主轴所在的进动锥面；只要提供某一时刻对称主轴的指向作为初值，即可得到刚体任意时刻的姿态。该工作已投稿《Celestial Mechanics and Dynamical Astronomy》。

研究了高层大气密度模型的动态改正方法。选择了几十颗在轨运行的大椭圆低轨卫星，建立了建模星座，通过对其一段时间内 TLE 数据的处理，并融合星载高精度大气探测资料，实现了对大气模型参数的动态测定，建立了短期适用的大气模型，并将其应用在多颗重要低轨卫星的定轨和预报中，提高了预报精度。

卫星精密定轨及应用研究

CCD 相机研制实验室

本年度主要开展了如下工作：初步完成修购专项-天文光学成像探测器研发平台；完成了一项 863 项目的结题验收工作，为一国防应用提供合格的 CCD 相机；参与申请的天文联合基金重点项目“天文近红外相机关键技术的研究”获得资助；参与了新一代大视场望远镜项目的总体设计工作，并完成了望远镜主焦面 CCD 系统的初步整体设计工作；将研制的多 CCD 拼接平台及多口读出的相机进行了硬件的升级和优化。

基本完成“天文光学成像探测器研发平台”的搭建。该平台针对不同种类的 CCD 芯片，例如大靶面、高帧频、高灵敏度等，均可在天文光学成像探测器研发平台上进行硬件和软件的研发测试和性能评估。

IV. 行星科学和深空探测研究部

近地天体探测和太阳系天体研究

本年度开展了太阳系小天体轨道动力学演化研究，深入调研了特洛伊小行星的形成和演化的研究现状，对其轨道演化及形成稳定区域的机制进行了分析研究，重点研究了海王星特洛伊小行星的可能形成机制；针对海王星特洛伊小行星（NTs）的轨道特点，通过数值模拟研究了行星迁移背景下 NTs 的轨道分布，同时，研究了不同原柯伊伯带群的初始轨道分布对最终俘获的 NTs 轨道分布的影响，完成论文 2 篇；在彗星研究方面，对活动的半人马怪天体 166P/2001 T4 (NEAT) 进行了测光和活动性研究；在上年度工作的基础上，依据测光资料研究了远距离彗星的活动性，发表论文 1 篇；开展系外行星大气研究，利用透射光谱研究了热木星的大气成分，使用 GROND 成像设备搜寻了 4 颗热木星的白昼大气热发射信号，并研究了热木星 WASP-43b 的大气化学组成及其丰度，发表论文 3 篇。顺利完成国家自然科学基金重点项目的结题工作。

主要成果和进展包括：

1）远距离彗星的活动性和活动机制研究。对远距离彗星 228P/LINEAR，C/2006 S3 (LONEOS)和 29P/Schwassmann-Wachmann 1 进行观测和测光研究，得出了这些彗星的彗核半径上限、表面亮度轮廓、彗发颜色以及 Afρ 值和尘埃生成率等物理参数，并利用一些图像处理方法研究彗发中可能存在的结构特征，最后对这些彗星在大的日心距保持活动性的原因进行了分析。结果显示(1)彗星 228P/LINEAR，C/2006 S3 (LONEOS) 和 29P/Schwassmann-Wachmann 1 在日心距大于 3 AU 处都具有明显的活动性，2)彗星的表面亮度轮廓梯度差异明显，对彗星 29P/Schwassmann-Wachmann 1 ，内部区域亮度轮廓

较陡,这可用彗核附近存在一个"加速度区"来解释,在这个区域内,从彗核抛出的尘埃颗粒被加速到终极速度,外部区域与其他彗星相同,是由于彗核源区的活动性变化引起的。

2)利用透射光谱研究热木星的大气成分。首次探测发现 HAT-P-1b 的昼夜交界大气中的钾原子共振双线吸收,其吸收轮廓拥有很窄的线心、缺乏压力致宽的线翼,说明可能存在云霾、或者钾原子丰度相对较低。通过对大范围大气透射光谱的诊断,大气中存在气态 TiO 和 VO 分子的可能性被排除、瑞利散射云霾存在的可能性也被排除。结合哈勃望远镜在 1.1-1.7 微米的光谱观测,HAT-P-1b 的大气可以由含有钠、钾、水和甲烷的近太阳化学组成的模型来解释。同时,研究结果表明,哈勃望远镜在光学波段的光谱观测中所发现的无法解释的未知光谱吸收特征并不存在,很可能并非起源于大气本身。研究了 HAT-P-32 的空间未分辨的 M 型伴星对光谱数据的稀释效应,在排除污染后,发现 HAT-P-32b 的大气可以有两种模型解释:高层大气中存在光厚云,从而遮盖了光谱特征;或者,大气由含有 TiO 和 VO 的太阳化学成分组成。如果无视光谱最蓝端的测量,后者数据与模型符合极好,很可能是该行星大气存在 TiO 和 VO 的观测证据,这两种分子对于热木星大气温度结构中逆温层的研究有着重要的意义。

历算和天文参考系研究

参与院学部基本天文学及其应用发展战略研究报告的修改完善工作,完成了其中有关历书天文学部分的章节。在保质保量地完成了天文历书常规编算工作的同时,与海军出版社合作完成了军标项目"航海天文历编制规范"的征求意见稿,完成了国家标准"农历的编算和颁行"草案的修改完善和有关项目的申报工作,该项目已正式立项。

在基础研究方面取得的主要进展和成果有:在太阳系主要天体基本历表研究方面,完成了行星月球历表分析表达模块和拟合模块的研制及验证工作,同时继续开展了自主观测研究工作。在双星和多星系统运动学和动力学研究方面,发表了 4 篇分别有关于分光双星的光心轨道、含蓝离散星的双星轨道和物理特征、恒星经验质光关系、以及三星稳定性统计研究方面的 ISTP 会议论文。在等级三星系统运动学模型精化和拟合方面取得实质性进展。发表了 5 篇引力理论检验方面的学术论文,以及 1 篇天体力学数学基础方面的论文。

太阳和太阳系等离子体研究

在 2014 年度,我们在太阳射电和动力学阿尔文波两个方面取得重要进展。在太阳射电爆发现象中,有两种类型最为重要——II 型射电暴和 III 型射电暴,这两种射电爆发被认为分别与太阳爆发活动产生的激波和高能电子束流相关。然而,激波和高能电子束流如何产生 II 型和 III 型射电暴,却是亟待解决的两个科学问题。在对太阳 II 型射电暴的研究中,我们提出了一个日冕激波产生射电辐射的物理模型。该模型主要针对近似垂直激波,认为辐射源区位于激波波前背景磁场与激波面相切的附近区域,即离子和电子 foreshock 边界的重合区。其中,激波加速产生的离子束流通过束流不稳定性激发阿尔文波,并进而通过波压作用形成沿束流方向的密度掏空导管。而激波加速产生的电子束流进入此导管并激发电子回旋脉泽辐射,因此激发并捕获在导管内的同频率基波和谐波将在相同的高度逃脱。该模型首次自然地解释了太阳 II 型爆发观测中出现的同频率辐射源区重合现象。在对太阳 III 型射电暴的研究中,有学者曾建议电子回旋脉泽辐射机制对应 III 型暴的产生。然而,有两个困难一直制约着电子回旋脉泽辐射机制的适用性。一个是电子回旋频率难以大于等离子体频率,另一个是单纯的电子束流无法提供激发电子回旋脉泽辐射的垂直自由能。基于这一现状,我们考虑到电子束流自身会激发阿尔文波这一效应,进而提出了一种新的自洽的电子回旋脉泽辐射模型。该模型成功克服了以上两个困难,进而使得电子回旋脉泽辐射有效发生。

另一方面,我们在阿尔文波的线性特性研究上取得重要成果。(1)基于双流体模型,在理论上给出了一般等离子体环境下的斜阿尔文波色散关系和偏振的完整解析表达式,并且详细比较了阿尔文波和慢波的特性区别。发现阿尔文波可以从低频(频率远小于离子回旋频率)延伸到电子回旋频率,而慢波频率一直低于离子回旋频率。发现在高 beta 等离子体中斜阿尔文波和慢波具有反相位的磁压-热压关系、以及总压强扰动近似为零。我们给出高 beta 等离子体中动力学尺度的阿尔文波和慢波具有以下不同特性:阿尔文波为右旋偏振,慢波为左旋偏振;阿尔文波磁螺度为 1,慢波磁螺度为-1;阿尔文波的 Alfven ratio 远小于 1,

慢波 Alfven ratio 远大于 1。以上特性可以用来判断太阳风中 PBS 结构中的波的模式。(2)对动力学阿尔文波的双流体和回旋动力论两种描述结果进行比较，发现在特定的离子-电子温度比情况下 ,两种模型不仅在长波区（远大于离子回旋半径）保持一致，而且在接近或远小于离子回旋半径（仍远大于电子回旋半径）的短波区也能保持一致。对以前认为流体模型不能描述小于离子回旋尺度动力学阿尔文波特征的观点形成有益的补充，对太阳和空间等离子体中动力学阿尔文波的数值模拟也具有重要意义。

在动力学阿尔文波激发的研究上取得重要成果。（1）基于磁场 - 等离子体相互作用的基本理论，探讨了太阳大气和地球磁层中等离子体场向电流的形成机制，发现电子束流或离子束流所产生的等离子体电流可以有效地激发动力学阿尔文波，并且详细地分析了不同微观驱动源下的动力学阿尔文波不稳定生长模式。由于动力学阿尔波在粒子能化上的重要作用，我们的研究结果为太阳大气和地球磁层诸多活动现象中的能量输运、积累和释放的微观物理机制的研究上提供了一个值得探索的方向。(2)提出太阳风中磁流体尺度阿尔文波直接激发动力学尺度阿尔文波和慢波的非线性机制，分析了反向激发（激发向前传播的慢波和向后传播的阿尔文波）和同向激发（激发的阿尔文波和慢波都向前传播）的两种激发渠道，发现波能通过这两种渠道都可以从大尺度直接传输到小尺度。这种非局域激发机制引起的谱传输可在太阳风中动力学尺度阿尔文波湍流的形成中起重要作用。

此外，我们在太阳风中阿尔文波观测和大尺度相关结构激发等问题研究上取得重要结果。(1)提出分析太阳风中阿尔文扰动的新方法，该方法不依赖于传统的 de Hoffmann−Teller 坐标系。对稳定的太阳风而言，新方法和以前的分析方法都能得到一致结果，但对具有一些结构（如多个小束流）的太阳风而言，新方法能更好地预期其中的阿尔文扰动。该方法对更好地理解太阳风中阿尔文扰动和湍流具有重要意义。(2) 提出非均匀等离子体条件下漂移阿尔文波可自组织激发一种大尺度涡旋结构，其中波能可以从小尺度输运到大尺度。发现不同传播方向的漂移阿尔文波可激发不同的结构（Zonal flow 和 Streamer），而且离子抗磁和电子抗磁模式都可以有效激发 Zonal flow 和 Streamer。该结果指出了一种多尺度扰动的关联现象。

天体化学和行星科学实验室

本年度重点开展的科研工作有如下几个方面 :(1) 原始球粒陨石中贵金属颗粒的成因研究 ;(2) 我国新疆陨石富集区的确定和申报 ;(3) 国内新发现的 18 块普通球粒陨石的矿物岩石学研究 ;(4) 月球陨石中磷灰石的挥发组分研究 ;(5) 碳质球粒陨石中富铝球粒的氧同位素和成因研究 ;(6)HED 陨石中磷灰石的矿物岩石学研究 ;(7) 铁陨石的矿物学研究等。

本年度的科研工作进展主要有以下几方面：

（1）选取 CV3 群碳质球粒陨石 NWA 2140，对其中的难熔包体内的贵金属颗粒进行岩石学观察和化学成分测定。根据成分分析结果推测该包体经历的热力学过程，辨识出两类贵金属合金颗粒，这两类贵金属分别为早期冷凝产物和原生金属的后期蚀变产物。

（2）成功申报我国新发现的 4 个陨石富集区：Xingdi, Argan, Loulan Yizhi 和 Lop Nur。它们位于新疆塔克拉玛干沙漠以东的罗布泊地区. 新富集区的地质、地形条件非常有利于陨石的野外搜寻工作。发现并确认 13 块平衡型普通球粒陨石。与南极陨石相比, 在国内沙漠富集区回收陨石具有诸多优势. 新富集区的确立为国内沙漠陨石的回收工作提供了理论依据和前提保障, 我国的沙漠陨石回收工作亟待进行.

（3）对十多块钙长辉长无球粒陨石进行了岩石学普查，在其中发现了十多颗磷灰石颗粒。磷灰石颗粒是测定陨石年龄的目标矿物之一，也是研究 H\Cl\F 等挥发组分的合适对象，目前的工作成果为后续离子探针分析工作的开展奠定了基础。

盱眙天文观测站

盱眙天文观测站 2014 年上半年通过继续开展太阳系天体巡天观测，共计获得 43863 个太阳系小天体的 202062 个观测数据，在全球 422 个台站中观测量据第八，在观测量最多的十个大站中精度最高。观测整理得到超过 5000 条小行星的光变曲线，得到 1000 余个小行星 gri 多色测光数据，开展了相应的小行星分类研究和光变数据库的建立。为后续开展近地天体监测预警中心的建设，开展小行星地面观测研究和小行星深空探测的地基观测，开展大样本太阳系天体物理性质的观测研究，提供了有力的支撑。下半年主要

开展了 10K 和 4K 两个 CCD 相机维修过程中的测试和讨论。

开展国内外的合作研究：开展了北天窄波段巡天观测的试观测、完成了 40cm 双筒望远镜观测资料文档的电子化和底片库改造等合作项目。与澳科大进行了利用 Cellinoid 模型进行小行星形状反演研究，已发表论文 1 篇。参与北京大学开展反银心数据的分析研究，开展了反银心数据的天体测量定标、三维消光分析、银晕密度特征等的研究，并参与发表了 3 篇论文。参与了 Vesta 族小行星的测光观测，参与发表论文 1 篇。

推进项目进展：根据台内发展要求，参与了中等口径大视场望远镜的项目研究论证。全程参与了大视场望远镜的光学和机械设计的讨论。开展了我国近地天体监测预警中心的规划。代表我国参加了联合国外空委 SMPAG 会议，向相关部门提供了建议。

盱眙站成为多用途观测站的建设，2014 年度完成了转发式卫星导航试验系统测定轨副站场地的建设任务，同时完成了测定轨分系统试验任务，掌握了相关天线及信道设备的操作、维护、观测等流程。配合主站完成观测站设备的子系统级、分系统级联调测试。另外配合中科院大气物理研究所在盱眙站安放了高层闪电监视仪开展雷暴云上方的中高层大气放电的观测研究。

行星科学与深空探测实验室（筹）

本年度主要围绕小行星深空探测和系外行星等开展研究工作。

主要成果与进展如下：

1）小行星深空探测方面：

（1）“利用嫦娥二号数据对图塔蒂斯小行星研究取得重要成果” 获得 2013 年度“十大天文科技进展”

利用嫦娥二号探测器对 4179 号小行星图塔蒂斯飞越探测获取的光学图像，我们研究了该小行星的物理特性、表面特征、内部结构以及可能的起源等。从嫦娥二号获取的高分辨率图像中，我们发现图塔蒂斯拥有不规则形状和不平坦表面，其形似一根生姜，由较小的一端“头部”（head）与较大的一端“身体”（body）组成。通过分析获得了图塔蒂斯表面的一些新特征（图 1）：在“身体”端部存在一个直径大约 800 米的巨型盆地，在小行星的表面找到了超过 50 处较为明显的、大小不一的陨石坑，其中包括两个先后产生在同一位置附近相互有部分遮盖的陨坑；“颈部”则以近乎垂直角度连接着“头部”和“身体”；其表面存在超过 30 个有巨石特征的区域；通过图像甚至可分辨出尺寸较小的线状结构等特征（图 2）。从这些特征可推断图塔蒂斯很可能是一颗具有碎石堆结构的密近双小行星，可能由两个独立小天体缓慢靠近形成或是约普(YORP)效应作用的结果，抑或是大规模的撞击造成。这些研究对认识太阳系中小行星的形成与演化与近地天体的空间防护具有重要科学价值。

该研究成果在线发表在 Nature 出版集团旗下期刊《Scientific Reports》(《科学报告》) 上，这是探月工程（二期）的重要成果，也是我国在此首次行星际探测活动中，多目标新模式探测、小行星新领域开拓的成功尝试，工程实践与科学研究相融合的成功范例，获得国际同行的关注和好评。Nature 英文网站作为首页头条推介此文，《Nature》中文版推荐为研究亮点，全球多个知名媒体也进行了报道。该项成果获得 2013 年度“十大天文科技进展”。

（2）完成小行星一体化采样装置研制与验收。作为小行星深空探测任务的关键载荷“有机组分分析仪”的重要组成部分，小行星一体化采样装置研制成功并通过验收。该装置在研制过程中进行了多项关键技术攻关，具有以下技术创新点：弱引力下的高硬度钻取技术；采样、转移、密封、加热等功能装置一体化设计集成技术；高温密封加热技术和空间环境适应性技术。新技术的攻关使得该装置无论在体积、重量、功耗和性能上均达到设计要求。

（3）研究双小行星 1996 FG3 的表面物理性质。通过 ATPM 对三组中红外观测数据的拟合，我们较准确地估算了近地小行星 1996 FG3 的平均热惯量、反照率、有效直径、粗糙度等物理性质，得到 1996 FG3 的有效直径、几何反照率、表面平均热惯量、粗糙度等参数；1996 FG 主星表面可能覆盖着一层颗粒很小的松散物质（风化层），其平均厚度大约为 5-20 mm (Yu, Ji & Wang,MNRAS,2014)。

（4）统计分析图塔蒂斯小行星表面碎石分布揭示其形成演化。我们根据嫦娥二号飞越探测图塔蒂斯小行星数据，对其正面的碎石进行了统计分析。

（5）基于嫦娥二号数据，研究图塔蒂斯小行星

的空间指向和自转动力学。

2）系外行星科学方面研究：

（1）揭示 Kepler 一类近共振系统的形成机制。针对三颗行星的系统，我们提出了一种可能形成这种系统构型的形成机制：首先三颗行星形成在远离中心恒星的位置处；在气体盘的作用下，三颗行星向内进行第一类轨道迁移，并在迁移过程中相互俘获进入平运动共振；在靠近中心恒星位置处，恒星的潮汐作用使行星脱离共振形成目前的近共振构型。影响这一过程的主要因素有：中心恒星的磁场强度和吸积率、第一类轨道迁移的速度以及系统中行星的质量。我们针对这四种因素进行了大量的数值计算，通过统计分析获得了形成近 3:2 和 2:1 共振的几个条件：恒星磁场对最终构型的影响比较小；恒星吸积率高易形成 2:1 共振而吸积率低则易形成 3:2 共振构型；较慢的第一类轨道迁移易于形成共振构型；行星系统中存在相等质量的行星更易形成共振构型。该机制提供了一种解释近 3:2 和 2:1 共振构型形成的机制（Wang & Ji, ApJ, 2014）。

（2）揭示 Kepler 空间望远镜所探测的候选体在半径分布中存在大气逃逸特征。在已发现的系外行星中，大多数离中央恒星非常近，其轨道半长径甚至小于 0.01 AU （公转周期小于 1 天），这些行星有可能经历了与太阳系内的行星迥然不同的形成与演化过程。在如此之近的距离内，行星很可能接受到来自年轻恒星的强烈 X-Ray 和 EUV 辐射。恒星辐射不仅会在行星大气上层产生一个比较厚的辐射区域，还可驱动流体动力学机制下的逃逸气流。在这项研究中，我们将行星大气逃逸、行星形成的核吸积模型与行星的热演化结合起来，模拟了整个行星族群从星子诞生到最终阶段的整个演化过程，并着重分析了大气逃逸对行星族群整体分布的影响，探讨了所产生的大气逃逸特征与大气模型相关的物理参数的关系。研究人员发现由于行星大气逃逸的存在，导致位于两个地球半径附近的行星数目明显减少，即形成所谓的“大气逃逸谷”。通过与计算结果的比较，我们还发现 Kepler 候选体的半径分布特征可用大气逃逸来解释，排除了不含大气逃逸的模型及加热效率为 100%的大气逃逸模型 (Jin et al., ApJ, 2014)。该项研究成果入选 2014 年中科院战略先导项目（B 类）研究亮点工作。

3）其他方面科研工作：

（1）月球空间数据分析研究。通过对 Artemis 卫星观测数据的分析，计算了月球邻近空间的磁场湍流。观测结果表明太阳风受到阻碍作用，在月球邻边诱发了等离子体动力学不稳定性，使动力学尺度湍流强度显著增强。

（2）嫦娥三号—VNIS 的谱像存在一定的相对移位，利用相关性分析，可以对谱像的局域移位进行修正。这些方法可以用于对 VNIS 数据的预处理，并有效提升相关分析的数据可靠性。

（3）普通球粒陨石中富铝球粒的氧同位素研究。富铝球粒（ARC）在岩矿学和同位素组成等方面兼具富钙富铝难熔包体（CAI）和镁铁质球粒的特征，可以揭示其成因及时空关系因而成为天体化学重要的研究对象之一。我们研究了三个普通球粒陨石中发现的七个富铝球粒。与前人研究结果相比，更缓的斜率及更贫 16O 的成分进一步表明普通球粒陨石中的富铝球粒不是 CAI 与镁铁质球粒简单混合形成的。相反，他们很有可能在多次熔融过程中与贫 16O 的星云气体储库经历了更高程度的氧同位素交换（蒋云等，中国科学，2014）。

（4）适用于大偏心率轨道的半分析解研究。在考虑 J22 非球形摄动影响下，给出了大偏心率轨道的一阶短周期半分析解。椭率项（J22 项）摄动对许多大天体和小天体的环绕轨道有重要影响，对于形状不规则的小行星来说其影响尤甚。而对于快自转天体来说，其大偏心率轨道卫星的分析解很难建立，若用传统的偏心率级数展开法将无法避免地遇到拉普拉斯极限问题。为了解决此问题，我们的工作采用了傅里叶级数展开方法，将最终结果表示为一个紧凑的半分析形式，既可保留了分析解的优点，又完全避开了拉普拉斯极限问题。从数值模拟的结果来看，该半分析解完全适用于 e<1 的情形（Hu et al., RAA, 2014）。

（5）与美国 Los Alamos 国家实验室建立了合作研究关系，开展原行星盘流体数值模拟方面的合作研究。这项工作将针对原行星盘开展流体数值模拟研究，并在原行星盘的观测领域与 ALMA 团队开展合作。

三、 学术交流与合作

1、国际合作与交流概况

全年出访申请 127 人次（71 团组，72 人，其中有 5 人次赴中国台湾地区访问），完成出访任务 114

人次（其中中国台湾地区 5 人次），涉及 21 个国家/地区，出访形式主要包括所级协议合作研究（62 人次）和国际会议（52 人次）等，出访国家/地区以美国（30 人次）、瑞士（23 人次）、俄罗斯（12 人次）、日本（12 人次）等为主。出访活动中，国际会议大会报告、分会报告或墙报等 46 人次。全年来访 147 人次（90 团，142 人），涉及 31 个国家/地区，主要为参加在华举办国际学术会议、合作研究等。与其他国家/地区人员合作发表论文 72 篇。

2014 年，紫台执行与国外研究机构和大学签订国际合作协议 13 项，其中新增 1 项。人才培养方面，执行中欧联合培养博士研究生 11 人，其中 2014 年新增 2 人。国际合作（人才）项目方面，执行“爱因斯坦讲席教授”1 项、“外国专家特聘研究员计划”1 项，“发展中国家访问学者计划”1 项，新立项国际合作重点项目 1 项。主办/承办的国际会议共 3 场，分别是“从暗物质晕到星系形成国际会议（第十届中德星系宇宙学会议）”、“第 3 届南极巡天望远镜国际合作会议暨 973 项目会议”和“探索太阳爆发的起源——先进天基太阳天文台国际论坛”。

2014 年，紫台完成了“一三五”国际专家诊断评估。来自美国、日本、德国、英国、意大利、瑞士和中国台湾等研究机构的 9 位国际知名天文学家对紫金山天文台“一三五”规划及实施情况进行了为期 3 天的诊断评估。

2、 重要国际合作项目进展

1）暗物质粒子探测合作研究

紫台主导的 A 类先导专项项目“暗物质粒子探测卫星（DAMPE）”探测器系统已经完成了工程样机的研制。为了测试探测器的性能，项目组赴瑞士欧洲核子中心（CERN）进行束流试验（编号 RE29 DAMPE）。欧洲核子中心向暗物质粒子探测器提供以下束流：PS-T9 的低能粒子、SPS-T2-H4 的高能电子/质子、SPS-T4-H8 重离子，以测试“暗物质粒子探测卫星（DAMPE）”探测器的性能。整个束流试验期间，完成了：电子的能量扫描（0.5GeV-250GeV）、能量分辨、能量泄露测试、触发效率测试；利用强子（Pion，Proton）完成能量扫描，探测器标定等；光子的测试（0-20GeV）等。测试结果显示，DAMPE 工作正常，电性能、探测器性能稳定，DAMPE 对电子、光子等的响应和预期相符。

作为暗物质粒子探测器的一个部分，硅阵列探测器的封装工作由意大利佩鲁贾大学完成。2014 年，紫台 A 类先导专项项目“暗物质粒子探测卫星（DAMPE）”工作人员考察硅阵列探测器的封装现场，并和佩鲁贾大学的工作人员讨论整个硅探测器的测试过程。

2）南极天文合作研究及中澳天文联合研究中心成立

在国家科技部资助的 973 项目“利用南极巡天望远镜在超新星宇宙学及太阳系外行星方面的前沿研究”支持下，由紫台主办的“第 3 届南极巡天望远镜国际合作会议暨 973 项目会议”于 2014 年 6 月在南京顺利举行。来自国内以及澳大利亚、法国、美国、英国的 80 多位专家学者参加了此次会议，并对以下内容展开了广泛的交流与深入的讨论：1) 南极巡天望远镜： a) 漠河测试，b) 2014/2015 南极科考计划，c) 第 3 台南极巡天望远镜进红外科学与进展，d) 南极巡天望远镜和澳大利亚 ASKAP 射电望远镜暂现源巡天；2) KDUST 南极昆仑暗宇宙巡天望远镜：a)工程及科学进展报告，b)国际合作进展报告；3) 未来的机遇及合作：欧盟 2020 展望，zETA 南极红移 20（z Equals 20 from Antarctica）。

根据中国科学院与澳大利亚工业、创新、科研和高等教育部签署的天文学合作谅解备忘录，“中澳天文联合研究中心”（简称中澳天文中心；英文名称为 Australia-ChinA ConsortiuM for Astrophysical Research，缩写为 ACAMAR）于 2014 年 12 月成立。中澳天文中心（中方）挂靠在紫金山天文台，紫台王力帆研究员任中方主任，杨戟研究员为科学家小组成员；中澳天文中心（澳方）依托澳大利亚国立大学，由澳大利亚国立大学教授，诺贝尔物理学奖获得者 Brain Schmidt 为澳方主任。该中心的成立将推进中澳在天文学领域深入和广泛的合作，领域包括射电、光学、红外以及南极天文学研究和相关设备研制、设施运行，基于射电平方公里阵（SKA）的组织成员和项目建设准备及随后各期出资方地位，以及双方在天文学领域具体合作与相关协议的协商与商判等。

3）太赫兹天文探测技术合作研究

基于紫台与日本理化学研究所（RIKEN）的合作协议，双方展开了关于太赫兹超导动态电感探测器（MKIDs）的合作研究，有利于推动紫金山天文台正

在承担的国家重大仪器设备研制专项“超导成像频谱仪”的顺利进行。基于紫台与法国巴黎天文台 LERMA 研究小组的合作协议，双方主要进行了 1.4 THz 频段超导热电子混频器混频特性的合作研究。基于紫台与“台湾中研院天文及天文物理研究所（ASIAA）”的长期合作基础，双方合作开展太赫兹超导探测器的制备工作，积累了太赫兹超导探测器制备工作的经验。

在开展合作研究的同时，积极参加“第 25 届空间太赫兹技术国际研讨会”（俄罗斯）、“第三届中美射电会议”（美国）、“应用超导电子学国际会议”（美国）、“第十五届东亚地区亚毫米波接收机技术研讨会”（日本），对紫台及我国目前在该领域中取得的成绩和进展进行了介绍，并同与会的其他国家的专家一起就目前空间太赫兹技术的发展进行了详尽讨论。

4）代表国家相关部门开展空间碎片等国际交流与合作

紫金山天文台代表以国家航天局的名义参加了 2014 年 6 月在奥地利维也纳举办的联合国外空委科技小组委员会第 51 届会议，与各国代表围绕第二次空间任务计划咨询组（SMPAG）的职责范围（ToR）、拟开展的关于行星防御的空间计划活动以及 SMPAG 的后续工作安排行了讨论交流。

紫金山天文台代表以国家航天局的名义参加了 2014 年 5 月在北京举办的机构间空间碎片协调委员会第 32 界会议第一工作组会议，与各国代表围绕过去一年空间碎片探测方法、探测技术、探测设备的进展及探测结果进行交流讨论，并讨论过去一年的联合测量结果以及未来联合测量工作开展的相关细节。

5）银河系结构和分子云与恒星形成系列合作研究

继续与德国马普射电天文所（MPIfR）和美国哈佛史密松天体物理中心（CfA）等联合开展大型国际合作计划——银河系棒和旋臂结构巡天（BeSSeL），与 BeSSeL 项目组成员交流讨论数据处理的结果及其中存在的问题，选择合适的观测目标源，并安排了下一年度的观测计划。

与美国哈佛-史密松天体物理中心、加州理工学院、约翰霍普金斯大学合作开展恒星形成物理过程的高分辨研究、Herschel、ALMA 项目的观测与合作研究。

6）太阳物理合作研究

2014 年，积极参加中欧联合空间科学卫星任务研讨，共同提出 ESA-CAS 联合空间科学卫星 SEEPE 提案。参加第 13 届 RHESSI 学术会议（瑞士），全面展示了紫台在太阳高能物理方面的研究进展，了解国际上学科的最新动向。参加第 40 届 COSPAR 大会（俄罗斯），与莫斯科大学和国家核研究大学同行讨论，在太阳伽马射线方面达成进一步合作意向。

执行基金委中俄合作项目，年内邀请俄罗斯科学院空间科学研究所等 2 人次来访，并 3 人次回访，针对太阳耀斑能量及高能多波段辐射开展合作研究。

7）星系形成合作研究

2014 年，紫金山天文台中德马普伙伴小组顺利通过中期国际评审。2014 年 5 月，第十届中德星系宇宙学国际会议“从暗物质到星系”在西安顺利召开，该会议由中国科学院紫金山天文台和德国马普天文所联合成立的中德马普伙伴小组主办。与会的学者就星系宇宙学领域的最新进展进行了热烈讨论，涵盖的主题有：星系中央黑洞和活动星系核、银河系和近邻星系群、引力透镜、星系形成、宇宙学。

ABSTRACT LIST OF PUBLICATIONS IN 2014

I. Dark Matter & Space Astronomy

Cosmology, Dark Matter and High-Energy Astrophysics

第 1 条，共 222 条

Problems Related To Gauge Invariance And Momentum, Spin Decomposition In Nucleon Structure Study

Wang, F (Wang, Fan); Sun, WM (Sun, W. M.); Chen, XS (Chen, X. S.); Zhang, PM (Zhang, P. M.)
PHYSICS OF PARTICLES AND NUCLEI

卷: 45 期: 4 页: 808-816

How do the quark and gluon share the nucleon momentum? How does the nucleon spin distribute among its constituents? What means the quark and gluon momentum, spin and orbital angular momentum? These problems are analyzed and a solution is proposed based on gauge invariance principle, canonical quantization rule and Poincar, covariance.

第 2 条，共 222 条

Shock Wave Evolution And Discontinuity Propagation For Relativistic Superfluid Hydrodynamics With Spontaneous Symmetry Breaking

Zhang, S (Zhang, Sun)
PHYSICS LETTERS B

卷: 729 页: 136-142

In this Letter, we have studied the shock wave and discontinuity propagation for relativistic superfluid with spontaneous U(1) symmetry breaking in the framework of hydrodynamics. General features of shock waves are provided, the propagation of discontinuity and the sound modes of shock waves are also presented. The first sound and the second sound are identified as the propagation of discontinuity, and the results are in agreement with earlier theoretical studies. Moreover, a differential equation, called the growth equation, is obtained to describe the decay and growth of the discontinuity propagating along its normal trajectory. The solution is' in an integral form and special cases of diverging waves are also discussed.

第 3 条，共 222 条

Constraints On Dark Energy From New Observations Including Pan-STARRS

Zhang, W (Zhang, Wei); Li, SY (Li, Si-Yu); Li, H (Li, Hong); Xia, JQ (Xia, Jun-Qing); Li, MZ (Li, Mingzhe); Lu, T (Lu, Tan)
JOURNAL OF COSMOLOGY AND ASTROPARTICLE PHYSICS

期: 8 文献号: 030

In this paper, we set the new limits on the equation of state parameter (EoS) of dark energy with the observations of cosmic microwave background radiation (CMB) from Planck satellite, the type Ia supernovae from Pan-STARRS and the baryon acoustic oscillation (BAO). We consider two parametrization forms of EoS: a constant w and time evolving w(a) = w(0) + w(a)(1 - a). The results show that with a constant EoS, w = -1.141 +/- 0.075 (68% C.L.), which is consistent with ACDM at about 2 sigma confidence level. For a time evolving w(a) model, we get w(0) = -1.09(-0.18)(+0.16) (l sigma C.L.), w(a) = -0.34(-0.51)(+0.87) (l sigma C.L.), and in this case ACDM can be comparable with our observational data at l sigma confidence level. In order to do the parametrization independent analysis, additionally we adopt the so called principal component analysis (PCA) method, in which we divide redshift range into several bins and assume w as a constant in each redshift bin (bin-w). In such bin-w scenario, we find that for most of the bins cosmological constant can be comparable with the data, however, there exists few bins which give w deviating from ACDM at more than 2 sigma confidence level, which shows a weak hint for the time evolving behavior of dark energy. To further confirm this hint, we need more data with higher

precision.

第 4 条，共 222 条

Constraints On Ultracompact Minihalos Using Neutrino Signals From Gravitino Dark Matter Decay

Zheng, YL (Zheng, Yun-Long); *Yang, YP* (Yang, Yu-Peng); Li, MZ (Li, Ming-Zhe); Zong, HS (Zong, Hong-Shi)
RESEARCH IN ASTRONOMY AND ASTROPHYSICS
卷: 14 期: 10 页: 1215-1220

Ultracompact dark matter minihalos (UCMHs) would be formed during the early universe if there were large density perturbations. If dark matter can decay into particles described by the standard model, such as neutrinos, these objects would become potential astrophysical sources of emission which could be detected by instruments such as IceCube. In this paper, we investigate neutrino signals from nearby UCMHs due to gravitino dark matter decay and compare these signals with the background neutrino flux which is mainly from the atmosphere to obtain constraints on the abundance of UCMHs.

第 5 条，共 222 条

Discontinuity Evolution And Sonic Propagation For Superfluidity Hydrodynamics With Small Superfluid Entropy

Zhang, S (Zhang Sun); Dong, YQ (Dong Yi-Qiao)
COMMUNICATIONS IN THEORETICAL PHYSICS
卷: 62 期: 5 页: 729-736

In this paper, we have studied discontinuity evolution and sonic propagation for the two-fluid model with small superfluid entropy in the framework of hydrodynamics. General features of the transverse mode and the longitudinal mode are provided. The fourth sound and the sixth sound are identified as the propagation of discontinuity, in agreement with earlier theoretical studies. Moreover, the growth equation is obtained to describe the decay and growth of the discontinuity propagating along its normal trajectory. The solution is in an integral form and various cases are discussed. Important discriminations between the case of fourth sound and that of sixth sound are also presented, which may be meaningful for future's experiments to identify the sixth sound and the small superfluid entropy.

Gamma-Ray Burst, Neutron Star and relevant physics

第 6 条，共 222 条

Spectral Softening In The X-Ray Afterglow Of Grb 130925a As Predicted By The Dust Scattering Model

Zhao, YN (Zhao, Yi-Nan); *Shao, L* (Shao, Lang)
ASTROPHYSICAL JOURNAL
卷: 789 期: 1 文献号: 74

Gamma-ray bursts (GRBs) usually occur in a dense star-forming region with a massive circumburst medium. The small-angle scattering of intense prompt X-ray emission off the surrounding dust grains will have observable consequences and sometimes can dominate the X-ray afterglow. In most of the previous studies, only the Rayleigh-Gans (RG) approximation is employed for describing the scattering process, which works accurately for the typical size of grains (with radius of a <= 0.1 mu m) in the diffuse interstellar medium. When the size of the grains may significantly increase, as in a more dense region where GRBs would occur, the RG approximation may not be valid enough for modeling detailed observational data. In order to study the temporal and spectral properties of the scattered X-ray emission more accurately with potentially larger dust grains, we provide a practical approach using the series expansions of anomalous diffraction (AD) approximation based on the complicated Mie theory. We apply our calculations to understand the puzzling X-ray afterglow of recently observed GRB 130925A that showed a significant spectral softening. We find that the X-ray scattering scenarios with either AD or RG approximation adopted could well reproduce both the temporal and spectral profile simultaneously. Given the plateau present in the early X-ray light curve, a typical distribution of smaller grains as in the interstellar medium would be suggested for GRB 130925A.

第 7 条，共 222 条

Quasi-Periodic Variations In X-Ray Emission And Long-Term Radio Observations: Evidence For A Two-Component Jet In Sw J1644+57

Wang, JZ (Wang, Jiu-Zhou); *Lei, WH* (Lei, Wei-Hua); Wang, DX (Wang, Ding-Xiong); Zou, YC (Zou,

Yuan-Chuan); Zhang, B (Zhang, Bing); Gao, H (Gao, He); Huang, CY (Huang, Chang-Yin)
ASTROPHYSICAL JOURNAL
卷: 788 期: 1 文献号: 32

The continued observations of Sw J1644+57 in X-ray and radio bands accumulated a rich data set to study the relativistic jet launched in this tidal disruption event. The X-ray light curve of Sw J1644+57 from 5-30 days presents two kinds of quasi=periodic variations: a 200 s quasi=periodic oscillation (QPO) and a 2.7 day quasi=periodic variation. The latter has been interpreted by a precessing jet launched near the Bardeen-Petterson radius of a warped disk. Here we suggest that the similar to 200 s QPO could be associated with a second, narrower jet sweeping the observer line-of-sight periodically, which is launched from a spinning black hole in the misaligned direction with respect to the black hole's angular momentum. In addition, we show that this two-component jet model can interpret the radio light curve of the event, especially the re-brightening feature starting similar to 100 days after the trigger. From the data we infer that inner jet may have a Lorentz factor of Gamma(j) similar to 5.5 and a kinetic energy of E-k,E-iso similar to 3.0 x 10(52) erg, while the outer jet may have a Lorentz factor of Gamma(j) similar to 2.5 and a kinetic energy of E-k,E-iso similar to 3.0 x 10(53) erg.

第 8 条 , 共 222 条

The Redshift Dependence Of Long Gamma-Ray Burst Intrinsic Properties

Zhang, FW (Zhang, Fu-Wen); Shao, L (Shao, Lang); Fan, YZ (Fan, Yi-Zhong); Wei, DM (Wei, Da-Ming)
ASTROPHYSICS AND SPACE SCIENCE
卷: 350 期: 2 页: 691-699

We performed a statistical analysis of the intrinsic properties and their redshift dependence of long gamma-ray bursts (GRBs) mainly detected by Swift satellite. The intrinsic quantities are the (z- and K-corrected) rest-frame duration, T (90,rest), the rest-frame peak energy, E (p,rest), the isotropic equivalent energy, E (iso), and the peak isotropic luminosity, L (iso), of the prompt emission. We find that the distributions of T (90,rest), E (p,rest), E (iso) and L (iso) all span a wide range and their central values are T (90,rest)similar to 10 s, E (p,rest)similar to 500 keV, E (iso)similar to 10(53) erg and L (iso similar to)3x10(52) erg/s. We also show that E (p,rest) and L (iso) are independent with T (90,rest), but E (iso) is correlated with T (90,rest). Moreover, we find the observed peak energy is independent with redshift, but the intrinsic peak energy, the isotropic energy and the peak luminosity all show some dependence on redshift, where the truncation effect is taken into account.

第 9 条 , 共 222 条

Long-Term Optical Observations Of The Be/X-Ray Binary X Per

Li, H (Li, Hui); Yan, JZ (Yan, Jingzhi); Zhou, JN (Zhou, Jianeng); Liu, QZ (Liu, Qingzhong)
ASTRONOMICAL JOURNAL
卷: 148 期: 6 文献号: 113

We present optical spectroscopic observations of X Per from 1999 to 2013 with the 2.16 m telescope at Xinglong Station and the 2.4 m telescope at Lijiang Station, National Astronomical Observatories of China. Combining these observations with the public optical photometric data, we find certain epochs of anti-correlations between the optical brightness and the intensity of the Ha and He I 6678 lines, which may be attributed to the mass ejections from the Be star; however, alternative explanations are also possible. The variability of the Fe II 6317 line in the spectra of X Per might also be caused by the shocked waves formed after the mass ejections from the Be star. The X-ray activities of the system might also be connected with the mass ejection events from the Be star. When the ejected materials were transported from the surface of the Be star to the orbit of the neutron star, an X-ray flare could be observed in its X-ray light curves. We use the neutron star as a probe to constrain the motion of the ejected material in the circumstellar disk. With the diffusion time of the ejected material from the surface of the Be star to the orbit of neutron star, the viscosity parameter a of the circumstellar disk is estimated to be 0.39 and 0.28 for the different times, indicating that the disk around the Be star may be truncated by the neutron star at the 2:1 resonance radius and that a Type I X-ray outburst is unlikely to be observed in X Per.

第 10 条 , 共 222 条

The Type B QPO Phenomena In The Transient Black Hole Candidate GX 339-4

Gao, HQ (Gao, H. Q.); Qu, JL (Qu, J. L.); Zhang, Z (Zhang, Z.); Li, ZB (Li, Z. B.); Zhang, S (Zhang, S.); Chen, L (Chen, L.); Ge, MY (Ge, M. Y.); *Zhou, JN*

(Zhou, J. N.); Song, LM (Song, L. M.); Wang, JM (Wang, J. M.)
MONTHLY NOTICES OF THE ROYAL ASTRONOMICAL SOCIETY
卷: 438 期: 1 页: 341-351

We investigated the spectral and timing properties of the type B quasi-periodic oscillations (QPOs) showing up in the transient black hole binary GX 339-4 during its four outbursts observed by Rossi X-ray Timing Explorer (RXTE)/PCA and HEXTE in 2002, 2004, 2007 and 2010. We find that, the dependence on variability of the accretion flow turns out to be similar for the type B QPOs occurring in these four outbursts. We therefore take the results from the 2010 outburst for presentation. Our spectral results obtained from both the energy and time domains show that, the occurrence of the type B QPO is accompanied with sudden increase of hard component flux, relatively smaller inner disk radius, stable disk but variable corona. The latter may be understood in a scenario of variable input of seed photons for Comptonization in the corona. Further clues to probing the possible origination of the type B QPO come from our analysis of time lag and its energy dependence. The energy dependence of type B QPO amplitude suggests that the hard component dominate the variability and the time lag spectral analysis results suggests the type B QPO could be related to inverse Compton scattering. The time lag between hard and soft energy band is about 10 ms and found to depend on frequency. in a form of v(-0.7) for type B QPOs in the rising phase. Finally we put these results in a context of a blob mechanism at work.

High-Energy Solar Astrophysics

第 11 条 , 共 222 条

A Solar Type Ii Radio Burst From Coronal Mass Ejection-Coronal Ray Interaction: Simultaneous Radio And Extreme Ultraviolet Imaging

Chen, Y (Chen, Yao); Du, GH (Du, Guohui); *Feng, L* (Feng, Li); Feng, SW (Feng, Shiwei); Kong, XL (Kong, Xiangliang); Guo, F (Guo, Fan); Wang, B (Wang, Bing); Li, G (Li, Gang)
ASTROPHYSICAL JOURNAL
卷: 787 期: 1 文献号: 59

Simultaneous radio and extreme ultraviolet (EUV)/white-light imaging data are examined for a solar type II radio burst occurring on 2010 March 18 to deduce its source location. Using a bow-shock model, we reconstruct the three-dimensional EUV wave front (presumably the type-II-emitting shock) based on the imaging data of the two Solar TErrestrial RElations Observatory spacecraft. It is then combined with the Nancay radio imaging data to infer the three-dimensional position of the type II source. It is found that the type II source coincides with the interface between the coronal mass ejection (CME) EUV wave front and a nearby coronal ray structure, providing evidence that the type II emission is physically related to the CME-ray interaction. This result, consistent with those of previous studies, is based on simultaneous radio and EUV imaging data for the first time.

第 12 条 , 共 222 条

Temporal Evolution Of The Magnetic Topology Of The Noaa Active Region 11158

Zhao, J (Zhao, Jie); Li, H (Li, Hui); Pariat, E (Pariat, Etienne); Schmieder, B (Schmieder, Brigitte); Guo, Y (Guo, Yang); Wiegelmann, T (Wiegelmann, Thomas)
ASTROPHYSICAL JOURNAL
卷: 787 期: 1 文献号: 88

We studied the temporal evolution of the magnetic topology of the active region (AR) 11158 based on the reconstructed three-dimensional magnetic fields in the corona. The non-linear force-free field extrapolation method was applied to the 12 minute cadence data obtained with the Helioseismic and Magnetic Imager on board the Solar Dynamics Observatory during 5 days. By calculating the squashing degree factor Q in the volume, the derived quasi-separatrix layers (QSLs) show that this AR has an overall topology, resulting from a magnetic quadrupole, including a hyperbolic flux tube (HFT) configuration that is relatively stable at the timescale of the flare (similar to 1-2 hr). A strong QSL, which corresponds to some highly sheared arcades that might be related to the formation of a flux rope, is prominent just before the M6.6 and X2.2 flares, respectively. These facts indicate the close relationship between the strong QSL and the high flare productivity of AR 11158. In addition, with a close inspection of the topology, we found a small-scale HFT that has an inverse tear-drop structure above the aforementioned QSL before the X2.2 flare. It indicates the existence of magnetic flux rope at this place. Even though a

global configuration (HFT) is recognized in this AR, it turns out that the large-scale HFT only plays a secondary role during the eruption. In conclusion, we dismiss a trigger based on the breakout model and highlight the central role of the flux rope in the related eruption.

第 13 条，共 222 条

A Chain Of Winking (Oscillating) Filaments Triggered By An Invisible Extreme-Ultraviolet Wave

Shen, YD (Shen, Yuandeng); Ichimoto, K (Ichimoto, Kiyoshi); Ishii, TT (Ishii, Takako T.); Tian, ZJ (Tian, Zhanjun); Zhao, RJ (Zhao, Ruijuan); Shibata, K (Shibata, Kazunari)
ASTROPHYSICAL JOURNAL
卷: 786 期: 2 文献号: 151

Winking (oscillating) filaments have been observed for many years. However, observations of successive winking filaments in one event have not yet been reported. In this paper, we present the observations of a chain of winking filaments and a subsequent jet that are observed right after the X2.1 flare in AR11283. The event also produced an extreme-ultraviolet (EUV) wave that has two components: an upward dome-like wave (850 km s(-1)) and a lateral surface wave (554 km s(-1)) that was very weak (or invisible) in imaging observations. By analyzing the temporal and spatial relationships between the oscillating filaments and the EUV waves, we propose that all the winking filaments and the jet were triggered by the weak (or invisible) lateral surface EUV wave. The oscillation of the filaments last for two or three cycles, and their periods, Doppler velocity amplitudes, and damping times are 11-22 minutes, 6-14 km s(-1), and 25-60 minutes, respectively. We further estimate the radial component magnetic field and the maximum kinetic energy of the filaments, and they are 5-10 G and similar to 10(19) J, respectively. The estimated maximum kinetic energy is comparable to the minimum energy of ordinary EUV waves, suggesting that EUV waves can efficiently launch filament oscillations on their path. Based on our analysis results, we conclude that the EUV wave is a good agent for triggering and connecting successive but separated solar activities in the solar atmosphere, and it is also important for producing solar sympathetic eruptions.

第 14 条，共 222 条

Solar Magnetized Tornadoes: Rotational Motion In A Tornado-Like Prominence

Su, Y (Su, Yang); Gomory, P (Goemoery, Peter); Veronig, A (Veronig, Astrid); Temmer, M (Temmer, Manuela); Wang, TJ (Wang, Tongjiang); Vanninathan, K (Vanninathan, Kamalam); *Gan, WQ* (Gan, Weiqun); Li, YP (Li, YouPing)
ASTROPHYSICAL JOURNAL LETTERS
卷: 785 期: 1 文献号: L2

Su et al. proposed a new explanation for filament formation and eruption, where filament barbs are rotating magnetic structures driven by underlying vortices on the surface. Such structures have been noticed as tornado-like prominences when they appear above the limb. They may play a key role as the source of plasma and twist in filaments. However, no observations have successfully distinguished rotational motion of the magnetic structures in tornado-like prominences from other motions such as oscillation and counter-streaming plasma flows. Here we report evidence of rotational motions in a tornado-like prominence. The spectroscopic observations in two coronal lines were obtained from a specifically designed Hinode/EIS observing program. The data revealed the existence of both cold and million-degree-hot plasma in the prominence leg, supporting the so-called prominence-corona transition region. The opposite velocities at the two sides of the prominence and their persistent time evolution, together with the periodic motions evident in SDO/AIA dark structures, indicate a rotational motion of both cold and hot plasma with a speed of similar to 5 km s(-1).

第 15 条，共 222 条

On The Possible Mechanism Of The First Ground Level Enhancement In Cosmic Ray Intensity Of Solar Cycle 24

Firoz, KA (Firoz, Kazi A.); *Gan, WQ* (Gan, W. Q.); *Li, YP* (Li, Y. P.); Rodriguez-Pacheco, J (Rodriguez-Pacheco, J.)
ASTROPHYSICS AND SPACE SCIENCE
卷: 350 期: 1 页: 21-32

We have carried out this work to comprehend the possible mechanisms of the first ground level enhancement (GLE71 17 May 2012 01:50 UT) in cosmic ray intensity of the solar cycle 24. For this, the cosmic ray intensities registered by neutron monitors at several sites have been analyzed and studied with concurrent solar flares of different energy channels. To assess empirically whether

the GLE might have been caused by the energy released from solar flare or CME-driven shock, we identify the possible time line in terms of the lowest spectral index determined from proton fluxes. If the GLE is caused by the energy released from particle acceleration in solar flare, the intensive phase of the flare representing the extreme emission should exist within/around the possible time line. In this respect, it is observed that the possible time line lies within the prominent phase of CME-driven shock. For better understanding, we have checked the possible relativistic energy with respect to solar flare as well as CME-driven shock. As witnessed, if the extreme emission phase of the flare is considered as the reason for the causation of GLE peak, the flare components procured insufficient amount of energy (a parts per thousand currency signa1/40.085 GeV) to produce a GLE. If the extreme emission phase of the flare is also considered as the dominator along GLE onset, the possible energy procurement (a parts per thousand currency signa1/40.414 GeV) is still not adequate to produce a GLE. In contrast, the CME-driven shock is capable of procuring enough possible relativistic energy (a parts per thousand yena1/41.21 GeV) that is sufficient amount of the energy for a GLE production. Any amount of the energy (< 0.414 GeV) released from preceding flare components is supposed to have been contributed to the shock process. Thus, it is assumed that the GLE71 was possibly caused by the energy released from the shock acceleration, which might have been boosted by the energy emanated from preceding flare.

第 16 条，共 222 条

Onset Of Electron Acceleration In A Flare Loop

Sharykin, I (Sharykin, Ivan); Liu, SM (Liu, Siming); Fletcher, L (Fletcher, Lyndsay)
ASTROPHYSICAL JOURNAL
卷: 793 期: 1 文献号: 25

We carried out a detailed analysis of X-ray and radio observations of a simple flare loop that occurred on 2002 August 12, with the impulsive hard X-ray (HXR) light curves dominated by a single pulse. The emission spectra of the early impulsive phase are consistent with an isothermal model in the coronal loop with a temperature reaching several keV. A power-law high-energy spectral tail is evident near the HXR peak time, in accordance with the appearance of footpoints at high energies, and is well correlated with the radio emission. The energy content of the thermal component keeps increasing gradually after the disappearance of this nonthermal component. These results suggest that electron acceleration only covers the central period of a longer and more gradual energy dissipation process and that the electron transport within the loop plays a crucial role in the formation of the inferred power-law electron distribution. The spectral index of power-law photons shows a very gradual evolution, indicating that the electron accelerator is in a quasi-steady state, which is confirmed by radio observations. These results are consistent with the theory of stochastic electron acceleration from a thermal background. Advanced modeling with coupled electron acceleration and spatial transport processes is needed to explain these observations more quantitatively, which may reveal the dependence of the electron acceleration on the spatial structure of the acceleration region.

第 17 条，共 222 条

An Interpretation Of Gle71 Concurrent Cme-Driven Shock Wave

Firoz, KA (Firoz, Kazi A.); Zhang, QM (Zhang, Q. M.); Gan, WQ (Gan, W. Q.); Li, YP (Li, Y. P.); Rodriguez-Pacheco, J (Rodriguez-Pacheco, J.); Moon, YJ (Moon, Y. -J.); Kudela, K (Kudela, K.); Park, YD (Park, Y. -D.); Dorman, LI (Dorman, Lev I.)
ASTROPHYSICAL JOURNAL SUPPLEMENT SERIES
卷: 213 期: 2 文献号: 24

Particle accelerations in solar flares and CME-driven shocks can sometimes result in very high-energy particle events (>= 1 GeV) that are known as ground level enhancements (GLEs). Recent studies on the first GLE event (GLE71 2012 May 17 01:50 UT) of solar cycle 24 suggested that CME-driven shock played a leading role in causing the event. To verify this claim, we have made an effort to interpret the GLE71 concurrent shock wave. For this, we have deduced the possible speed and height of the shock wave in terms of the frequency (MHz) of the solar radio type II burst and its drift rate (MHz min(-1)), and studied the temporal evolution of the particle intensity profiles at different heights of the solar corona. For a better perception of the particle acceleration in the shock, we have studied the solar radio type II burst with concurrent solar radio and electron fluxes. When the particle intensity profiles are necessarily shifted in time at similar to 1 AU, it is found that the growth phases of the electron and

cosmic ray intensity fluxes are strongly correlated (>0.91; >= 0.87) with the frequency drift rate of the type II burst, which is also consistent with the intensive particle accelerations at upper coronal heights (similar to >= 0.80 R-S < 1.10 R-S). Thus, we conclude that the CME-driven shock was possibly capable of producing the high-energy particle event. However, since the peaks of some flare components are found to be strongly associated with the fundamental phase of the type II burst, the preceding flare is supposed to contribute to the shock acceleration process.

第 18 条，共 222 条

Solar Eruptive Events：Mystery Of The Engine

SU Y, GAN Wei-Qun,

卷: 43；期: 1；页: 2-11

physics

Among solar activities, flares and coronal mass ejections (CMEs) are the most powerful energy release in solar system and the main factors in the changes of space weather. Magnetic field reconnection has been believed to be the driver of these solar eruptive events. However, the solid evidence of the whole process are still missing. Now, the Solar Dynamics Observatory (SDO) finally captured complete evidence of magnetic reconnection in the corona. In this article, we briefly review the history of studies on solar eruptive events, present the latest results, and discusson the main research subjects in future.

第 19 条，共 222 条

Space Solar Physics in 2012-2014

Gan WQ

Chinese Journal of Space Science

卷: 34 期: 5 页: 563-564

The main activities of Chinese space solar physics in 2012-2014 include: to continue studying the mid and long-term (2016-2030) plan of Chinese space solar physics; to arrange a group of pre-study projects of space solar physics; to initiate and continue a few solar mission-level projects. This paper summarizes all these activities briefly.

第 20 条，共 222 条

Fitting Power-Law Frequency Distribution With A Modified Maximum Likelihood Estimator

Li YP

卷: 55；期: 5；页: 437-443

Acta Astronomica Sinica

We developed a new correction formula for fitting the frequency distribution with saturation data. Through comparing four cases (with/without the saturation data and with/without the modified formula) to fit the tested numerical data, we found that the correction formula is the best for the data excluding the saturation data, although the original MLE (Maximum Likelihood Estimator) may be acceptable for the data including the saturation data and for a larger index. We therefore suggest to use the modified MLE to fit power-law frequency distribution, and the saturation data should be rejected first. Key words methods: statistical, methods: numerical, methods: data analysis.

Multi-Band Observation of Solar Activity

第 21 条，共 222 条

Well-Observed Dynamics Of Flaring And Peripheral Coronal Magnetic Loops During An M-Class Limb Flare

Shen, JH (Shen, Jinhua); *Zhou, TH* (Zhou, Tuanhui); Ji, HS (Ji, Haisheng); Wiegelmann, T (Wiegelmann, Thomas); Inhester, B (Inhester, Bernd); Feng, L (Feng, Li)

ASTROPHYSICAL JOURNAL

卷: 791 期: 2 文献号: 83

In this paper, we present a variety of well-observed dynamic behaviors for the flaring and peripheral magnetic loops of the M6.6 class extreme limb flare that occurred on 2011 February 24 (SOL2011-02-24T07:20) from EUV observations by the Atmospheric Imaging Assembly on the Solar Dynamics Observatory and X-ray observations by RHESSI. The flaring loop motion confirms the earlier contraction-expansion picture. We find that the U-shaped trajectory delineated by the X-ray corona source of the flare roughly follows the direction of a filament eruption associated with the flare. Different temperature structures of the coronal source during the contraction and expansion phases strongly suggest different kinds of magnetic reconnection processes. For some peripheral loops, we discover that their dynamics are closely correlated with the filament eruption. During the slow rising to abrupt, fast rising of the filament, overlying peripheral

magnetic loops display different responses. Two magnetic loops on the elbow of the active region had a slow descending motion followed by an abrupt successive fast contraction, while magnetic loops on the top of the filament were pushed outward, slowly being inflated for a while and then erupting as a moving front. We show that the filament activation and eruption play a dominant role in determining the dynamics of the overlying peripheral coronal magnetic loops.

第 22 条，共 222 条

New Vacuum Solar Telescope And Observations With High Resolution

Liu, Z (Liu, Zhong); Xu, J (Xu, Jun); Gu, BZ (Gu, Bo-Zhong); Wang, S (Wang, Sen); *You, JQ* (You, Jian-Qi); Shen, LX (Shen, Long-Xiang); Lu, RW (Lu, Ru-Wei); Jin, ZY (Jin, Zhen-Yu); Chen, LF (Chen, Lin-Fei); Lou, K (Lou, Ke); Li, Z (Li, Zhi); Liu, GQ (Liu, Guang-Qian); Xu, Z (Xu, Zhi); Rao, CH (Rao, Chang-Hui); Hu, QQ (Hu, Qi-Qian); Li, RF (Li, Ru-Feng); Fu, HW (Fu, Hao-Wen); Wang, F (Wang, Feng); Bao, MX (Bao, Men-Xian); Wu, MC (Wu, Ming-Chan); Zhang, BR (Zhang, Bo-Rong)
RESEARCH IN ASTRONOMY AND ASTROPHYSICS
卷: 14 期: 6 页: 705-718

The New Vacuum Solar Telescope (NVST) is a one meter vacuum solar telescope that aims to observe fine structures on the Sun. The main goals of NVST are high resolution imaging and spectral observations, including measurements of the solar magnetic field. NVST is the primary ground-based facility used by the Chinese solar research community in this solar cycle. It is located by Fuxian Lake in southwest China, where the seeing is good enough to perform high resolution observations. We first introduce the general conditions at the Fuxian Solar Observatory and the primary science cases of NVST. Then, the basic structures of this telescope and instruments are described in detail. Finally, some typical high resolution data of the solar photosphere and chromosphere are also shown.

第 23 条，共 222 条

Dependence Of The Length Of Solar Filament Threads On The Magnetic Configuration

Zhou, YH (Zhou, Yu-Hao); Chen, PF (Chen, Peng-Fei); *Zhang, QM* (Zhang, Qing-Min); Fang, C (Fang, Cheng)
RESEARCH IN ASTRONOMY AND ASTROPHYSICS
卷: 14 期: 5 页: 581-588

High-resolution H alpha observations indicate that filaments consist of an assembly of thin threads. In quiescent filaments, the threads are generally short, whereas in active region filaments, the threads are generally long. In order to explain these observational features, we performed one-dimensional radiative hydrodynamic simulations of filament formation along a dipped magnetic flux tube in the framework of the chromospheric evaporation-coronal condensation model. The geometry of a dipped magnetic flux tube is characterized by three parameters, i.e., the depth (D), the half-width (w) and the altitude (h) of the magnetic dip. A survey of the parameters in numerical simulations shows that when allowing the filament thread to grow in 5 days, the maximum length (L-th) of the filament thread increases linearly with w, and decreases linearly with D and h. The dependence is fitted into a linear function L-th = 0.84w - 0.88D - 2.78h + 17.31 (Mm). Such a relation can qualitatively explain why quiescent filaments have shorter threads and active region filaments have longer threads.

第 24 条，共 222 条

Reciprocatory Magnetic Reconnection In A Coronal Bright Point

Zhang, QM (Zhang, Q. M.); Chen, PF (Chen, P. F.); Ding, MD (Ding, M. D.); *Ji, HS* (Ji, H. S.)
ASTRONOMY & ASTROPHYSICS
卷: 568 文献号: A30

Context. Coronal bright points (CBPs) are small-scale and long-duration brightenings in the lower solar corona. They are often explained in terms of magnetic reconnection.
Aims. We aim to study the substructures of a CBP and clarify the relationship among the brightenings of different patches inside the CBP.
Methods. The event was observed by the X-ray Telescope (XRT) aboard the Hinode spacecraft on 2009 August 22-23.
Results. The CBP showed repeated brightenings (or CBP flashes). During each of the two successive CBP flashes, that is, weak and strong flashes that were separated by similar to 2 hr, the XRT images revealed that the CBP was composed of two chambers, patches A and B. During the weak flash, patch A brightened first, and patch B brightened similar to 2 min later. During the transition, the right leg of a large-scale coronal loop drifted from

the right side of the CBP to the left side. During the strong flash, patch B brightened first, and patch A brightened similar to 2 min later. During the transition, the right leg of the large-scale coronal loop drifted from the left side of the CBP to the right side. In each flash, the rapid change of the connectivity of the large-scale coronal loop is strongly suggestive of the interchange reconnection.
Conclusions. For the first time we found reciprocatory reconnection in the CBP, which means that reconnected loops in the outflow region of the first reconnection process serve as the inflow of the second reconnection process.

第 25 条，共 222 条

Blobs In Recurring Extreme-Ultraviolet Jets

Zhang, QM (Zhang, Q. M.); *Ji, HS* (Ji, H. S.)
ASTRONOMY & ASTROPHYSICS
卷: 567 文献号: A11

Context. Coronal jets are one type of ubiquitous small-scale activity that is caused by magnetic reconnection in the solar corona. They are often associated with cool surges in the chromosphere.
Aims. In this paper, we report our discovery of blobs in the recurrent and homologous jets that occurred at the western edge of the NOAA active region 11259 on 2011 July 22.
Methods. The jets were observed in the seven extreme-ultraviolet (EUV) filters of the Atmospheric Imaging Assembly instrument aboard the Solar Dynamics Observatory. Using the base-difference images of the six filters (94, 131, 171, 211, 193, and 335 angstrom), we carried out the differential emission measure (DEM) analyses to explore the thermodynamic evolutions of the jets. The jets were accompanied by cool surges observed in the H alpha line center of the ground-based telescope in the Big Bear Solar Observatory.
Results. The jets that had lifetimes of 20-30 min recurred at the same place for three times with an interval of 40-45 min. Interestingly, each of the jets intermittently experienced several upward eruptions at the speed of 120-450 km s(-1). After reaching the maximum heights, they returned back to the solar surface, showing near-parabolic trajectories. The falling phases were more evident in the low-T filters than in the high-T filters, indicating that the jets experienced cooling after the onset of eruptions. We identified bright and compact blobs in the jets during their rising phases. The simultaneous presence of blobs in all the EUV filters were consistent with the broad ranges of the DEM profiles of the blobs (5.5 <= log T <= 7.5), indicating their multi-thermal nature. The median temperatures of the blobs were similar to 2.3 MK. The blobs that were similar to 3 Mm in diameter had lifetimes of 24-60 s.
Conclusions. To our knowledge, this is the first report of blobs in coronal jets. We propose that these blobs are plasmoids created by the magnetic reconnection as a result of tearing-mode instability and are ejected out along the jets.

第 26 条，共 222 条

Long-Period Pulsations Of The Thermal Microwave Emission Of The Solar Flare Of June 2, 2007 From Data With High Spatial Resolution

Kupriyanova, EG (Kupriyanova, E. G.); Melnikov, VF (Melnikov, V. F.); Puzynya, VM (Puzynya, V. M.); Shibasaki, K (Shibasaki, K.); *Ji, HS* (Ji, H. S.)
ASTRONOMY REPORTS
卷: 58 期: 8 页: 573-577

Data from the Nobeyama Radioheliograph at 17 GHz with high spatial and temporal resolution are used to detect quasi-periodic pulsations with periods from 55 to 250 s in the thermal component of the microwave emission of a solar flare loop observed on June 2, 2007. Observed pulsations with periods of about 110-120 s are co-phased along the entire loop axis. The observed periodicity is most likely due to modulation of the radio emission by slow magnetoacoustic waves trapped in the filamentary flare loop.

第 27 条，共 222 条

Investigation Of The Moving Structures In A Coronal Bright Point

Ning, ZJ (Ning, Zongjun); Guo, Y (Guo, Yang)
ASTROPHYSICAL JOURNAL
卷: 794 期: 1 文献号: 79

We have explored themoving structures in a coronal bright point (CBP) observed by the Solar Dynamic Observatory Atmospheric Imaging Assembly (AIA) on 2011 March 5. This CBP event has a lifetime of similar to 20 minutes and is bright with a curved shape along a magnetic loop connecting a pair of negative and positive fields. AIA imaging observations show that a lot of bright structures are moving intermittently along the loop legs toward the two footpoints from the CBP brightness core. Such moving bright structures are

clearly seen at AIA 304 angstrom. In order to analyze their features, the CBP is cut along the motion direction with a curved slit which is wide enough to cover the bulk of the CBP. After integrating the flux along the slit width, we get the spacetime slices at nine AIA wavelengths. The oblique streaks starting from the edge of the CBP brightness core are identified as moving bright structures, especially on the derivative images of the brightness spacetime slices. They seem to originate from the same position near the loop top. We find that these oblique streaks are bi-directional, simultaneous, symmetrical, and periodic. The average speed is about 380 km s(-1), and the period is typically between 80 and 100 s. Nonlinear force-free field extrapolation shows the possibility that magnetic reconnection takes place during the CBP, and our findings indicate that thesemoving bright structures could be the observational outflows aftermagnetic reconnection in the CBP.

第 28 条，共 222 条

Interaction And Merging Of Two Sinistral Filaments

Jiang, YC (Jiang, Yunchun); Yang, JY (Yang, Jiayan); Wang, HM (Wang, Haimin); *Ji, HS* (Ji, Haisheng); Liu, Y (Liu, Yu); Li, HD (Li, Haidong); Li, JP (Li, Jianping)

ASTROPHYSICAL JOURNAL

卷: 793 期: 1 文献号: 14

In this paper, we report the interaction and subsequent merging of two sinistral filaments (F1 and F2) occurring at the boundary of AR 9720 on 2001 December 6. The two filaments were close and nearly perpendicular to each other. The interaction occurred after F1 was erupted and the eruption was impeded by a more extended filament channel (FC) standing in the way, in which F2 was embedded. The erupted material ran into FC along its axis, causing F1 and F2 to merge into a single structure that subsequently underwent a large-amplitude to-and-fro motion. A significant plasma heating process was observed in the merging process, making the mixed material largely disappear from the H alpha passband, but appear in Extreme Ultraviolet Telescope 195 angstrom images for a while. These observations can serve as strong evidence of merging reconnection between the two colliding magnetic structures. A new sinistral filament was formed along FC after the cooling of the merged and heated material. No coronal mass ejection was observed to be associated with the event; though, the eruption was accompanied by a two-ribbon flare with a separation motion, indicating that the eruption had failed. This event shows that, in addition to overlying magnetic fields, such an interaction is an effective restraint to make a filament eruption fail in this way.

第 29 条，共 222 条

The progress of Chinese Giant Solar Telescope

Z Liu , Zhenyu Jin , Shu Yuan , Jun Lin,Yuangong Deng, *Ji HS*, Yihua Yan

卷：9145 期： 26 页：1-1

SPIE 会议论文

Chinese Giant Solar Telescope (CGST) is the next generation ground-based solar telescope which was formally listed into the National Plans of Major Science and Technology Infrastructures. We have got series progresses of CGST in the recent years, from site testing to detailed designs. CGST is currently designed to be an 8m Ring Solar Telescope (RST). As an 8-meter solar telescope, the designing of CGST still faces some serious problems, although the ring structure is propitious to the thermo con。

第 30 条，共 222 条

The Chinese Giant Solar Telescope

Z Liu , Zhenyu Jin , Shu Yuan , Jun Lin,Yuangong Deng, *Ji HS*, Yihua Yan

卷：300 期： 1 页：349-354

IAU 会议论文

Chinese Giant Solar Telescope is the next generation ground-based solar telescope. The main science task of this telescope is to observe the ultra fine structures of the solar magnetic field and dynamic field. Due to the advantages in polarization detection and thermal controlling with a symmetrical circular system, the current design of CGST is a 6~8 meter circular symmetrical telescope. The results of simulations and analysis showed that the current design could meet the demands of most scienc

第 31 条，共 222 条

A swirling flare-related EUV jet

Zhang, QM (Zhang, Q. M.); Ji, HS (Ji, H. S.)

ASTRONOMY & ASTROPHYSICS

卷: 561 文献号: A134

Aims. We report our observations of a swirling flare-related extreme-ultraviolet (EUV) jet on 2011 October 15 at the edge of NOAA active region 11314. Methods. We used the multiwavelength observations in the EUV passbands from the Atmospheric Imaging Assembly (AIA) aboard the Solar Dynamics Observatory (SDO). We extracted a wide slit along the jet axis and 12 thin slits across its axis to investigate the longitudinal motion and transverse rotation. We also used data from the Extreme-Ultraviolet Imager (EUVI) aboard the Solar TErrestrial RElations Observatory (STEREO) spacecraft to investigate the three-dimensional (3D) structure of the jet. Ground-based Ha images from the El Teide Observatory, a member of the Global Oscillation Network Group (GONG), provide a good opportunity to explore the relationship between the cool surge and the hot jet. Line-of-sight magnetograms from the Helioseismic and Magnetic Imager (HMI) aboard SDO enable us to study the magnetic evolution of the flare/jet event. We carried out potential-field extrapolation to calculate the magnetic configuration associated with the jet. Results. The onset of jet eruption coincided with the start time of the C1.6 flare impulsive phase. The initial velocity and acceleration of the longitudinal motion were 254 +/- 10 km s(-1) and -97 +/- 5 m s(-2), respectively. The jet presented helical structure and transverse swirling motion at the beginning of its eruption. The counter-clockwise rotation slowed down from an average velocity of similar to 122 km s(-1) to similar to 80 km s(-1). The interwinding thick threads of the jet untwisted into multiple thin threads during the rotation that lasted for one cycle with a period of similar to 7 min and an amplitude that increases from similar to 3.2 Mm at the bottom to similar to 11 Mm at the upper part. Afterwards, the curtain-like leading edge of the jet continued rising without rotation, leaving a dimming region behind, before falling back to the solar surface. The appearance/disappearance of dimming corresponded to the longitudinal ascending/descending motions of jet. Cospatial Ha surge and EUV dimming imply that the dimming resulted from the absorption of hot EUV emission by the cool surge. The flare/jet event was caused by continuous magnetic cancellation before the start of the flare. The jet was associated with the open magnetic fields at the edge of AR 11314.

Imaging Observations of X-Ray Quasi-periodic Oscillations at 3-6 keV in the 26 December 2002 Solar Flare

Ning, ZJ (Ning, Zongjun)
SOLAR PHYSICS
卷: 289 期: 4 页: 1239-1256

Quasi-periodic oscillations in soft X-rays (SXR) are not well known due to the instrument limitations, especially the absence of imaging observations of SXR oscillations. We explore the quasi-periodic oscillations of SXR at 3-6 keV in a solar flare observed by the Reuven Ramaty High Energy Solar Spectroscopic Imager (RHESSI) on 26 December 2002. This was a B8.1 class event and showed three X-ray sources (S-1, S-2, and S-3) at 3-6 keV and two sources (S-1 and S-2) at 12 -25 keV. The light curves of the total fluxes display a two-minute oscillation at 3-6 keV, but not in the energy bands above 8 keV. To investigate imaging observations of the oscillations, we prepared CLEAN images at seven energy bands between 3 keV and 20 keV with an eight-second integration. The light curves of three sources were analyzed after integrating the flux of each source region. We used the Fourier method to decompose each source light curve into rapidly varying and slowly varying components. The rapidly varying components show seven individual peaks which are well fitted with a sine function. Then we used the wavelet method to analyze the periods in the rapidly varying component of each source. The results show that three sources display damped quasi-periodic oscillations with a similar two-minute period. The damped oscillations timescale varies between 2.5 to 6 minutes. Source S-1 oscillates with the same phase as S-3, but is almost in anti-phase with S-2. Analyzing the flaring images in more detail, we found that these oscillation peaks are well consistent with the appearance of S-3, which seems to split from or merge with S-2 with a period of two minutes. The flare images with a high cadence of one second at 3-6 keV show that source S-3 appears with a rapid period of 25 seconds. The two-minute oscillation shows the highest spectral power. Source S-3 seems to shift its position along the flare loop with a mean speed of 130 km s(-1), which is of the same order as the local sound speed. This connection between the oscillation peaks and emission enhancement appears to be an observational constraint on the emission mechanism at 3-6 keV.

第 33 条，共 222 条

Multi-wavelength Analysis to Solar Corona Heating Events

Yang Xu; Ji Haisheng; Li Haochuan

Acta Astronomica Sinica

卷: 55 期: 3 页: 193-202

With the advent and Successful running of the 1.6 meter aperture New Solar Telescope at Big Bear Solar Observatory(BBSO/NST),solar observation has entered the era of 0.1 arc second.This permits us to carry out case studies for single coronal heating event,accumulating original high.resolution observational evidences for a final resolving of the coronal heating problem.By combining the high-resolution Helium I 10830 A.TiO 7057 A,and H_alpha-0.7 A imaging data from NST,and the satellite data from the Atmospheric Imaging Assembly(AIA)and Helioseismic and Magnetic Imager(HMI)on board the Solar Dynamics Observatory(SDO),we analyze the evolution of magnetic field in the roots of two tiny dynamical events originating from the Suns intergranular lanes as seen from Helium I 10830 A images.The two events caused subsequent brightening in the corona,but no obvious feature is found at H_alpha-0.7 A images.We find that the two events are rooted at one side of magnetic polarity inversion 1ine.One event is apparently accompanied by the disappearance of a tiny magnetic element,while,in another event,weakening of a magnetlc concentration area is found.Changes for granules are also found during the two events. The results suggest that the two heating events are caused by smallscale magnetic actlvltles in intergranular lanes driven by constant granule convection.It appears that ubiquitous small-scale magnetic activities produce outflow of cold matter as seen at 10830 A and hot matter as seen at extreme ultraviolet bands.

Laboratory for Dark Matter and Space Astronomy

第 34 条，共 222 条

Production Rates Of Cosmogenic Nuclei On The Lunar Surface

Dong, TK (Dong Tie-Kuang); Yun, SJ (Yun Su-Jun); Ma, T (Ma Tao); Chang, J (Chang Jin); Dong, WD (Dong Wu-Dong); Zhang, XP (Zhang Xiao-Ping); Li, GL (Li Guo-Long); Ren, ZZ (Ren Zhong-Zhou)

CHINESE PHYSICS C

卷: 38 期: 7 文献号: 075101

A physical model for Geant4-based simulation of the galactic cosmic ray (GCR) particles' interaction with the lunar surface matter has been developed to investigate the production rates of cosmogenic nuclei. In this model the GCRs, mainly very high energy protons and alpha particles, bombard the surface of the Moon and produce many secondary particles, such as protons and neutrons: The energies of protons and neutrons at different depths are recorded and saved as ROOT files, and the analytical expressions for the differential proton and neutron fluxes are obtained through the best-fit procedure using ROOT software. To test the validity of this model, we calculate the production rates of the long-lived nuclei Be-10 and Al-26 in the Apollo 15 long drill core by combining the above differential fluxes and the newly evaluated spoliation reaction cross sections. Our numerical results show that the theoretical production rates agree quite well with the measured data, which means that this model works well. Therefore, it can be expected that this model can be used to investigate the cosmogenic nuclei in future lunar samples returned by the Chinese lunar exploration program and can be extended to study other objects, such as meteorites and the Earth's atmosphere.

第 35 条，共 222 条

Probing Cosmic Rays In Nearby Giant Molecular Clouds With The Fermi Large Area Telescope

Yang, RZ (Yang, Rui-zhi); Wilhelmi, ED (de Ona Wilhelmi, Emma); Aharonian, F (Aharonian, Felix)

ASTRONOMY & ASTROPHYSICS

卷: 566 文献号: A142

We report the results of our study of the energy spectra and absolute fluxes of cosmic rays (CRs) in the Local Galaxy based on a five-year gamma-ray observation with the Fermi Large Area Telescope (LAT) of eight nearby giant molecular clouds (GMCs) belonging to the Gould Belt. The gamma-ray signals obtained with high statistical significance allow the determination of gamma-ray spectra above 300 MeV with adequate precision for extraction of the energy distributions of CRs in these clouds. Remarkably, both the derived spectral indices and the absolute fluxes of CR protons in the energy interval 10-100 GeV

agree with the recent direct measurements of local CRs by the PAMELA experiment. This is strong evidence of a quite homogeneous distribution of CRs, at least within several hundred parsecs of the Local Galaxy. Combined with the well established energy-dependent time of escape of CRs from the Galaxy, tau(E) proportional to E-delta with delta approximate to 0.5-0.6, the measured spectrum implies a CR spectral index of the (acceleration) source of approximate to E-2.3. At low energies, the spectra of gamma rays appear to vary from one cloud to another. This implies spatial variations of the energy spectra of CRs below 10 GeV, which at such low energies could be explained naturally by both the impact of the propagation effects and the contribution of CR locally accelerated inside the clouds.

第 36 条，共 222 条

Grb 131231a: Implications Of The Gev Emission

Liu, B (Liu, Bin); Chen, W (Chen, Wei); Liang, YF (Liang, Yun-Feng); Zhou, B (Zhou, Bei); He, HN (He, Hao-Ning); Tam, PHT (Tam, Pak-Hin Thomas); Shao, L (Shao, Lang); Jin, ZP (Jin, Zhi-Ping); Fan, YZ (Fan, Yi-Zhong); Wei, DM (Wei, Da-Ming)
ASTROPHYSICAL JOURNAL LETTERS

卷: 787 期: 1 文献号: L6

GRB 131231A was detected by the Large Area Telescope on board the Fermi Space Gamma-ray Telescope. The high-energy gamma-ray (>100 MeV) afterglow emission spectrum is F-nu proportional to nu(-0.54 +/- 0.15) in the first similar to 1300 s after the trigger and the most energetic photon has an energy of similar to 62 GeV, arriving at t similar to 520 s. With reasonable parameters of the gamma-ray burst (GRB) outflow as well as the density of the circum-burst medium, the synchrotron radiation of electrons or protons accelerated at an external forward shock have difficulty accounting for the data. Rather, the synchrotron self-Compton radiation of the forward shock-accelerated electrons can account for both the spectrum and temporal behavior of the GeV afterglow emission. We also show that the prospect for detecting GRB 131231A-like GRBs with the Cherenkov Telescope Array is promising.

第 37 条，共 222 条

Circular Polarization In The Optical Afterglow Of GRB 121024A

Wiersema, K (Wiersema, K.); Covino, S (Covino, S.); Toma, K (Toma, K.); van der Horst, AJ (van der Horst, A. J.); Varela, K (Varela, K.); Min, M (Min, M.); Greiner, J (Greiner, J.); Starling, RLC (Starling, R. L. C.); Tanvir, NR (Tanvir, N. R.); Wijers, RAMJ (Wijers, R. A. M. J.); Campana, S (Campana, S.); Curran, PA (Curran, P. A.); *Fan, Y* (Fan, Y.); Fynbo, JPU (Fynbo, J. P. U.); Gorosabel, J (Gorosabel, J.); Gomboc, A (Gomboc, A.); Gotz, D (Goetz, D.); Hjorth, J (Hjorth, J.); Jin, ZP (Jin, Z. P.); Kobayashi, S (Kobayashi, S.); Kouveliotou, C (Kouveliotou, C.); Mundell, C (Mundell, C.); O'Brien, PT (O'Brien, P. T.); Pian, E (Pian, E.); Rowlinson, A (Rowlinson, A.); Russell, DM (Russell, D. M.); Salvaterra, R (Salvaterra, R.); Alighieri, SD (Alighieri, S. di Serego); Tagliaferri, G (Tagliaferri, G.); Vergani, SD (Vergani, S. D.); Elliott, J (Elliott, J.); Farina, C (Farina, C.); Hartoog, OE (Hartoog, O. E.); Karjalainen, R (Karjalainen, R.); Klose, S (Klose, S.); Knust, F (Knust, F.); Levan, AJ (Levan, A. J.); Schady, P (Schady, P.); Sudilovsky, V (Sudilovsky, V.); Willingale, R (Willingale, R.)
NATURE

卷: 509 期: 7499 页: 201-202

Gamma-ray bursts (GRBs) are most probably powered by collimated relativistic outflows (jets) from accreting black holes at cosmological distances. Bright afterglows are produced when the outflow collides with the ambient medium. Afterglow polarization directly probes the magnetic properties of the jet when measured minutes after the burst, and it probes the geometric properties of the jet and the ambient medium when measured hours to days after the burst(1-5). High values of optical polarization detected minutes after the burst of GRB 120308A indicate the presence of large-scale ordered magnetic fields originating from the central engine(5) (the power source of the GRB). Theoretical models predict low degrees of linear polarization and no circular polarization at late times(6-8), when the energy in the original ejecta is quickly transferred to the ambient medium and propagates farther into the medium as a blast wave. Here we report the detection of circularly polarized light in the afterglow of GRB 121024A, measured 0.15 days after the burst. We show that the circular polarization is intrinsic to the afterglow and unlikely to be produced by dust scattering or plasma propagation effects. A possible explanation is to invoke anisotropic (rather than the commonly assumed isotropic) electron pitch-angle distributions, and we suggest that new models are required to produce the complex microphysics of realistic shocks in

relativistic jets(9-11).

第 38 条，共 222 条

The Spatial Distribution Of Dark Matter Annihilation Originating From A Gamma-Ray Line Signal

Lu, TS (Lu, Tong-Suo); Dong, TK (Dong, Tie-Kuang); Wu, J (Wu, Jian)

RESEARCH IN ASTRONOMY AND ASTROPHYSICS

卷: 14 期: 5 页: 520-526

The GeV - TeV gamma-ray line signal is the smoking gun signature of dark matter annihilation or decay. The detection of such a signal is one of the main targets of some space-based telescopes, including Fermi-LAT and the upcoming missions CALET, DAMPE and Gamma-400. An important feature of gamma-ray line photons that originate from dark-matter-annihilation is that they are concentrated at the center of the Galaxy. So far, no reliable gamma-ray line has been detected by Fermi-LAT, and the upper limits on the cross section of annihilation into gamma-rays have been reported. We use these upper limits to estimate the "maximal" number of gamma-ray line photons detectable for Fermi-LAT, DAMPE and Gamma-400, and then investigate the spatial distribution of these photons. We show that the center of the distribution will usually be offset from the Galactic center (Sgr A*) due to the limited statistics. Such a result is almost independent of models of the dark matter distribution, and will render the reconstruction of the dark matter distribution with the gamma-ray line signal very challenging for foreseeable space-based detectors.

第 39 条，共 222 条

Fermi Large Area Telescope Detection Of Supernova Remnant Rcw 86

Yuan, Q (Yuan, Qiang); *Huang, XY* (Huang, Xiaoyuan); Liu, SM (Liu, Siming); Zhang, B (Zhang, Bing)

ASTROPHYSICAL JOURNAL LETTERS

卷: 785 期: 2 文献号: L22

Using 5.4 yr Fermi Large Area Telescope data, we report the detection of GeV. gamma- ray emission from the shell-type supernova remnant RCW 86 (G315.4-2.3) with a significance of similar to 5.1 sigma. The data slightly favors an extended emission of this supernova remnant. The spectral index of RCW 86 is found to be very hard, Gamma similar to 1.4, in the 0.4-300 GeV range. A one-zone leptonic model can well fit the multi-wavelength data from radio to very high energy gamma-rays. The very hard GeV gamma-ray spectrum and the inferred low gas density seem to disfavor a hadronic origin for the gamma-rays. The. - ray behavior of RCW 86 is very similar to several other TeV shell-type supernova remnants, e. g., RX J1713.7- 3946, RX J0852.0-4622, SN 1006, and HESS J1731-347.

第 40 条，共 222 条

A Preliminary Research On The Development Of The Hard X-Ray Imaging Telescope

Zheng C X; Cai Mingsheng; Hu Yiming; Huang Yongyi; Gong Yizhong

卷: 55 期: 2 页: 154-169

Acta Astronomica Sinica

Since the 1860s, astronomers have explored a new field with the discovery of X-ray. Instead of the conventional imaging technique by using mirrors or lens, which can not work in the high-energy bands, direct imaging, coded aperture, and Fourier transform are used for the high-energy imaging. It can be implemented in various hardware configurations, among which the spatial modulation collimator are widely used. We adopt the grating collimator based on Fourier transform that is discussed in detail. This paper makes an investigation on the fabrication process of grating. The key components of the hard X-ray telescope based on the spatial modulation are developed, which contains 8 Csl-detector modules, 8-channel shaping amplifiers, and data acquisition system. The preliminary test results of readout electronics system are obtained.

第 41 条，共 222 条

The Design And Realization Of Linear Calibration System Of A Large Dynamic Range Readout Unit For A BGO Calorimeter

Xie MG; Guo Jianhua; Wu Jian; Chang Jin

卷: 55 期: 2 页:170-179

Acta Astronomica Sinica

The DArk Matter Particle Explorer (DAMPE) is proposed by Purple Mountain Observatory, Chinese Academy of Sciences. This project expects to find the evidence of the existence of dark matter particle in the universe via the detection of high-energy electron and gamma-ray. A major component of the payload is a BGO (Bismuth Germanate Oxide) calorimeter, which is used to detect the particles in the energy range from 5

GeV to 10 TeV. According to a physical simulation, the dynamic range of each BGO detection unit is about 1.5x10~5. In order to test the linearity of BGO detection readout unit, we implement a simple linearity calibration system covering such a large dynamic range. The experimental result shows that the nonlinearity of the entire dynamic range is less than 2.7%.

第 42 条，共 222 条

Fermi Large Area Telescope Observations Of The Supernova Remnant HESS J1731-347

Yang, RZ (Yang, Rui-zhi); Zhang, X (Zhang, Xiao); Yuan, Q (Yuan, Qiang); Liu, SM (Liu, Siming)
ASTRONOMY & ASTROPHYSICS

卷: 567 文献号: A23

Context. HESS J1731-347 has been identified as one of the few TeV-bright shell type supernova remnants (SNRs). These remnants are dominated by nonthermal emission. and the nature of TeV emission has been continuously debated for nearly a decade. Aims. We carry out the detailed modeling of the radio to gamma-ray spectrum of HESS J1731-347 to constrain the magnetic field and energetic particles sources, which we compare with those of the other TeV-bright shell-type SNRs explored before.
Methods. Four years of data from Fermi Large Area Telescope (LAT) observations for regions around this remnant are analyzed, leading to no detection correlated with the source discovered in the TeV band. The Markov chain Monte Carlo method is used to constrain parameters of one-zone models for the overall emission spectrum. Results. Based on the 99.9% upper limits of fluxes in the GeV range, one-zone hadronic models with an energetic proton spectral slope greater than 1.8 can be ruled out, which favors a leptonic origin for the gamma-ray emission, making this remnant a sibling of the brightest TeV SNR RX J1713.7-3946, the Vela Junior SNR RX J0852.0-4622. and RCW 86. The best fit leptonic model has an electron spectral slope of 1.8 and a magnetic field of similar to 30 mu G. which is at least a factor of 2 higher than those of RX 31713.7-3946 and RX 30852.0-4622. posing a challenge to the distance estimate and/or the energy equipartition between energetic electrons and the magnetic field of this source. A measurement of the shock speed will address this challenge and has implications on the magnetic field evolution and electron acceleration driven by shocks of SNRs.

第 43 条，共 222 条

The Fermi Bubbles Revisited

Yang, RZ (Yang, Rui-zhi); Aharonian, F (Aharonian, Felix); Crocker, R (Crocker, Roland)
ASTRONOMY & ASTROPHYSICS

卷: 567 文献号: A19

We analyze 60 months of all-sky data from the Fermi-LAT. The Fermi bubble structures discovered previously are clearly revealed by our analysis. With more data, hence better statistics, we can now divide each bubble into constant longitude slices to investigate their gross gamma-ray spectral morphology. While the detailed spectral behavior of each slice derived in our analysis is somewhat dependent on the assumed background model, we find, robustly, a relative deficit in the flux at low energies (i.e., hardening) toward the top of the south bubble. In neither bubble does the spectrum soften with longitude. The morphology of the Fermi bubbles is also revealed to be energy-dependent: at high energies they are more extended. We conclude from the gamma-ray spectrum at high latitudes that a low energy break in the parent cosmic ray population is required in both leptonic and hadronic models. We briefly discuss possible leptonic and hadronic interpretations of this phenomenology.

第 44 条，共 222 条

Spectral Modeling Of The Charge-Exchange X-Ray Emission From M82

Zhang, SN (Zhang, Shuinai); Wang, QD (Wang, Q. Daniel); Ji, L (Ji, Li); Smith, RK (Smith, Randall K.); Foster, AR (Foster, Adam R.); Zhou, X (Zhou, Xin)
ASTROPHYSICAL JOURNAL

卷: 794 期: 1 文献号: 61

It has been proposed that the charge-exchange (CX) process at the interface between hot and cool interstellar gases could contribute significantly to the observed soft X-ray emission in star-forming galaxies. We analyze the XMM-Newton/reflection grating spectrometer (RGS) spectrum of M82 using a newly developed CX model combined with a single-temperature thermal plasma to characterize the volume-filling hot gas. The CX process is largely responsible for not only the strongly enhanced forbidden lines of the Ka triplets of various He-like ions but also good fractions of the Ly alpha transitions of C (similar to 87%), 0 VIII, and N VII (>= 50%) as well. In total

about a quarter of the X-ray flux in the RGS 6-30 angstrom band originates in the CX. We infer an ion incident rate of 3 x 10(51) s(-1) undergoing CX at the hot and cool gas interface and an effective area of the interface of 2 x 1045 cm2 that is one order of magnitude larger than the cross section of the global biconic outflow. With the CX contribution accounted for, the best-fit temperature of the hot gas is 0.6 keV, and the metal abundances are approximately solar. We further show that the same CX/thermal plasma model also gives an excellent description of the EPIC-pn spectrum of the outflow Cap, projected at 11.6 kpc away from the galactic disk of M82. This analysis demonstrates that the CX is potentially an important contributor to the X-ray emission from starburst galaxies and also an invaluable tool to probe the interface astrophysics.

第 45 条，共 222 条

Spins And Parities Of The Odd-A P Isotopes Within A Relativistic Mean-Field Model And Elastic Magnetic Electron-Scattering Theory

Wang, ZJ (Wang, Zaijun); Ren, ZZ (Ren, Zhongzhou); *Dong, TK* (Dong, Tiekuang); Xu, C (Xu, Chang)
PHYSICAL REVIEW C

卷: 90 期: 2 文献号: 024307

The ground-state spins and parities of the odd-A phosphorus isotopes P25-47 are studied with the relativistic mean-field (RMF) model and relativistic elastic magnetic electron-scattering theory (REMES). Results of the RMF model with the NL-SH, TM2, and NL3 parameters show that the 2s(1/2) and 1d(3/2) proton level inversion may occur for the neutron-rich isotopes P37-47, and, consequently, the possible spin-parity values of P37-47 may be 3/2(+), which, except for P-47, differs from those given by the NUBASE2012 nuclear data table by Audi et al. Calculations of the elastic magnetic electron scattering of P37-47 with the single valence proton in the 2s(1/2) and 1d(3/2) state show that the form factors have significant differences. The results imply that elastic magnetic electron scattering can be a possible way to study the 2s(1/2) and 1d(3/2) level inversion and the spin-parity values of P37-47. The results can also provide new tests as to what extent the RMF model, along with its various parameter sets, is valid for describing the nuclear structures. In addition, the contributions of the upper and lower components of the Dirac four-spinors to the form factors and the isotopic shifts of the magnetic form factors are discussed.

第 46 条，共 222 条

Fast Radio Bursts As A Cosmic Probe?

Zhou, B (Zhou, Bei); Li, X (Li, Xiang); Wang, T (Wang, Tao); Fan, YZ (Fan, Yi-Zhong); Wei, DM (Wei, Da-Ming)
PHYSICAL REVIEW D

卷: 89 期: 10 文献号: 107303

We discuss the possibility of using fast radio bursts (FRBs)-if cosmological-as a viable cosmic probe. We find that the contribution of the host galaxies to the detected dispersion measures can be inapparent for the FRBs that are not from galaxy centers or star-forming regions. The inhomogeneity of the intergalactic medium (IGM), however, causes significant deviation of the dispersion measure from that predicted in the simplified homogeneous IGM model for an individual event. Fortunately, with sufficient FRBs along different sightlines but within a very narrow redshift interval (e. g., Delta z similar to 0.05), the mean obtained from averaging observed dispersion measures does not suffer such a problem and hence may be used as a cosmic probe. We show that in the optimistic case (e. g., about 20 FRBs in each Delta z have been measured; the most distant FRBs were at redshift >= 3; the host galaxies and the FRB sources contribute little to the detected dispersion measures) and with all the uncertainties (i.e., the inhomogeneity of the IGM, the contribution and uncertainty of host galaxies, and the evolution and error of f(IGM)) considered, FRBs could help constrain the equation of state of dark energy.

第 47 条，共 222 条

Association Of Cmes With Solar Surface Activity During The Rise And Maximum Phases Of Solar Cycles 23 And 24

Gao, PX (Gao, Peng-Xin); Li, T (Li, Ting); Zhang, J (Zhang, Jun)
RESEARCH IN ASTRONOMY AND ASTROPHYSICS

卷: 14 期: 10 页: 1289-1290

The cyclical behaviors of sunspots, flares and coronal mass ejections (CMEs) for 54 months from 2008 November to 2013 April after the onset of Solar Cycle (SC) 24 are compared, for the first time, with those of SC 23 from 1996 November to 2001 April. The results are summarized below. (i) During the maximum phase, the number of sunspots in SC 24 is significantly smaller than that for SC 23

and the number of flares in SC 24 is comparable to that of SC 23. (ii) The number of CMEs in SC 24 is larger than that in SC 23 and the speed of CMEs in SC 24 is smaller than that of SC 23 during the maximum phase. We individually survey all the CMEs (1647 CMEs) from 2010 June to 2011 June. A total of 161 CMEs associated with solar surface activity events can be identified. About 45% of CMEs are associated with quiescent prominence eruptions, 27% of CMEs only with solar flares, 19% of CMEs with both active-region prominence eruptions and solar flares, and 9% of CMEs only with active-region prominence eruptions. Comparing the association of the CMEs and their source regions in SC 24 with that in SC 23, we notice that the characteristics of source regions for CMEs during SC 24 may be different from those of SC 23.

第 48 条，共 222 条

Model-Dependent Estimate On The Connection Between Fast Radio Bursts And Ultra High Energy Cosmic Rays

Li, X (Li, Xiang); Zhou, B (Zhou, Bei); He, HN (He, Hao-Ning); Fan, YZ (Fan, Yi-Zhong); Wei, DM (Wei, Da-Ming)

ASTROPHYSICAL JOURNAL

卷: 797 期: 1 文献号: 33

The existence of fast radio bursts (FRBs), a new type of extragalatic transient, has recently been established, and quite a few models have been proposed. In this work, we discuss the possible connection between the FRB sources and ultra high energy (>10(18) eV) cosmic rays. We show that in the blitzar model and the model of merging binary neutron stars, which includes the huge energy release of each FRB central engine together with the rather high rate of FRBs, the accelerated EeV cosmic rays may contribute significantly to the observed ones. In other FRB models, including, for example, the merger of double white dwarfs and the energetic magnetar radio flares, no significant EeV cosmic ray is expected. We also suggest that the mergers of double neutron stars, even if they are irrelevant to FRBs, may play a nonignorable role in producing EeV cosmic ray protons if supramassive neutron stars are formed in a sufficient fraction of mergers and the merger rate is greater than or similar to 10(3) yr(-1) Gpc(-3). Such a possibility will be unambiguously tested in the era of gravitational wave astronomy.

第 49 条，共 222 条

The Realization Of The Test System For The Trigger Logic In The DAMPE

Zhang L; Guo Jianhua; Zhang Yongqiang

卷: 55 期: 6 页: 522-533

Acta Astronomica Sinica

As a part of DAMPE (Dark Matter Particle Explorer), the trigger system is mainly used for triggering the target particles: high-energy electrons and gamma-ray. The trigger system is composed of the trigger detectors (the BGO (Bi_2O_3-GeO_2) calorimeter in DAMPE), which generates the hit signals, and triggers the coincidence logic. This paper describes the design of the test system for the trigger logic of DAMPE, which uses the hit signal generator board to test the trigger logic. Furthermore, we also implement a coincidence system to trigger cosmic ray, which is used to test the trigger efficiency of DAMPE for muon particle.

第 50 条，共 222 条

The Uniform K Distribution Of The Mare Deposits In The Orientale Basin: Insights From Chang'E-2 Gamma-Ray Spectrometer

Meng-Hua, *Chang J,* Changb, Minggang Xiea, Jörg Fritzc, Vera A. Fernandesc, e, Wing-Huen Ipa,d, Tao Mab, Aoao Xua

Earth and Planetary Science Letters

卷: 143；期: 1；页: 1-9

The composition of mare basalt units in the Orientale Basin are investigated by using the potassium (K) map derived from Chang'E-2 gamma-ray spectrometer (CE-2 GRS) and FeO map derived from Clementine UV–Vis data set. Together with crater retention ages of the mare basalts from literature data, we aim to investigate possible magma sources underneath the Orientale Basin and their chemical evolution over time. Analyses of the chemical composition of the resurfaced mare basalts together with the reported eruption ages suggest a unique magma generating process for the resurfaced mare deposits. The early mare basalts in the central Mare Orientale and the later resurfaced mare deposits probably derived from magma generated by heat release due to high radioactive element concentrations. Based on forward modeling, the

similar K abundances observed in the small mare deposits of the SW polygon area, Lacus Veris, and Lacus Autumni and those in the central Mare Orientale imply the same heat source for these lava eruptions. The chemical similarities (e.g., K, FeO, and TiO_2) of these regions suggest that mare basalts within the Orientale Basin are a result of multiple eruptions from a relatively homogeneous source underneath the Basin.
Gadget timed out while loading

第 51 条，共 222 条

AMS-02 Positron Excess: New Bounds On Dark Matter Models And Hint For Primary Electron Spectrum Hardening

Feng, L (Feng, Lei); Yang, RZ (Yang, Rui-Zhi); He, HN (He, Hao-Ning); Dong, TK (Dong, Tie-Kuang); Fan, YZ (Fan, Yi-Zhong); Chang, J (Chang, Jin)
PHYSICS LETTERS B
卷: 728 页: 250-255

The data collected by ATIC, CREAM and PAMELA all display remarkable cosmic ray nuclei spectrum hardening above the magnetic rigidity similar to 240 GV. One natural speculation is that the primary electron spectrum also gets hardened (possibly at similar to 80 CV) and the hardening partly accounts for the electron/positron total spectrum excess discovered by ATIC, HESS and Fermi-LAT. If it is the case, the increasing behavior of the subsequent positron-to-electron ratio will get flattened and the spectrum hardening should be taken into account in the joint fit of the electron/positron data otherwise the inferred parameters will be biased. Our joint fits of the latest AMS-02 positron fraction data together with the PAMELA/Fermi-LAT electron/positron spectrum data suggest that the primary electron spectrum hardening is needed in most though not all modelings. The bounds on dark matter models have also been investigated. In the presence of spectrum hardening of primary electrons, the amount of dark-matter-originated electron/positron pairs needed in the modeling is smaller. Even with such a modification, the annihilation channel chi chi ->mu(+) mu(-) has been tightly constrained by the Fermi-EAT Galactic diffuse emission data. The decay channel chi ->mu(+) mu(-) is found to be viable.

第 52 条，共 222 条

High Energy Emission Of Grb 130821a: Constraining The Density Profile Of The Circum-Burst Medium As Well As The Initial Lorentz Factor Of The Outflow

Liang, YF (Liang, Yun-Feng); Zhou, B (Zhou, Bei); He, HN (He, Hao-Ning); Tam, PHT (Tam, Pak-Hin Thomas); Fan, YZ (Fan, Yi-Zhong); Wei, DM (Wei, Da-Ming)
ASTROPHYSICAL JOURNAL
卷: 781 期: 2 文献号: 74

GRB 130821A was detected by Fermi-GBM/LAT, Konus-WIND, SPI-ACS/INTEGRAL, RHESSI and Mars Odyssey-HEND. Although the data of GRB 130821A are very limited, we show in this work that the high energy gamma-ray emission (i.e., above 100 MeV) alone imposes tight constraint on the density profile of the circumburst medium as well as the initial Lorentz factor of the outflow. The temporal behavior of the high energy gamma-ray emission is consistent with the forward shock synchrotron radiation model, and the circum-burst medium likely has a constant-density profile. The Lorentz factor is about a few hundred, similar to other bright GRBs.

第 53 条，共 222 条

Observational Results Of The Change-1 Solar X-Ray Monitor

Cui, XZ (Cui, X. Z.); Wang, HY (Wang, H. Y.); Peng, WX (Peng, W. X.); Zhang, CM (Zhang, C. M.); Liang, XH (Liang, X. H.); Wang, JZ (Wang, J. Z.); Gao, M (Gao, M.); Yang, JW (Yang, J. W.); Cao, XL (Cao, X. L.); Zhang, JY (Zhang, J. Y.); Wu, MY (Wu, M. Y.); *Chang, J* (Chang, J.); Sun, HX (Sun, H. X.); OuYang, ZY (OuYang, Z. Y.); Zhou, YL (Zhou, Y. L.); Li, CL (Li, C. L.)
SOLAR PHYSICS
卷: 289 期: 5 页: 1597-1606

We present the primary observations of the Solar X-ray Monitor (SXM) payload onboard the ChangE-1 lunar exploration satellite, which was launched on 24 October 2007. The SXM payload uses a solid-state silicon P-I-N photo-diode (Si-PIN) whose dynamic energy ranges from 1 keV to 10 keV. The long-term integrated spectra at different solar-activity levels as observed by the SXM are presented. By fitting these spectra with an optically thin plasma model, the two-minute temperature variation of the solar coronal plasma

during a solar flare is also presented.

第 54 条，共 222 条

Phase Relationships Between The CME-Energy Cycle, The Sunspot-Area Cycle And The Flare-Index Cycle

Gao, PX (Gao, P. X.); Xie, JL (Xie, J. L.); Zhong, J (Zhong, J.)

SOLAR PHYSICS

卷: 289 期: 5 页: 1831-1841

We study the phase relationships between the coronal-mass-ejection (CME) energy cycle, the sunspot-area cycle, and the flare-index cycle from 1996 to 2010. The results show the following: i) The activity cycle of the flare index significantly leads the activity cycle of the sunspot area. ii) The activity cycle of the CME energy is inferred to be almost in phase with the activity cycle of the sunspot area; the activity cycle of the CME energy at low latitudes slightly leads the activity cycle of the sunspot area; the CME energy at high latitudes is shown to significantly lag behind the sunspot area. iii) The CME energy is shown to significantly lag behind the flare index; the CME energy at low latitudes is shown to slightly lag behind the flare index; the CME energy at high latitudes is shown to significantly lag behind the flare index.

第 55 条，共 222 条

Probe The 2s(1/2) And 1d(3/2) State Level Inversion With Electron-Nucleus Scattering

Wang, ZJ (Wang Zai-Jun); Ren, ZZ (Ren Zhong-Zhou); *Dong, TK* (Dong Tie-Kuang)

CHINESE PHYSICS C

卷: 38 期: 2 文献号: 024102

The neutron-rich even-even nuclei Mg26-40, S28-46, and Ar32-56 are calculated with the RMF model and the phase-shift electron scattering method. Results show that level inversion of the 2s(1/2) and 1d(3/2) proton states may occur for the magnesium, silicon, sulphur, and argon isotopes with more neutrons away from the stability line. Calculations show that the variation of the central charge densities for S30-48, and Ar32-56 are very sensitive to the 2s(1/2) and 1d(3/2) proton state level inversion, and the level inversion can lead to a large measurable central charge depletion to the charge density distributions for the neutron-rich isotopes. Calculations also show that the charge density differences between the isotopes with and without central charge depletion can reveal not only the level inversion of the 2s(1/2) and 1d(3/2) proton states but also the behavior of the proton wave functions of both states. The results can provide references for the possible study of the nuclear level inversion and nuclear bubble phenomenon with electron scattering off short-lived nuclei at RIKEN or/and GSI in the future. In addition, direct nuclear reaction S-44(n, d)(43)p S-44(H-3, alpha)P-43 might also be a possible way to study the 2s(1/2) and 1d(3/2) proton state level inversion.

第 56 条，共 222 条

Midterm Periods Of Solar Filaments

Zou, P (Zou, Peng); Li, QX (Li, Qixiu)

JOURNAL OF GEOPHYSICAL RESEARCH-SPACE PHYSICS

卷: 119 期: 12

On the basis of the Carte Synoptique catalogue of solar filaments from March 1919 to December 1989, we measure power spectra of detrended full-disk (FSFNs, latitudinal bands: 0 degrees-90 degrees), low-latitude (LSFNs, latitudinal bands: <50 degrees), and high-latitude (HSFNs, latitudinal bands: >= 50 degrees) solar filament numbers by Maximum Entropy Method (MEM) and Continuous wavelet transform to detect midterm periods. It is found as the following: (1) FSFNs and LSFNs have the same midterm periodicity, while HSFNs show a different midrange periodicity. Some periods frequently mentioned in other solar indices are also detected from the solar filament numbers, such as 2-3 year period (quasi-biennial oscillation-QBO), similar to 1.7 year, similar to 1.3 year, similar to 1 year, 150-157 day period (Rieger period), and 6.0-6.4 months (Rieger-type period). These periods are intermittent during considered time span. Some of them are missing in some solar cycles. (2) QBO is detected from total data and most solar cycles of FSFNs, LSFNs, and HSFNs. It may be related to oscillation of magnetic field of solar surface. (3) Approximately 1.3 year period occasionally appears, but similar to 1.7 year period is hardly seen. These two periods probably are seasonal effects. (4) Approximately 1 year period is detected from both total data and every solar cycle of FSFNs and LSFNs but hardly detected from HSFNs. It is perhaps connected with sunspot activity. (5) Rieger period of 5.0-5.2 months is detected in total data and even solar cycles of HSFNs. Rieger-type period of 6.0-6.4 months is

found in total data and most solar cycles, except cycle 18 of LSFNs and FSFNs. These periods seem to be subharmonics of similar to 11 year period.

第 57 条，共 222 条

Nonlinear Relativistic Mean-Field Theory Studies On He Isotopes

Fan, GW (Fan Guang-Wei); *Dong, TK* (Dong Tie-Kuang); Nishimura, D (Nishimura, D.)

卷: 38 期: 12

CHINESE PHYSICS C

The ground state properties of He isotopes are studied in the nonlinear relativistic mean-field (RMF) theory with force parameters NL-SH and TM2. The modified Glauber model is introduced as a gatekeeper to check the calculations. The investigation shows that the RMF theory provides a good description on the properties of He isotopes. The many-body space information of He-4 + neutrons is obtained reliably. As a product, the calculation gives strong evidence for a neutron halo in He-5.

第 58 条，共 222 条

An Updated Analysis Of Inert Higgs Doublet Model In Light Of The Recent Results From LUX, PLANCK, AMS-02 And LHC

Arhrib, A (Arhrib, Abdesslam); Tsai, YLS (Tsai, Yue-Lin Sming); *Yuan, Q* (Yuan, Qiang); Yuan, TC (Yuan, Tzu-Chiang)

期: 6 文献号: 030

JOURNAL OF COSMOLOGY AND ASTROPARTICLE PHYSICS

In light of the recent discovery by the ATLAS and CMS experiments at the Large Hadron Collider (LHC) of a Higgs-like particle with a narrow mass range of 125-126GeV, we perform an updated analysis on one of the popular scalar dark matter models, the Inert Higgs Doublet Model (IHDM). We take into account in our likelihood analysis of various experimental constraints, including recent relic density measurement, dark matter direct and indirect detection constraints as well as the latest collider constraints on the invisible decay width of the Higgs boson and monojet search at the LHC. It is shown that if the invisible decay of the standard model Higgs boson is open, LHC as well as direct detection experiments like LUX and XENON100 could put stringent limits on the Higgs boson couplings to dark matter. We find that the most favoured parameter space for IHDM corresponds to dark matter with a mass less than 100 GeV or so. In particular, the best-fit points are at the dark matter mass around 70 GeV where the invisible Higgs decay to dark matter is closed. Scalar dark matter in the higher mass range of 0.5-4 TeV is also explored in our study. Projected sensitivities for the future experiments of monojet at LHC-14, XENON1T and AMS-02 one year antiproton flux are shown to put further constraints on the existing parameter space of IHDM.

第 59 条，共 222 条

Dark Matter Particle Explorer: The First Chinese Cosmic Ray And Hard Gamma-Ray Detector In Space

Chang J

Chinese Journal of Space Science

卷: 34 期: 5 页: 550-557

The Dark Matter Particle Explorer (DAMPE) mission is one of the five scientific space science missions within the framework of the Strategic Pioneer Program on Space Science of the Chinese Academy of Science (CAS) approved in 2011. The main scientific objective of DAMPE is to detect electrons and photons in the range of 5 GeV-10 TeV with unprecedented energy resolution (1.5% at 100 GeV) in order to identify possible Dark Matter (DM) signatures. It will also measure the flux of nuclei up to above 500TeV with excellent energy resolution (40% at 800GeV), which will bring new insights to the origin and propagation high energy cosmic rays. With its excellent photon detection capability, the DAMPE mission is well placed for new discoveries in high energy-ray astronomy as well.

第 60 条，共 222 条

中国空间站的高能宇宙辐射探测设施

张双南 徐明 董永伟 *常进*

期: 432 页 7-16

Space science

大量的天文观测证据表明，暗物质不但存在，而且主导宇宙的物质分布。但是目前人类对于暗

物质粒子的性质还几乎一无所知，关键就在于还没有探测到暗物质粒子，这是人类对宇宙认识的重大缺憾之一。现代物理学理论的有些模型预言了种类繁多的候选暗物质粒子，但是无法明确说明哪种粒子就是暗物质粒子，所以最终探测到并且测量暗物质粒子的性质将能够对于基础物理学理论的发展起到巨大的推动作用。根据不同的理论模型所预测的暗物质粒子的性质，对于这些候选暗物质粒子有不同的探测和搜寻手段。最近几年的地下、地面和空间暗物质探测对暗物质粒子的性质给出了一些约束、甚至有一些探测到的迹象，但是暗物质粒子存在的可靠证据仍然十分缺乏，使得暗物质粒子的探测成为国际科学前沿竞争最为激烈的研究领域。国际上不断有各种各样新的暗物质粒子探测或者搜寻的实验投入运行或者部署中，尤其是"国际空间站"已经成为国际上最重要的通过探测高能宇宙辐射探测和搜寻暗物质的国际实验室，而且其规模正在迅速地大幅度扩展。中国科学家利用后发优势，制定了中国的空间暗物质搜寻路线图，规划了两个实验，一个是正在建造的"暗物质粒子探测卫星"(DAMPE)，另外一个就是将在中国空间站部署的高能宇宙辐射探测设施(HERD)，这两个实验的先后实施将使中国在这个领域保持领先并且做出重大科学发现，这是中国科学界的一个重大机遇。毫无疑问，HERD 实验将成为中国空间站的标志性实验。

II. Antarctic Astronomy Radio Astronomy

Stellar Structure, Evolution and Pulsation

第 61 条 , 共 222 条

Nsvs4484038, A Contact Binary System At The Short-Period Cutoff

Zhang, XB (Zhang, X. B.); Deng, LC (Deng, L. C.); Wang, K (Wang, K.); Yan, ZZ (Yan, Z. Z.); Tian, JF (Tian, J. F.); Peng, YJ (Peng, Y. J.); Pan, Y (Pan, Y.); Luo, ZQ (Luo, Z. Q.); *Sun, JJ* (Sun, J. J.); Liu, QL (Liu, Q. L.); Xin, HQ (Xin, H. Q.); Zhou, Q (Zhou, Q.)

ASTRONOMICAL JOURNAL

卷: 148 期: 3 文献号: 40

We present a photometric study of the short-period eclipsing binary NSVS4484038. Time-series CCD photometry of the star in the B and V band was carried out. An orbital period of 0.218551 days was determined for the eclipsing binary and a revised linear ephemeris was given. The first photometric solution of the binary system was detected through light-curve synthesis using the Wilson Devinney method. It reveals an overcontact configuration for the system with a filling-out factor of about 10%. The mass ratio was determined to be 2.74 with an inclination of 72 degrees.1 The less massive secondary component is found to have a higher surface temperature than the primary by about 90 K, indicating that NSVS4484038 could be a contact system of W subtype. The star is then identified to be a new member of W UMa systems at the short-period cutoff. Comparisons with known contact binaries at the short-period cutoff, the properties, and the evolutionary status of the binary system are discussed.

第 62 条 , 共 222 条

Dependence Of Pulsation Stability On Helium Abundance Of Stellar Convection Envelope

Xiong DR; Deng Licai; Wang kun

卷: 55 期: 4 页: 279-287

Acta Astronomica Sinica

By using a non-local and time-dependent theory of convection, the linear non-adiabatic oscillations of radial and low-degree nonradial F-p8 modes for the evolutionary models in the mass range of 1.4-3.0 M⊙ and with three helium abundances of convective envelope (Y=0.28, 0.13, 0.00; Z=0.02) are calculated. The numerical results show that the red edge of theoretical delta Scuti instability strip almost does not change with the helium abundance. The blue edge of delta Scuti instability strip moves towards low temperature. With decrease of helium abundance, the high-temperature stars on the hot side of instability strip become more stable, and the low-temperature stars on the cold side of instability strip become more unstable. It seems impossible to explain the nonvariable stars in delta Scuti strip by using diffusion of helium. However, the ratios of nonvariable stars to variable stars in the hot and cold sides of the delta Scuti strip may be as an observational evidence of helium diffusion.

Center for Antarctic Astronomy

第 63 条 , 共 222 条

Variability Of The Giant X-Ray Bump In GRB 121027A And Its Possible Origin

Hou, SJ (Hou, Shu-Jin); Gao, H (Gao, He); Liu, T (Liu, Tong); Gu, WM (Gu, Wei-Min); Lin, DB (Lin, Da-Bin); Li, YP (Li, Ya-Ping); Men, YP (Men, Yun-Peng); Wu, XF (Wu, Xue-Feng); Lei, WH (Lei,

Wei-Hua); Lu, JF (Lu, Ju-Fu)
MONTHLY NOTICES OF THE ROYAL ASTRONOMICAL SOCIETY

卷: 441 期: 3 页: 2375-2379

The giant X-ray bump of GRB 121027A observed by Swift is different from the typical X-ray flares in gamma-ray bursts. The observed structural variability in the rise and decay phases of the bump has four components. Of these four components, only the data in the bump from about 5300 to about 6100 s is of good enough quality to be analysed using the stepwise filter correlation method. A 86(-9.4)(+5.9)s periodic oscillation is postulated, which is confirmed by the Lomb-Scargle method. A jet precession model is proposed to account for this variability.

第 64 条，共 222 条

A Comparison Of Cosmological Models Using Time Delay Lenses

Wei, JJ (Wei, Jun-Jie); Wu, XF (Wu, Xue-Feng); Melia, F (Melia, Fulvio)
ASTROPHYSICAL JOURNAL

卷: 788 期: 2 文献号: 190

The use of time-delay gravitational lenses to examine the cosmological expansion introduces a new standard ruler with which to test theoretical models. The sample suitable for this kind of work now includes 12 lens systems, which have thus far been used solely for optimizing the parameters of ACDM. In this paper, we broaden the base of support for this new, important cosmic probe by using these observations to carry out a one-on-one comparison between competing models. The currently available sample indicates a likelihood of similar to 70%-80% that the R-h = ct universe is the correct cosmology versus similar to 20%-30% for the standard model. This possibly interesting result reinforces the need to greatly expand the sample of time-delay lenses, e.g., with the successful implementation of the Dark Energy Survey, the VST ATLAS survey, and the Large Synoptic Survey Telescope. In anticipation of a greatly expanded catalog of time-delay lenses identified with these surveys, we have produced synthetic samples to estimate how large they would have to be in order to rule out either model at a similar to 99.7% confidence level. We find that if the real cosmology is ACDM, a sample of similar to 150 time-delay lenses would be sufficient to rule out R-h = ct at this level of accuracy, while similar to 1000 time-delay lenses would be required to rule out ACDM if the real universe is instead R-h = ct. This difference in required sample size reflects the greater number of free parameters available to fit the data with ACDM.

第 65 条，共 222 条

Color-Magnitude Distribution Of Face-On Nearby Galaxies In Sloan Digital Sky Survey Dr7

Jin, SW (Jin, Shuo-Wen); Gu, QS (Gu, Qiusheng); Huang, S (Huang, Song); Shi, Y (Shi, Yong); Feng, LL (Feng, Long-Long)
ASTROPHYSICAL JOURNAL

卷: 787 期: 1 文献号: 63

We have analyzed the distributions in the color-magnitude diagram (CMD) of a large sample of face-on galaxies to minimize the effect of dust extinctions on galaxy color. About 300,000 galaxies with log(a/b) < 0.2 and redshift z < 0.2 are selected from the Sloan Digital Sky Survey DR7 catalog. Two methods are employed to investigate the distributions of galaxies in the CMD, including one-dimensional (1D) Gaussian fitting to the distributions in individual magnitude bins and two-dimensional (2D) Gaussian mixture model (GMM) fitting to galaxies as a whole. We find that in the 1D fitting, two Gaussians are not enough to fit galaxies with the excess present between the blue cloud and the red sequence. The fitting to this excess defines the center of the green valley in the local universe to be (u -r) (0.1) = -0.121M(r, 0.1)-0.061. The fraction of blue cloud and red sequence galaxies turns over around M-r,M- 0.1 similar to -20.1 mag, corresponding to stellar mass of 3 x 10(10) M-circle dot . For the 2D GMM fitting, a total of four Gaussians are required, one for the blue cloud, one for the red sequence, and the additional two for the green valley. The fact that two Gaussians are needed to describe the distributions of galaxies in the green valley is consistent with some models that argue for two different evolutionary paths from the blue cloud to the red sequence.

第 66 条，共 222 条

The Origin Of The Plateau And Late Rebrightening In The Afterglow Of Grb 120326a

Hou, SJ (Hou, S. J.); Geng, JJ (Geng, J. J.); Wang, K (Wang, K.); Wu, XF (Wu, X. F.); Huang, YF (Huang, Y. F.); Dai, ZG (Dai, Z. G.); Lu, JF (Lu, J. F.)

ASTROPHYSICAL JOURNAL

卷: 785 期: 2 文献号: 113

GRB 120326A is an unusual gamma-ray burst (GRB) that has a long plateau and a very late rebrightening in both X-ray and optical bands. The similar behavior of the optical and X-ray light curves suggests that they may share a common origin. The long plateau starts at several hundred seconds and ends at tens of thousands of seconds, and the peak time of the late rebrightening is about 30,000 s. We analyze the energy injection model by means of numerical and analytical solutions, considering both the wind environment and the interstellarmedium environment for GRB afterglows. We particularly study the influence of the injection starting time, ending time, stellar wind density (or density of the circumburst environment), and injection luminosity on the shape of the afterglow light curves, respectively. In the wind model, we find that the light curve is largely affected by the parameters and that there is a "bump" in the late stage. In the wind environment, we found that the longer the energy is injected, the more obvious the rebrightening will be. We also find that the peak time of the bump is determined by the stellar wind density. We use the late continuous injection model to interpret the unusual afterglow of GRB 120326A. The model fits the observational data well; however, we find that the timescale of the injection must be higher than 10,000 s, which implies that the timescale of the central engine activity must also be more than 10,000 s. This information can give useful constraints on the central engines of GRBs-we consider a newborn millisecond pulsar with a strong magnetic field to be the central engine. On the other hand, our results suggest that the circumburst environment of GRB 120326A is very likely a stellar wind.

第 67 条 , 共 222 条

Cosmological Tests Using Gamma-Ray Bursts, The Star Formation Rate And Possible Abundance Evolution

Wei, JJ (Wei, Jun-Jie); Wu, XF (Wu, Xue-Feng); Melia, F (Melia, Fulvio); Wei, DM (Wei, Da-Ming); Feng, LL (Feng, Long-Long)

MONTHLY NOTICES OF THE ROYAL ASTRONOMICAL SOCIETY

卷: 439 期: 4 页: 3329-3341

The principal goal of this paper is to use attempts at reconciling the Swift long gamma-ray bursts (LGRBs) with the star formation history (SFH) to compare the predictions of Lambda cold dark matter (Lambda CDM) with those in the R-h = ct Universe. In the context of the former, we confirm that the latest Swift sample of GRBs reveals an increasing evolution in the GRB rate relative to the star formation rate (SFR) at high redshifts. The observed discrepancy between the GRB rate and the SFR may be eliminated by assuming a modest evolution parametrized as (1 + z)(0.8) - perhaps indicating a cosmic evolution in metallicity. However, we find a higher metallicity cut of Z = 0.52 Z(circle dot) than was seen in previous studies, which suggested that LGRBs occur preferentially in metal-poor environments, i.e. Z similar to 0.1-0.3 Z(circle dot). We use a simple power-law approximation to the high-z (greater than or similar to 3.8) SFH, i.e. R-SF proportional to [(1 + z)/4.8](alpha), to examine how the high-z SFR may be impacted by a possible abundance evolution in the Swift GRB sample. For an expansion history consistent with Lambda CDM, we find that the Swift redshift and luminosity distributions can be reproduced with reasonable accuracy if alpha = -2.41(-2.09)(+1.87). For the R-h = ct Universe, the GRB rate is slightly different from that in Lambda CDM, but also requires an extra evolutionary effect, with a metallicity cut of Z = 0.44 Z(circle dot). Assuming that the SFR and GRB rate are related via an evolving metallicity, we find that the GRB data constrain the slope of the high-z SFR in R-h = ct to be alpha = -3.60(-2.45)(+2.45). Both cosmologies fit the GRB/SFR data rather well. However, in a one-on-one comparison using the Akaike information criterion, the best-fitting R-h = ct model is statistically preferred over the best-fitting Lambda CDM model with a relative probability of similar to 70 per cent versus

similar to 30 per cent.

第 68 条，共 222 条

Planetary Transit Candidates In The Cstar Field: Analysis Of The 2008 Data

Wang, SH (Wang, Songhu); Zhang, H (Zhang, Hui); Zhou, JL (Zhou, Ji-Lin); Zhou, X (Zhou, Xu); Yang, M (Yang, Ming); *Wang, LF* (Wang, Lifan); Bayliss, D (Bayliss, D.); Zhou, G (Zhou, G.); Ashley, MCB (Ashley, M. C. B.); Fan, Z (Fan, Zhou); Feng, LL (Feng, Long-Long); Gong, XF (Gong, Xuefei); Lawrence, JS (Lawrence, J. S.); Liu, HG (Liu, Huigen); Liu, Q (Liu, Qiang); Luong-Van, DM (Luong-Van, D. M.); Ma, J (Ma, Jun); Meng, ZY (Meng, Zeyang); Storey, JWV (Storey, J. W. V.); Wittenmyer, RA (Wittenmyer, R. A.); Wu, ZY (Wu, Zhenyu); Yan, J (Yan, Jun); Yang, HG (Yang, Huigen); Yang, J (Yang, Ji); Yang, JY (Yang, Jiayi); Yuan, XY (Yuan, Xiangyan); Zhang, TM (Zhang, Tianmeng); Zhu, ZX (Zhu, Zhenxi); Zou, H (Zou, Hu)
ASTROPHYSICAL JOURNAL SUPPLEMENT SERIES
卷: 211 期: 2 文献号: 26

The Chinese Small Telescope ARray (CSTAR) is a group of four identical, fully automated, static 14.5 cm telescopes. CSTAR is located at Dome A, Antarctica and covers 20 deg(2) of sky around the South Celestial Pole. The installation is designed to provide high-cadence photometry for the purpose of monitoring the quality of the astronomical observing conditions at Dome A and detecting transiting exoplanets. CSTAR has been operational since 2008, and has taken a rich and high-precision photometric data set of 10,690 stars. In the first observing season, we obtained 291,911 qualified science frames with 20 s integrations in the i band. Photometric precision reaches similar to 4 mmag at 20 s cadence at i = 7.5 and is similar to 20 mmag at i = 12. Using robust detection methods, 10 promising exoplanet candidates were found. Four of these were found to be giants using spectroscopic follow-up. All of these transit candidates are presented here along with the discussion of their detailed properties as well as the follow-up observations.

第 69 条，共 222 条

Cold Stream Stability During Minor Mergers

Wang, L (Wang, Liang); Zhu, WS (Zhu, Weishan); Feng, LL (Feng, Long-Long); Maccio, AV (Maccio, Andrea V.); Chang, J (Chang, Jiang); Kang, X (Kang, Xi)
MONTHLY NOTICES OF THE ROYAL ASTRONOMICAL SOCIETY
卷: 439 期: 1 页: L85-L89

We use high-resolution Eulerian simulations to study the stability of cold gas flows in a galaxy size dark matter halo (10(12) M-circle dot) at redshift z = 2. Our simulations show that a cold stream penetrating a hot gaseous halo is stable against thermal convection and Kelvin-Helmholtz instability. We then investigate the effect of a satellite orbiting the main halo in the plane of the stream. The satellite is able to perturb the stream and to inhibit cold gas accretion towards the centre of the halo for 0.5 Gyr. However, if the supply of cold gas at large distances is kept constant, the cold stream is able to re-establish itself after 0.3 Gyr. We conclude that cold streams are very stable against a large variety of internal and external perturbations.

第 70 条，共 222 条

Gamma-Ray Burst Prompt Emission Light Curves And Power Density Spectra In The Icmart Model

Zhang, B (Zhang, Bo); Zhang, B (Zhang, Bing)
ASTROPHYSICAL JOURNAL
卷: 782 期: 2 文献号: 92

In this paper, we simulate the prompt emission light curves of gamma-ray bursts (GRBs) within the framework of the Internal-Collision-induced MAgnetic Reconnection and Turbulence (ICMART) model. This model applies to GRBs with a moderately high magnetization parameter sigma in the emission region. We show that this model can produce highly variable light curves with both fast and slow components. The rapid variability is caused by many locally Doppler-boosted mini-emitters due to turbulent magnetic reconnection in a moderately high s flow. The runaway growth and subsequent depletion of these mini-emitters as a function of time define a broad slow component for each ICMART event. A GRB light curve is usually composed of multiple ICMART events that are fundamentally driven by the erratic GRB central engine activity. Allowing variations of the model parameters, one is able

to reproduce a variety of light curves and the power density spectra as observed.

第 71 条，共 222 条

Sky Brightness Values In The SDSS G And R Bands At The Dome A Of The Antarctica In 2009

Zong Weikai; Fu Jianning; Niu Jiashu; Ashley Michael C B; Gong Xuefei; Lawrence Jon S; Liu Qiang; Luong-Van Daniel; Pennypacker Carl R; Storey John W V; Wang Lingzhi; *Wang Lifan*; Yang Huigen; Yuan Xiangyan; York Donald G; Zhu Zhenxi

卷: 11 期: 1 页: 89-94

Astronomical Research & Technology

For an astronomical observation site its sky brightness is among the most important factors for observation. In this paper we investigate the sky brightness values in the SDSS g and r bands at the Dome A on the Antarctica Plateau by using the data collected with the Chinese Small Telescope Array (CSTAR) during the winter of 2009. There are 251310 and 536383 image frames in the g and r bands, respectively. These frames correspond to total exposures of 969 hours and 2349 hours, respectively. In the data reduction we use two super-flat images combined from images taken at the Dome A,and use two bias images taken at the Xinglong Station of the National Astronomical Observatories of China. Variations of the sky brightness at the Dome A are mainly caused by changes in the solar elevation angle and the lunar phase. The CSTAR worked for a shorter time in the g band than in the r band. Nearly half of all images in the g band were taken when the sun was far below the horizon at the Dome A. The results show that in 74% of the g-band images and 91% of the r-band images sky brightness values are less than 100ADU/s. In less than 20% of the g-band images and less than 2% of the r-band images sky brightness values are over 300ADU/ s. The median sky brightness values are 40ADU/s in the g-band and 28ADU/s in the r-band in the entire 2009 observational duty cycle of the CSTAR. Since most pixels in an image are in the sky region,the median values of the sky brightness values (in ADU per pixel) are evaluated using all the pixel values in the images. We use calibrated g- and r-band magnitudes of stars in the TYCHO catalog for photometric calibration. We have derived the zero points, g_0 =3.76 0.07mag and r_0= 3.940. 06mag for the g and r bands ，respectively, based on 12 of the brightest stars in the field of view of the CSTAR. Using the definition of the instrumental magnitudes in the CSTAR photometric system, a pixel size of 15 arcsec, and the zero points, we transform the sky brightness values in ADU/s into magnitudes. We do not consider the atmospheric extinctions since they are less than the errors of the zero points in clear photometric nights. We conclude that the median sky brightness values are 19.9mag/arcsec~2 in the g band and 20.1mag/arcsec~2 in the r band in the entire 2009 observational duty cycle of the CSTAR.

第 72 条，共 222 条

The Optical Luminosity Function Of Gamma-Ray Bursts Deduced From Rotse-Iii Observations

Cui, XH (Cui, X. H.); Wu, XF (Wu, X. F.); Wei, JJ (Wei, J. J.); Yuan, F (Yuan, F.); Zheng, WK (Zheng, W. K.); Liang, EW (Liang, E. W.); Akerlof, CW (Akerlof, C. W.); Ashley, MCB (Ashley, M. C. B.); Flewelling, HA (Flewelling, H. A.); Gogus, E (Gogus, E.); Guver, T (Guver, T.); Kiziloglu, U (Kiziloglu, U.); Mckay, TA (Mckay, T. A.); Pandey, SB (Pandey, S. B.); Rykoff, ES (Rykoff, E. S.); Rujopakarn, W (Rujopakarn, W.); Schaefer, BE (Schaefer, B. E.); Wheeler, JC (Wheeler, J. C.); Yost, SA (Yost, S. A.)

ASTROPHYSICAL JOURNAL

卷: 795 期: 2 文献号: 103

We present the optical luminosity function (LF) of gamma-ray bursts (GRBs) estimated from a uniform sample of 58 GRBs from observations with the Robotic Optical Transient Search Experiment III (ROTSE-III). Our GRB sample is divided into two sub-samples: detected afterglows (18 GRBs) and those with upper limits (40 GRBs). We derive R-band fluxes for these two sub-samples 100 s after the onset of the burst. The optical LFs at 100 s are fitted by assuming that the co-moving GRB rate traces the star formation rate. While fitting the optical LFs using Monte Carlo simulations, we take into account the detection function of ROTSE-III. We find that the cumulative distribution of optical emission at 100 s is well described by an exponential rise and power-law decay, a broken power law, and Schechter LFs. A single

power-law (SPL) LF, on the other hand, is ruled out with high confidence.

第 73 条，共 222 条

Photosphere Emission In The X-Ray Flares Of Swift Gamma-Ray Bursts And Implications For The Fireball Properties

Peng, FK (Peng, Fang-Kun); Liang, EW (Liang, En-Wei); Wang, XY (Wang, Xiang-Yu); *Hou, SJ* (Hou, Shu-Jin); Xi, SQ (Xi, Shao-Qiang); Lu, RJ (Lu, Rui-Jing); Zhang, J (Zhang, Jin); Zhang, B (Zhang, Bing)

ASTROPHYSICAL JOURNAL

卷: 795 期: 2 文献号: 155

X-ray flares of gamma-ray bursts (GRBs) are usually observed in the soft X-ray range and the spectral coverage is limited. In this paper, we present an analysis of 32 GRB X-ray flares that are simultaneously observed by both Burst Alert Telescope and X-Ray Telescope on board the Swift mission, so that a joint spectral analysis with a wider spectral coverage is possible. Our results show that the joint spectra of 19 flares are fitted with the absorbed single power law or the Band function models. More interestingly, the joint spectra of the other 13 X-ray flares are fitted with the absorbed single power-law model plus a blackbody component. Phenomenally, the observed spectra of these 13 flares are analogous to several GRBs with a thermal component, but only with a much lower temperature of kT = 1 similar to 3 keV. Assuming that the thermal emission is the photosphere emission of the GRB fireball, we derive the fireball properties of the 13 flares that have redshift measurements, such as the bulk Lorentz factor Gamma(ph) of the outflow. The derived Gamma(ph) range from 50 to 150 and a relation of Gamma(ph) to the thermal emission luminosity is found. It is consistent with the Gamma(0) - L-iso relations that are derived for the prompt gamma-ray emission. We discuss the physical implications of these results within the content of jet composition and the radiation mechanism of GRBs and X-ray flares.

第 74 条，共 222 条

Distributions Of Gamma-Ray Bursts And Blazars In The L-P-E-P-Plane And Possible Implications For Their Radiation Physics

Lyu, F (Lyu, Fen); Liang, EW (Liang, En-Wei); Liang, YF (Liang, Yun-Feng); Wu, XF (Wu, Xue-Feng); Zhang, J (Zhang, Jin); Sun, XN (Sun, Xiao-Na); Lu, RJ (Lu, Rui-Jing); Zhang, B (Zhang, Bing)

ASTROPHYSICAL JOURNAL

卷: 793 期: 1 文献号: 36

We present a spectral analysis for a sample of redshift-known gamma-ray bursts (GRBs) observed with Fermi/GBM. Together with the results derived from our systematical spectral energy distribution modeling with the leptonic models for a Fermi/LAT blazar sample, we compare the distributions of the GRBs and the blazars by plotting the synchrotron peak luminosity (L-s) and the corresponding peak photon energy E-s of blazars in the L-p-E-p-plane of GRBs, where L-p and E-p are the peak luminosity and peak photon energy of the GRB time-integrated nu f(nu) spectrum, respectively. The GRBs are in the high-L-p, high-E-p corner of the plane and a tight L-p-E-p relation is found, i.e., L-p alpha E-p(2.13-0.46) (+0.54). Both flat spectrum radio quasars (FSRQs) and low-synchrotron peaking BL Lac objects (LBLs) are clustered in the low-Ep, low-Lp corner. Intermediate-and high-synchrotron peaking BL Lac objects (IBLs and HBLs) have E-s similar to 2 x 10(-3)-10(2) keV and L-s similar to 10(44)-10(47) erg s(-1), but no dependence of L-s on E-s is found. We show that the tight L-p-E-p relation of GRBs is potentially explained with the synchrotron radiation of fast-cooling electrons in a highly magnetized ejecta, and the weak anti-correlation of L-s-E-s for FSRQs and LBLs may be attributed to synchrotron radiation of slow-cooling electrons in a moderately magnetized ejecta. The distributions of IBLs and HBLs in the L-p-E-p-plane may be interpreted with synchrotron radiation of fast-cooling electrons in a matter-dominated ejecta. These results may present a unified picture for the radiation physics of relativistic jets in GRBs and blazars within the framework of the leptonic synchrotron radiation models.

第 75 条，共 222 条

Revisiting The Emission From Relativistic Blast Waves In A Density-Jump Medium

Geng, JJ (Geng, J. J.); *Wu, XF* (Wu, X. F.); Li, L (Li, Liang); Huang, YF (Huang, Y. F.); Dai, ZG (Dai, Z. G.)

ASTROPHYSICAL JOURNAL

卷: 792 期: 1 文献号: 31

Re-brightening bumps are frequently observed in gamma-ray burst afterglows. Many scenarios have been proposed to interpret the origin of these bumps, of which a blast wave encountering a density-jump in the circumburst environment has been questioned by recent works. We develop a set of differential equations to calculate the relativistic outflow encountering the density-jump by extending the work of Huang et al. This approach is a semi-analytic method and is very convenient. Our results show that late high-amplitude bumps cannot be produced under common conditions, rather only a short plateau may emerge even when the encounter occurs at an early time (< 10(4) s). In general, our results disfavor the density-jump origin for those observed bumps, which is consistent with the conclusion drawn from full hydrodynamics studies. The bumps thus should be caused by other scenarios.

第 76 条，共 222 条

Matched Filter Optimization Of Ksz Measurements With A Reconstructed Cosmological Flow Field

Li, M (Li, Ming); Angulo, RE (Angulo, R. E.); White, SDM (White, S. D. M.); Jasche, J (Jasche, J.)

MONTHLY NOTICES OF THE ROYAL ASTRONOMICAL SOCIETY

卷: 443 期: 3 页: 2311-2326

We develop and test a new statistical method to measure the kinematic Sunyaev-Zel'dovich (kSZ) effect. A sample of independently detected clusters is combined with the cosmic flow field predicted from a galaxy redshift survey in order to derive a matched filter that optimally weights the kSZ signal for the sample as a whole given the noise involved in the problem. We apply this formalism to realistic mock microwave skies based on cosmological N-body simulations, and demonstrate its robustness and performance. In particular, we carefully assess the various sources of uncertainty, cosmic microwave background primary fluctuations, instrumental noise, uncertainties in the determination of the velocity field, and effects introduced by miscentring of clusters and by uncertainties of the mass-observable relation (normalization and scatter). We show that available data (Planck maps and the MaxBCG catalogue) should deliver a 7.7 sigma detection of the kSZ. A similar cluster catalogue with broader sky coverage should increase the detection significance to similar to 13 sigma. We point out that such measurements could be binned in order to study the properties of the cosmic gas and velocity fields, or combined into a single measurement to constrain cosmological parameters or deviations of the law of gravity from General Relativity.

第 77 条，共 222 条

Meteorological Data For The Astronomical Site At Dome A, Antarctica

Hu, Y (Hu, Yi); Shang, ZH (Shang, Zhaohui); Ashley, MCB (Ashley, Michael C. B.); Bonner, CS (Bonner, Colin S.); Hu, KL (Hu, Keliang); Liu, Q (Liu, Qiang); Li, YS (Li, Yuansheng); Ma, B (Ma, Bin); Wang, LF (Wang, Lifan); Wen, HK (Wen, Haikun)

PUBLICATIONS OF THE ASTRONOMICAL SOCIETY OF THE PACIFIC

卷: 126 期: 943 页: 868-881

We present an analysis of the meteorological data collected at Dome A, Antarctica by the Kunlun Automated Weather Station, including temperatures and wind speeds at eight elevations above the snow surface between 0 m and 14.5 m. The average temperatures at 2 m and 14.5 m are -54 degrees C and -46 degrees C, respectively. We find that a strong temperature inversion existed at all heights for more than 70% of the time, and the temperature inversion typically lasts longer than 25 hr, indicating an extremely stable atmosphere. The temperature gradient is larger at lower elevations than at higher elevations. The average wind speed was 1.5 ms(-1) at 4 m elevation. We find that the temperature inversion is stronger when the wind speed is lower, and the temperature gradient decreases sharply at a specific wind speed for each elevation. The strong temperature inversion and low wind speed

result in a shallow and stable boundary layer with weak atmospheric turbulence above it, suggesting that Dome A should be an excellent site for astronomical observations. All the data from the weather station are available for download.

第 78 条，共 222 条

The High Energy Cosmic-Radiation Detection (HERD) Facility Onboard China's Space Station

S. N. Zhang，O. Adriani，S. Albergo，*Chang,J*，范一中

卷: 9144 期: 1 页: 9144-9144

Proceedings of the SPIE 会议论文

The High Energy cosmic-Radiation Detection (HERD) facility is one of several space astronomy payloads of the cosmic lighthouse program onboard China's Space Station, which is planned for operation starting around 2020 for about 10 years. The main scientific objectives of HERD are indirect dark matter search, precise cosmic ray spectrum and composition measurements up to the knee energy, and high energy gamma-ray monitoring and survey. HERD is composed of a 3-D cubic calorimeter (CALO) surrounded by microstrip silicon trackers (STKs) from five sides except the bottom. CALO is made of about 10 4 cubes of LYSO crystals, corresponding to about 55 radiation lengths and 3 nuclear interaction lengths, respectively. The top STK microstrips of seven X-Y layers are sandwiched with tungsten converters to make precise directional measurements of incoming electrons and gamma-rays. In the baseline design, each of the four side SKTs is made of only three layers microstrips. All STKs will also be used for measuring the charge and incoming directions of cosmic rays, as well as identifying back scattered tracks. With this design, HERD can achieve the following performance: energy resolution of 1% for electrons and gamma-rays beyond 100 GeV, 20% for protons from 100 GeV to 1 PeV; electron/proton separation power better than 10 -5 ; effective geometrical factors of >3 m 2 sr for electron and diffuse gamma-rays, >2 m 2 sr for cosmic ray nuclei. R and D is under way for reading out the LYSO signals with optical fiber coupled to image intensified CCD and the prototype of one layer of CALO. 漏 (2014) COPYRIGHT Society of Photo-Optical Instrumentation Engineers (SPIE). Downloading of the abstract is permitted for personal use only.

第 79 条，共 222 条

GRB 130427A/SN 2013cq And The Gamma-Ray Burst/Supernova Associations

Wang Shanqin; Dai Zigao; *Wu Xuefeng*

卷: 32 期: 4 页: 481-515

Progress in Astronomy

Eleven gamma-ray burst (GRB)/supernova (SN) associations have been identified since the first possible connection between GRB 980425 and SN 1998bw was discovered in April 1998. The most recent association is GRB 130831A/SN 2013fu which was identified in September 2013. By studying these GRB/SN associations in details, our understanding of GRBs as well as type Ic SNe has been greatly deepened, and the study of the evolution, death as well as explosion of massive stars has been advanced. The observations and analysis of their multi-band afterglows and supernova spectra have gradually unveiled the GRB/SN central engines. GRB 130427A is the only-known unique energetic and luminous GRB discovered in the local universe. The GeV gamma-ray emission of GRB 130427A challenges current GRB radiation mechanisms. The bright optical flash from GRB 130427A provides valuable clues about the nature of the explosion. The kinetic energy of SN 2013cq accompanied GRB 130427A is one of the largest kinetic energy of all SNe associated with GRBs. The non-detection of neutrinos from GRB 130427A/SN 2013cq can put useful constraint on the models for GRB prompt emission. In this review, we summarize the important observational properties of GRB 130427A/SN 2013cq, which are very valuable for exploring the nature of GRB-SN association and the detailed properties of the prompt and afterglow emission.

第 80 条，共 222 条

中国南极昆仑站天文台

Liu,L Wu,XF

卷: 26 期: 5 页: 60-64

现代物理知识

南极,位于地球最南端,也叫"第七大陆",是人类最后到达的大陆。这里无定居居民,仅有一些来自于其他大陆国家的科学考察人员。根据 1961 年 6 月通过的《国际南极条约》规定,南极不属于任何一个国家,它属于全人类,只用于和平目的。

第 81 条，共 222 条

A Double Neutron Star Merger Origin For The Cosmological Relativistic Fading Source Ptf11agg?

Wu, XF (Wu, Xue-Feng); Gao, H (Gao, He); Ding, X (Ding, Xuan); Zhang, B (Zhang, Bing); Dai, ZG (Dai, Zi-Gao); Wei, JY (Wei, Jian-Yan)
ASTROPHYSICAL JOURNAL LETTERS

卷: 781 期: 1 文献号: L10

The Palomar Transient Factory (PTF) team recently reported the discovery of a rapidly fading optical transient source, PTF11agg. A long-lived scintillating radio counterpart was identified, but the search for a high-energy counterpart showed negative results. The PTF team speculated that PTF11agg may represent a new class of relativistic outbursts. Here we suggest that a neutron star (NS)-NS merger system with a supra-massive magnetar central engine could be a possible source to power such a transient, if our line of sight is not on the jet axis direction of the system. These systems are also top candidates for gravitational wave sources to be detected in the advanced LIGO/Virgo era. We find that the PTF11agg data could be explained well with such a model, suggesting that at least some gravitational wave bursts due to NS-NS mergers may be associated with such a bright electromagnetic counterpart without a gamma-ray trigger.

第 82 条，共 222 条

An Estimation Of Local Bulk Flow With The Maximum-Likelihood Method

Ma, YZ (Ma, Yin-Zhe); *Pan, J* (Pan, Jun)
MONTHLY NOTICES OF THE ROYAL ASTRONOMICAL SOCIETY

卷: 437 期: 2 页: 1996-2004

A maximum-likelihood method, tested as an unbiased estimator from numerical simulations, is used to estimate cosmic bulk flow from peculiar velocity surveys. The likelihood function is applied to four observational catalogues (ENEAR, SFI++, A1SN and SC) constructed from galaxy peculiar velocity surveys and Type Ia supernovae data at low redshift (z <= 0.03). We find that the Spiral Field I-band catalogue constrains the bulk flow to be V = 290 +/- 30 km s(-1) towards l = 281 degrees +/- 7 degrees, b = 8 degrees(+ 6 degrees)(-5 degrees) on effective scales of 58 h(-1) Mpc, which is the tightest constraints achievable at the present time. By comparing the amplitudes of our estimated bulk flows with theoretical prediction, we find excellent agreement between the two. In addition, directions of estimated bulk flows are also consistent with measurements in other studies.

第 83 条，共 222 条

Optically Selected BLR-Less Active Galactic Nuclei From The SDSS Stripe82 Database - I. The Sample

Zhang, XG (Zhang, Xue-Guang)
MONTHLY NOTICES OF THE ROYAL ASTRONOMICAL SOCIETY

卷: 438 期: 1 页: 557-572

This is the first paper in a dedicated series to study the properties of the optically-selected broad-line-region-less (BLR-less) active galactic nuclei (AGNs; with no-hidden central broad emission line regions). We carried out a systematic search for the BLR-less AGNs through the Sloan Digital Sky Survey Legacy Survey (SDSS Stripe82 Database). Based on the spectral decomposition results for all the 136 676 spectroscopic objects (galaxies and quasars) with redshift less than 0.35 covered by the SDSS Stripe82 region, our spectroscopic sample for the BLR-less AGNs includes 22 693 pure narrow line objects without broad emission lines but with apparent AGN continuum emission R-AGN > 0.3 and apparent stellar lights R-ssp > 0.3. Then, using the properties of the photometry magnitude RMS (RMS) and Pearson's coefficients (R-1,R- 2) between two different SDSS band light curves: RMSk > 3 x RMSMk and R-1,R- 2 > similar to 0.8, the final 281 pure narrow line objects with true photometry variabilities are our selected reliable candidates for the BLR-less AGNs. The selected candidates

with higher confidence levels not only have the expected spectral features of the BLR-less AGNs, but also show significant true photometry variabilities. The reported sample enlarges at least four times the current sample of the BLR-less AGNs, and will provide more reliable information to explain the lack of the BLRs of AGNs in our following studies.

第 84 条，共 222 条

Relationship Between The Kinetic Power And Bolometric Luminosity Of Jets: Limitation From Black Hole X-Ray Binaries, Active Galactic Nuclei, And Gamma-Ray Bursts

Ma, RY (Ma, Renyi); Xie, FG (Xie, Fu-Guo); *Hou, SJ* (Hou, Shujin)
ASTROPHYSICAL JOURNAL LETTERS
卷: 780 期: 1 文献号: L14

The correlation between the kinetic power P-jet and intrinsic bolometric luminosity L-jet of jets may reveal the underlying jet physics in various black hole systems. Based on the recent work by Nemmen et al., we re-investigate this correlation with additional sources of black hole X-ray binaries (BXBs) in hard/quiescent states and low-luminosity active galactic nuclei (LLAGNs). The new sample includes 29 sets of data from 7 BXBs and 20 LLAGNs, with P-jet and L-jet being derived from spectral modeling of the quasi-simultaneous multi-band spectra under the accretion jet scenario. Compared to previous works, the range of luminosity is now enlarged to more than 20 decades, i.e., from similar to 10(31) erg s(-1) to similar to 10(52) erg s(-1), which allows for better constraining of the correlation. One notable result is that the jets in BXBs and LLAGNs almost follow the same P-jet-L-jet correlation that was obtained from blazars and gamma-ray bursts. The slope indices we derived are 1.03+/-0.01 for the whole sample, 0.85+/-0.06 for the BXB subsample, 0.71+/-0.11 for the LLAGN subsample, and 1.01+/-0.05 for the LLAGN-blazar subsample, respectively. The correlation index around unit implies the independence of jet efficiency on the luminosity or kinetic power. Our results may further support the hypothesis that similar physical processes exist in the jets of various black hole systems.

第 85 条，共 222 条

Time Evolution Of Flares In Grb 130925a: Jet Precession In A Black Hole Accretion System

Hou, SJ (Hou, Shu-Jin); Liu, T (Liu, Tong); Gu, WM (Gu, Wei-Min); Lin, DB (Lin, Da-Bin); Sun, MY (Sun, Mou-Yuan); Wu, XF (Wu, Xue-Feng); Lu, JF (Lu, Ju-Fu)
ASTROPHYSICAL JOURNAL LETTERS
卷: 781 期: 1 文献号: L19

GRB 130925A, composed of three gamma-ray emission episodes and a series of orderly flares, has been detected by Swift, Fermi, Konus-Wind, and INTEGRAL. If the third weakest gamma-ray episode can be considered a giant flare, we find that after the second gamma-ray episode observed by INTEGRAL located at about 2000 s, a positive relation exists between the time intervals of the adjacent flares and the time since the episode. We suggest that the second gamma-ray episode and its flares originate from the resumption of the accretion process due to the fragments from the collapsar falling back; such a relation may be related to a hyperaccretion disk around a precessed black hole (BH). We propose that the origin and time evolution of the flares, and the approximately symmetrical temporal structure and spectral evolution of the single flare can be explained well by a jet precession model. In addition, the mass and spin of the BH can be constrained, which indicates a stellar-mass, fast-rotating BH located in the center of GRB 130925A.

第 86 条，共 222 条

The Nonlinear Photon Transfer Curve Of Ccds And Its Effects On Photometry

Ma bin ,Shang, Zhaohui, *Wang,LF*, Hu,Yi;Liu, Qiang Wei,peng
Volume 9154, id. 91541U 10 pp. (2014)
Proceedings of the SPIE

The photon transfer curve (PTC, variance vs. signal level) is a commonly used and effective tool in characterizing CCD performance. It is theoretically linear in the range where photon shot noise dominates, and its slope is utilized to derive the gain of the CCD. However, recent researches on different CCDs have revealed that the variance progressively drops at high signal levels, while the linearity shown by signal versus exposure time is still excellent and unaffected.

On the other hand, bright stars are found to exhibit fatter point spread function (PSF). Both nonlinear PTC and the brighter-fatter effect are regarded as the result of spreading of charges between pixels, an interaction progress increasing with signal level. In this work we investigate the nonlinear PTC based on the images with a STA1600FT CCD camera, whose PTC starts to become nonlinear at about 1/3 full well. To explain the phenomenon, we present a model to characterize the charge-sharing PSF. This signal-dependent PSF can be derived from flat-field frames, and allow us to quantify the effects on photometry and measured shape of stars. This effect is essentially critical for projects requiring accurate photometry and shape parameters.

第 87 条，共 222 条

A New Method Of CCD Dark Current Correction Via Extracting The Dark Information From Scientific Images

Ma bin ,Shang, Zhaohui, *Wang,LF* Hu,Yi;Liu, Qiang Wei,peng
Volume 9154, id. 91541T 8 pp
Proceedings of the SPIE
We have developed a new method to correct dark current at relatively high temperatures for Charge-Coupled Device (CCD) images when dark frames cannot be obtained on the telescope. For images taken with the Antarctic Survey Telescopes (AST3) in 2012, due to the low cooling efficiency, the median CCD temperature was -46°C, resulting in a high dark current level of about 3e-/pix/sec, even comparable to the sky brightness (10e-/pix/sec). If not corrected, the nonuniformity of the dark current could even overweight the photon noise of the sky background. However, dark frames could not be obtained during the observing season because the camera was operated in frame-transfer mode without a shutter, and the telescope was unattended in winter. Here we present an alternative, but simple and effective method to derive the dark current frame from the scientific images. Then we can scale this dark frame to the temperature at which the scientific images were taken, and apply the dark frame corrections to the scientific images. We have applied this method to the AST3 data, and demonstrated that it can reduce the noise to a level roughly as low as the photon noise of the sky brightness, solving the high noise problem and improving the photometric precision. This method will also be helpful for other projects that suffer from similar issues.

第 88 条，共 222 条

Kunlun Dark Universe Survey Telescope

Zhu,Yongtian;*Wang,LF*,Yuan,Xiangyuan;Gu,Bozhong;Li,xinnan;Yang,shihai
Volume 9145, id. 91450E 17 pp.
Proceedings of the SPIE
Chinese Antarctic Observatory has been listed as National large research infrastructure during twelfth five-year plan. Kunlun Dark Universe Survey Telescope, one of two major facility of Chinese Antarctic Observatory, is a 2.5-meter optic/infrared telescope and will be built at the Chinese Antarctic Kunlun Station. It is intended to take advantage of the exceptional seeing conditions, as well as the low temperature reducing background for infrared observations. KDUST will adopt an innovative optical system, which can deliver very good image quality over a 2 square degree flat field of view. All of parts of it have been designed carefully to endure the extremely harsh environment. KDUST will be perched on a 14.5-meter-high tower to lift it above the turbulence layer. In this paper, preliminary design and key technology pre-research of KDUST will be introduced.

第 89 条，共 222 条

Asteroseismology from Dome A, Antarctica

Fu,J,N;Zong,W.K;Yang,Y;Moore,A;Ashley,M.C.B.;Cui,X,Q;Feng,L,L;Gong,X,F;Lawrence,J,S;Luong-Van,D.Storev,J.W.V;Wang,L.Z.;*Wang,L.F*;
Volume 301, pp. 409-410
Precision Asteroseismology, Proceedings of the International Astronomical Union, IAU Symposium,
Gattini and CSTAR have been installed at Dome A, Antarctica, which provide time-series photometric data for a large number of pulsating variable stars. We present the study for several variable stars with the data collected with the two facilities in 2009 to demonstrate the scientific potential of observations from Dome A for asteroseismology.

Galaxy Cosmology and Dark Energy

第 90 条，共 222 条

Satellite Alignment. I. Distribution Of Substructures And Their Dependence On Assembly History From N-Body Simulations

Wang, YO (Wang, Yang Ocean); Lin, WP (Lin, W. P.); *Kang, X* (Kang, X.); Dutton, A (Dutton, Aaron); Yu, Y (Yu, Yu); Maccio, AV (Maccio, Andrea V.)
ASTROPHYSICAL JOURNAL
卷: 786 期: 1 文献号: 8

Observations have shown that the spatial distribution of satellite galaxies is not random, but aligned with the major axes of central galaxies. This alignment is dependent on galaxy properties, such that red satellites are more strongly aligned than blue satellites. Theoretical work conducted to interpret this phenomenon has found that it is due to the non-spherical nature of dark matter halos. However, most studies overpredict the alignment signal under the assumption that the central galaxy shape follows the shape of the host halo. It is also not clear whether the color dependence of alignment is due to an assembly bias or an evolution effect. In this paper we study these problems using a cosmological N-body simulation. Subhalos are used to trace the positions of satellite galaxies. It is found that the shapes of dark matter halos are mis-aligned at different radii. If the central galaxy shares the same shape as the inner host halo, then the alignment effect is weaker and agrees with observational data. However, it predicts almost no dependence of alignment on the color of satellite galaxies, though the late accreted subhalos show stronger alignment with the outer layer of the host halo than their early accreted counterparts. We find that this is due to the limitation of pure N-body simulations where satellite galaxies without associated subhalos ("orphan galaxies") are not resolved. These orphan (mostly red) satellites often reside in the inner region of host halos and should follow the shape of the host halo in the inner region.

第 91 条，共 222 条

A Semi-analytical Model of Quasar Formation

Yang AH
卷: 55 期: 1 页: 8-19
Acta Astronomica Sinica

We model the cosmological co-evolution of galaxies and their central supermassive black holes in a series of high-resolution N-body simulations by using the semi-analytical approach. Our model is based on the semi-analytical model of galaxy formation and evolution of Kang et al. Under the hypothesis that quasar activity is triggered by galaxy mergers, we derive the quasar bolometric luminosity function, black hole mass function in the redshift range $0 < z < 4.5$,and the projected two point correlation function at $z = 1.0$. Our results show that the history of black hole accretion can not be well reproduced with the constant Eddington ratio, and the Eddington ratio needs to increase with the redshift in a specific range. The major merger of galaxies is an efficient mechanism to trigger quasar activity. The minor mergers only have influence on the low and moderate luminosity quasars, and have little effect on very luminous ones. At $z = 1.0$, the very luminous quasars are more strongly clustered than the others.

第 92 条，共 222 条

The Distribution Of Satellites Around Central Galaxies In A Cosmological Hydrodynamical Simulation

Dong, XC (Dong, X. C.); Lin, WP (Lin, W. P.); *Kang, X* (Kang, X.); Wang, YO (Wang, Yang Ocean); Dutton, AA (Dutton, Aaron A.); Maccio, AV (Maccio, Andrea V.)
ASTROPHYSICAL JOURNAL LETTERS
卷: 791 期: 2 文献号: L33

Observations have shown that the spatial distribution of satellite galaxies is not random, but rather is aligned with the major axes of central galaxies (CGs). The strength of the alignment is dependent on the properties of both the satellites and centrals. Theoretical studies using dissipationless N-body simulations are limited by their inability to directly predict the shape of CGs. Using hydrodynamical simulations including gas cooling, star formation, and feedback, we carry out a study of galaxy alignment and its dependence on the galaxy

properties predicted directly from the simulations. We found that the observed alignment signal is well produced, as is the color dependence: red satellites and red centrals both show stronger alignments than their blue counterparts. The reason for the stronger alignment of red satellites is that most of them stay in the inner region of the dark matter halo where the shape of the CG better traces the dark matter distribution. The dependence of alignment on the color of CGs arises from the halo mass dependence, since the alignment between the shape of the central stellar component and the inner halo increases with halo mass. We also find that the alignment of satellites is most strongly dependent on their metallicity, suggesting that the metallicity of satellites, rather than color, is a better tracer of galaxy alignment on small scales. This could be tested in future observational studies.

第 93 条，共 222 条

Measuring The X-Ray Luminosities Of SDSS DR7 Clusters From ROSAT All Sky Survey

Wang, L (Wang, Lei); Yang, XH (Yang, Xiaohu); Shen, SY (Shen, Shiyin); Mo, HJ (Mo, H. J.); van den Bosch, FC (van den Bosch, Frank C.); Luo, WT (Luo, Wentao); Wang, Y (Wang, Yu); Lau, ET (Lau, Erwin T.); Wang, QD (Wang, Q. D.); Kang, X (Kang, Xi); Li, R (Li, Ran)

MONTHLY NOTICES OF THE ROYAL ASTRONOMICAL SOCIETY

卷: 439 期: 1 页: 611-622

We use ROSAT All Sky Survey broad-band X-ray images and the optical clusters identified from Sloan Digital Sky Survey Data Release 7 to estimate the X-ray luminosities around similar to 65 000 candidate clusters with masses greater than or similar to 10(13) h(-1) M-circle dot based on an optical to X-ray (OTX) code we develop. We obtain a catalogue with X-ray luminosity for each cluster. This catalogue contains 817 clusters (473 at redshift z <= 0.12) with signal-to-noise ratio >3 in X-ray detection. We find about 65 per cent of these X-ray clusters have their most massive member located near the X-ray flux peak; for the rest 35 per cent, the most massive galaxy is separated from the X-ray peak, with the separation following a distribution expected from a Navarro-Frenk-White profile. We investigate a number of correlations between the optical and X-ray properties of these X-ray clusters, and find that the cluster X-ray luminosity is correlated with the stellar mass (luminosity) of the clusters, as well as with the stellar mass (luminosity) of the central galaxy and the mass of the halo, but the scatter in these correlations is large. Comparing the properties of X-ray clusters of similar halo masses but having different X-ray luminosities, we find that massive haloes with masses greater than or similar to 10(14) h(-1) M-circle dot contain a larger fraction of red satellite galaxies when they are brighter in X-ray. An opposite trend is found in central galaxies in relative low-mass haloes with masses less than or similar to 10(14) h(-1) M-circle dot where X-ray brighter clusters have smaller fraction of red central galaxies. Clusters with masses greater than or similar to 10(14) h(-1) M-circle dot that are strong X-ray emitters contain many more low-mass satellite galaxies than weak X-ray emitters. These results are also confirmed by checking X-ray clusters of similar X-ray luminosities but having different characteristic stellar masses. A cluster catalogue containing the optical properties of member galaxies and the X-ray luminosity is available at http://gax.shao.ac.cn/data/Group.html.

第 94 条，共 222 条

Resolving The Problem Of Galaxy Clustering On Small Scales: Any New Physics Needed?

Kang, X (Kang, X.)

MONTHLY NOTICES OF THE ROYAL ASTRONOMICAL SOCIETY

卷: 437 期: 4 页: 3385-3395

Galaxy clustering sets strong constraints on the physics governing galaxy formation and evolution. However, most current models fail to reproduce the clustering of low-mass galaxies on small scales ($r < 1$ Mpc h(-1)). In this paper, we study the galaxy clusterings predicted from a few semi-analytical models. We first compare two Munich versions, Guo et al. and De Lucia & Blaizot. The Guo11 model well reproduces the galaxy stellar mass function, but overpredicts the clustering of low-mass galaxies on small scales. The DLB07 model provides a better fit to the clustering on small scales, but overpredicts the stellar mass function. These seem to be puzzling. The clustering on small scales is

dominated by galaxies in the same dark matter halo, and there is slightly more fraction of satellite galaxies residing in massive haloes in the Guo11 model, which is the dominant contribution to the clustering discrepancy between the two models. However, both models still overpredict the clustering at 0.1 < r < 10 Mpc h(-1) for low-mass galaxies. This is because both models overpredict the number of satellites by 30 per cent in massive haloes than the data. We show that the Guo11 model could be slightly modified to simultaneously fit the stellar mass function and clusterings, but that cannot be easily achieved in the DLB07 model. The better agreement of DLB07 model with the data actually comes as a coincidence as it predicts too many low-mass central galaxies which are less clustered and thus brings down the total clustering. Finally, we show the predictions from the semi-analytical models of Kang et al. We find that this model can simultaneously fit the stellar mass function and galaxy clustering if the supernova feedback in satellite galaxies is stronger. We conclude that semi-analytical models are now able to solve the small-scales clustering problem, without invoking of any other new physics or changing the dark matter properties, such as the recent favoured warm dark matter.

Star Formation in Galaxies

第 95 条，共 222 条

Characterizing Ultraviolet And Infrared Observational Properties For Galaxies. Ii. Features Of Attenuation Law

Mao, YW (Mao, Ye-Wei); Kong, X (Kong, Xu); Lin, L (Lin, Lin)
ASTROPHYSICAL JOURNAL

卷: 789 期: 1 文献号: 76

Variations in the attenuation law have a significant impact on observed spectral energy distributions for galaxies. As one important observational property for galaxies at ultraviolet and infrared wavelength bands, the correlation between infrared-to-ultraviolet luminosity ratio and ultraviolet color index (or ultraviolet spectral slope), i.e., the IRX-UV relation (or IRX-beta relation), offered a widely used formula for correcting dust attenuation in galaxies, but the usability appears to be in doubt now because of considerable dispersion in this relation found by many studies. In this paper, on the basis of spectral synthesis modeling and spatially resolved measurements of four nearby spiral galaxies, we provide an interpretation of the deviation in the IRX-UV relation with variations in the attenuation law. From both theoretical and observational viewpoints, two components in the attenuation curve, the linear background and the 2175 angstrom bump, are suggested to be the parameters in addition to the stellar population age (addressed in the first paper of this series) in the IRX-UV function; different features in the attenuation curve are diagnosed for the galaxies in our sample. Nevertheless, it is often difficult to ascertain the attenuation law for galaxies in actual observations. Possible reasons for preventing the successful detection of the parameters in the attenuation curve are also discussed in this paper, including the degeneracy of the linear background and the 2175 angstrom bump in observational channels, the requirement for young and dust-rich systems to study, and the difficulty in accurate estimates of dust attenuations at different wavelength bands.

第 96 条，共 222 条

Molecular Gas Heating Mechanisms, And Star Formation Feedback In Merger/Starbursts: Ngc 6240 And Arp 193 As Case Studies

Papadopoulos, PP (Papadopoulos, Padelis P.); *Zhang, ZY* (Zhang, Zhi-Yu); Xilouris, EM (Xilouris, E. M.); Weiss, A (Weiss, Axel); van der Werf, P (van der Werf, Paul); Israel, FP (Israel, F. P.); Greve, TR (Greve, T. R.); Isaak, KG (Isaak, Kate G.); Gao, Y (Gao, Y.)
ASTROPHYSICAL JOURNAL

卷: 788 期: 2 文献号: 153

We used the SPIRE/FTS instrument aboard the Herschel Space Observatory to obtain the Spectral Line Energy Distributions (SLEDs) of CO from J= 4-3 to J= 13-12 of Arp 193 and NGC 6240, two classical merger/starbursts selected from our molecular line survey of local Luminous Infrared Galaxies (L-IR >= 10(11) L-circle dot). The high-J CO SLEDs are then combined with ground-based low-J CO, (CO)-C-13, HCN, HCO+,

CS line data and used to probe the thermal and dynamical states of their large molecular gas reservoirs. We find the two CO SLEDs strongly diverging from J = 4-3 onward, with NGC 6240 having a much higher CO line excitation than Arp 193, despite their similar low-J CO SLEDs and LFIR/LCO, 1-0, LHCN/LCO (J = 1-0) ratios (proxies of star formation efficiency and dense gas mass fraction). In Arp 193, one of the three most extreme starbursts in the local universe, the molecular SLEDs indicate a small amount (similar to 5%-15%) of dense gas (n >= 10(4) cm(-3)) unlike NGC 6240 where most of the molecular gas (similar to 60%-70%) is dense (n similar to (10(4)-10(5)) cm(-3)). Strong star-formation feedback can drive this disparity in their dense gas mass fractions, and also induce extreme thermal and dynamical states for the molecular gas. In NGC 6240, and to a lesser degree in Arp 193, we find large molecular gas masses whose thermal states cannot be maintained by FUV photons from Photon-Dominated Regions. We argue that this may happen often in metal-rich merger/starbursts, strongly altering the initial conditions of star formation. ALMA can now directly probe these conditions across cosmic epoch, and even probe their deeply dust-enshrouded outcome, the stellar initial mass function averaged over galactic evolution.

第 97 条，共 222 条

Warm Molecular Gas In Luminous Infrared Galaxies

Lu, N (Lu, N.); *Zhao, Y* (Zhao, Y.); Xu, CK (Xu, C. K.); Gao, Y (Gao, Y.); Armus, L (Armus, L.); Mazzarella, JM (Mazzarella, J. M.); Isaak, KG (Isaak, K. G.); Petric, AO (Petric, A. O.); Charmandaris, V (Charmandaris, V.); Diaz-Santos, T (Diaz-Santos, T.); Evans, AS (Evans, A. S.); Howell, J (Howell, J.); Appleton, P (Appleton, P.); Inami, H (Inami, H.); Iwasawa, K (Iwasawa, K.); Leech, J (Leech, J.); Lord, S (Lord, S.); Sanders, DB (Sanders, D. B.); Schulz, B (Schulz, B.); Surace, J (Surace, J.); van der Werf, PP (van der Werf, P. P.)
ASTROPHYSICAL JOURNAL LETTERS

卷: 787 期: 2 文献号: L23

We present our initial results on the CO rotational spectral line energy distribution (SLED) of the J to J-1 transitions from J = 4 up to 13 from Herschel SPIRE spectroscopic observations of 65 luminous infrared galaxies (LIRGs) in the Great Observatories All-Sky LIRG Survey. The observed SLEDs change on average from one peaking at J <= 4 to a broad distribution peaking around J similar to 6 to 7 as the IRAS 60-to-100 mu m color, C(60/100), increases. However, the ratios of a CO line luminosity to the total infrared luminosity, L-IR, show the smallest variation for J around 6 or 7. This suggests that, for most LIRGs, ongoing star formation (SF) is also responsible for a warm gas component that emits CO lines primarily in the mid-J regime (5 less than or similar to J less than or similar to 10). As a result, the logarithmic ratios of the CO line luminosity summed over CO (5-4), (6-5), (7-6), (8-7) and (10-9) transitions to L-IR, log R-midCO, remain largely independent of C(60/100), and show a mean value of -4.13 (log R-midCO(SF)) and a sample standard deviation of only 0.10 for the SF-dominated galaxies. Including additional galaxies from the literature, we show, albeit with a small number of cases, the possibility that galaxies, which bear powerful interstellar shocks unrelated to the current SF, and galaxies, in which an energetic active galactic nucleus contributes significantly to the bolometric luminosity, have their R-midCO higher and lower than R-midCO(SF), respectively.

第 98 条，共 222 条

Probing Asymmetric Structures In The Outskirts Of Galaxies

Wen, ZZ (Wen, Zhang Zheng); Zheng, XZ (Zheng, Xian Zhong); An, FX (An, Fang Xia)
ASTROPHYSICAL JOURNAL

卷: 787 期: 2 文献号: 130

Upcoming large imaging surveys will allow detailed studies of the structure and morphology of galaxies aimed at addressing how galaxies form and evolve. Computational approaches are needed to characterize their morphologies over large samples. We introduce an automatic method to quantify the outer structure of galaxies. The key to our approach is the division of a galaxy image into two sections delineated by the isophote, which encloses half the total brightness of the galaxy. We call the central section the inner half-flux region (IHR) and the outer section the outer half-flux region (OHR). From this division, we derive two parameters: A(o), which measures the

asymmetry of the OHR, and D-o, which measures the deviation of the intensity weighted centroid of the OHR from that of the IHR relative to the effective radius. We derive the two parameters from HST/ACS z(850)-band images for a sample of 764 galaxies with z(850) < 22 mag and 0.35 < z < 0.9 selected from the GEMS and GOODS-South surveys. We show that the sample galaxies having strong asymmetric structures, particularly tidal tails, are well-separated from those with regular morphologies in the A(o)-D-o space. Meanwhile, the widely used CAS and Gini-M-20 methods turn out to be insensitive to such morphological features. We stress that the A(o)-D-o method is an efficient way to select galaxies with significant asymmetric features like tidal tails and study galaxy mergers in the dynamical phase traced by these delicate features.

第 99 条，共 222 条

Alma Observations Of Warm Molecular Gas And Cold Dust In Ngc 34

Xu, CK (Xu, C. K.); Cao, C (Cao, C.); Lu, N (Lu, N.); *Gao, Y* (Gao, Y.); van der Werf, P (van der Werf, P.); Evans, AS (Evans, A. S.); Mazzarella, JM (Mazzarella, J. M.); Chu, J (Chu, J.); Haan, S (Haan, S.); Diaz-Santos, T (Diaz-Santos, T.); Meijerink, R (Meijerink, R.); Zhao, YH (Zhao, Y. -H.); Appleton, P (Appleton, P.); Armus, L (Armus, L.); Charmandaris, V (Charmandaris, V.); Lord, S (Lord, S.); Murphy, EJ (Murphy, E. J.); Sanders, DB (Sanders, D. B.); Schulz, B (Schulz, B.); Stierwalt, S (Stierwalt, S.)

ASTROPHYSICAL JOURNAL

卷: 787 期: 1 文献号: 48

We present Atacama Large Millimeter Array (ALMA) Cycle-0 observations of the CO (6-5) line emission (rest-frame frequency = 691.473 GHz) and of the 435 mu m dust continuum emission in the nuclear region of NGC 34, a local luminous infrared galaxy at a distance of 84 Mpc (1 '' = 407 pc) which contains a Seyfert 2 active galactic nucleus (AGN) and a nuclear starburst. The CO emission is well resolved by the ALMA beam (0.'' 26x 0.'' 23), with an integrated flux of fCO(6-5) = 1004 (+/- 151) Jy km s-1. Both the morphology and kinematics of the CO (6-5) emission are rather regular, consistent with a compact rotating disk with a size of 200 pc. A significant emission feature is detected on the redshifted wing of the line profile at the frequency of the (HCN)-C-13 (8-7) line, with an integrated flux of 17.7 +/- 2.1(random) +/- 2.7(systematic) Jy km s(-1). However, it cannot be ruled out that the feature is due to an outflow of warm dense gas with a mean velocity of 400 km s(-1). The continuum is resolved into an elongated configuration, and the observed flux corresponds to a dustmass ofM(dust) = 10(6.97 +/- 0.13) M circle dot. An unresolved central core (radius +/- 50 pc) contributes 28% of the continuum flux and 19% of the CO (6-5) flux, consistent with insignificant contributions of the AGN to both emissions. Both the CO (6-5) and continuum spatial distributions suggest a very high gas column density (>= 104 M circle dot pc (2)) in the nuclear region at radius <= 100 pc.

第 100 条，共 222 条

The Properties Of H Alpha Emission-Line Galaxies At Z=2.24

An, FX (An, Fang Xia); Zheng, XZ (Zheng, Xian Zhong); Wang, WH (Wang, Wei-Hao); Huang, JS (Huang, Jia-Sheng); Kong, X (Kong, Xu); Wang, JX (Wang, Jun-Xian); Fang, GW (Fang, Guan Wen); Zhu, FF (Zhu, Feifan); Gu, QS (Gu, Qiu-Sheng); Wu, H (Wu, Hong); Hao, L (Hao, Lei); Xia, XY (Xia, Xiao-Yang)

ASTROPHYSICAL JOURNAL

卷: 784 期: 2 文献号: 152

Using deep narrowband H(2)S1 and K-s-band imaging data obtained with CFHT/WIRCam, we identify a sample of 56 H alpha emission-line galaxies (ELGs) at z = 2.24 with the 5 sigma depths of H(2)S1 = 22.8 and K-s = 24.8 (AB) over a 383 arcmin(2) area in the Extended Chandra Deep Field South. A detailed analysis is carried out with existing multi-wavelength data in this field. Three of the 56 H alpha ELGs are detected in Chandra 4 Ms X-ray observations and two of them are classified as active galactic nuclei. The rest-frame UV and optical morphologies revealed by HST/ACS and WFC3 deep images show that nearly half of the H alpha ELGs are either merging systems or have a close companion, indicating that the merging/interacting processes play a key role in regulating star formation at cosmic epoch z = 2-3. About 14% are too faint to be resolved in the rest-frame UV morphology due to high dust extinction. We estimate dust extinction from

spectral energy distributions. We find that dust extinction is generally correlated with Ha luminosity and stellar mass. Our results suggest that H alpha ELGs are representative of star-forming galaxies. Applying extinction corrections to individual objects, we examine the intrinsic Ha luminosity function (LF) at z = 2.24, obtaining a best-fit Schechter function characterized by a faint-end slope of alpha similar or equal to -1.3. This is shallower than the typical slope of a z-1.6 in previous works based on constant extinction correction. We demonstrate that this difference is mainly due to the different extinction corrections. The proper extinction correction is thus the key to recovering the intrinsic LF as the extinction globally increases with H alpha luminosity. Moreover, we find that our H alpha LF mirrors the stellar mass function of star-forming galaxies at the same cosmic epoch. This finding indeed reflects the tight correlation between star formation rate and stellar mass for star-forming galaxies, i.e., the so-called main sequence.

第 101 条，共 222 条

Dense Gas Tracers And Star Formation Laws In Active Galaxies: Apex Survey Of Hcn J=4 -> 3, Hco+ J=4 -> 3, And Cs J=7 -> 6

Zhang, ZY (Zhang, Zhi-Yu); Gao, Y (Gao, Yu); Henkel, C (Henkel, Christian); Zhao, YH (Zhao, Yinghe); Wang, JZ (Wang, Junzhi); Menten, KM (Menten, Karl M.); Gusten, R (Guesten, Rolf)
ASTROPHYSICAL JOURNAL LETTERS

卷: 784 期: 2 页: 1-7

We report HCN J = 4 --> 3, HCO+ J = 4 --> 3, and CS J = 7 --> 6 observations in 20 nearby star-forming galaxies with the Atacama Pathfinder EXperiment 12 m telescope. Combined with four HCN, three HCO+, and four CS detections from the literature, we probe the empirical link between the luminosity of molecular gas (L'(gas)) and that of infrared emission (L-IR), up to the highest gas densities (similar to 10(6) cm(-3)) that have been probed so far. For nearby galaxies with large radii, we measure the IR luminosity within the submillimeter beam size (14 ''-18 '') to match the molecular emission. We find linear slopes for L'(CS J=7-6)-L-IR and L'(HCNJ=4-3)-L-IR, and a slightly super-linear slope for L'(HCO+ J=4-3)-L-IR. The correlation of L'(CS J=7-6)-L-IR even extends over eight orders of luminosity magnitude down to Galactic dense cores, with a fit of log(L-IR) = 1.00(+/-0.01)xlog(L'(CS J=7-6)) + 4.03(+/-0.04). Such linear correlations appear to hold for all densities >10(4) cm(-3), and indicate that star formation rate is not related to the free-fall timescale for dense molecular gas.

第 102 条，共 222 条

[30] Garnett D R, Shields G A, Skillman E D, Et Al. Apj, 1997, 489: 63 Spectroscopic Observations Of The Star Formation Regions In Nearby Galaxies

Kong X; Lin Lin; Li Jinrong; Zhou X; Zou Hu; Li Hongyu; Chen Fuzhen; Du Wei; Fan Zhou; *Mao YW*; Wang Jing; Zhu Yinan; Zhou Zhimin

卷: 55 期: 1 页: 29-39

Acta Astronomica Sinica

During the late 1990s and the first decade of the 21st century, the 8 ~10 m scale ground-based telescopes are helping astronomers learn much more about how galaxies develop. The existing 2 ~4 m scale telescopes become less important for astrophysical researches. To use the existing 2 ~4 m scale telescopes to address important issues in cosmology and extragalactic and galactic astronomy, we have to consider very carefully which kind of things we can do, and which we can not. For this reason, the Time Allocation Committee (TAC) of the National Astronomical Observatories of China (NAOC) 2.16 m telescope decides to support some key projects since 2013. Nearby galaxies supply us with the opportunity to study galaxy dynamics and star formation on large scales, yet are close enough to reveal the details. Star formation regions in nearby galaxies provide an excellent laboratory to study the star formation processes, the evolution of massive stars, and the properties of the surrounding interstellar medium. A wealth of information can be obtained from the spectral analysis of the bright emission lines and the stellar continuum. Considering these, we proposed a long-term project "Spectroscopic Observations of the Star Formation Regions in Nearby Galaxies", and it becomes the key project of the NAOC 2.16 m telescope since 2013, supported with 30 dark/grey nights per year. The primary goal of this project is to observe the spectroscopy of star formation regions in 20 nearby galaxies, with the NAOC 2.16 m telescope and the

Hectospec/MMT (Multiple Mirror Telescope) multifiber spectrograph by Telescope Access Program (TAP). With the spectra of a large sample of star formation regions, combining multi-wavelength data from UV to IR, we can investigate, understand, and quantify the nature of the deviation from the starbursts' IRX-beta (the IR/UV ratio "IRX" versus the UV color "beta") correlation. It will be important for a better understanding of the interaction of dust and radiation specifically in nearby galaxies, but it also has direct consequences for our understanding and interpretation of galaxy evolution in a general context. As the first paper of this project, we describe the sample and scientific objectives, review the observation, and present initial results in this paper. We have obtained spectrophotometric data for 80 star formation regions in the spiral galaxy NGC 2403, and have determined the radial gas-phase oxygen abundance and dust extinction gradient of NGC 2403.

第 103 条，共 222 条

Dust And Gas In Luminous Proto-Cluster Galaxies At Z=4.05: The Case For Different Cosmic Dust Evolution In Normal And Starburst Galaxies

Tan, Q (Tan, Q.); Daddi, E (Daddi, E.); Magdis, G (Magdis, G.); Pannella, M (Pannella, M.); Sargent, M (Sargent, M.); Riechers, D (Riechers, D.); Bethermin, M (Bethermin, M.); Bournaud, F (Bournaud, F.); Carilli, C (Carilli, C.); da Cunha, E (da Cunha, E.); Dannerbauer, H (Dannerbauer, H.); Dickinson, M (Dickinson, M.); Elbaz, D (Elbaz, D.); Gao, Y (Gao, Y.); Hodge, J (Hodge, J.); Owen, F (Owen, F.); Walter, F (Walter, F.)
ASTRONOMY & ASTROPHYSICS
卷: 569 页: A98 (1)-A98(17)

We measure the dust and gas content of the three submillimeter galaxies (SMGs) in the GN20 proto-cluster at z = 4.05 using new IRAM Plateau de Bure interferometer (PdBI) CO(4-3) and 1.2-3.3 mm continuum observations. All these three SMGs are heavily dust obscured, with UV-based star formation rate (SFR) estimates significantly smaller than the ones derived from the bolometric infrared (IR), consistent with the spatial offsets revealed by HST and CO imaging. Based also on evaluations of the specific SFR, CO-to-H-2 conversion factor and gas depletion timescale, we classify all the three galaxies as starbursts (SBs), although with a lower confidence for GN20.2b that might be a later stage merging event. We place our measurements in the context of the evolutionary properties of main sequence (MS) and SB galaxies. ULIRGs have 3-5 times larger L'(CO)/M-dust and M-dust/M-star ratios than z = 0 MS galaxies, but by z similar to 2 the difference appears to be blurred, probably due to differential metallicity evolution. SB galaxies appear to slowly evolve in their L'(CO)/M-dust and M-dust/M-star ratios all the way to z > 6 (consistent with rapid enrichment of SB events), while MS galaxies rapidly increase in M-dust/M-star from z = 0 to 2 (due to gas fraction increase, compensated by a decrease of metallicities). While no IR/submm continuum detection is available for indisputably normal massive galaxies at z > 2.5, we show that if metallicity indeed decrease rapidly for these systems at z > 3 as claimed in the literature, we should expect a strong decrease of their M-dust/M-star, consistent with recent PdBI and ALMA upper limits. We conclude that the M-dust/M-star ratio could be a powerful tool for distinguishing starbursts from normal galaxies at z > 4.

第 104 条，共 222 条

Physical Conditions Of Molecular Gas In The Circinus Galaxy Multi-J CO And C I P-3(1) -> P-3(0) Observations

Zhang, ZY (Zhang, Zhi-Yu); Henkel, C (Henkel, Christian); Gao, Y (Gao, Yu); Gusten, R (Guesten, Rolf); Menten, KM (Menten, Karl M.); Papadopoulos, PP (Papadopoulos, Padelis P.); Zhao, YH (Zhao, Yinghe); Ao, YP (Ao, Yiping); Kaminski, T (Kaminski, Tomasz)
ASTRONOMY & ASTROPHYSICS
卷: 568 文献号: A122

We report mapping observations of the (CO)-C-12 J = 3 -> 2, 4 -> 3, 6 -> 5, and 7 -> 6 transitions and the C I P-3(1) -> P-3(0) (C I) 492 GHz transition toward the central 40 '' x 40 '' region of the Circinus galaxy, using the Atacama Pathfinder EXperiment (APEX) telescope. We also detected (CO)-C-13 J = 3 -> 2 at the central position of Circinus. These observations are to date the highest CO transitions reported in

Circinus. With large velocity gradient (LVG) modeling and likelihood analysis we try to obtain density, temperature, and column density of the molecular gas in three regions: the nuclear region (D < 18 '' similar to 360 pc), the entire central 45 '' (D < 45 '' similar to 900 pc) region, and the star-forming (S-F) ring (18 '' < D < 45 ''). In the nuclear region, we can fit the CO excitation with a single excitation component, yielding an average condition of nH(2) similar to 10(3.2) cm(-3), T-kin similar to 200 K, and dv/dr similar to 3 km s(-1) pc(-1). In the entire 45 '' region, which covers both the nucleus and the S-F ring, two excitation components are needed with nH(2) similar to 10(4.2) cm(-3) and 10(3.0) cm(-3), T-kin similar to 60 K and 30 K, and MH2 similar to 2.3 x 10(7) M-circle dot and 6.6 x 10(7) M-circle dot, respectively. The gas excitation in the S-F ring can also be fitted with two LVG components, after subtracting the CO fluxes in the 18 '' nuclear region. The S-F ring region contributes 80% of the molecular mass in the 45 '' region. For the entire 45 '' region, we find a standard conversion factor of N(H-2)/I-CO (1 -> 0) = 0.37 x 10(20) cm(-2) (K km s(-1))(-1), about 1/5 of the Galactic disk value. The luminosity ratios of C I and (CO)-C-12 J = 3 -> 2 (R-CI/(CO) (3 -> 2)) in Circinus basically follow a linear trend, similar to that obtained in high-redshift galaxies. The average R-CI/(CO) (J =) (3 -> 2) in Circinus is found to be similar to 0.2, lying at an intermediate value between non-AGN nuclear regions and high-redshift galaxies.

第 105 条，共 222 条

Star Formation Relations And Co Spectral Line Energy Distributions Across The J-Ladder And Redshift

Greve, TR (Greve, T. R.); Leonidaki, I (Leonidaki, I.); Xilouris, EM (Xilouris, E. M.); Weiss, A (Weiss, A.); Zhang, ZY (Zhang, Z. -Y.); van der Werf, P (van der Werf, P.); Aalto, S (Aalto, S.); Armus, L (Armus, L.); Diaz-Santos, T (Diaz-Santos, T.); Evans, AS (Evans, A. S.); Fischer, J (Fischer, J.); *Gao, Y* (Gao, Y.); Gonzalez-Alfonso, E (Gonzalez-Alfonso, E.); Harris, A (Harris, A.); Henkel, C (Henkel, C.); Meijerink, R (Meijerink, R.); Naylor, DA (Naylor, D. A.); Smith, HA (Smith, H. A.); Spaans, M (Spaans, M.); Stacey, GJ (Stacey, G. J.); Veilleux, S (Veilleux, S.); Walter, F (Walter, F.)

ASTROPHYSICAL JOURNAL

卷: 794 期: 2 文献号: 142

We present FIR [50-300 mu m]-CO luminosity relations (i.e., log L-FIR = alpha log L'(CO) + beta) for the full CO rotational ladder from J = 1-0 up to J = 13-12 for a sample of 62 local (z <= 0.1) (Ultra) Luminous InfraredGalaxies (LIRGs; LIR[8-1000 mu m] > 10(11) L-circle dot) using data from Herschel SPIRE-FTS and ground-based telescopes. We extend our sample to high redshifts (z > 1) by including 35 submillimeter selected dusty star forming galaxies from the literature with robust CO observations, and sufficiently well-sampled FIR/submillimeter spectral energy distributions (SEDs), so that accurate FIR luminosities can be determined. The addition of luminous starbursts at high redshifts enlarge the range of the FIR-CO luminosity relations toward the high-IR-luminosity end, while also significantly increasing the small amount of mid-J/high-J CO line data (J = 5-4 and higher) that was available prior to Herschel. This new data set (both in terms of IR luminosity and J-ladder) reveals linear FIR-CO luminosity relations (i.e., a similar or equal to 1) for J = 1-0 up to J = 5-4, with a nearly constant normalization (beta similar to 2). In the simplest physical scenario, this is expected from the (also) linear FIR-(molecular line) relations recently found for the dense gas tracer lines (HCN and CS), as long as the dense gas mass fraction does not vary strongly within our (merger/starburst)-dominated sample. However, from J = 6-5 and up to the J = 13-12 transition, we find an increasingly sublinear slope and higher normalization constant with increasing J. We argue that these are caused by a warm (similar to 100 K) and dense (>10(4) cm(-3)) gas component whose thermal state is unlikely to be maintained by star-formation-powered far-UV radiation fields (and thus is no longer directly tied to the star formation rate). We suggest that mechanical heating (e.g., supernova-driven turbulence and shocks), and not cosmic rays, is the more likely source of energy for this component. The global CO spectral line energy distributions, which remain highly excited from J = 6-5 up to J = 13-12, are found to be a generic feature of the (U)LIRGs in our sample, and further support the presence of this gas component.

第 106 条，共 222 条

Hermes: Point Source Catalogues From Herschel-SPIRE Observations II

Wang, L (Wang, L.); Viero, M (Viero, M.); Clarke, C (Clarke, C.); Bock, J (Bock, J.); Buat, V (Buat, V.); Conley, A (Conley, A.); Farrah, D (Farrah, D.); *Guo, K* (Guo, K.); Heinis, S (Heinis, S.); Magdis, G (Magdis, G.); Marchetti, L (Marchetti, L.); Marsden, G (Marsden, G.); Norberg, P (Norberg, P.); Oliver, SJ (Oliver, S. J.); Page, MJ (Page, M. J.); Roehlly, Y (Roehlly, Y.); Roseboom, IG (Roseboom, I. G.); Schulz, B (Schulz, B.); Smith, AJ (Smith, A. J.); Vaccari, M (Vaccari, M.); Zemcov, M (Zemcov, M.)

MONTHLY NOTICES OF THE ROYAL ASTRONOMICAL SOCIETY

卷: 444 期: 3 页: 2870-2883

The Herschel Multi-tiered Extragalactic Survey (HerMES) is the largest Guaranteed Time Key Programme on the Herschel Space Observatory. With a wedding cake survey strategy, it consists of nested fields with varying depth and area totalling similar to 380 deg(2). In this paper, we present deep point source catalogues extracted from Herschel-Spectral and Photometric Imaging Receiver (SPIRE) observations of all HerMES fields, except for the later addition of the 270 deg(2) HerMES Large-Mode Survey (HeLMS) field. These catalogues constitute the second Data Release (DR2) made in 2013 October. A sub-set of these catalogues, which consists of bright sources extracted from Herschel-SPIRE observations completed by 2010 May 1 (covering similar to 74 deg(2)) were released earlier in the first extensive data release in 2012 March. Two different methods are used to generate the point source catalogues, the SUSSEXTRACTOR point source extractor used in two earlier data releases (EDR and EDR2) and a new source detection and photometry method. The latter combines an iterative source detection algorithm, STARFINDER, and a De-blended SPIRE Photometry algorithm. We use end-to-end Herschel-SPIRE simulations with realistic number counts and clustering properties to characterize basic properties of the point source catalogues, such as the completeness, reliability, photometric and positional accuracy. Over 500 000 catalogue entries in HerMES fields (except HeLMS) are released to the public through the HeDAM (Herschel Database in Marseille) website

第 107 条，共 222 条

Inefficient Star Formation In Extremely Metal Poor Galaxies

Shi, Y (Shi, Yong); Armus, L (Armus, Lee); Helou, G (Helou, George); Stierwalt, S (Stierwalt, Sabrina); *Gao, Y* (Gao, Yu); Wang, JZ (Wang, Junzhi); Zhang, ZY (Zhang, Zhi-Yu); Gu, QS (Gu, Qiusheng)

NATURE

卷: 514 期: 7522 页: 335-339

The first galaxies contain stars born out of gas with few or no 'metals' (that is, elements heavier than helium). The lack of metals is expected to inhibit efficient gas cooling and star formation(1,2), but this effect has yet to be observed in galaxies with an oxygen abundance (relative to hydrogen) below a tenth of that of the Sun(2-4). Extremely metal poor nearby galaxies may be our best local laboratories for studying in detail the conditions that prevailed in low metallicity galaxies at early epochs. Carbon monoxide emission is unreliable as a tracer of gas at low metallicities(5-7), and while dust has been used to trace gas in low-metallicity galaxies(5,8-10), low spatial resolution in the far-infrared has typically led to large uncertainties(9,10). Here we report spatially resolved infrared observations of two galaxies with oxygen abundances below ten per cent of the solar value, and show that stars formed very inefficiently in seven star-forming clumps in these galaxies. The efficiencies are less than a tenth of those found in normal, metal rich galaxies today, suggesting that star formation may have been very inefficient in the early Universe.

第 108 条，共 222 条

Quantifying The Heating Sources For Mid-Infrared Dust Emissions In Galaxies: The Case Of M 81

Lu, N (Lu, N.); Bendo, GJ (Bendo, G. J.); Boselli, A (Boselli, A.); Baes, M (Baes, M.); Wu, H (Wu, H.); Madden, SC (Madden, S. C.); De Looze, I (De Looze, I.); Remy-Ruyer, A (Remy-Ruyer, A.); Boquien, M (Boquien, M.); Wilson, CD (Wilson, C. D.); Galametz, M (Galametz, M.); Lam, MI (Lam,

M. I.); Cooray, A (Cooray, A.); Spinoglio, L (Spinoglio, L.); *Zhao, Y* (Zhao, Y.)
ASTROPHYSICAL JOURNAL
卷: 797 期: 2 文献号: 129

With the newly available photometric images at 250 and 500 mu m from the Herschel Space Observatory, we study quantitative correlations over a sub-kiloparsec scale among three distinct emission components in the interstellar medium of the nearby spiral galaxy M81 (NGC 3031): (1) I-8 or I-24, the surface brightness of the mid-infrared emission observed in the Spitzer Space Telescope 8 or 24 mu m band, with I-8 and I-24 being dominated by the emissions from polycyclic aromatic hydrocarbons (PAHs) and very small grains (VSGs) of dust, respectively; (2) I-500, that of the cold dust continuum emission in the Herschel Space Observatory 500 mu m band, dominated by the emission from large dust grains heated by evolved stars; and (3) I-H alpha, a nominal surface brightness of the H alpha line emission, from gas ionized by newly formed massive stars. The results from our correlation study, free from any assumption on or modeling of dust emissivity law or dust temperatures, present solid evidence for significant heating of PAHs and VSGs by evolved stars. In the case of M81, about 67% (48%) of the 8 mu m (24 mu m) emission derives its heating from evolved stars, with the remainder attributed to radiation heating associated with ionizing stars.

第 109 条，共 222 条

Sio And CH3OH Mega-Masers In NGC 1068

Wang, JZ (Wang, Junzhi); Zhang, JS (Zhang, Jiangshui); *Gao, Y* (Gao, Yu); Zhang, ZY (Zhang, Zhi-Yu); Li, D (Li, Di); Fang, M (Fang, Min); Shi, Y (Shi, Yong)
NATURE COMMUNICATIONS
卷: 5 文献号: 5449
NATURE COMMUNICATIONS

Maser is an acronym for microwave amplification by stimulated emission of radiation; in astronomy mega-masers are masers in galaxies that are >= 10(6) times more luminous than typical galactic maser sources. Observational studies of mega-masers can help us to understand their origins and characteristics. More importantly, mega-masers can be used as diagnostic tracers to probe the physical properties of their parent galaxies. Since the late 1970s, only three types of molecules have been found to form mega-masers: H2O, OH and H2CO. Here we report the detection of both SiO and CH3OH mega-masers near the centre of Seyfert 2 galaxy NGC 1068 at millimetre wavelengths, obtained using the IRAM 30-m telescope. We argue that the SiO mega-maser originated from the nuclear disk and the CH3OH mega-maser originated from shock fronts. High-resolution observations in the future will enable us to investigate AGN feedback and determine the masses of central supermassive black holes in such galaxies.

第 110 条，共 222 条

Mapping Observations Of The Nearby Spiral Galaxy M51 In HCN J=1-0

Chen H; Gao Yu
Scientia Sinica Physica, Mechanica & Astronomica
卷: 44 期: 9 页: 993-1002

We have mapped the Whirlpool galaxy M51 in HCN J=1-0 transition with the IRAM 30m telescope in order to investigate the distribution of dense molecular gas in M51. The map covers an extent of 4'*5' with a spatial resolution of 28", which is the largest HCN map of M51. Comparing with the CO map observed by the NRO 45m telescope, convolved to the same resolution as our HCN map, we discuss the different distribution (and correlation) between the molecular gas and dense molecular gas traced by CO and HCN respectively. HCN shows a concentration in the center, the integrated intensity of the central regions is 3-4 times of the outer disk. The inner spiral arms traced nicely in CO map are all detected in HCN. The total HCN integrated intensity of M51 is 5 times of the central beam (kpc scales), illustrating that there is an extended dense molecular gas distribution outside of the ~1 kpc nuclear region. The ratio of HCN/CO decreases along the radii in the central 42" (roughly corresponding to the stellar bulge component) and stays flat at larger radii in the spiral disk. For most of the regions in the disk, HCN correlates tightly with CO, following a nearly linear relation with a slope of 1.2. Whereas in the bulge the correlation slope is much higher (2.3). All these suggest a dramatic difference in the dense molecular gas

properties (e.g., content, excitation or HCN abundances) between the bulge and spiral disk regions.

Molecular Clouds and Star Formation

第 111 条，共 222 条

Herbig-Haro Objects And Mid-Infrared Outflows In The Vela C Molecular Cloud

Zhang, MM (Zhang, Miaomiao); Wang, HC (Wang, Hongchi); Henning, T (Henning, Thomas)
ASTRONOMICAL JOURNAL

卷: 148 期: 2 文献号: 26

We have performed a deep [S II] lambda lambda 6717/6731 wide field Herbig-Haro (HH) object survey toward the Vela C molecular cloud with a sky coverage of about 2 deg(2). In total, 18 new HH objects, HH 1090-1107, are discovered and the two previously known HH objects, HH 73-74, are also detected in our [S II] images. We also present an investigation of mid-infrared outflows in the Vela C molecular cloud using the Wide-field Infrared Survey Explorer images taken from AllWISE data release. Using the method suggested by Zhang & Wang, 11 extended green objects (EGOs) are identified to be the mid-infrared outflows, including 6 new mid-infrared outflows that have not been detected previously at other wavelengths and 5 mid-infrared counterparts of the HH objects detected in this work. Using the AllWISE Source Catalog and the source classification scheme suggested by Koenig et al., we have identified 56 young stellar object (YSO) candidates in the Vela C molecular cloud. The possible driving sources of the HH objects and EGOs are discussed based on the morphology of HH objects and EGOs and the locations of HH objects, EGOs and YSO candidates. Finally we associate 12 HH objects and 5 EGOs with 10 YSOs and YSO candidates. The median length of the outflows in Vela C is 0.35 pc and the outflows seem to be oriented randomly.

第 112 条，共 222 条

Carbon And Oxygen Isotope Ratios In Starburst Galaxies: New Data From NGC 253 And Mrk 231 And Their Implications

Henkel, C (Henkel, C.); Asiri, H (Asiri, H.); *Ao, Y* (Ao, Y.); Aalto, S (Aalto, S.); Danielson, ALR (Danielson, A. L. R.); Papadopoulos, PP (Papadopoulos, P. P.); Garcia-Burillo, S (Garcia-Burillo, S.); Aladro, R (Aladro, R.); Impellizzeri, CMV (Impellizzeri, C. M. V.); Mauersberger, R (Mauersberger, R.); Martin, S (Martin, S.); Harada, N (Harada, N.)
ASTRONOMY & ASTROPHYSICS

卷: 565 文献号: A3

Carbon and oxygen isotope ratios are excellent measures of nuclear processing, but few such data have been taken toward extragalactic targets so far. Therefore, using the IRAM 30-m telescope, CN and CO isotopologues have been measured toward the nearby starburst galaxy NGC 253 and the prototypical ultraluminous infrared galaxy Mrk 231. Toward the center of NGC 253, the CN and (CN)-C-13 N = 1 -> 0 lines indicate no significant deviations from expected local thermodynamical equilibrium after accounting for moderate saturation effects (10 and 25%) in the two detected spectral components of the main species. Including calibration uncertainties, which dominate the error budget, the C-12/C-13 ratio becomes 40 +/- 10. This is larger than the ratio in the central molecular zone of the Galaxy, suggesting a higher infall rate of poorly processed gas toward the central region. Assuming that the ratio also holds for the CO emitting gas, this yields O-16/O-18 = 145 +/- 36 and O-16/O-17 = 1290 +/- 365 and a S-32/S-34 ratio close to the one measured for the local interstellar medium (2025). No indication of vibrationally excited CN is found in the lower frequency fine structure components of the N = 1 -> 0 and 2 -> 1 transitions at rms noise levels of 3 and 4 mK (15 and 20 mJy) in 8.5 km s-1 wide channels. Peak line intensity ratios between NGC 253 and Mrk 231 are similar to 100 for (CO)-C-12-O-16 and (CO)-C-12-O-18 J = 1 -> 0, while the ratio for (CO)-C-13-O-16 J = 1 -> 0 is similar to 250. This and similar (CO)-C-13 and (CO)-O-18 line intensities in the J = 1 -> 0 and 2 -> 1 transitions of Mrk 231 suggest C-12/C-13 similar to 100 and O-16/O-18 similar to 100, in agreement with values obtained for the less evolved ultraluminous merger Arp 220. Also, when

accounting for other (scarcely available) extragalactic data, C-12/C-13 ratios appear to vary over a full order of magnitude, from >100 in ultraluminous high redshift galaxies to similar to 100 in more local such galaxies to similar to 40 in weaker starbursts that are not undergoing a large scale merger to 25 in the central molecular zone of the Milky Way. With C-12 being predominantly synthesized in massive stars, while C-13 is mostly ejected by longer lived lower mass stars at later times, this is qualitatively consistent with our results of decreasing carbon isotope ratios with time and rising metallicity. It is emphasized, however, that both infall of poorly processed material, initiating a nuclear starburst, and the ejecta from newly formed massive stars (in particular in the case of a top-heavy stellar initial mass function) can raise the carbon isotope ratio for a limited amount of time.

第 113 条，共 222 条

Observed Spectral Energy Distribution Of The Thermal Emission From The Dayside Of WASP-46b

Chen, G (Chen, G.); van Boekel, R (van Boekel, R.); Wang, H (Wang, H.); Nikolov, N (Nikolov, N.); Seemann, U (Seemann, U.); Henning, T (Henning, Th)

ASTRONOMY & ASTROPHYSICS

卷: 567 文献号: A8

Alms, We aim to construct a spectral energy distribution (SED) for the emission from the dayside atmosphere of the hot Jupiter WASP -46b and to investigate its energy budget.

Methods, We observed a secondary eclipse of WASP-46b simultaneously in the g'r;i'z'JHK bands using the GROND instrument on the MPG/ESO 2.2 m telescope. Eclipse depths of the acquired light curves were derived to infer the brightness temperatures at multibands that cover the SED peak.

Results. We report the first detection of the thermal emission from the dayside of WASP -46b in the K band at 4.2 sigma level and tentative detections in the H (2.50 sigma) and J (2.3 sigma) bands, with flux ratios of 0.253(-0.060)(+0.063)% 0.194 +/- 0.078%, and 0.129 +/- 0.055%, respectively. The derived brightness temperatures (2306(-187)(+177) K, 2462(-302)(+245) K, and 2453(-0.060)(+0.063)% K, respectively) are consistent with an isothermal temperature profile of 2386 K, which is significantly higher than the dayside-averaged equilibrium temperature, indicative of very poor heat redistribution efficiency. We also investigate the tentative detections in the g'r'i' bands and the 30 sigma upper limit in the z' band, which might indicate the existence of reflective clouds if these tentative detections do not arise from systematics.

第 114 条，共 222 条

Star-Forming Regions Of The Aquila Rift Cloud Complex II. Turbulence In Molecular Cores Probed By NH3 Emission

Levshakov, SA (Levshakov, S. A.); Henkel, C (Henkel, C.); Reimers, D (Reimers, D.); *Wang, M* (Wang, M.)

ASTRONOMY & ASTROPHYSICS

卷: 567 文献号: A78

Aims. We intend to derive statistical properties of stochastic gas motion inside the dense, low-mass star-forming molecular cores that are traced by NH3(1, 1) and (2, 2) emission lines.

Methods. We use the spatial two-point autocorrelation (ACF) and structure functions calculated from maps of the radial velocity fields.

Results. The observed ammonia cores are characterized by complex intrinsic motions of stochastic nature. The measured kinetic temperature ranges between 8.8 K and 15.1 K. From NH3 excitation temperatures of 3.5-7.3 K, we determine H-2 densities with typical values of n(H2) similar to (1-6) x 10(4) cm(-3). The ammonia abundance, X = [NH3]/[H-2], varies from 2 x 10(-8) to 1.5 x 10(-7). We find oscillating ACFs, which eventually decay to zero with increasing lags on scales of 0.04 less than or similar to l less than or similar to 0.5 pc. The current paradigm supposes that the star-formation process is controlled by the interplay between gravitation and turbulence with the latter preventing molecular cores from a rapid collapse due to their own gravity. Thus, oscillating ACFs may indicate a damping of the developed turbulent flows surrounding the dense but less turbulent core, a transition to dominating gravitational forces and, hence, to gravitational collapse.

第 115 条，共 222 条

Ground-Based Detection Of The Near-Infrared Emission From The Dayside Of WASP-5b

Chen, G (Chen, G.); van Boekel, R (van Boekel, R.); Madhusudhan, N (Madhusudhan, N.); Wang, H (Wang, H.); Nikolov, N (Nikolov, N.); Seemann, U (Seemann, U.); Henning, T (Henning, Th.)
ASTRONOMY & ASTROPHYSICS

卷: 564 文献号: A6

Context. Observations of secondary eclipses of hot Jupiters allow one to measure the dayside thermal emission from the planets' atmospheres. The combination of ground-based near-infrared observations and space-based observations at longer wavelengths constrains the atmospheric temperature structure and chemical composition. Aims. This work aims at detecting the thermal emission of WASP-5b, a highly irradiated dense hot Jupiter orbiting a G4V star every 1.6 days, in the J, H and K near-infrared photometric bands. The spectral energy distribution is used to constrain the temperature-pressure profile and to study the energy budget of WASP-5b. Methods. We observed two secondary-eclipse events of WASP-5b in the J, H, K bands simultaneously using the GROND instrument on the MPG/ESO 2.2 m telescope. The telescope was in nodding mode for the first observation and in staring mode for the second observation. The occultation light curves were modeled to obtain the flux ratios in each band, which were then compared with atmospheric models. Results. Thermal emission of WASP-5b is detected in the J and K bands in staring mode. The retrieved planet-to-star flux ratios are 0.168(-0.052)(+0.050)% in the J band and 0.269 +/- 0.062% in the K band, corresponding to brightness temperatures of 2996(-261)(+212) K and 2890(-269)(+246) K, respectively. No thermal emission is detected in the H band, with a 3 sigma upper limit of 0.166% on the planet-to-star flux ratio, corresponding to a maximum temperature of 2779 K. On the whole, our J, H, K results can be explained by a roughly isothermal temperature profile of similar to 2700 K in the deep layers of the planetary dayside atmosphere that are probed at these wavelengths. Together with Spitzer observations, which probe higher layers that are found to be at similar to 1900 K, a temperature inversion is ruled out in the range of pressures probed by the combined data set. While an oxygen-rich model is unable to explain all the data, a carbon-rich model provides a reasonable fit but violates energy balance. The nodding-mode observation was not used for the analysis because of unremovable systematics. Our experience reconfirms that of previous authors: staring-mode observations are better suited for exoplanet observations than nodding-mode observations.

第 116 条，共 222 条

Broad-Band Transmission Spectrum And K-Band Thermal Emission Of WASP-43b As Observed From The Ground

Chen, G (Chen, G.); van Boekel, R (van Boekel, R.); Wang, H (Wang, H.); Nikolov, N (Nikolov, N.); Fortney, JJ (Fortney, J. J.); Seemann, U (Seemann, U.); Wang, W (Wang, W.); Mancini, L (Mancini, L.); Henning, T (Henning, Th.)
ASTRONOMY & ASTROPHYSICS

卷: 563 文献号: A40

Aims. WASP-43b is the closest-orbiting hot Jupiter, and it has high bulk density. It causes deep eclipse depths in the system's light curve in both transit and occultation that is attributed to the cool temperature and small radius of its host star. We aim to secure a broad-band transmission spectrum and to detect its near-infrared thermal emission in order to characterize its atmosphere.
Methods. We observed one transit and one occultation event simultaneously in the g', r', i', z', J, H, K bands using the GROND instrument on the MPG/ESO 2.2-m telescope, where the telescope was heavily defocused in staring mode. After modeling the light curves, we derived wavelength-dependent transit depths and flux ratios and compared them to atmospheric models.
Results. From the transit event, we have independently derived WASP-43's system parameters with high precision and improved the period to be 0.81347437(13) days based on all the available timings. No significant variation in transit depths is detected, with the largest deviations coming from the i'-, H-, and K-bands. Given the observational uncertainties, the broad-band transmission spectrum can be explained by either (i) a flat featureless straight

line that indicates thick clouds; (ii) synthetic spectra with absorption signatures of atomic Na/K, or molecular TiO/VO that in turn indicate cloud-free atmosphere; or (iii) a Rayleigh scattering profile that indicates high-altitude hazes. From the occultation event, we detected planetary dayside thermal emission in the K-band with a flux ratio of 0.197 +/- 0.042%, which confirms previous detections obtained in the 2.09 mu m narrow band and K-S-band. The K-band brightness temperature 1878(-116)(+108) K favors an atmosphere with poor day-to nightside heat redistribution. We also have a marginal detection in the i'-band (0.037(0.021)(+0.023)%), corresponding to T-B = 2225(225)(+139) K, which is either a false positive, a signature of non-blackbody radiation at this wavelength, or an indication of reflective hazes at high altitude.

第 117 条，共 222 条

Herschel Photometry Of Disks Around Low-Mass Stars In The R Cra Cloud

Harvey, PM (Harvey, Paul M.); Henning, T (Henning, Thomas); *Liu, Y* (Liu, Yao); Wolf, S (Wolf, Sebastian)

ASTROPHYSICAL JOURNAL

卷: 795 期: 1 文献号: 21

We report photometric results from a subset of a Herschel-PACS program to observe cool dust in disks around low-mass stars as a complement to our earlier program to measure far-infrared emission from brown dwarfs. In this latest study we observed five low-mass objects in the nearby R Corona Australis region and detected at least three at 70 mu m. Using a Monte Carlo radiative transfer code we have investigated the disk masses and geometry based on detailed spectral energy distribution (SED) modeling, and we compare these new results to those from our earlier larger sample of brown dwarfs. In particular, our SED analysis for these five objects shows again that disk geometries of brown dwarfs or low-mass stars are generally similar to their higher mass counterparts like T Tauri disks, but the range of disk mass extends to well below the value found in T Tauri stars.

第 118 条，共 222 条

The 3-D Extinction Law In The 2nd Quadrant Of The Galactic Disk

Chao Liu, *Fang M*, Yue Wu, Kenneth Carrell, Xiangxiang Xue and Glenn v an d e Ven

卷：期：298 页：243-243

IAU

We estimate the 3D extinction law in the optical-NIR bands for a line of sight in the 2nd quadrant of the Galactic disk. Two dust lanes are identified at ~9 and ~10.25 kpc in both A V and R V , indicating that the size of the dust grains in the spiral arms is larger than that in the inter-arm regions.

第 119 条，共 222 条

Deep Near-Infrared Imaging Of W3 Main: Constraints On Stellar Cluster Formation

Bik, A (Bik, A.); Stolte, A (Stolte, A.); Gennaro, M (Gennaro, M.); Brandner, W (Brandner, W.); Gouliermis, D (Gouliermis, D.); Hussmann, B (Hussmann, B.); Tognelli, E (Tognelli, E.); Rochau, B (Rochau, B.); Henning, T (Henning, Th.); Adamo, A (Adamo, A.); Beuther, H (Beuther, H.); Pasquali, A (Pasquali, A.); *Wang, Y* (Wang, Y.)

ASTRONOMY & ASTROPHYSICS

卷: 561 文献号: A12

Context. Embedded clusters like W3 Main are complex and dynamically evolving systems that represent an important phase in the star formation process.

Aims. We aim to characterize of the entire stellar content of W3 Main in a statistical sense, which will then identify possible differences in the evolutionary phase of the stellar populations and find clues about the formation mechanism of this massive embedded cluster.

Methods. Deep JHK(s) imaging is used to derive the disk fraction, K-s-band luminosity functions, and mass functions for several subregions in W3 Main. A two-dimensional completeness analysis using artificial star experiments is applied as a crucial ingredient for assessing realistic completeness limits for our photometry.

Results. We find an overall disk fraction of 7.7 +/- 2.3%, radially varying from 9.4 +/- 3.0% in the central 1 pc to 5.6 +/- 2.2% in the outer parts of W3 Main. The mass functions derived for three subregions are consistent with a Kroupa and Chabrier mass function. The mass function of IRSN3 is complete down to 0.14

M-circle dot and shows a break at M similar to 0.5 M-circle dot.
Conclusions. We interpret the higher disk fraction in the center as evidence that the cluster center is younger. We find that the evolutionary sequence observed in the low-mass stellar population is consistent with the observed age spread among the massive stars. An analysis of the mass function variations does not show evidence of mass segregation. W3 Main is currently still actively forming stars, showing that the ionizing feedback of OB stars is confined to small areas (similar to 0.5 pc). The FUV feedback might be influencing large regions of the cluster as suggested by the low overall disk fraction.

第 120 条，共 222 条

Molecular Clouds In The North American And Pelican Nebulae: Structures

Zhang, SB (Zhang, Shaobo); Xu, Y (Xu, Ye); Yang, J (Yang, Ji)
ASTRONOMICAL JOURNAL
卷: 147 期: 3 文献号: 46

We present observations of a 4.25 deg(2) area toward the North American and Pelican Nebulae in the J = 1-0 transitions of (CO)-C-12, (CO)-C-13, and (CO)-O-18. Three molecules show different emission areas with their own distinct structures. These different density tracers reveal several dense clouds with a surface density of over 500 M-circle dot pc(-2) and a mean H-2 column density of 5.8, 3.4, and 11.9 x 10(21) cm(-2) for (CO)-C-12, (CO)-C-13, and (CO)-O-18, respectively. We obtain a total mass of 5.4 x 104 M-circle dot ((CO)-C-12), 2.0 x 10(4) M-circle dot ((CO)-C-13), and 6.1 x 10(3) M-circle dot ((CO)-O-18) in the complex. The distribution of excitation temperature shows two phases of gas: cold gas (similar to 10 K) spreads across the whole cloud; warm gas (>20 K) outlines the edge of the cloud heated by the W80 H II region. The kinetic structure of the cloud indicates an expanding shell surrounding the ionized gas produced by the H II region. There are six discernible regions in the cloud: the Gulf of Mexico, Caribbean Islands and Sea, and Pelican's Beak, Hat, and Neck. The areas of (CO)-C-13 emission range within 2-10 pc(2) with mass of (1-5) x 10(3) M-circle dot and line width of a few km s(-1). The different line properties and signs of star-forming activity indicate they are in different evolutionary stages. Four filamentary structures with complicated velocity features are detected along the dark lane in LDN 935. Furthermore, a total of 611 molecular clumps within the (CO)-C-13 tracing cloud are identified using the ClumpFind algorithm. The properties of the clumps suggest that most of the clumps are gravitationally bound and at an early stage of evolution with cold and dense molecular gas.

Laboratory for Millimeter & Sub-Millimeter Wave

第 121 条，共 222 条

Extraction Of Material Parameters Of A Bi-Layer Structure Using Terahertz Time-Domain Spectroscopy

Jin, BB (Jin BiaoBing); Zhang, CH (Zhang CaiHong); *Shen, XF* (Shen XiaoFang); Ma, JL (Ma JinLong); Chen, J (Chen Jian); Shi, SC (Shi ShengCai); Wu, PH (Wu PeiHeng)
SCIENCE CHINA-INFORMATION SCIENCES
卷: 57 期: 8 文献号: 082408

For a bi-layer structure consisting of a film deposited on a substrate, a new extraction method is proposed using which we can extract both the material parameters of the film and the thickness of the substrate from the measured Terahertz transmission through it, so long as the complex refractive index of the substrate is known beforehand. This method is applicable to a range of refractive indices of the film less than the refractive index of the substrate and a very wide range of layer thicknesses from 20 mu m to at least 200 mu m. It is very useful in some cases where the thickness of the substrate cannot be determined using conventional methods such as a Vernier caliper or micrometer screw.

第 122 条，共 222 条

Temperature Dependence Of The Receiver Noise Temperature And IF Bandwidth Of Superconducting Hot Electron Bolometer Mixers

Zhang, W (Zhang, W.); Miao, W (Miao, W.);

Zhong, JQ (Zhong, J. Q.); Shi, SC (Shi, S. C.); Hayton, DJ (Hayton, D. J.); Vercruyssen, N (Vercruyssen, N.); Gao, JR (Gao, J. R.); Goltsman, GN (Goltsman, G. N.)
SUPERCONDUCTOR SCIENCE & TECHNOLOGY
卷: 27 期: 8 文献号: 085013

In this paper we study the temperature dependence of the receiver noise temperature and IF noise bandwidth of superconducting hot electron bolometer (HEB) mixers. Three superconducting NbN HEB devices of different transition temperatures (T-c) are measured at 0.85 THz and 1.4 THz at different bath temperatures (T-bath) between 4 K and 9 K. Measurement results demonstrate that the receiver noise temperature of superconducting NbN HEB devices is nearly constant for T-bath/T-c, less than 0.8, which is consistent with the simulation based on a distributed hot-spot model. In addition, the IF noise bandwidth appears independent of T-bath/T-c, indicating the dominance of phonon cooling in the investigated HEB devices.

第 123 条，共 222 条

Terahertz Direct-Detection Behavior Of Niobium Nitride Superconducting Tunnel Junctions Above Liquid Helium Temperature

Wang, Z (Wang, Zheng); Liu, D (Liu, Dong); Li, SL (Li, Shao-liang); Li, J (Li, Jing); Shi, SC (Shi, Sheng-Cai)
SUPERCONDUCTOR SCIENCE & TECHNOLOGY
卷: 27 期: 7 文献号: 075003

Niobium nitride (NbN) superconducting tunnel junctions (STJs) have an energy gap nearly double that of niobium STJs, making them potential sensitive detectors that operate at higher frequencies and temperatures. In this paper, we investigate the direct-detection behavior (i.e. the spectral response, current responsivity, noise characteristics, and noise equivalent power (NEP)) of a 500 GHz NbN STJ detector at temperatures from approximately 5 to 9 K. The detector shows an uncorrected NEP of 3.8 x 10(-13) W/root Hz around 5 K and 1.5 x 10(-12) W/root Hz at 9 K. Its performance can be further improved by adopting a cryogenically cooled readout circuit and fabricating the device with a wiring layer of higher critical-transition temperatures.

第 124 条，共 222 条

A Quasi-Optical Vector Near-Field Measurement System At Terahertz Band

Lou, Z (Lou, Zheng); Hu, J (Hu, Jie); Zhou, KM (Zhou, Kang-Min); Miao, W (Miao, Wei); Shi, SC (Shi, Sheng-Cai)
REVIEW OF SCIENTIFIC INSTRUMENTS
卷: 85 期: 6 文献号: 064702

This paper describes a vector near-field measurement system at terahertz band based on a high sensitivity superconducting receiver equipped with a quasi-optical probe for high resolution near-field sensing. A novel single-receiver rather than commonly used dual-receiver configuration is adopted for vector measurement. Performances of the measurement system including stability and dynamic range are studied. Vector near-field measurement of a diagonal feedhorn at 850 GHz is presented and shows good agreement with simulation and direct far-field measurement. (C) 2014 AIP Publishing LLC.

第 125 条，共 222 条

A Novel Compact Butler Matrix Without Phase Shifter

Tian, G (Tian, Ge); *Yang, JP* (Yang, Jin-Ping); Wu, W (Wu, Wen)
IEEE MICROWAVE AND WIRELESS COMPONENTS LETTERS
卷: 24 期: 5 页: 306-308

A novel compact 4 x 4 Butler matrix using only microstrip couplers and a crossover is proposed in this letter. Compared with the conventional Butler matrix, the proposed one avoids the interconnecting mismatch loss and imbalanced amplitude introduced by the phase shifter. The measurements show accurate phase differences of 45 +/- 0.8 degrees and -135 +/- 0.9 degrees with an amplitude imbalance less than 0.4 dB. The 10 dB return loss bandwidth is 20.1%.

第 126 条，共 222 条

Nonlinear Analysis Of A 5-Layer Beam-Like Piezoelectric Transformer Near Resonance

Wang, HR (Wang, Hairen); Xie, X (Xie, Xuan); Hu, YT (Hu, Yuantai); Wang, J (Wang, Ji)

ACTA MECHANICA SOLIDA SINICA
卷: 27 期: 2 页: 195-201

The paper examines the weakly nonlinear behavior of a 5-layer beam-like piezoelectric transformer operating near resonance, where the main structure of the device consists of properly poled and electroded flexible piezoceramic four-layers separated by a central metallic layer. Nonlinear effects of the large deflection to induce the incidental in-plane extension near resonance are considered, which is shown that on one side of the resonant frequency the output-input relation becomes nonlinear, and the other side output voltage experiences jumps.

第 127 条，共 222 条

Weakly Nonlinear Characteristics Of A Three-Layer Circular Piezoelectric Plate-Like Power Harvester Near Resonance

Wang, HR (Wang, H. R.); Xie, X (Xie, X.); Hu, YT (Hu, Y. T.); Wang, J (Wang, J.)
JOURNAL OF MECHANICS
卷: 30 期: 1 页: 97-102

The nonlinear characteristics of a simply-supported three-layer circular piezoelectric plate-like power harvester near resonance are examined in the paper, where the energy-scavenging structure consists of two properly poled piezoceramic layers separated by a central metallic layer. The structure is subjected to a uniform harmonic pressure on the upper surface. Nonlinear effects of large deflection near resonance to induce the incidental in-plane extension are considered. Results on output powers are presented, which exhibit multi-valuedness and jump phenomena.

第 128 条，共 222 条

Recent Advances On Rotational Spectroscopy And Microwave Spectroscopic Techniques

Li, L (Li Li); Sun, M (Sun Ming); Li, XH (Li Xiao-Hua); Zhao, ZW (Zhao Zhen-Wen); Ma, HM (Ma Hui-Min); Gan, HY (Gan Hai-Yong); *Lin, ZH* (Lin Zhen-Hui); Shi, SC (Shi Sheng-Cai); Ziurys, LM (Ziurys, Lucy M.)
CHINESE JOURNAL OF ANALYTICAL CHEMISTRY
卷: 42 期: 9 页: 1369-1378

Rotational spectroscopy is a branch of fundamental science to study the rotational spectra of molecules, free radicals and ions based on the quantum mechanics. It has great applications on many fields such as radio astronomy and atmospheric remote sensing. In this paper we reviewed the basic theory of rotational spectroscopy, two different types of Fourier transform microwave spectrometers, spectroscopic analysis of certain typical cases, and future prospect of the microwave spectroscopic techniques as well.

第 129 条，共 222 条

4 K High Frequency Pulse Tube Cryocooler Used For Terahertz Space Application

Quan, J (Quan, Jia); Liu, YJ (Liu, Yanjie); *Liu, D* (Liu, Dong); Zhang, K (Zhang, Kun); Liang, JT (Liang, Jingtao); Li, J (Li, Jing); Yao, QJ (Yao, Qijun); Shi, SC (Shi, Shengcai)
CHINESE SCIENCE BULLETIN
卷: 59 期: 27 页: 3490-3494

Terahertz (THz) frequency region, defined from 0.1 to 10 THz, is an important frequency band for radio astronomy and atmospheric science. As NbN Superconductor-Insulator-Superconductor (SIS) mixers used for terahertz detection, which are studied by the Purple Mountain Observatory (PMO), Chinese Academy of Sciences (CAS), work at 8-10 K, and require condition of micro vibrations, its astronomical observation in aerospace is limited by suitable refrigeration method. 4 K high frequency pulse tube cryocooler developed by Key Laboratory of Space Energy Conversion Technologies (SECT), Technical Institute of Physics and Chemistry (TIPC), CAS, offers an opportunity for the application of SIS mixers. This article introduces the progress of the two-stage high frequency pulse tube cryocooler researched by TIPC. The cryocooler has reached a no load temperature of 4.5 K which is the lowest temperature for this kind of cryocooler reported so far. The successful coupling between the THz component and the high frequency pulse tube cryocooler lays a solid foundation for space detection in the terahertz band.

第 130 条，共 222 条

A 3.7 Thz Third-Order Distributed Feedback Quantum Cascade Laser As The Local Oscillator Of A Superconducting Hot Electron Bolometer Receiver

缪巍,张文,娄峥,李邵亮,钟加强,周康敏,任远,张坤,姚骑均,史生才

期: 1 页: 1-34

会议论文,会议名称:General Assembly and Scientific Symposium (URSI GASS)

In this paper, we report on the investigation of a 3.7 THz phase-matched third-order distributed feedback (DFB) quantum cascade laser (QCL) as the local oscillator (LO) of a superconducting hot electron bolometer (HEB) heterodyne receiver. Due to the incorporation of the third-order Bragg gratings, the beam pattern of the QCL was found much improved. Beam pattern measurements show that the QCL has a narrow beam with ~12×18 degree divergence, which is in good agreement with simulations by considering the gratings as an array of phased linear sources. Using this QCL as LO, we measured the noise temperature of a log-spiral antenna coupled superconducting HEB mixer at 3.7 THz. The lowest double-sideband (DSB) receiver noise temperature is about 4000 K, and reduced to 1100 K after correcting the optical losses. This result shows that phase-matched third-order DFB QCLs are very promising device as a LO in THz heterodyne receivers.

第 131 条,共 222 条

Characterization Of Terahertz Detectors Based On Niobium Nitride Superconducting Tunnel Junctions

Wang Z,S Li,D Liu

期: 31 页: 1-4

会议论文,会议名称:General Assembly and Scientific Symposium (URSI GASS)

Terahertz direct detectors based on superconducting tunnel junctions (STJs) have the merits of short response time, large dynamic range and relatively high operating temperature, providing a good choice for terahertz detection. Compared with commonly used niobium STJs, niobium nitride (NbN) ones have a high transition temperature close to 16K. Hence they might be useful for terahertz detection operating at temperatures well above the LHe temperature of 4.2K. In this paper, we investigate the properties of NbN STJ detectors at different bath temperatures. Detailed experiment results are given.

第 132 条,共 222 条

The Control System For The 13.7m Millimeter Wavelength Telescope Equipped With Multibeam Receiver

Duan WY; Jixian Sun ; Qijun Yao ; Yingxi Zuo ; Jinjiang Sun ; Shaoliang Li ; Zhenhui Lin ;Xuguo Zhang ; Wenlei Shan ; Shengcai Shi ; Ji Yang

期: 9 页: 1696-1701

会议论文,会议名称:2013 Ninth International Conference on. IEEE

An upgraded version of the control system for the Delingha 13.7m millimeter wavelength telescope is recently introduced. This new control system adapts the new installed multi-beam receiver operated between 85 and 115 GHz. This paper presents a general overview of this new control system, which performs many operational functions including star acquisition and tracking, receiver setting and monitoring, spectra analyzing and data storage, and observation scheduling based on a distributed computing system. Special descriptions are given to the frontend and backend control of the multi-beam receiver.

第 133 条,共 222 条

A W-Band Subharmonic Schottky Mixer For Millimeter Imaging

Hu,Jie Cheng-Jiang Zhang, Qing Ding, Zheng Lou , Sheng-Cai Shi

卷: 9275,期: 927514,页: 9275-1-9275-6

Proc. of SPIE

A 100GHz Schottky diode mixer based on quartz substrate is presented, which will be used as the detector for the millimeter imaging. The Schottky diode is modeled based on its physical dimension thus its high frequency parasitic parameters can be fully taken into consideration. The measured conversionloss is better than 10dBm over 95~105GHz with 8dBm LO pump at 49.53GHz. The measured result is also in

excellent accord with the simulated model.

第 134 条，共 222 条

Investigation Of Superconducting Nbn Hot-Electron Bolometers For Terahertz Direct Detection

Zhong JQ, Wei MIAO, Wen ZHANG, Sheng-cai SHI, and François PAJOT

期: 31，页:1-4

会议论文，会议名称：General Assembly and Scientific Symposium (URSI GASS)

In this paper, we report on the terahertz (THz) direct detection performance of two superconducting niobium nitride (NbN) hot-electron bolometers (HEBs) of different micro-bridge sizes. At the optimum bias point, the two HEB devices show similar thermal conductance (~80nW/K). The measured responsivity coincides well with the electrical responsivity calculated from the measured current-voltage (IV) curves at different bath temperatures. The noise equivalent power (NEP) of the two HEB devices is found to be about 10W/√Hz.

第 135 条，共 222 条

Frequency Spectrum Of A Thz QCL In Pulse Mode Measured By An FTS System

Li SL, Wei Miao, Zhen-Hui Lin, Qi-Jun Yao and Sheng-Cai Shi

卷: 9275，期: 9275，页: 927515-927515

会议论文，会议名称：Proc. SPIE 9275, Infrared, Millimeter-Wave, and Terahertz Technologies III

In this paper, we report on the spectrum measurement of a terahertz (THz) pulse signal using a Fourier transform spectroscopy (FTS) system. The THz pulse signal is a quantum cascade laser (QCL) at 3.7THz with changeable repeating frequency and duty cycle. With a fixed duty cycle, the repeating frequency is changed to investigate the maximum value that can be measured with an FTS system. The relationship between the spectrum intensity and the pulse width is investigated through the variance of the duty cycle with a given repeating frequency. Detailed experimental results will be presented.

第 136 条，共 222 条

Far-Field Beam-Pattern Of A Twin-Slot HEB Mixer At 600ghz

Zhou KM, Yan Delorme, Roland Lefevre, Frederic.Dauplay,
Alexandre.Feret, Thibaut Vacelet, Zheng Lou and Sheng-Cai Shi

卷: 9275，期: 9275，页: 9275Z1-9275Z7

会议论文，会议名称：Proc. SPIE 9275, Infrared, Millimeter-Wave, and Terahertz Technologies III

In this paper, we report on the measured and simulated far-field beam-patterns of a quasi-optical NbNsuperconducting hot electron bolometer (HEB) mixer at 600GHz. This superconducting HEB mixer consists of an extended hemispherical lens with a diameter of 12.7mm and an extension length of 2.45mm, a twin-slot planar antenna (two slots measuring 148.5μm x 10.4μm with a separation of 78.98μm) and a 5.5-nm thick NbN thin-film micro-bridge with an area of 2μm x0.2μm . The far-field beam pattern of this mixer is measured by a direct-detection technique with a dynamic range of nearly 25dB, showing an FWHM beam angle of 2.7°and -18dB level of the first side-lobe. The measured beam of the quasi-optical mixer is nearly collimated and has good Gaussian beam efficiency. In addition, the far-field beam-pattern is measured at different DC bias voltages of the superconducting HEB mixer and at different bath temperatures. The measured results are compared with the ones simulated by two different methods. Detailed measurement and simulation results will be presented.

第 137 条，共 222 条

Nonlinear Characteristics Of Circular-Cylinder Piezoelectric Power Harvester Near Resonance Based On Flow-Induced Flexural Vibration Mode

Wang, HR (Wang, Hai-ren); Xie, JM (Xie, Jie-min); Xie, X (Xie, Xuan); Hu, YT (Hu, Yuan-tai); Wang, J (Wang, Ji)

APPLIED MATHEMATICS AND MECHANICS-ENGLISH EDITION

卷: 35 期: 2 页: 229-236

The nonlinear behaviors of a circular-cylinder piezoelectric power harvester (CCPPH) near resonance are analyzed based on the flow-induced flexural vibration mode. The

geometrically-nonlinear effect of the cylinder is studied with considering the in-plane extension incidental to the large deflection. The boundary electric charges generated from two deformation modes, flexure and in-plane extension, were distinguished with each other because the charge corresponding to the latter mode produces no contribution to the output current. Numerical results on output powers show that there are multivaluedness and jump behaviors.

第 138 条，共 222 条

Non-Uniform Absorption Of Terahertz Radiation On Superconducting Hot Electron Bolometer Microbridges

Miao, W (Miao, W.); Zhang, W (Zhang, W.); Zhong, JQ (Zhong, J. Q.); Shi, SC (Shi, S. C.); Delorme, Y (Delorme, Y.); Lefevre, R (Lefevre, R.); Feret, A (Feret, A.); Vacelet, T (Vacelet, T.)

APPLIED PHYSICS LETTERS

卷: 104 期: 5 文献号: 052605

We interpret the experimental observation of a frequency-dependence of superconducting hot electron bolometer (HEB) mixers by taking into account the non-uniform absorption of the terahertz radiation on the superconducting HEB microbridge. The radiation absorption is assumed to be proportional to the local surface resistance of the HEB microbridge, which is computed using the Mattis-Bardeen theory. With this assumption the dc and mixing characteristics of a superconducting niobium-nitride (NbN) HEB device have been modeled at frequencies below and above the equilibrium gap frequency of the NbN film. (C) 2014 AIP Publishing LLC.

第 139 条，共 222 条

Research On The Equivalent Circuit Model Of The Three-Port T-Junction And Its Applications To High-Performance Branch-Line Coupler

Tian G; *Yang JP*; Shi Shengcai; Wu Wen

卷: 42 期: 1 页: 199-203

Tien Tzu Hsueh Pao/Acta Electronica Sinica

This method extracts parameters of the equivalent circuit model with high accuracy in ultra wideband. In order to control the effect of the parasitic capacitance, two improved T-junctions with concave and convex segments are proposed. The effect in the equivalent circuit model and parasitic capacitance due to different connection ways of three-port T-junction is also investigated. Then the improved T-ju

第 140 条，共 222 条

The Study Of Purity Improvement On Tl-1223 Thin Films By DC Sputtering And Post-Annealing Method

Gao, XX (Gao, X. X.); Xie, W (Xie, W.); *Wang, Z* (Wang, Z.); Zhao, XJ (Zhao, X. J.); He, M (He, M.); Zhang, X (Zhang, X.); Yan, SL (Yan, S. L.); Ji, L (Ji, L.)

JOURNAL OF SUPERCONDUCTIVITY AND NOVEL MAGNETISM

卷: 27 期: 7 页: 1665-1670

Un-substituted TlBa2Ca2Cu3O (x) (Tl-1223)-superconducting thin films have been fabricated on a LaAlO3 (001) substrate in oxygen by using a two-step method, which includes direct current (DC) magnetron sputtering and post-annealing process. Thallium (Tl) content in amorphous precursor films is found to be important to the crystallization of Tl-superconducting phase. Using the nominal composition of Tl1+delta Ba2Ca2Cu3 O (8) (delta = 0.1 similar to 0.2) precursor films, the formation is promoted to Tl-1223 and Tl-2223 phase rather than Tl-1212 and Tl-1223 phase with accompanying Tl-rich source pellets. When the annealing process continues, Tl-2223 phase will be converted to Tl-1223 phase at a suitable annealing time and temperature. From the X-ray diffraction pattern, only Tl-1223 (00l) peaks are observed, which shows that the purity of Tl-1223 film is improved significantly by this method. The critical temperature T (c) of Tl-1223 film is characterized at 110 K, and the critical current density J (c) (77 K, T = 0) is up to 1.5 MA/cm(2).

Qinhai Observation Station

第 141 条，共 222 条

Discovery Of A Pre-Existing Molecular Filament Associated With Supernova Remnant G127.1+0.5

Zhou, X (Zhou, Xin); Yang, J (Yang, Ji); Fang, M (Fang, Min); Su, Y (Su, Yang)
ASTROPHYSICAL JOURNAL

卷: 791 期: 2 文献号: 109

We performed millimeter observations in CO lines toward the supernova remnant (SNR) G127.1+0.5. We found a molecular filament at 4-13 km s(-1) consisting of two distinct parts: a straight part coming out of the remnant region and a curved part in the remnant region. The curved part is coincides well with the bright SNR shell detected in 1420 MHz radio continuum and mid-infrared observations in the northeastern region. In addition, redshifted line wing broadening is found only in the curved part of the molecular filament, which indicates a physical interaction. These provide strong evidences, for the first time, to confirm the association between an SNR and a pre-existing long molecular filament. Multi-band observations in the northeastern remnant shell could be explained by the interaction between the remnant shock and the dense molecular filament. RADEX radiative transfer modeling of the quiet and shocked components yield physical conditions consistent with the passage of a non-dissociative J-type shock. We argue that the curved part of the filament is fully engulfed by the remnant's forward shock. A spatial correlation between aggregated young stellar objects (YSOs) and the adjacent molecular filament close to the SNR is also found, which could be related to the progenitor's activity.

第 142 条，共 222 条

Trigonometric Parallaxes Of Star Forming Regions In The Perseus Spiral Arm

Choi, YK (Choi, Y. K.); Hachisuka, K (Hachisuka, K.); Reid, MJ (Reid, M. J.); Xu, Y (Xu, Y.); Brunthaler, A (Brunthaler, A.); Menten, KM (Menten, K. M.); Dame, TM (Dame, T. M.)
ASTROPHYSICAL JOURNAL

卷: 790 期: 2 文献号: 99

We report trigonometric parallaxes and proper motions of water masers for 12 massive star forming regions in the Perseus spiral arm of the Milky Way as part of the Bar and Spiral Structure Legacy (BeSSel) Survey. Combining our results with 14 parallax measurements in the literature, we estimate a pitch angle of 9 degrees.9 +/- 1 degrees.5 for a section of the Perseus arm. The three-dimensional Galactic peculiar motions of these sources indicate that on average they are moving toward the Galactic center and slower than the Galactic rotation.

第 143 条，共 222 条

Trigonometric Parallaxes Of Star-Forming Regions In The Sagittarius Spiral Arm

Wu, YW (Wu, Y. W.); Sato, M (Sato, M.); Reid, MJ (Reid, M. J.); Moscadelli, L (Moscadelli, L.); Zhang, B (Zhang, B.); Xu, Y (Xu, Y.); Brunthaler, A (Brunthaler, A.); Menten, KM (Menten, K. M.); Dame, TM (Dame, T. M.); Zheng, XW (Zheng, X. W.)
ASTRONOMY & ASTROPHYSICS

卷: 566 文献号: A17

We report measurements of parallaxes and proper motions of ten high-mass star-forming regions in the Sagittarius spiral arm of the Milky Way as part of the BeSSeL Survey with the VLBA. Combining these results with eight others from the literature, we investigated the structure and kinematics of the arm between Galactocentric azimuths beta approximate to -2 degrees. and 65 degrees. We found that the spiral pitch angle is 7 degrees.3 +/- 1 degrees.5; the arm's half-width, defined as the rms deviation from the fitted spiral, is approximate to 0.2 kpc; and the nearest portion of the Sagittarius arm is 1.4 +/- 0.2 kpc from the Sun. Unlike for adjacent spiral arms, we found no evidence for significant peculiar motions of sources in the Sagittarius arm opposite to Galactic rotation.

第 144 条，共 222 条

Review Of Galactic And Extragalactic Searches For Class I Methanol Masers

Chen, X (Chen, Xi); Ellingsen, SP (Ellingsen, Simon P.); Gan, CG (Gan, Conggui); Xu, Y (Xu, Ye); Shen, ZQ (Shen, Zhiqiang)
CHINESE SCIENCE BULLETIN

卷: 59 期: 11 页: 1066-1077

Class I methanol masers are important tools for investigations of star formation throughout the

Universe. Recently, a series of surveys for class I methanol masers at the 95 GHz transition toward samples of young stellar objects have been undertaken. These surveys have resulted in the detection of about 200 new class I methanol masers and combined with previous observations they have increased the number of known class I methanol masers in our Galaxy to similar to 400. From analysis of the relationship between class I methanol maser emission and associated astrophysical objects, it has been shown that the intensity of the class I methanol maser emission is closely correlated with the properties of the 1.1 mm Bolocam Galactic Plane Survey (BGPS) dust continuum sources and outflow properties. This further supports the hypothesis that class I methanol masers are collisionally pumped and excited in shocked regions. Based on these observations, it can be inferred that the BGPS catalog is likely to provide more reliable samples for targeting further class I methanol maser searches. A new survey for class I methanol masers toward a larger size sample of BGPS sources to test this is currently underway. The prospects for detecting class I methanol megamasers in extragalactic sources is discussed, and observations constituting the first sensitive search have been proposed.

第 145 条，共 222 条

Trigonometric Parallaxes Of High Mass Star Forming Regions: The Structure And Kinematics Of The Milky Way

Reid, MJ (Reid, M. J.); Menten, KM (Menten, K. M.); Brunthaler, A (Brunthaler, A.); Zheng, XW (Zheng, X. W.); Dame, TM (Dame, T. M.); *Xu, Y* (Xu, Y.); Wu, Y (Wu, Y.); Zhang, B (Zhang, B.); Sanna, A (Sanna, A.); Sato, M (Sato, M.); Hachisuka, K (Hachisuka, K.); Choi, YK (Choi, Y. K.); Immer, K (Immer, K.); Moscadelli, L (Moscadelli, L.); Rygl, KLJ (Rygl, K. L. J.); Bartkiewicz, A (Bartkiewicz, A.)

ASTROPHYSICAL JOURNAL

卷: 783 期: 2 文献号: 130

Over 100 trigonometric parallaxes and proper motions for masers associated with young, high-mass stars have been measured with the Bar and Spiral Structure Legacy Survey, a Very Long Baseline Array key science project, the European VLBI Network, and the Japanese VLBI Exploration of Radio Astrometry project. These measurements provide strong evidence for the existence of spiral arms in the MilkyWay, accurately locating many arm segments and yielding spiral pitch angles ranging from about 7 degrees to 20 degrees. The widths of spiral arms increase with distance from the Galactic center. Fitting axially symmetric models of the MilkyWay with the three- dimensional position and velocity information and conservative priors for the solar and average source peculiar motions, we estimate the distance to the Galactic center, R-0, to be 8.34 +/- 0.16 kpc, a circular rotation speed at the Sun, Theta(0), to be 240 +/- 8 km s(-1), and a rotation curve that is nearly flat (i. e., a slope of -0.2 +/- 0.4 km s(-1) kpc(-1)) between Galactocentric radii of approximate to 5 and 16 kpc. Assuming a " universal" spiral galaxy form for the rotation curve, we estimate the thin disk scale length to be 2.44 +/- 0.16 kpc. With this large data set, the parameters R-0 and Theta(0) are no longer highly correlated and are relatively insensitive to different forms of the rotation curve. If one adopts a theoretically motivated prior that high-mass star forming regions are in nearly circular Galactic orbits, we estimate a global solar motion component in the direction of Galactic rotation, V-circle dot = 14.6 +/- 5.0 km s(-1). While Theta(0) and V-circle dot are significantly correlated, the sum of these parameters is well constrained, Theta(0) + V circle dot = 255.2 +/- 5.1 km s(-1), as is the angular speed of the Sun in its orbit about the Galactic center, (Theta(0) + V-circle dot)/R-0 = 30.57 +/- 0.43 km s(-1) kpc(-1). These parameters improve the accuracy of estimates of the accelerations of the Sun and the Hulse-Taylor binary pulsar in their Galactic orbits, significantly reducing the uncertainty in tests of gravitational radiation predicted by general relativity.

第 146 条，共 222 条

6.7 Ghz Methanol Maser Survey Toward GLIMPSE Point Sources And BGPS 1.1 Mm Dust Clumps

Sun, Y (Sun, Yan); Xu, Y (Xu, Ye); Chen, X (Chen, Xi); Zhang, B (Zhang, Bo); Wu, YW (Wu, Yuan-Wei); Henkel, C (Henkel, Christian); Brunthaler, A (Brunthaler, Andreas); Choi, YK (Choi, Yoon Kyung); Zheng, XW (Zheng, Xing-Wu)

ASTRONOMY & ASTROPHYSICS

卷: 563 文献号: A130

We present the results of a 6.7 GHz methanol maser survey from the Effelsberg 100 m radio telescope. A sample of 404 sources from the Bolocam Galactic Plane Survey (BGPS) 1.1 mm dust clump survey that met specific Galactic Legacy Infrared Mid-Plane Survey Extraodinaire (GLIMPSE) point-source color criteria was selected and 318 of these were observed. The new observations resulted in the detection of 29 methanol masers, including 12 new ones. Together with the additional 74 detections from the literature, this means that a total of 103 methanol masers are coincident with 1.1 mm dust clumps, yielding an overall detection rate of 26%. A comparison of the properties of a 1.1 mm dust clump and a 6.7 GHz methanol maser indicates that methanol masers with a higher flux density and/or luminosity are generally associated with more massive but less dense 1.1 mm dust clumps. The overall detection rate of 26% appears to vary as a function of the derived H-2 column density of the associated 1.1 mm dust clump. The methanol masers were primarily detected toward the brighter and more massive 1.1 mm dust clumps. A subsample of 194 sources that overlapped sources with observations of the 95 GHz methanol line was investigated in more detail for the properties of 1.1 mm dust clumps. The statistical analysis reveals that 1.1 mm dust clumps with both class I and II counterparts have much higher mean and median values of mass, column density, and flux density than those with only class I or II counterparts. Based on our much larger sample, we slightly revise the boundary defined previously for selecting BGPS sources associated with a class II methanol maser, wherein similar to 80% of expected class II methanol masers will be detected with a detection rate in the range of 40-50%.

第 147 条，共 222 条

Interaction Between Supernova Remnant G22.7–0.2 And The Ambient Molecular Clouds

Su,Y Ji Yang, Xin Zhou, Ping Zhou, and Yang Chen

卷: 796 期:2 页: 122-130

ASTROPHYSICAL JOURNAL

We have carried out ^{12}CO (J = 1-0 and 2-1), ^{13}CO (J = 1-0), and C^{18}O (J = 1-0) observations in the direction of the supernova remnant (SNR) G22.7-0.2. A filamentary molecular gas structure, which is likely part of a larger molecular complex with V_{LSR} ~ 75-79 km s^{-1}, is detected and is found to surround the southern boundary of the remnant. In particular, the high-velocity wing (77-110 km s^{-1}) in the ^{12}CO (J = 1-0 and J = 2-1) emission shows convincing evidence of the interaction between SNR G22.7-0.2 and the 75-79 km s^{-1} molecular clouds (MCs). Spectra with redshifted profiles, a signature of shocked molecular gas, are seen in the southeastern boundary of the remnant. The association between the remnant and the 77 km s^{-1} MCs places the remnant at the near distance of 4.4 ± 0.4 kpc, which agrees with a location on the Scutum-Crux arm. We suggest that SNR G22.7-0.2, SNR W41, and H II region G022.760-0.485 are at the same distance and are associated with GMC G23.0-0.4.

第 148 条，共 222 条

Star Formation Associated With A Large-Scale Infrared Bubble

Xu, JL (Xu, Jin-Long); *Ju, BG* (Ju, Bing-Gang)

ASTRONOMY & ASTROPHYSICS

卷: 569 文献号: A36

Aims. To investigate how a large-scale infrared bubble centered at l = 53.9 degrees and b = 0.2 degrees forms, and to study if star formation is taking place at the periphery of the bubble, we performed a multiwavelength study.

Methods. Using the data from the Galactic Ring Survey (GRS) and Galactic Legacy Infrared Mid-Plane Survey Extraordinaire (GLIMPSE), we performed a study of a large-scale infrared bubble with a size of about 16 pc at a distance of 2.0 kpc. We present the (CO)-C-12 J = 1-0, (CO)-C-13 J = 1-0, and (CO)-O-18 J = 1-0 observations of HII region G53.54-0.01 (Sh2-82) obtained at the Purple Mountain Observation (PMO) 13.7 m radio telescope to investigate the detailed distribution of associated molecular material. In addition, we also used radiorecombination line and VLA data. To select young stellar objects (YSOs) consistent with this region, we used the GLIMPSE I catalog.

Results. The large-scale infrared bubble shows a half-shell morphology at 8 mu m. The H II regions of G53.54-0.01, G53.64+0.24, and

G54.09-0.06 are situated on the bubble. Comparing the radio recombination line velocities and associated (CO)-C-13 J = 1-0 components of the three H II regions, we found that the 8 mu m emission associated with H II region G53.54-0.01 should belong to the foreground emission, and only overlap with the large-scale infrared bubble in the line of sight. Three extended green objects (EGOs, the candidate massive young stellar objects), as well as three H II regions and two small-scale bubbles are found located in the G54.09-0.06 complex, indicating an active massive star-forming region. Emission from (CO)-O-18 at J = 1-0 presents four cloud clumps on the northeastern border of H II region G53.54-0.01. By comparing the spectral profiles of (CO)-C-12 J = 1-0, (CO)-C-13 J = 1-0, and (CO)-O-18 J = 1-0 at the peak position of each clump, we found the collected gas in the three clumps, except for the clump coinciding with a massive YSO (IRAS 19282+1814). Using the evolutive model of the H II region, we derived that the age of H II region G53.54-0.01 is 1.5 x 10(6) yr. The significant enhancement of several Class I and Class II YSOs around G53.54-0.01 indicates the presence of some recently formed stars, which may be triggered by this H II region through the collect-and-collapse process.

第 149 条，共 222 条

A CO Observation Of The Galactic Methanol Masers

Ren, ZY (Ren, Zhiyuan); Wu, YF (Wu, Yuefang); Liu, T (Liu, Tie); Li, LX (Li, Lixin); Li, D (Li, Di); *Ju, BG* (Ju, Binggang)

ASTRONOMY & ASTROPHYSICS

卷: 567 文献号: A40

Context We investigated the molecular gas associated with 6.7 GHz methanol masers throughout the Galaxy using a J = 1-0 transition of the CO isotopologues. Aims. The methanol maser at 6.7 GHz is an ideal tracer for young high mass star forming cores. Based CM molecular line emissions in the maser sources throughout the Galaxy, we can estimate their physical parameters and, thereby, investigate the forming conditions of the high-mass stars.

Methods, Using the 13.7-m telescope at the Purple Mountain Observatory (PMO), we have obtained (CO)-C-12 and (CO)-C-13 (1-0) lines for 160 methanol masers sources from the first to the third Galactic quadrants. We made efforts to resolve the distance ambiguity by careful comparison with the radio continuum and HI 21 em observations. We examined the statistical properties in three aspects: first. the variation throughout the Galaxy; second, the correlation between the different parameters; third, the difference between the maser sources and the infrared dark clouds. In addition, we have also carried out (CO)-C-13 mapping for 33 sources in our sample.

Results. First, the maser sources show increased (CO)-C-13 line widths toward the Galactic center suggesting that the molecular gas are more turbulent toward the Galactic center. This trend can be noticeably traced by the (CO)-C-13 line width. In comparison, the Galactic variation for the IT column density and the (CO)-C-12 excitation temperature are less significant. Second, the (CO)-C-12 1 excitation temperature shows a noticeable correlation with the H-2 column density. A possible explanation consistent with the collapse model is that the higher surface-density gas is more efficient to the stellar heating and/or has a higher formation rate of high mass stars. Third.comparing the infrared dark clouds, the maser sources on average have significantly lower H-2 column densities, moderately higher temperatures, and similar line widths. Fourth, In the mapped regions around 33 masers, 51 (CO)-C-13 cores have been revealed. Among them, only 17 coincide with the radio continuum emission (F-cm > 6 mty). while a larger fraction (30 cores) coincide with the infrared emissions. Only one maser source has no significant IR emission. The IR-bright and radio bright sources exhibit significantly higher (CO)-C-12 excitation temperatures than the IR-faint and radio-faint sources, respectively.

Conclusions. The 6.7 GHz masers show a moderately low ionization rate but have a common existing stellar heating that generates the IR emissions, The relevant properties can be characterized by the (CO)-C-12 and (CO)-C-12 (1-0) emissions in several aspects as described above.

第 150 条，共 222 条

Trigonometric Parallaxes Of Star Forming Regions In The Scutum Spiral Arm

Sato, M (Sato, M.); *Wu, YW* (Wu, Y. W.); Immer, K (Immer, K.); Zhang, B (Zhang, B.); Sanna, A (Sanna, A.); Reid, MJ (Reid, M. J.); Dame, TM (Dame, T. M.); Brunthaler, A (Brunthaler, A.); Menten, KM (Menten, K. M.)

ASTROPHYSICAL JOURNAL

卷: 793 期: 2 文献号: 72

We report measurements of trigonometric parallaxes for six high-mass star-forming regions in the Scutum spiral arm of the Milky Way as part of the BeSSeL Survey. Combining our measurements with 10 previous measurements from the BeSSeL Survey yields a total sample of 16 sources in the Scutum arm with trigonometric parallaxes in the Galactic longitude range from 5 degrees to 32 degrees. Assuming a logarithmic spiral model, we estimate a pitch angle of 19 degrees.8 +/- 3 degrees.1 for the Scutum arm, which is larger than pitch angles reported for other spiral arms. The high pitch angle of the arm may be due to the arm's proximity to the Galactic bar. The Scutum arm sources show an average peculiar motion of 4 km s(-1) slower than the Galactic rotation and 8 km s(-1) toward the Galactic center. While the direction of this non-circular motion has the same sign as determined for sources in other spiral arms, the motion toward the Galactic center is greater for the Scutum arm sources.

第 151 条，共 222 条

Molecular Environment Of The Supernova Remnant Ic 443: Discovery Of The Molecular Shells Surrounding The Remnant

Su, Y (Su, Yang); Fang, M (Fang, Min); Yang, J (Yang, Ji); Zhou, P (Zhou, Ping); Chen, Y (Chen, Yang)

ASTROPHYSICAL JOURNAL

卷: 788 期: 2 文献号: 122

We have carried out (CO)-C-12, (CO)-C-13, and (CO)-O-18 observations toward the mixed morphology supernova remnant (SNR) IC 443. The observations cover a 1.5(degrees) x 1.5 degrees area and allow us to investigate the overall molecular environment of the remnant. Some northern and northeastern partial shell structure of CO gas is around the remnant. One of the partial shells, about 5' extending beyond the northeastern border of the remnant's bright radio shell, seems to just confine the faint radio halo. On the other hand, some faint CO clumps can be discerned along the eastern boundary of the faint remnant's radio halo. Connecting the eastern CO clumps, the northeastern partial shell structures, and the northern CO partial shell, we can see that a half molecular ring structure appears to surround the remnant. The LSR velocity of the half-ring structure is in the range of -5 km s(-1) to -2 km s(-1), which is consistent with that of the -4 km s(-1) molecular clouds. We suggest that the half-ring structure of the CO emission at V-LSR similar to -4 km s(-1) is associated with the SNR. The structures are possibly swept up by the stellar winds of SNR IC 443's massive progenitor. Based on theWide-field Infrared Survey Explorer and the Two Micron All Sky Survey near-IR database, 62 young stellar object (YSO) candidates are selected within the radio halo of the remnant. These YSO candidates concentrated along the boundary of the remnant's bright radio shell are likely to be triggered by the stellar winds from the massive progenitor of SNR IC 443.

第 152 条，共 222 条

Thermal Deformation Of The Delingha 13.7 M Telescope

Sun JX; Zuo Yingxi; Yang Ji; Li Yang; Ma Junmei; Lu Dengrong

卷: 55 期: 3 页: 246-255

Acta Astronomica Sinica

Thermal deformation is one of the key causes that degrade the performance of a large millimeter-wave antenna. It will affect the axis and focus of the antenna, increase the error of the reflector, and further result in not only the decrease of pointing and efficiency of the telescope but also the degradation of their long-term stability. Moreover, the diurnal motion of the sun will cause a variation of temperature difference of the pedestal structure, resulting in a tilt variation of the azimuth axis. In this paper, we present a study on the thermal deformation behavior of the Delingha 13.7 m millimeter-wave radio telescope by means of several methods. The relation between the defocus and the temperature difference of the antenna structure along the normal direction of

the main reflector has been investigated. Consequently, the real-time focusing of the antenna has been realized by adaptive adjustment of the subreflector, thereby the antenna efficiency has been significantly improved. The pointing error as a function of the temperature difference across the reflector aperture has been studied and corrected. The thermal induced pedestal tilt variation is also one of the sources of the pointing error. By wrapping the tower legs with thermal insulation materials, the peak of the pedestal tilt variation is reduced from 7'' to 3'',and the related pointing error is reduced from 3'' to 1.5''.

第 153 条，共 222 条

The Parallax Of W43: A Massive Star-Forming Complex Near The Galactic Bar

Zhang, B (Zhang, B.); Moscadelli, L (Moscadelli, L.); Sato, M (Sato, M.); Reid, MJ (Reid, M. J.); Menten, KM (Menten, K. M.); Zheng, XW (Zheng, X. W.); Brunthaler, A (Brunthaler, A.); Dame, TM (Dame, T. M.); *Xu, Y* (Xu, Y.); Immer, K (Immer, K.)
ASTROPHYSICAL JOURNAL

卷: 781 期: 2 文献号: 89

We report trigonometric parallax measurements of masers in the massive star-forming complex W43 from Very Long Baseline Array observations as part of the Bar and Spiral Structure Legacy Survey. Based on measurements of three 12 GHz methanol maser sources (G029.86-00.04, G029.95-00.01, and G031.28+00.06) and one 22 GHz water maser source (G031.58+ 00.07) toward W43, we derived a distance of 5.49(-0.34)(+0.39) kpc to W43. By associating the masers with CO molecular clouds, and associating the clouds kinematically with CO longitude-velocity spiral features, we assign W43 to the Scutum spiral arm, close to the near end of the Galactic bar. The peculiar motion of W43 is about 20 km s(-1) toward the Galactic Center and is very likely induced by the gravitational attraction of the bar.

第 154 条，共 222 条

Photometric Study Of The Pulsating, Eclipsing Binary OO DRA

Zhang, XB (Zhang, X. B.); Deng, LC (Deng, L. C.); Tian, JF (Tian, J. F.); Wang, K (Wang, K.); *Sun, JJ* (Sun, J. J.); Liu, QL (Liu, Q. L.); Xin, HQ (Xin, H. Q.); Zhou, Q (Zhou, Q.); Yan, ZZ (Yan, Z. Z.); Luo, ZQ (Luo, Z. Q.); Luo, CQ (Luo, C. Q.)

卷: 148 期: 6 文献号: 106

ASTRONOMICAL JOURNAL

We present a comprehensive photometric study of the pulsating, eclipsing binary OO Dra. Simultaneous B- and V-band photometry of the star was carried out on 14 nights. A revised orbital period and a new ephemeris were derived from the data. The first photometric solution of the binary system and the physical parameters of the component stars are determined. They reveal that OO Dra could be a detached system with a less-massive secondary component nearly filling its Roche lobe. By subtracting the eclipsing light changes from the data, we obtained the intrinsic pulsating light curves of the hotter, massive primary component. A frequency analysis of the residual light yields two confident pulsation modes in both B- and V-band data with the dominant frequency detected at 41.865 c/d. A brief discussion concerning the evolutionary status and the pulsation nature of the binary system is finally given.

III. Applied Celestial Mechanics and Space Object & Debris Research

Center for Space Object and Debris Research

第 155 条，共 222 条

Long Term Evolution Of Molniya Orbit Under The Effect Of Earth's Non-Spherical Gravitational Perturbation

Zhu, TL (Zhu, Ting-Lei); Zhao, CY (Zhao, Chang-Yin); Zhang, MJ (Zhang, Ming-Jiang)
ADVANCES IN SPACE RESEARCH

卷: 54 期: 2 页: 197-208

A double resonance model is applied to study the long term evolution of a Molniya orbit, which is highly elliptical (e >= 0.7), critically inclined (i approximate to 63.4 degrees), and in the state of the 2:1 mean motion resonance with the Earth rotation. The dynamics of a Molniya orbit can be divided into three kinds: short (12
h), intermediate (several years) and long (several centuries) period motions, with the latter two studied in this paper. The J(2) and J(12) (l = 2, 3,..., 8) harmonics are modelled, based on a careful selection. The analytic solution for the intermediate period motion is obtained, a first integral, (I) over bar (3), for the long period motion is derived analytically, and the phase structures are obtained by the level curves of (I) over bar (3). Three types of the phase structures, depending on the equilibria and stabilities, are observed when the Hamiltonian constant varies. Compared with the near circular 12-h satellite orbits and with the critically inclined orbits without mean motion resonance with the Earth rotation, the features of the Molniya orbits are discussed in detail. It is pointed out that (1) unlike the case of near circular orbits, the J(32) term does not dominate the 2:1 mean motion resonance problem (intermediate period motion), and that (2) instead of the J(2)(2) terms, the resonant tesseral harmonics dominate the critical inclination problem (long period motion).

第 156 条，共 222 条

An Adaptive Threshold Method For Improving Astrometry Of Space Debris CCD Images

Sun, RY (Sun, Rong-yu); Zhao, CY (Zhao, Chang-yin)

ADVANCES IN SPACE RESEARCH

卷: 53 期: 11 页: 1664-1674

Optical survey is a main technique for observing space debris, and precisely measuring the positions of space debris is of great importance. Due to several factors, e.g. the angle object normal to the observer, the shape as well as the attitude of the object, the variations of observed characteristics for low earth orbital space debris are distinct. When we look at optical CCD images of observed objects, the size and brightness are varying, hence it's difficult to decide the threshold during centroid measurement and precise astrometry. Traditionally the threshold is given empirically and constantly in data reduction, and obviously it's not suitable for data reduction of space debris. Here we offer a solution to provide the threshold. Our method assumes that the PSF (point spread function) is Gaussian and estimates the signal flux by a directly two-dimensional Gaussian fit, then a cubic spline interpolation is performed to divide each initial pixel into several sub-pixels, at last the threshold is determined by the estimation of signal flux and the sub-pixels above threshold are separated to estimate the centroid. A trail observation of the fast spinning satellite Ajisai is made and the CCD frames are obtained to test our algorithm. The calibration precision of various threshold is obtained through the comparison between the observed equatorial position and the reference one, the latter are obtained from the precise ephemeris of the satellite. The results indicate that our method reduces the total errors of measurements, it works effectively in improving the centering precision of space debris images.

第 157 条，共 222 条

Attitude Stability Of A Spacecraft With Two Flexible Solar Arrays On A Stationary Orbit Around An Asteroid Subjected To Gravity Gradient Torque

Zhang, MJ (Zhang, Ming-Jiang); Zhao, CY (Zhao, Chang-Yin)

ASTROPHYSICS AND SPACE SCIENCE

卷: 351 期: 2 页: 507-524

In the gravity field of an asteroid with the second order and degree harmonics C (20) and C (22), the attitude stability of a spacecraft with two flexible solar arrays on a stationary orbit subjected to the fourth-order gravity gradient torque is investigated in this paper. The sufficient conditions of attitude stability of the spacecraft are obtained, the effect of the direction of the flexible solar arrays and some special cases are discussed. Taking the asteroids 4769 Castalia, 25143 Itokawa and the imaginary asteroids as examples, the attitude stability domains, determined by the sufficient

conditions, of the spacecrafts moving on stationary orbits around them are presented. It is found that the attitude stability domains of the spacecraft with two flexible solar arrays are evidently different when the solar arrays are installed in different directions; the effect of the harmonics C (20) and C (22) of the asteroids has the significant influence on the attitude stability domains of the spacecrafts with flexible appendages moving on stationary orbits; in the certain case, the effect of the harmonics C (20) and C (22) of the asteroids has no influence on the attitude stability domains of the rigid spacecrafts moving on stationary orbits, but in the other cases, the effect of the harmonics C (20) and C (22) of the asteroids has also the significant influence on the attitude stability domains of the rigid spacecrafts moving on stationary orbits; whether the harmonics C (20) and C (22) of the asteroids are considered or not, the effect of flexible appendages decreases the attitude stability domains.

第 158 条，共 222 条

A Method For Calculating Probability Of Collision Between Space Objects

Xu, XL (Xu, Xiao-Li); Xiong, YQ (Xiong, Yong-Qing)
RESEARCH IN ASTRONOMY AND ASTROPHYSICS

卷: 14 期: 5 页: 601-609

A method is developed to calculate probability of collision. Based on geometric features of space objects during the encounter, it is reasonable to separate the radial orbital motions from those in the cross section for most encounter events that occur in a near-circular orbit. Therefore, the probability of collision caused by differences in both altitude of the orbit in the radial direction and the probability of collision caused by differences in arrival time in the cross section are calculated. The net probability of collision is expressed as an explicit expression by multiplying the above two components. Numerical cases are applied to test this method by comparing the results with the general method. The results indicate that this method is valid for most encounter events that occur in near-circular orbits.

第 159 条，共 222 条

A Research On Adaptability Of Collision Criterion

Li JI; Xiong Jianning; Xu Xiaoli; Zhao Changyin
Acta Astronomica Sinica

卷: 55 期: 5 页: 404-414

With the rising number of space debris, people pay more and more atten- tion to the space debris collision avoidance system (SDCAS). In the early 1990s, the BOX method is commonly used as a collision criterion to decide whether the avoiding maneuver is necessary for spacecraft. But this method has low practicability, so the method of collision probability is developed. In this way, both the relative distance and the geometrical param- eters at the closest approach time are taken into consideration. However, the mathematical model of this collision criterion depends highly on the covariance, so it may lead to some inaccurate results. In this paper, the rendezvous of two orbits are simulated, and the errors are considered, then the relative distance at the closest approach time and the collision prob- ability are calculated. The results indicate that the covariance plays an indispensable role in measuring the risk of collision. When the precision of orbit prediction is not very good, it is better to combine the BOX method and the collision probability method in the SDCAS.

第 160 条，共 222 条

The Mid-Term Forecast Method Of Solar Radiation Index F_(10.7)

Wang HB; Xiong Jianning; Zhao Changyin
Acta Astronomica Sinica

卷: 55 期: 4 页: 302-312

In the low earth orbit satellite's orbit computation, the solar radiation index F_(10.7) is an important parameter, which is usually used to describe the solar activity's effect on the thermosphere density and the orbit perturbation. So the accuracy of index F_(10.7) will affect the precision of orbit prediction. In this paper, based on the characteristics of the solar 27-day short-term activity, we bring up a forecast method of F_(10.7) which can use the historical indices of the past 135 days to predict the solar radiation indices in the next 54 days. That is to say, the method is able to forecast the variations of solar radiation for about two

rotation-cycles in the future. In this paper, we compare this method with those widely-used methods. The detail results are as follows: (1) This paper's method is observably better than the traditional triangle function method; (2) In the short-term forecast (7 days), this paper's method is little better than the method developed by Space Weather Prediction Center in America, since the root mean square could be reduced by about 19% when using this paper's method; (3) In the mid-term forecast (27 days), the accuracy of this paper's method is almost equal to the 54-order self-regression method which is used widely in our country. However, fewer parameters and observation data are needed in this paper's method, leading to the more convenient application in orbit computation. Moreover, on the 54th day the correlation coefficient between the prediction and actual index is still greater than 0.92, implying that the method can keep stable in mid-term forecast. All in all, the advantage of this paper's method is that it could use fewer historical indices to predict the mid-term solar radiation independent of extra solar real-time observation, and it is very helpful to the orbit short- and mid-term predictions in some space flight missions.

第 161 条，共 222 条

Statistics And Analysis Of LEO Objects' Luminosities

Zhang YP; Zhao Changyin; Zhang Xiaoxiang; Ping Yiding; Zhang Chen

Acta Astronomica Sinica

卷: 55 期: 4 页: 322-337

As a basic property of space objects, luminosity is frequently used for the identification of space objects, as well as for the calculation of their scattering cross sections. In general, space objects shine only by reflecting sunlight. The luminosity observed by ground stations was affected by many factors. Since the multi-objective photometric observation equipment operated 5 years ago, a large number of photometric data have been accumulated. This article estimates the overall accuracies of the data, and lists some situations through the relation between phase angle and magnitude (PA-m). And the statistics is conducted on the luminosities of more than two thousand low earth orbit (LEO) objects.

第 162 条，共 222 条

A Comparison Of Digital Centering Algorithms For High Earth Orbital Space Debris

Sun RY; Zhao Changyin; Zhu Tinglei; Lu Yao

卷: 44 期: 6 页: 656-664

Scientia Sinica Physica, Mechanica & Astronomica

The applications of digital centering algorithms have a major impact on precise astrometry. In optical observations of space debris, due to the observing strategies and methods, the image degradation is distinct, which affects the centroid computing of CCD images. Adopting the four widely-used centering algorithms, including modified moment, one-dimensional Gaussian fit, two-dimensional Gaussian fit and median, tests are made on raw CCD images of space debris. With the observation positions obtained by astronomical calibration and the reference ones from ephemeris, the precision of variable algorithms and the influence of different threshold settings are acquired. The results indicate that the median reveals performs best for right ascension coordinates and others reveals a better results for declination coordinates. For Gaussian fit, no threshold may improve the centering precision.

第 163 条，共 222 条

Improved Astrometry Of Space Debris With Image Restoration

Sun, RY (Sun, Rong-Yu); Zhao, CY (Zhao, Chang-Yin)

RESEARCH IN ASTRONOMY AND ASTROPHYSICS

卷: 14 期: 8 页: 992-1000

In order to implement an observing strategy, image degradation that occurs during optical observation of space debris is ineluctable and has distinct characteristics. Image restoration is presented as a way to remove the influence of degradation in CCD images of space debris, based on assumed PSF models with the same FWHM as images of the object. In the process of image restoration, the maximum entropy method is adopted. The results of reduction using observed raw CCD images indicate that the precision in estimating positions of objects is

improved and the effects of degradation are reduced. Improving the astrometry of space debris using image restoration is effective and feasible.

第 164 条，共 222 条

Restoration Of Space Object Images By Using Maximum Entropy Method

Sun RY; Zhao Changyin

卷: 55 期: 3 页: 237-245

Acta Astronomica Sinica

Due to the survey strategy and specialized hardware design, the imaging degradation of optical space object observation is serious and distinct. Thus, the imaging process is affected, and the precision of astrometric reduction on object CCD images is reduced. To improve the astrometry of space objects, the maximum entropy method is adopted for image restoration, with the apriori PSF (Point Spread Function) models. The measurement errors of objects before and after restoration are compared to investigate the effect and efficiency of image restoration. The experiment results indicate that the influences of imaging degradation are reduced and the astrometric precision of space objects is improved with the maximum entropy method.

第 165 条，共 222 条

Searching For Space Debris In GEO

SUN RY , ZHAO Chang-Yin

卷：14 期: 2 页 14-18

Space Debris Research and Application

A method combined with geometrical morphology identification and linear correlation is adopted for the data calibration of IADC (the Inter –Agency Space Debris Coordination Committee) AI23.4. The main aim for this action is detecting the debris in GEO region. During calibration, the pointing errors of telescope are corrected , and 1137 detection are obtained from the raw CCD images. Finally 139 tracklets are acquired, of which 116 tracklets are correlated with the catalogue. The distributions of magnitude, semi-major axis, inclination and longitude of ascending node of these objects are obtained as well.

第 166 条，共 222 条

A Robotic Identification Method For Space Object Tracking

Xu Z ，L Wu，X Wang

期：1，页：399-408

会议论文，会议名称：Proceedings of the 27th Conference of Spacecraft TT&C Technology in China

A practical method is proposed for the robotic identification and capture of space object in tracking mode. Method chooses proper tracking speed of the telescope and exposure time of the sensor to achieve the image which generates significant difference between the static and moving objects. Algorithm, which recognizes moving object with single frame and correlate moving path on multiple frames, drastically reduces the computational resources compared to the traditional image-differencing method. Path correlation methods are given separately for both low and high altitude object. Practical experiments show that the method is effective and convenient, realizes the fully robotic tracking for electro-optical facilities well as the key technology for the network observation system.

第 167 条，共 222 条

Design And Implementation Of CNEOST Image Database Based On Nosql System

WANG,X

卷: 38 期: 2 页:211-221

Chinese Asronomy and Astrophyscs

The China Near Earth Object Survey Telescope is the largest Schmidt telescope in China, and it has acquired more than 3 TB astronomical image data since it saw the first light in 2006. After the upgrade of the CCD camera in 2013, over 10 TB data will be obtained every year. The management of the massive images is not only an indispensable part of data processing pipeline but also the basis of data sharing. Based on the analysis of requirement, an image management system is designed and implemented by employing the nonrelational database.

第 168 条，共 222 条

Orbit Determination With Mixture Observations Of Multiple Objects

Wang X

卷: 55 期: 6 页: 488-497

Acta Astronomica Sinica

In the operational orbit determination with optical measurements of space ob jects, some observations of different ob jects are tagged as the same ob ject. For this kind of data, the orbit improvement according to the tag is failed because of the composition of multiple objects. A method is proposed from the view of maximum likelihood, and it combines the orbit improvement and identification by employing the EM (Expectation Maximum) method. In the implementation of this method, a robust estimation is also given. Corresponding numerical simulations show that the method is feasible, effective, and convenient.

第 169 条，共 222 条

Improving The Precision Of Astrometry For Space Debris

Sun, RY (Sun, Rongyu); Zhao, CY (Zhao, Changyin); Zhang, XX (Zhang, Xiaoxiang)

ASTRONOMICAL JOURNAL

卷: 147 期: 3 文献号: 58

The data reduction method for optical space debris observations has many similarities with the one adopted for surveying near-Earth objects; however, due to several specific issues, the image degradation is particularly critical, which makes it difficult to obtain precise astrometry. An automatic image reconstruction method was developed to improve the astrometry precision for space debris, based on the mathematical morphology operator. Variable structural elements along multiple directions are adopted for image transformation, and then all the resultant images are stacked to obtain a final result. To investigate its efficiency, trial observations are made with Global Positioning System satellites and the astrometry accuracy improvement is obtained by comparison with the reference positions. The results of our experiments indicate that the influence of degradation in astrometric CCD images is reduced, and the position accuracy of both objects and stellar stars is improved distinctly. Our technique will contribute significantly to optical data reduction and high-order precision astrometry for space debris.

Research and application of satellite precise orbit

第 170 条，共 222 条

An Orbit Determination Method Using Data Before And After Satellite-Rocket Separation

MAO YX; MA Jing yuan ,ZHANG Jing , SONG Ye-zhi

卷：35 期: 12 页 1360-1366

Journal of Astronautics

In a satellite launch task using spring separation mode the satellite obtains a velocity increment produced from the separating force of spring data of two segments before and after the epoch of satellite-rocket separation are not in the same orbit and c;an' t he used to c;alc;ulate the orbit together by using traditional method. To solve the problem a new method improved method of perturbed initial orbit determination based on Unit Vector Method is proposed to solve a position vector and two velocity vectors simultaneously in this paper. The results of simulated and measured data show that the method c;an realize combined orbit determination by using the measured data of two different orbits before and after the satellite-rocket separation. Because the orbit determination data is inc;reased the ac;c;urac;y of initial orbit determination in injection phase is also improved.

第 171 条，共 222 条

Recognition Of Free-Flight Trajectory And Rapid Early Warning

Yang D; Xu Jin; Chen Wushen

卷: 55 期: 3 页: 256-267

Acta Astronomica Sinica

A processing approach is proposed to identify the free-flight missiles and derive the launch and landing locations based on the orbital motion characteristics of the missiles. In this approach, the orbital elements of the target missile are

obtained by tracking the target in space, and recording the real-time orbital measurements using ground-based early-warning radar. The method has two parts: the two-body model and perturbation correction. The results indicate that, the approach has a fast convergence rate after just 6~8 times of iterations, and the calculation can satisfy the highly time-sensitive requirement of the early warning of missiles.

第 172 条，共 222 条

Timing Design of High-speed Mosaic CCD Camera

Zheng XL，YAO Dazhi，HUA Yuanyuan LIU Wei MEN Jinrui

卷: 34 期:3 页:210-212

Optoelectronic technology

The high-speed mosaic CCD camera is badly needed in China's Space Object and Debris Observation currently. The research on camera promotes the development capacity of China's high-speed mosaic CCD camera.With focus on the timing design of 16 channel high-speed mosaic CCD camera, the measured results of camera and application prospect of the camera are discussed

IV. Planetary Sciences and Deep Space Exploration

Near Earth Object Survey and Solar System Bodies

第 173 条，共 222 条

CCD Photometry Of Distant Active Comets 228P/LINEAR, C/2006 S3(LONEOS) And 29P/Schwassmann-Wachmann 1

Shi, JC (Shi, J. C.); Ma, YH (Ma, Y. H.); Zheng, JQ (Zheng, J. Q.)

MONTHLY NOTICES OF THE ROYAL ASTRONOMICAL SOCIETY

卷: 441 期: 1 页: 739-744

We presentphotometric investigations of three distant active comets, 228P/LINEAR, C/2006 S3 Lowell Observatory Near-Earth-Object Search (LONEOS) and 29P/Schwassmann-Wachmann 1. The data were obtained with the 1-m optical telescope at Lulin Observatory in Taiwan on 2011 February 5 and 6. These comets were observed at heliocentric distances larger than 3 au, all of them appeared to be active. By cometary morphological and photometric studies, the upper limits of the nuclei radii were derived. Also, the surface brightness profiles, Af rho parameters, mass production rates and the coma colours were measured. Finally, we discussed possible driver of activity in comets.

Ephemerial Astronomy and Astronomical Reference System

第 174 条，共 222 条

Comparisons And Evaluations Of JPL Ephemerides

Deng XM，Fan Min ,Xie Yi

卷: 54 期: 38 页: 330-341

Chinese Astronomy and Astrophysics

In the light of the wide applications of a series of ephemerides developed by the Jet Propulsion

Laboratory (JPL) of the National Aeronautics and Space Administration (NASA) of the USA to many aspects like the deep-space navigation and interplanetary exploration, it is necessary to make comparisons of their contents, applicable ranges, realizations and maintenances. In view of the fact that the explorations of the Venus and Mars are expected to carry out in China, their dynamical models and the adopted observational data are analysis by taking the DE405, DE421 and DE423 to be the examples. From the evaluations of the accuracies and performances of the above-mentioned ephemerides of different editions, their effects on the probes orbiting around the Venus or Mars are emphatically discussed, and a suggestion is given for their use that as far as the Venus missions are concerned, the use of the DE423 is recommend, and that the use of the DE421 or DE423 is recommended for the Mars Missions.

第 175 条，共 222 条

The Status And Trends Of Testing Relativity In Highly Accurate Level: Tests In The Solar System

Deng XM; Xie Yi

卷: 32 期: 2 页: 227-245

Progress in Astronomy

With the development of the unprecedented techniques for observations and the improvement of the advanced methods for measurements, general relativity has passed all of the tests in the solar system with flying colors, which included Einstein equivalence principle, the light deflection, the Shapiro time delay and the perihelion advance of Mercury. Even the gravitational wave predicted by the general relativity has been detected by using the timing model of binary pulsar systems indirectly. However, there are many important reasons to question the validity of general relativity and to determine where it will be violated. Thus, high-precision experiments in the solar system offer some new opportunities for probing gravitation in the spacetime. In this paper, the development status and trends of general relativity and its experimental tests are reviewed and outlooked, which include the main research content on highly accurate experimental tests of general relativity and some plan and progress in deep space missions for testing it. First of all, Einstein equivalence principle and its tests is presented. This principle is the cornerstone of the general relativity and it contains three parts: the weak equivalence principle, the local Lorentz invariance and the local position invariance. Second, experimental tests of relativistic gravitation's theories are discussed, which are mainly focused on measuring the parametrized post-Newtonian parameters. Focusing on Chinese deep space missions in the future, we give some advices on their application to gravitational tests.

第 176 条，共 222 条

Spacecraft Doppler Tracking With Possible Violations Of LLI And LPI: A Theoretical Modeling

Deng, XM (Deng, Xue-Mei); Xie, Y (Xie, Yi)

卷: 14 期: 3 页: 319-328

RESEARCH IN ASTRONOMY AND ASTROPHYSICS

Currently two-way and three-way spacecraft Doppler tracking techniques are widely used and play important roles in control and navigation of deep space missions. Starting from a one-way Doppler model, we extend the theory to two-way and three-way Doppler models by making them include possible violations of the local Lorentz invariance (LLI) and the local position invariance (LPI) in order to test the Einstein equivalence principle, which is the cornerstone of general relativity and all other metric theories of gravity. After taking the finite speed of light into account, which is the so-called light time solution (LTS), we make these models depend on the time of reception of the signal only for practical convenience. We find that possible violations of LLI and LPI cannot affect two-way Doppler tracking under a linear approximation of LTS, although this approximation is sufficiently good for most cases in the solar system. We also show that, in three-way Doppler tracking, possible violations of LLI and LPI are only associated with two stations, which suggests that it is better to set the stations at places with significant differences in velocities and gravitational potentials to obtain a high level of sensitivity for the tests.

第 177 条，共 222 条

Preliminary Limits On A Logarithmic Correction To The Newtonian Gravitational Potential In The Solar System

Deng, XM (Deng, Xue-Mei); Xie, Y (Xie, Yi)
ASTROPHYSICS AND SPACE SCIENCE

卷: 350；期: 1；页: 103-107

Using the supplementary advances of the perihelia provided by INPOP10a (IMCCE, France) and EPM2011 (IAA RAS, Russia) ephemerides, we obtain preliminary limits on a logarithmic correction to the Newtonian gravitational potential in the solar system. This kind of correction may originate from fundamental frameworks, like string theories or effective models of gravity due to quantum effects and the non-local gravity scheme. We estimate upper limit of Tohline-Kuhn-Kruglyak parameter lambda and lower bound of Fabris-Campos parameter alpha, which parametrize the correction and connect each other by alpha lambda=-1. In our estimation, we take the Lense-Thirring effect due to the Sun's angular momentum and the uncertainty of the Sun's quadrupole moment into account. These two factors were usually absent in previous works. We find that INPOP10a yields the upper limit as alpha=-(0.66 +/- 5.82)x10(-4) kpc(-1) [or the lower limit as lambda=(0.15 +/- 8.76)x10(5) kpc] while EPM2011 gives alpha=(0.52 +/- 1.74)x10(-4) kpc(-1) [or the lower limit as lambda=-(0.19 +/- 3.29)x10(5) kpc]. The limits of |lambda| are greater than the result based on the rotation curves of spiral galaxies by about 3 orders of magnitude, indicating its effects might be screened in high density regions.

第 178 条，共 222 条

Statistics And Dynamical Stability Of Observed Triple Stars

Xia F

卷: 482；页: 95-100

The Tenth Pacific Rim Conference on Stellar Astrophysics

In this paper, the dynamical stability of totally 127 observed triple stars and the statistical characteristics on mass parameters, orbital elements of these systems are studied. Using five stability criteria and numerical simulation of three-body evolution, most of the 127 triple stars are determined to be stable. The statistical conclusions on the observed systems are summarized: most of the observed triple stars have strong hierarchical configuration, the systems with very large period ratio usually have an inner eccentricity close to zero, most systems have two bodies with comparative mass and there is few system has a low mass third body. In the end of this paper, the stable systems with small parameters (e.g. small distance ratio, small eccentricity) are listed.

第 179 条，共 222 条

The Empirical Mass-Luminosity Relation

Xia F

卷: 482；页: 77-79

ASP Conference Series

The Tenth Pacific Rim Conference on Stellar Astrophysics The recent works devoted to improving empirical Mass-Luminosity Relation (MLR) for main sequence stars are reviewed in this paper. In the mass-luminosity plane, the observational data are subjected to non-negligible errors in both coordinates with different dimensions. In order to obtain more reliable results, a more reasonable weight-assigning scheme is needed. Such a scheme is developed, with which each data point can have its own due contribution. For low mass stars (smaller than _ 1M_), three-piecewise continuous improved MLRs in K, J and H bands are obtained respectively. For visual band, improved MLR for stars with mass spanning from 0.12M_ to 22.89 M_, and improved MMLR (mass-metallicity-luminosity relation) for low mass stars which is based on our K band MLR and available observational metallicity data are provided. Further improvements of MLR would have to come from future observations.

第 180 条，共 222 条

Revisiting Three Blue Straggler Binaries

Wang,XL，任树林

卷: 482；期：1 页: 271-274

ASP Conference Series

For blue stragglers in binary systems, two kinds of origin mechanisms, i.e., collision and mass transfer, are theoretically predicted and companion mass is one of the most important

probes to distinguish their origin mechanisms. By fitting the revised Hipparcos Intermediate Astrometric Data, we obtain the astrometric orbits of three single-lined spectroscopic binaries (HIP 39903, 55022, and 59750) with blue stragglers.

第 181 条，共 222 条

Hipparcos Photocentric Orbits And Component Masses Of 9 Double-Lined Spectroscopic Binaries

Ren,SL，王晓丽，李凡

卷: 482；期：1 页: 147-150

ASP Conference Series

For double-lined spectroscopic binaries (SB2s) in the 9th Catalogue of Orbits of Spectroscopic Binaries with reliable spectroscopic orbits of period between 50 days and 3.2 years, photocentric orbits are determined by fitting the revised Hipparcos Intermediate Astrometric Data in our present work. After a stringent assessment and screening process, we accept photocentric orbits of 9 systems.

第 182 条，共 222 条

On The (Im)Possibility Of Testing New Physics In Exoplanets Using Transit Timing Variations: Deviation From Inverse-Square Law Of Gravity

Xie, Y (Xie, Yi); *Deng, XM* (Deng, Xue-Mei)

MONTHLY NOTICES OF THE ROYAL ASTRONOMICAL SOCIETY

卷: 438；期: 2；页: 1832-1838

Ground-based and space-borne observatories studying exoplanetary transits now and in the future will considerably increase the number of known exoplanets and the precision of the measured times of transit minima. Variations in the transit times can not only be used to infer the presence of additional planets, but might also provide opportunities for testing new physics in the places beyond the Solar system. In this work, we take deviation from the inverse-square law of gravity as an example, focus on the fifth-force-like Yukawa-type correction to the Newtonian gravitational force which parameterizes this deviation, investigate its effects on the secular transit timing variations and analyse their observability in exoplanetary systems. It is found that the most optimistic values of Yukawa-type secular transit timing variations are at the level of similar to 0.1 s per year. Those values unfortunately appear only in rarely unique cases and, most importantly, they are still at least two orders of magnitude below the current capabilities of observations. Such a deviation from the inverse-square law of gravity is likely too small to detect for the foreseeable future. Meanwhile, systematic uncertainties, such as the presence of additional and unknown planets, will likely be exceptionally difficult to remove from a signal that should be seen.

第 183 条，共 222 条

Determination Of Reference Catalogs For Meridian Observations Using Statistical Method

Li ZY

Acta Astronomica Sinica

卷: 55 期: 5 页: 415-426

The meridian observational data are useful for developing high-precision plan- etary ephemerides of the solar system. These historical data are provided by the jet propul- sion laboratory (JPL) or the Institut De Mecanique Celeste Et De Calcul Des Ephemerides (IMCCE). However, we find that the reference systems (realized by the fundamental cata- logs FK3 (Third Fundamental Catalogue), FK4 (Fourth Fundamental Catalogue), and FK5 (Fifth Fundamental Catalogue), or Hipparcos), to which the observations are referred, are not given explicitly for some sets of data. The incompleteness of information prevents us from eliminating the systematic effects due to the different fundamental catalogs. The pur- pose of this paper is to specify clearly the reference catalogs of these observations with the problems in their records by using the JPL DE421 ephemeris. The data for the correspond- ing planets in the geocentric celestial reference system (GCRS) obtained from the DE421 are transformed to the apparent places with different hypothesis regarding the reference cat- alogs. Then the validations of the hypothesis are tested by two kinds of statistical quantities which are used to indicate the significance of difference between the original and transformed data series. As a result, this method is proved to be effective for specifying the reference catalogs, and the missed

information is determined unambiguously. Finally these meridian data are transformed to the GCRS for further applications in the development of planetary ephemerides.

The Sun and Solar System Plasmas

第 184 条，共 222 条

A Reduced Model For The Attenuation Of Sound Due To Molecular Collisions

LI Bing ，*WU DJ*

卷：38 期: 4 页 368-371

JOURNAL OF HEBEI NORMAL UNIVERSITY /Natural Science Edition

Based on a reduced two-fluid model for dry air and water vapor , the effect of water vapor on the attenuation of sound is studied. The results show that for waves with frequencies much less than the elastic collisional frequency between dry air molecule and water vapor molecule , the attenuation coefficient is insensitive to the mixing ratio. When the wave frequency becomes comparable or greater than the elastic collisional frequency , the attenuation due to water vapor becomes very strong. The result may help to understand the effects of molecular processes on the attenuation of sound.

第 185 条，共 222 条

Excitation Of Langmuir Waves By The Lower Energy Cutoff Behavior Of Power-Law Electrons

Tang, JF (Tang, Jianfei); Wu, DJ (Wu, Dejin); Zhao, GQ (Zhao, Guoqing); Chen, L (Chen, Ling); Tan, CM (Tan, Chengming)

ASTROPHYSICS AND SPACE SCIENCE

卷: 353 期: 1 页: 131-135

Langmuir waves (LWs), which are believed to play a crucial role in the plasma emission of solar radio bursts, can be excited by streaming instability of energetic electron beams. However, solar hard X-ray observations imply that the energetic flare electrons usually have a power-law energy distribution with a lower energy cutoff. In this paper, we investigate LWs driven by the power-law electrons. The results show that power-law electrons with the steepness cutoff behavior can excite LWs effectively because of the population inversion distribution below the cutoff energy (E (c)). The growth rate of LWs increases with the steepness index (delta) and decreases with the power-law index (alpha). The wave number of the fastest growing LWs (k lambda (D)), decreases with the characteristic velocity of the power-law electrons () and increases with the thermal velocity of ambient electrons (v (T)). This can be helpful for us to understand better the physics of LWs and the dynamics of energetic electron beams in space and astrophysical plasmas.

第 186 条，共 222 条

MHD Simulation Of Energy Transfer Across Magnetopause During Sudden Changes Of The IMF Orientation

Jing, H (Jing, H.); Lu, JY (Lu, J. Y.); Kabin, K (Kabin, K.); *Zhao, JS* (Zhao, J. S.); Liu, ZQ (Liu, Z. -Q.); Yang, YF (Yang, Y. F.); Zhao, MX (Zhao, M. X.); Wang, M (Wang, M.)

PLANETARY AND SPACE SCIENCE

卷: 97 页: 50-59

A three-dimensional adaptive magnetohydrodynamic (MHD) model is used to investigate the energy flow from the solar wind to the magnetosphere in response to sudden turnings of the interplanetary magnetic field (IMF) on 5 June 1998. During this dynamic period, the size of magnetospheric cavity and the energy input fluctuated enormously. Due to the positive earth dipole tilt angle during the event, the distribution of energy transfer between northern and southern hemispheres of magnetopause is asymmetrical, with most energy transferred in the north hemisphere sunward of X-GSE > ORE. The electromagnetic and mechanical energy inputs increase rapidly after the arrival of an interplanetary shock, while the electromagnetic energy rises much more slowly after IMF turns from north to south. With a nearly invariable By component of IMF, under southward IMF the most electromagnetic energy is transferred near the plane anti-parallel to IMF clock angle, the most significant mechanical energy input occurs in the polar cusp of north hemisphere. In contrast, for northward IMF the electromagnetic energy is mostly transferred near the plane perpendicular

to IMF clock angle, mechanical transferred energy occurs near equatorial plane of dayside magnetopause. Analyzing the distribution of the Poynting flux we show that the high-latitude reconnection causes different types of electromagnetic energy transfers into the magnetosphere during northward IMF especially with a large By component. It is also shown that the traditional energy transfer parameters from solar wind conditions do not include any of residual or hysteresis effects; therefore sometimes they do not reflect the right response to the solar wind variations.

第 187 条，共 222 条

Effect Of Alfven Waves On The Growth Rate Of The Electron-Cyclotron Maser Emission

Wu, DJ (Wu, D. J.)
PHYSICS OF PLASMAS
卷: 21 期: 6 文献号: 064506

By using the non-relativistic approximation for the calculation of growth rates, but taking account of the weakly relativistic modification for the electron-cyclotron resonance condition, it is shown that the effect of Alfven waves (AWs) on the electron-cyclotron maser emission leads to the significant increase of the O-mode growth rate, but has little effect on the X-mode growth rate. We propose that this is because the O-mode wave has the field-aligned polarization sense in the same as the field-aligned oscillatory current, which is created by the field-aligned oscillatory motion of the energetic electrons caused via the presence of AWs. It is this field-aligned oscillatory current that contributes a novel growth rate to the O-mode wave but has little effect on the X-mode wave.

第 188 条，共 222 条

A Novel Mechanism For Electron-Cyclotron Maser

Wu, DJ (Wu, D. J.); Chen, L (Chen, L.); Zhao, GQ (Zhao, G. Q.); Tang, JF (Tang, J. F.)
ASTRONOMY & ASTROPHYSICS
卷: 566 文献号: A138

Context. It has been a long-standing puzzle on how to produce natural radio bursts of various cosmic objects, ranging from remote active galactic nuclei and pulsars to the nearest solar radio bursts and terrestrial auroral kilometer radiations.
Aims. An electron-cyclotron maser (ECM) driven by fast electron beams trapped in magnetic fields has been suggested as a dominant mechanism of producing natural high-power radio radiation. However, there have been two serious difficulties: the magnetization condition of requiring the electron gyrofrequency over the plasma frequency and the inversion condition of the perpendicular velocity distribution of the fast electrons, which has held back the popularization of ECM in the astrophysical community.
Methods. By including effects of self-generated Alfven waves (AW) excited by the beam current, this paper proposes a novel, self-consistent ECM model.
Results. The results show that the self-generated AW can effectively make a density-depleted duct, in which the magnetization condition is easily satisfied, and result in the inversion condition of perpendicular velocity distribution of the beam electrons.
Conclusions. This self-consistent ECM model can effectively overcome the two difficulties, make ECM very easily occur, and, hence, has greatly interesting implications and general significance in radio astrophysics because of its self-consistency, simplicity, and efficiency.

第 189 条，共 222 条

A Model For Radio Emission From Solar Coronal Shocks

Zhao, GQ (Zhao, G. Q.); Chen, L (Chen, L.); Wu, DJ (Wu, D. J.)
ASTROPHYSICAL JOURNAL
卷: 786 期: 1 文献号: 47

Solar coronal shocks are very common phenomena in the solar atmosphere and are believed to be the drivers of solar type II radio bursts. However, the microphysical nature of these emissions is still an open question. This paper proposes that electron cyclotron maser (ECM) emission is responsible for the generation of radiation from the coronal shocks. In the present model, an energetic ion beam accelerated by the shock first excites the Alfven wave (AW), then the excited AW leads to the formation of a density-depleted duct along the

foreshock boundary of the shock. In this density-depleted duct, the energetic electron beam produced via the shock acceleration can effectively excite radio emission by ECM instability. Our results show that this model may potentially be applied to solar type II radio bursts.

第 190 条，共 222 条

Nonlinear Generation Of Kinetic-Scale Waves By Magnetohydrodynamic Alfven Waves And Nonlocal Spectral Transport In The Solar Wind

Zhao, JS (Zhao, J. S.); Voitenko, Y (Voitenko, Y.); Wu, DJ (Wu, D. J.); De Keyser, J (De Keyser, J.)

ASTROPHYSICAL JOURNAL

卷: 785 期: 2 文献号: 139

We study the nonlocal nonlinear coupling and generation of kinetic Alfven waves (KAWs) and kinetic slow waves (KSWs) by magnetohydrodynamic Alfven waves (MHD AWs) in conditions typical for the solar wind in the inner heliosphere. This cross-scale process provides an alternative to the turbulent energy cascade passing through many intermediate scales. The nonlinearities we study are proportional to the scalar products of wave vectors and hence are called "scalar" ones. Despite the strong Landau damping of kinetic waves, we found fast growing KAWs and KSWs at perpendicular wavelengths close to the ion gyroradius. Using the parametric decay formalism, we investigate two independent decay channels for the pump AW: forward decay (involving co-propagating product waves) and backward decay (involving counter-propagating product waves). The growth rate of the forward decay is typically 0.05 but can exceed 0.1 of the pump wave frequency. The resulting spectral transport is nonlocal and anisotropic, sharply increasing perpendicular wavenumbers but not parallel ones. AWs and KAWs propagating against the pump AW grow with about the same rate and contribute to the sunward wave flux in the solar wind. Our results suggest that the nonlocal decay of MHD AWs into KAWs and KSWs is a robust mechanism for the cross-scale spectral transport of the wave energy from MHD to dissipative kinetic scales in the solar wind and similar media.

第 191 条，共 222 条

Lower Energy Cutoff Behavior Of Negative Power-Law Electrons And Electron-Cyclotron Maser Emission

Tang JF

卷: 55 期: 1 页: 99-100

Acta Astronomica Sinica

The electron-cyclotron maser (ECM) emission is one of the most important radio emission mechanisms in astrophysics. It was first pointed out in the late 1950s. Because of the limitation of the nonrelativistic resonant condition, it is difficult to produce an amplified radiation that can escape from plasma. The ECM instability has been extensively applied to various coherent radio-burst phenomena since Wu & Lee (1979) utilized the weakly relativistic resonant condition.

第 192 条，共 222 条

Properties Of Short-Wavelength Oblique Alfven And Slow Waves

Zhao, JS (Zhao, J. S.); Voitenko, Y (Voitenko, Y.); Yu, MY (Yu, M. Y.); Lu, JY (Lu, J. Y.); Wu, DJ (Wu, D. J.)

ASTROPHYSICAL JOURNAL

卷: 793；期: 2；文献号: 107

Linear properties of kinetic Alfven waves (KAWs) and kinetic slow waves (KSWs) are studied in the framework of two-fluid magnetohydrodynamics. We obtain the wave dispersion relations that are valid in a wide range of the wave frequency. and plasma-to-magnetic pressure ratio beta. The KAW frequency can reach and exceed the ion-cyclotron frequency at ion kinetic scales, whereas the KSW frequency remains sub-cyclotron. At beta similar to 1, the plasma and magnetic pressure perturbations of both modes are in anti-phase, so that there is nearly no total pressure perturbations. However, these modes also exhibit several opposite properties. At high beta, the electric polarization ratios of KAWs and KSWs are opposite at the ion gyroradius scale, where KAWs are polarized in the sense of electron gyration (right-hand polarized) and KSWs are left-hand polarized. The magnetic helicity sigma similar to 1 for KAWs and sigma similar to -1 for KSWs, and the ion Alfven ratio R-Ai << 1 for KAWs and R-Ai >> 1 for

KSWs. We also found transition wavenumbers where KAWs change their polarization from left-handed to right-handed. These new properties can be used to discriminate KAWs and KSWs when interpreting kinetic-scale electromagnetic fluctuations observed in various solar-terrestrial plasmas. This concerns, in particular, identification of modes responsible for kinetic-scale pressure-balanced fluctuations and turbulence in the solar wind.

第 193 条，共 222 条

Excitation Of Kinetic Alfven Waves By Fast Electron Beams

作者: *Chen, L* (Chen, L.); Wu, DJ (Wu, D. J. p); Zhao, GQ (Zhao, G. Q.); Tang, JF (Tang, J. F.); Huang, J (Huang, J.)
ASTROPHYSICAL JOURNAL
卷: 793 期: 1 文献号: 13

Energetic electron beams, which are ubiquitous in a large variety of active phenomena in space and astrophysical plasmas, are one of the most important sources that drive plasma instabilities. In this paper, taking account of the return-current effect of fast electron beams, kinetic Alfven wave (KAW) instability driven by a fast electron beam is investigated in a finite-beta plasma of Q < beta < 1 (where beta is the kinetic-to-magnetic pressure ratio and Q = m(e)/m(i) is the mass ratio of electrons to ions). The results show that the kinetic resonant interaction of beam electrons is the driving source for KAW instability, unlike the case driven by a fast ion beam, where both the kinetic resonant interaction of beam ions and the return-current are the driving source for the KAW instability. KAW instability has a nonzero growth rate in the range of the perpendicular wave number, 0 < k(perpendicular to) < k(perpendicular to)(u), and the maximum growth rate, gamma(m), occurs between 0.5k(perpendicular to)(u) < k(perpendicular to)(m) < 0.8k(perpendicular to)(u). Both the maximal growing perpendicular wave number k(perpendicular to)(m) and the maximal growth rate gamma(m) depend sensitively on the velocity of electron beam upsilon(b), and the most favorable beam velocity occurs between 8 upsilon(A) < upsilon(b) < 10 upsilon(A). On the other hand, the excited KAWs are weakly dispersive with k(perpendicular to) rho(i) < 1 and have the maximum growth rate at relatively low perpendicular wave numbers in the range 0.3 < k(perpendicular to)(m) rho(i) < 0.6 for a beam velocity upsilon(b) < 10 upsilon(A). A possible application to the upward electron beams in the terrestrial magnetosphere is briefly discussed.

第 194 条，共 222 条

Comparison Of Two-Fluid And Gyrokinetic Models For Kinetic Alfven Waves In Solar And Space Plasmas

Yang, L (Yang, L.); Wu, DJ (Wu, D. J.); Wang, SJ (Wang, S. J.); Lee, LC (Lee, L. C.)
ASTROPHYSICAL JOURNAL
卷: 792 期: 1 文献号: 36

An analytical comparative study of a two-fluid and a gyrokinetic model of kinetic Alfven waves (KAWs) is presented for various solar and space plasma environments. Based on the linear KAW dispersion relation for gyrokinetics (Howes et al. 2006), the wave group velocity and electromagnetic polarizations are obtained analytically. Then the gyrokinetic wave properties are compared with those of the two-fluid model. The results show that both models agree well with each other not only in the long wavelength regime (>> the ion gyroradius rho(i)) for all cases considered, but also in wavelengths similar to rho(i) and <<rho(i) (still much larger than the electron gyroscale) for a moderate or low (less than or similar to 1) and a high (>> 1) ion/electron temperature ratio T-0i/T-0e, respectively. However, the fluid model calculations deviate strongly from the gyrokinetic model at scales <rho(i) for a relatively low T-0i/T-0e due to the electron gyroradius effect. Meanwhile, the plasma beta(i) can make the gyrokinetic dispersion relation of KAWs become complex and sometimes have an oscillation-like structure. With the inherent simplicity of the fluid theory, these results may improve our understanding of the applicability of the two-fluid model, and may have important implications for computer simulation studies of KAWs in the solar and space plasma surroundings.

第 195 条，共 222 条

A Study Of Line Widths And Kinetic Parameters Of Ions In The Solar Corona

Zhao, GQ (Zhao, G. Q.); Wu, DJ (Wu, D. J.); Wang, CB (Wang, C. B.)
ASTROPHYSICS AND SPACE SCIENCE
卷: 353；期: 2；页: 373-378

Solar extreme-ultraviolet (EUV) lines emitted by highly charged ions have been extensively studied to discuss the issue of coronal heating and solar wind acceleration. Based on observations of the polar corona by the SUMER/SOHO spectrometer, this paper investigates the relation between the line widths and kinetic parameters of ions. It is shown that there exists a strongly linear correlation between two variables (sigma/lambda)(2) and M (-1), where sigma, lambda and M are the half-width of the observed line profile at , the wavelength and the ion mass, respectively. The Pearson product-moment correlation coefficients exceed 0.9. This finding tends to suggest that the ions from a given height of polar corona have a common temperature and a common non-thermal velocity in terms of existing equation. The temperature and non-thermal velocity are obtained by linear least-square fit. The temperature is around 2.8 MK at heights of 57aEuro(3) and 102aEuro(3). The non-thermal velocity is typical 21.6 km s(-1) at height of 57aEuro(3) and 25.2 km s(-1) at height of 102aEuro(3).

第 196 条，共 222 条

Saturation Level Of Alfven Waves Driven By Kelvin-Helmholtz Instability

Chen, L (Chen, Ling); Wu, DJ (Wu, Dejin); Zhao, GQ (Zhao, Guoqing); Huang, J (Huang, Jing)
CHINESE SCIENCE BULLETIN
卷: 59 期: 28 页: 3536-3542

Alfv,n waves (AWs) can play an important role in the macroscopic dynamics as well as in the microscopic wave-particle interaction in various magneto-plasma environments. A very wide observed range of the relative amplitude of magnetic fluctuations of AWs from lower than 10(-3) in the terrestrial magnetosphere up to similar to 1 in the solar wind implies the complexity of saturation mechanisms of AWs. Taking account of the ion-neutral collision damping in a partially ionized plasma, the saturation level of AWs driven by the Kelvin-Helmholtz (K-H) instability is investigated in this paper. The intensified magnetic field due to the excited AWs may result in the saturation of the excited AWs when the growth rate is balanced by the damping rate. An equation determining the saturation level of the AWs is obtained. The results show that, for a fixed-frequency wave, the saturation level of the AWs considerably increases as the ionization degree increases as well as the sheared-flow velocity. On the other hand, for a fixed ionization degree the saturation level of the AWs slightly increases as the plasma beta increases but decreases as the wave frequency increases. These results have potential importance for us to estimate the saturation level of AWs in space and astrophysical plasmas.

第 197 条，共 222 条

Streamers Generation By Small-Scale Drift-Alfven Waves

Zhao, JS (Zhao, J. S.); Yu, MY (Yu, M. Y.)
PHYSICS OF PLASMAS
卷: 21 期: 10 文献号: 102302

Excitation of streamers by modulationally unstable small-scale drift-Alfven wave (SSDAW) is investigated. It is found that the excitation depends strongly on the propagation direction of the SSDAW, and the ion and electron diamagnetic drift waves are both unstable due to the generation of streamers. It is also shown that zonal flows can be effectively excited by the SSDAW with the propagation direction different from that for streamer excitation. (C) 2014 AIP Publishing LLC.

第 198 条，共 222 条

Effects Of Inelastic Collisions On Alfven Waves In Partially Ionized Plasmas

Li, B (Li, Bing); Chen, L (Chen, Ling); Wu, DJ (Wu, Dejin)
CHINESE SCIENCE BULLETIN
卷: 59 期: 8 页: 740-746

Based on a three-component description of partially ionized plasmas (i.e., electrons, ions, and neutral atoms), effects of inelastic collisions between ions (neutrals) and electrons on Alfv,n waves (AWs) in a partially ionized plasma are

studied. It is shown that for a fixed ionizability () or a fixed inelastic collision parameter (chi, i.e., the ratio of the inelastic to elastic collision frequency), the damping rate of AWs has a peak value round k (z) v (A)/nu (in) 1, where k (z) is the parallel wavenumber of AWs, v (A) is the Alfv,n velocity, and nu (in) is the elastic collision frequency between ions and neutrals. On the other hand, the damping rate of AWs decreases monotonously with the ionizability for a fixed inelastic collision parameter, but has a peak value when the inelastic collision parameter varies for sufficiently small ionizability (). For sufficiently large ionizability (), it is found that the damping rate decreases with the inelastic collision parameter. The results may help us to understand the physics of AWs in partially ionized plasmas.

第 199 条，共 222 条

Walen Test And De Hoffmann-Teller Frame Of Interplanetary Large-Amplitude Alfven Waves

Chao, JK (Chao, J. K.); Hsieh, WC (Hsieh, Wen-Chieh); *Yang, L* (Yang, L.); Lee, LC (Lee, L. C.)

ASTROPHYSICAL JOURNAL

卷: 786 期: 2 文献号: 149

In this study, three methods of analysis are compared to test the Walen relation. Method 1 requires a good de Hoffmann-Teller (HT) frame. Method 2 uses three components separately to find the frame that is slightly modified from Method 1. This method is intended to improve the accuracy of the HT frame and able to demonstrate the anisotropic property of the fluctuations. The better the relation is, the closer the slope of a regression fitting the data of plasma versus Alfven velocities is to 1. However, this criterion is based on an average HT frame, and the fitted slope does not always work for the Walen test because the HT frame can change so fast in the high-speed streams. We propose Method 3 to check the Walen relation using a sequence of data generated by taking the difference of two consecutive values of plasma and Alfven velocities, respectively. The difference data are independent of the HT frame. We suggest that the ratio of the variances between plasma and Alfven velocities is a better parameter to qualify the Walen relation. Four cases in two solar wind streams are studied using these three methods. Our results show that when the solar wind HT frame remains stable, all three methods can predict Alfvenic fluctuations well, but Method 3 can better predict the Walen relation when solar wind contains structures with several small streams. A simulated case also demonstrates that Method 3 is better and more robust than Methods 1 and 2. These results are important for a better understanding of Alfvenic fluctuations and turbulence in the solar wind.

Laboratory for Astrochemistry and Planetary Sciences

第 200 条，共 222 条

The Petrology And Mineralogy Analysis Of Noble Metal Alloys In The Inclusions Of Chondrite: An Implication On The Evolution Of The Solar Nebula

Wu YH; Xing Weifan; Xu Weibiao

卷: 55 期: 2 页: 105-115

Acta Astronomica Sinica

The Ca, Al-rich Inclusions (CAIs) in chondrites are believed to be the first solids to have formed in the solar system which retain the original information of the early solar nebula. However, in-depth researches reveal that most inclusions had experienced a complex history involving partial melting and secondary alteration. Studies on astrochemistry are focused on refractory and chemically stable noble metal alloys in the CAI of a CV meteorite (NWA 2140). The petrology and mineralogy of the alloys are analyzed. The compositional data analysis of the component can imply the thermal history of the CAI. Two kinds of noble metal alloys are identified, the primary condensates and secondary alteration products of pre-existing metals, respectively.

第 201 条，共 222 条

Effects Of Spectralon Absorption On Reflectance Spectra Of Typical Planetary Surface Analog Materials

Zhang, H (Zhang, Hao); Yang, YZ (Yang, Yazhou); Jin, WD (Jin, Weidong); Liu, CJ (Liu, Chujian); *Hsu,*

WB (Hsu, Weibiao)

卷: 22 期: 18 页: 21280-21291

OPTICS EXPRESS

Acquiring accurate visible and near-infrared (VisNIR) reflectance values of atmosphereless celestial bodies is very important in inferring the physical and geological properties of their surficial materials. When a calibration target with inherent non-trivial absorption features is used, the calibrated reflectance would essentially always contain spurious spectral features and the spectroscopic data may easily be misinterpreted if the artifact is not properly taken care of. We demonstrate with laboratory reflectance measurements that the VisNIR spectra of three typical planetary surface analog materials, lunar simulant JSC-1A, olivine and pyroxene grains, have an artificial peak at 2.1 mu m when Spectralon-type plaque made of polytetrafluoroethylene is used as the calibration target in the NIR region. The degree of severity of this artifact is dependent on the strength of the 2.0 mu m absorption feature of the mineral. Empirical methods are proposed to remove this artifact to bring the spectra close to that calibrated by a gold mirror which does not have any conspicuous absorption features in the NIR region. The correction methods may be applied to reflectance data acquired by the VisNIR imaging spectrometer onboard the Yutu Rover of the Chinese Chang'E 3 lunar mission which employed an onboard Spectralon-type calibration target. (C) 2014 Optical Society of America

第 202 条，共 222 条

The Fuhe Chondrite

Hsu, WB (Hsu, W.); Li, S (Li, S.)

METEORITICS & PLANETARY SCIENCE

卷: 49 特刊: SI 页: A174-A174

会议名称: 77th Annual Meeting of the Meteoritical-Society

This issue of the Meteoritical Bulletin reports on 1075 meteorites divided between 468 non-Antarctic and 607 Antarctic meteorites.Written descriptions are given for eight falls (Fuhe, Kemer, Lorton, Mason Gully, Mifflin, Red Canyon Lake, Varre-Sai, and Whetstone Mountains).Particularly notable are descriptions and chemical data for 42 new iron meteorites, many of which are unpaired. Also reported are seven Martian meteorites totaling 1447.1 g (four non-Antarctic) and 14 lunar meteorites totaling 9451 g(10non-Antarctic). Other noteworthy meteorites include NWA 5958, a C3.0-ung with an extremely 16O-rich bulk oxygen isotopic composition; Sayh al Uhaymir 493, an ungrouped achondrite with significant ferric iron, and Northwest Africa 6704, an unusual ungrouped achondrite characterized by relatively ferroan mafic silicate minerals with oxygen isotopic composition that plots within the field for acapulcoites-lodranites. Also reported are two new dense collection areas: Biduna Blowhole in Australia and Stump Spring in the United States. Antarctic meteorites reported include those recovered by the ANSMET (US) and NIPR (Japan) meteorite recovery programs.

第 203 条，共 222 条

Meteorites From Northwest Of China

Hsu, WB (Hsu, W.); Li, S (Li, S.)

METEORITICS & PLANETARY SCIENCE

卷: 49特刊: SI页: A173-A173

77th Annual Meeting of the Meteoritical Society, held September 7-12, 2014 in Casablanca, Morocco. LPI Contribution No. 1800, id.5080 Published in Sep 2014

Numerous meteorites are recently found in gobi deserts of Xinjiang province of China. Ten DCAs have been reported in the region.

第 204 条，共 222 条

New Dense Meteorite Collection Areas Were Found In Lop Nur, Xinjiang

Li Shaolin; *Hsu WB*

卷: 59期: 21页: 2091-2097

Chinese Science Bulletin

Xingdi, Argan, Loulan Yizhi and Lop Nur are four dense meteorite collection areas newly found in China. They are located on the east of the Taklimakan Desert, Xinjiang. The geological and morphological setting of these areas are suitable to meteorites collection and 13 equilibrated ordinary chondrites were first identified. Compared to other typical desert meteorites, these meteorites went through more intense weathering, which may be result of the

pre-coexisting high air humidity and evaporite. Collecting meteorites in deserts have several advantages over in Antarctic, and these dense meteorite collection areas provide possibility for mass collection of meteorites in desert of China.

第 205 条，共 222 条

Mineralogy And Oxygen Isotope Compositions Of A Ti-Rich Refractory Inclusion From The Ch Chondrite Sau 290

A. C. Zhang , C. Ma, N. Sakamoto , *Hsu, W. B.* R.C. Wang, and H. Yurimoto

45th Lunar and Planetary Science Conference

卷：0;号：1;页：1230-1231

Titanium has oxidation states Ti4+,Ti3+, and Ti2+, with the former two states observed innatural minerals. Proportions of different oxidationstates of Ti in minerals can be used to trace the redoxconditions under which Ti-bearing minerals formed.Since Ti is a refractory element, refractory inclusionsin chondrites, which are considered having formed inthe very early solar system, often include Ti-rich min-erals. Therefore, Ti behaves as one of the few refracto-ry elements that have been used to constrain the oxy-gen fugacity of the early solar nebula and its variation. In the literature, many investigations onvariation of the redox conditions in the early solarnebula were based on the data on Ti3+ /Titot values ofpyroxene in refractory inclusions. Recently, more attention has been paid to the various Ti3+/Titotvalues between different minerals with discovery ofnew Ti-rich mineralsand applicationsof XANES technique. In this study, we report Ti-mineralogy of a CAI (designed as A0031) fromthe CH chondrite SaU 290 and their oxygen isotopic compositions, and discuss their origins.

第 206 条，共 222 条

Origin Of P-O-Rich Sulfide In Cm Chondrites: More Constraints From Mineralogy And Oxygen Isotope Compositions

A.C.Zhang S .Itoh .H.Yurimoto *Hsu W.B.*

期: 1 页: 1360-1361

45th Lunar and Planetary Science Conference, held 17-21 March, 2014 at The Woodlands, Texas. LPI Contribution No. 1777, p.1360

Published in Mar 2014

P-O-rich sulfide in CM chondrites is an object whose origin is still a subject of debate. Here, we report its mineralogical features and O-isotope compositions.

Xuyi Observation Station

第 207 条，共 222 条

Cellinoid Shape Model For Asteroids

Lu, XP (Lu, Xiaoping); *Zhao, HB* (Zhao, Haibin); You, Z (You, Zhong)

EARTH MOON AND PLANETS

卷: 112 期: 1-4 页: 73-87

The ellipsoid shape model plays an important role in physical research on asteroids. However, its symmetric structure cannot practically simulate real asteroids. This article applies a general shape model, named the cellinoid, instead of the ellipsoid model to simulate the asymmetric shape of asteroids. The cellinoid shape model consists of eight octants of ellipsoids having different semi-axes, with the constraint that adjacent octants must have two equal semi-axes in common. Totally, the shape of the cellinoid model is controlled by six parameters, not three as in the case of the shape of the ellipsoid. Using this shape model, the brightness of asteroids observed from the Earth can be fitted numerically by the surface triangularization of the cellinoid. The Levenberg-Marquardt algorithm is also employed here to solve a nonlinear minimization problem. Owing to the asymmetric shape of the cellinoid, the physical parameters of asteroids, such as the rotation period and pole orientation, can be fitted more accurately than in the case of the ellipsoid model. Finally, this is confirmed numerically by applying the shape to both synthetic light curves and real light curves of asteroids. Additionally, the center of mass and moment of inertia of the cellinoid are analyzed explicitly.

第 208 条，共 222 条

Rr Lyrae In Xstps: The Halo Density Profile In The North Galactic Cap

Faccioli, L (Faccioli, L.); Smith, MC (Smith, M. C.); Yuan, HB (Yuan, H. -B.); Zhang, HH (Zhang, H. -H.); Liu, XW (Liu, X. -W.); *Zhao, HB* (Zhao, H. -B.); Yao, JS (Yao, J. -S.)

ASTROPHYSICAL JOURNAL

卷: 788 期: 2 文献号: 105

We present a catalog of RR Lyrae stars (RRLs) observed by the Xuyi Schmidt Telescope Photometric Survey (XSTPS). The area we consider is located in the north Galactic cap, covering approximate to 376.75 deg(2) at a approximate to 150 degrees and delta approximate to 27 degrees. down to a magnitude limit of i approximate to 19 Using the variability information afforded by the multi-epoch nature of our XSTPS data, combined with colors from the Sloan Digital Sky Survey, we are able to identify candidate RRLs. We find 318 candidates, derive distances to them, and estimate the detection efficiency. The majority of our candidates have more than 12 observations, and for these we are able to calculate periods. These also allow us to estimate our contamination level, which we predict is between 30% and 40%. Finally, we use the sample to probe the halo density profile in the 9-49 kpc range and find that it can be well fitted by a double power law. We find good agreement between this model and the models derived for the south Galactic cap using the Watkins et al. and Sesar et al. RRL data sets, after accounting for possible contamination in our data set from Sagittarius stream members. We consider non-spherical double power-law models of the halo density profile and again find agreement with literature data sets, although we have limited power to constrain the flattening due to our small survey area. Much tighter constraints will be placed by current and future wide-area surveys, most notably ESA's astrometric Gaia mission. Our analysis demonstrates that surveys with a limited number of epochs can effectively be mined for RRLs. Our complete sample is provided as accompanying online material; as an example the first few entries of each electronic table are shown in the text.

第 209 条，共 222 条

Spectral Diversity And Photometric Behavior Of Main-Belt And Near-Earth Vestoids And (4) Vesta: A Study In Preparation For The Dawn Encounter

Hicks, MD (Hicks, Michael D.); Buratti, BJ (Buratti, Bonnie J.); Lawrence, KJ (Lawrence, Kenneth J.); Hillier, J (Hillier, John); Li, JY (Li, Jian-Yang); Reddy, V (Reddy, Vishnu); Schroder, S (Schroeder, Stefan); Nathues, A (Nathues, Andreas); Hoffmann, M (Hoffmann, Martin); Le Corre, L (Le Corre, Lucille); Duffard, R (Duffard, Rene); *Zhao, HB* (Zhao, Hai-Bin); Raymond, C (Raymond, Carol); Russell, C (Russell, Christopher); Roatsch, T (Roatsch, Thomas); Jaumann, R (Jaumann, Ralf); Rhoades, H (Rhoades, Heath); Mayes, D (Mayes, Deronda); Barajas, T (Barajas, Tzitlaly); Truong, TT (Thien-Tin Truong); Foster, J (Foster, James); McAuley, A (McAuley, Amanda)

ICARUS

卷: 235 页: 60-74

In anticipation of the Dawn Mission to 4 Vesta, we conducted a ground-based campaign of Bessel BVRI filter photometry of five V-type near-Earth asteroids over a wide range of solar phase angles. We also obtained medium-resolution optical spectroscopy (0.38 mu m < lambda < 0.92 mu m; R similar to 500) of sixteen near-Earth and main-belt V-type asteroids in order to investigate their spectral diversity and to draw connections between spacecraft data of Vesta and V-type asteroids. Our disk-integrated photometry extended the excursion in solar phase angle beyond the maximum of 24 degrees available from Earth for Vesta to 87 degrees, which is more typical of the geometry during the Dawn approach and mapping phases. The majority of our broad-band observations were obtained at the JPL 0.6-m Table Mountain Observatory but multiple nights were also contributed by the Calar Alto 1.2-m and 2.2-m telescopes, as well as by the Purple Mountain 1-m Schmidt. Our results include a determination of rotation periods for 4 asteroids, identification of a binary candidate and four new V-type asteroids, including a confirmation of two main-belt V-type asteroids beyond the Jupiter 1:3 resonance (Cruikshank, D.P., Tholen, DJ., Bell, J.F., Hartmann, W.K., Brown, R.H. [1991]. Icarus 89,1-13; Lazzaro, D. et al. [2000]. Science 288, 2033-2035; Roig, F., Gil-Hutton, R.[20061. Icarus 183(2), 411-419; Moskovitz, N.A., Jedicke, R.,

Gaidos, E., Willman, M., Nesvorny, D., Fevig, R., Ivezic, Z. [2008]. Icarus 198,77-90). This latter finding supports the hypothesis that some vestoids may be crustal fragments of a disrupted basaltic parent body compositionally similar to 4 Vesta. We also obtained rotationally resolved medium resolution spectra of Vesta during the Dawn orbit insertion phase, which will be valuable for calibration and comparison of spacecraft data. Modeling of a composite V-type asteroid phase curve yielded a generic photometric model for V asteroids. We also find that a significant amount of the spectral diversity in the V class comes from changes in solar phase angle. A fit of a composite solar phase curve containing our vestoid observations, previously published groundbased observations of Vesta, and early disk-integrated Dawn observations show important differences with other asteroids. The macroscopic surface roughness of V-type asteroids is significantly larger than that of C-type or S-types (Helfenstein, P., Veverka, J. [1989]. Physical characterization of asteroid surfaces from photometric analysis. In: Binzel, R., Gehrels, T., Matthews, M.S. (Eds.), Asteroids II. University of Arizona Press, Tucson, pp. 557-593). This result is consistent with radar studies showing that igneous rocky asteroids - the E and V types - exhibit the largest surface roughness (Benner, L et al. [2008]. Icarus 198,294-304). The effects of what appears to be space weathering can be largely explained by phase reddening in our collection of V-type NEOs, but our finding that smaller vestoids, which have shorter lifetimes, are more similar to Vesta suggests that some type of alteration of the surface through time occurs. Our observations confirm that the south polar region of Vesta has a more diogenitic composition than its equatorial regions. The south pole, which is dominated by a large impact feature, thus may offer a view into the interior of Vesta. We derive a visible phase integral of 0.44 +/- 0.02 and a corresponding Bond albedo of 0.15 +/- 0.03 from our composite V-type asteroid solar phase curve. (C) 2014 Published by Elsevier Inc.

第 210 条，共 222 条

Astrometric Calibration Of The Xuyi Schmidt Telescope Photometric Survey Of The Galactic Anti-Center (XSTPS-GAC)

Zhang, HH (Zhang, Hui-Hua); Liu, XW (Liu, Xiao-Wei); Yuan, HB (Yuan, Hai-Bo); *Zhao, HB* (Zhao, Hai-Bin); Yao, JS (Yao, Jin-Sheng); Zhang, HW (Zhang, Hua-Wei); Xiang, MS (Xiang, Mao-Sheng); Huang, Y (Huang, Yang)

RESEARCH IN ASTRONOMY AND ASTROPHYSICS

卷: 14 期: 4 页: 456-470

We present astrometric calibration of the Xuyi Schmidt Telescope Photometric Survey of the Galactic Anti-center (XSTPS-GAC). XSTPS-GAC is the photometric part of the Digital Sky Survey of the Galactic Anti-center (DSS-GAC), which is a photometric and spectroscopic sky survey, in combination with LAMOST. In order to select an astrometric reference catalog, we made comparisons between the four widely used astrometric catalogs, GSC2.3, USNO-B1.0, UCAC3 and PPMXL. PPMXL shows relatively small systematic errors in positions and more homogeneous proper motion distributions toward the Galactic Anti-center (GAC), and was selected as the reference catalog. Based on the high quality and bright reference stars that were picked out from PPMXL, we performed a 4th-order polynomial fitting in image units, to construct the transformation relation between coordinates used by XSTPS-GAC and standard coordinates, and to simultaneously correct the image distortions in the CCD. Then we applied the derived relation to all sources to obtain their mean celestial coordinates based on the International Celestial Reference System. For bright point sources with r < 17.0 mag, the accuracy of astrometric calibration could reach about 80 mas for each of the g, r, i bands, with systematic errors being less than 10 mas. But for the faint sources at the brightness limit of the survey, which was r similar to 19.0 mag, the accuracy can still reach 200 mas. After combining all observations, the final weighted average coordinates could reach an accuracy of less than 70 mas for bright stars. For faint stars, the rms residuals of weighted coordinates decrease to similar to 110 mas. The final combined XSTPS-GAC coordinates show a good consistency with the Sloan Digital Sky Survey.

第 211 条，共 222 条

A Three-Dimensional Extinction Map Of The Galactic Anticentre From Multiband Photometry

Chen, BQ (Chen, B. -Q.); Liu, XW (Liu, X. -W.); Yuan, HB (Yuan, H. -B.); Zhang, HH (Zhang, H. -H.); Schultheis, M (Schultheis, M.); Jiang, BW (Jiang, B. -W.); Huang, Y (Huang, Y.); Xiang, MS (Xiang, M. -S.); *Zhao, HB* (Zhao, H. -B.); Yao, JS (Yao, J. -S.); Lu, H (Lu, H.)

MONTHLY NOTICES OF THE ROYAL ASTRONOMICAL SOCIETY

卷: 443 期: 2 页: 1192-1210

We present a three-dimensional extinction map in the r band. The map has a spatial angular resolution, depending on latitude, between 3 and 9 arcmin and covers the entire Xuyi Schmidt Telescope Photometric Survey of the Galactic Anticentre (XSTPS-GAC) survey area of over 6000 deg(2) for Galactic longitude 140 < l < 240 deg and latitude -60 < b < 40 deg. By cross-matching the photometric catalogue of the XSTPS-GAC with those of 2MASS and WISE, we have built a multiband photometric stellar sample of about 30 million stars and applied spectral energy distribution (SED) fitting to the sample. By combining photometric data from the optical to the near-infrared, we are able to break the degeneracy between the intrinsic stellar colours and the amounts of extinction by dust grains for stars with high photometric accuracy, and trace the extinction as a function of distance for low Galactic latitude and thus highly extincted regions. This has allowed us to derive the best-fitting extinction and distance information of more than 13 million stars, which are used to construct the three-dimensional extinction map. We have also applied a Rayleigh-Jeans colour excess (RJCE) method to the data using the 2MASS and WISE colour (H - W2). The resulting RJCE extinction map is consistent with the integrated two-dimensional map deduced using the best-fitting SED algorithm. However for individual stars, the amounts of extinction yielded by the RJCE method suffer from larger errors than those given by the best-fitting SED algorithm.

第 212 条，共 222 条

GRB 140219A: Xuyi And Nanshan Upper Limits

D. Xu (DARK/NBI), *Wei,D.-M.* H.-B. Zhao, Y. Xia (PMO), C.-H. Bai, X. Zhang, H.-B. Niu, A. Esamdin, L. Ma (XAO), Y. Osorio (NOT)

GCN CIRCULAR

期：15873

We observed the whole IPN field and its surrounding region of GRB 140219A (Hurley et al., GCN 15864). The first epoch was done at ~15:40 UT on 2014-02-20 using the 1m telescope located at Xuyi, Jiangsu, China, equipped with a 3x3 deg^2 CCD camera. The second epoch was done at ~17:50 UT on 2014-02-20 using the 1m telescope located at Nanshan, Xinjiang, China, equipped with a 1.2x1.2 deg^2 CCD camera. For both epochs, a series of R-band 120s exposures were obtained.The depths of the images of the two epochs are largely comparable and it has R~19 mag. Within the IPN field, we found two relatively bright sources, but they can be ruled out to be an afterglow by cross checking the Xuyi, Nanshan, and DSS images. A third epoch was done at the 2.5m Nordic Optical Telescope (NOT) and the NOT images confirm the above ruling-out. Therefore, assuming GRB 140219A is a conventional cosmological burst happening within the IPN field, its afterglow would be fainter than R~19 mag at T~20 hrs post-burst, which is a possible case according to previous GRB follow-ups. Inspection of some surrounding region of the IPN field also leads to no credible afterglow candidate detection. For the reported two Swift/XRT sources in the central part of the IPN field (Mangano et al., GCN 15872), S2 is not present in the Xuyi and Nanshan images as well, while S1 is a known source.

Laboratory for Planetary Science and Deep Space Exploration

第 213 条，共 222 条

Shape, Thermal And Surface Properties Determination Of A Candidate Spacecraft Target Asteroid (175706) 1996 FG3

Yu, LL (Yu, LiangLiang); Ji, JH (Ji, Jianghui); Wang, S (Wang, Su)

MONTHLY NOTICES OF THE ROYAL ASTRONOMICAL SOCIETY
卷: 439 期: 4 页: 3357-3370

In this paper, a 3D convex shape model of (175706) 1996 FG3, which consists of 2040 triangle facets and 1022 vertices, is derived from the known light curves. The best-fitting orientation of the asteroid's spin axis is determined to be lambda = 237 degrees.7 and beta = -83 degrees.8 considering the observation uncertainties, and its rotation period is similar to 3.5935 h. Using the derived shape model, we adopt the so-called advanced thermophysical model (ATPM) to fit three published sets of mid-infrared observations of 1996 FG3, so as to evaluate its surface properties. Assuming the primary and the secondary bear identical shape, albedo, thermal inertia and surface roughness, the best-fitting parameters are obtained from the observations. The geometric albedo and effective diameter of the asteroid are reckoned to be p(v) = 0.045 +/- 0.002, D-eff = 1.69(-0.02)(+0.05) km. The diameters of the primary and secondary are determined to be D-1 = 1.63(-0.03)(+0.04) km, respectively. The surface thermal inertia Gamma is derived to be a low value of 80 +/- 40 Jm(-2) s(-0.5) K-1 with a roughness fraction f(R) of 0.8(-0.4)(+0.2). This indicates that the primary possibly has a regolith layer on its surface, which is likely to be covered by a mixture of dust, fragmentary rocky debris and sand. The minimum regolith depth is estimated to be 5-20 mm from the simulations of subsurface temperature distribution, indicating that 1996 FG3 could be a very suitable target for a sample return mission.

第 214 条，共 222 条

Formation And Internal Structure Of Terrestrial Planets, And Atmospheric Escape

Jin S

卷: 55 期: 6 页: 534-536
Acta Astronomica Sinica

As of 2014 April 21, over 1490 confirmed exoplanets and 3705 Kepler candidates have been detected. This implies that exoplanets may be ubiquitous in the universe. In this paper, we focus on the formation, evolution, and internal structure of terrestrial planets, and the atmospheric escape of close-in planets.

第 215 条，共 222 条

Ground-Based Radar Detection Of Near-Earth Asteroids

Zhang X; Ji Jianghui

卷: 32 期: 1 页: 24-39
Progress in Astronomy

Ground-based radar detection may act as a powerful means to determine the shape and physical properties of the asteroids in our Solar system. By measuring time delay and doppler frequency of the received echoes, radar systems provide information in ranging and radial velocity of the asteroids. Over the past few decades, more than 500 asteroids (mostly near-Earth objects) were detected using radar observations. There are two categories of radar detection: (1) The continuous wave detection, which is adopted to determine the roughness of an asteroid's surface. (2) The delay-Doppler detection , which is likely to produce its three-dimensional model, and to define the rotational state. In the delay-Doppler detection, target asteroids are resolved in line-of-sight distance and line-of-sight velocity, providing two-dimensional images with spatial resolution as fine as meter-scale. Besides radar detection, several other techniques would also provide the shape model of the asteroids, among which the lightcurve inverse method is the most popular one to do that. In comparison with other methods, radar observation may have an advantage on spacial resolution. The lightcurves cannot reveal elaborate information on small features, and the intermediate-scale features of the inversed model are only suggestive. By contrast, radar detection produces resolved images. In this review, we present the radar observation technique and the method for reconstructing three-dimensional models of asteroids from radar measurements. In addition, we also provide several examples of asteroid models by radar detection, and then compare them with other observations for the shape reconstruction for the asteroids.

第 216 条，共 222 条

Planetary Population Synthesis Coupled With Atmospheric Escape: A Statistical View Of Evaporation

Jin, S (Jin, Sheng); Mordasini, C (Mordasini, Christoph); Parmentier, V (Parmentier, Vivien); van Boekel, R (van Boekel, Roy); Henning, T (Henning, Thomas); Ji, JH (Ji, Jianghui)
ASTROPHYSICAL JOURNAL

卷: 795 期: 1 文献号: 65

We apply hydrodynamic evaporation models to different synthetic planet populations that were obtained from a planet formation code based on the core-accretion paradigm. We investigated the evolution of the planet populations using several evaporation models, which are distinguished by the driving force of the escape flow (X-ray or EUV), the heating efficiency in energy-limited evaporation regimes, or both. Although the mass distribution of the planet populations is barely affected by evaporation, the radius distribution clearly shows a break at approximately 2R(circle plus). We find that evaporation can lead to a bimodal distribution of planetary sizes and to an "evaporation valley" running diagonally downward in the orbital distance-planetary radius plane, separating bare cores from low-mass planets that have kept some primordial H/He. Furthermore, this bimodal distribution is related to the initial characteristics of the planetary populations because low-mass planetary cores can only accrete small primordial H/He envelopes and their envelope masses are proportional to their core masses. We also find that the population-wide effect of evaporation is not sensitive to the heating efficiency of energy-limited description. However, in two extreme cases, namely without evaporation or with a 100% heating efficiency in an evaporation model, the final size distributions show significant differences; these two scenarios can be ruled out from the size distribution of Kepler candidates.

第 217 条，共 222 条

Near 3:2 And 2:1 Mean Motion Resonance Formation In The Systems Observed By Kepler

Wang, S (Wang, Su); Ji, JH (Ji, Jianghui)
ASTROPHYSICAL JOURNAL

卷: 795 期: 1 文献号: 85

The Kepler mission has released similar to 4229 transiting planet candidates. There are approximately 222 candidate systems with three planets. Among them, the period ratios of planet pairs near 1.5 and 2.0 reveal that two peaks exist for which the proportions of the candidate systems are similar to 7.0% and 18.0%, respectively. In this work, we study the formation of mean motion resonance (MMR) systems, particularly for the planetary configurations near 3:2 and 2:1 MMRs, and we concentrate on the interplay between the resonant configuration and the combination of stellar accretion rate, stellar magnetic field, speed of migration, and additional planets. We perform more than 1000 runs by assuming a system with a solar-like star and three surrounding planets. From the statistical results, we find that under the formation scenario, the proportions near 1.5 and 2.0 can reach 14.5% and 26.0%, respectively. In addition, (M) over dot = 0.1 x 10(-8) M-circle dot yr(-1) is propitious toward the formation of 3:2 resonance, whereas (M) over dot = 2 x 10(-8) M-circle dot yr(-1) contributes to the formation of 2:1 resonance. The speed-reduction factor of type I migration f(1) >= 0.3 facilitates 3:2 MMRs, whereas f(1) >= 0.1 facilitates 2:1 MMRs. If additional planets are present in orbits within the innermost or beyond the outermost planet in a three-planet system, 3:2:1 MMRs can be formed, but the original systems trapped in 4:2:1 MMRs are not affected by the supposed planets. In summary, we conclude that this formation scenario will provide a likely explanation for Kepler candidates involved in 2:1 and 3:2 MMRs.

第 218 条，共 222 条

The Configuration Formation Of Planetary Systems Observed By Kepler

Wang, S，Ji, Jianghui

Volume 293, pp. 106-109

Proceedings IAU Symposium

The Kepler mission has found many planetary systems, among them more than 80 systems host three planet candidates which reveal a configuration of near 4:2:1 mean motion resonance. In this paper, we focus on the configuration formation of resonant systems. As shown from our model and N-body simulations,

we find that 3:2 mean motion resonance always forms at the early stage of star evolution and planets undergo high rate of migration, while 2:1 mean motion resonance happens at the late stage of the star formation, more often.

第 219 条，共 222 条

Progress Of Thermophysical Investigations On Asteroids

Ji JH; Yu Liangliang

卷: 32 期: 28-29 页: 104-108

Science & Technology Review

In this work, we review two kinds of thermophysical models widely adopted in the thermophysical investigations of asteroids, i.e., TPM and ATPM, and further discuss their scientific applications and applicable scopes in the investigations. In general, TPM can be used to derive thermal inertia of the asteroid, whereas ATPM can not only be applied to the of thermophysical characteristics of the asteroids such as thermal inertia, surface roughness, etc., but also reveal the YORP effect of asteroids. It is shown that TPM and ATPM are applicable to effective exploration of the asteroids thermophysical properties in terms of present observation accuracy. The likely engineering application for future asteroid missions is also briefly discussed.

第 220 条，共 222 条

Investigation Of Thermal Inertia And Surface Properties For Near-Earth Asteroid (162173) 1999 JU3

YU LL, JI Jiang-hui, WANG Su

Chinese Astronomy and Astrophysics

Volume 38, Issue 3, July–September 2014, Pages 317–329

In order to obtain the substantial information about the surface physics and thermal property of the target asteroid (162173) 1999 JU3, which will be visited by Hayabusa 2 in a sample return mission, with the Advanced Thermal Physical Model (ATPM) we estimate the possible thermal inertia distribution over its surface, and infer the major material composition of its surface materials. In addition, the effective diameter and geometric albedo are derived to be Deff = 1.13 ± 0.03 km, pv = 0.042 ± 0.003, respectively, and the average thermal inertia is estimated to be about (300 ± 50) J m-2 s-0.5 K-1 According to the derived thermal inertia distribution, we infer that the major area on the surface of the target asteroid may be covered by loose materials, such as rock debris, sands, and so on, but few bare rocks may exist in a very small region. In this sense, the sample return mission of Hayabusa 2 is feasible, when it is performed successfully, it will certainly bring significant scientific information to the research of asteroids.

第 221 条，共 222 条

月球火山碎屑堆积物光谱研究

Zhang, XW，Jiang Y，LIU Han，ZHANG Xunyu，ZHOU Xiafeng，CHEN Yuan ，TANG Xiao，WU Yunzhao

期 21 页 137-149

Earth Science frontiers

Lunar pyroclastic deposits (LPDs) originating from the explosive volcanism represent the deeper materials than the basalts in mare; they arc the prior target for the lunar exploration. Reflectance spectroscopy is an important tool to study LPDs. We studied the spectrum of 29 LPDs which have been identified previously,established the distinguishing indicator of volcanic glass and proposed a new idea to compare the relative contents of FeO anTiO2among the glass-richLPDs.The result shows that Sulpicius Uallus, Uauss, Walthcr A，Birt E and Aristarchus arc glass-rich LPDs.The titanium contents of Aristarchus, Sulpicius Uallus and Birt E arc lower than those of Walther A and Uauss.The Birt E has the shallower absorption depth, and the left shoulder moves to shorter wavelength at 1 um band. It may be caused by the very low Fe^{2+} content of Birt E or by its more mature material.

第 222 条，共 222 条

A Research On Tidal Evolution Of Extrasolar Planets（博士论文选登）

Dong Y

卷: 55 期: 3 页 271-272

Acta Astronomica Sinica

In this paper, we perform numerical simulations to investigate the tidal evolution of three single-planet systems, including WASP-43, GJ 1214, and Kepler-10 (in which KeplerlOc is considered as a perturber), and two multiple-planet systems, CoRoT-7 and Kepler-10. For the three single-planet systems, the results of the orbital evolution show that tidal decay and circularization may play a very significant role in shaping their final orbits. Especially, for Kepler-lOb, considering the general relativity, a perturbed companion, and the stellar quadrupole, the results show that all these effects can be ignored during the tidal evolution. However, the above three kinds of effects, as well as planetary tide, may contribute to the apsidal precession for Kepler-lOb, whose numerical precession period agrees quite well with that of the prediction of theory.For the two-planet cases, the tidal evolution of CoRoT-7 system is similar to previous works on the two planets migrating into the host star as well as circularization. But for Kepler-10 system, Kepler-lOb may undergo orbital decay and circularization due to its extremely approximate to the host star. However, Kepler-lOc's orbit simply performs slight oscillations in the semi-major axis and eccentricity owing to its much farther distance from the star than the inner planet's. In order to compare our results with those of CoRoT-7 system, we fabricate a two-planet system based on Kepler-10 system, in which Kepler-lOc with an assumed nonzero eccentricity is located in a closer place within 0.05 au, accompanied with Kepler-lOb whose initial eccentricity is assumed to be zero. The numerical results of orbital evolution for the fabricated system are well consistent with the tidal theory. Moreover, additional simulations with alternative values of dissipation factor are carried out to explore tidal evolution for two planets of Kepler-10, whose outcomes may be indicative of a possible range of 50 -200, and show that the role of in the eccentricity may solely affect the damping timescale rather than the final semi-major axis. Furthermore, considering the density comparable to terrestrial planets in the solar system and the previous models, we provide a possible constraint on the mass of Kepler-lOc with 7 M.m2(20 M. (Mb isthe mass of the earth) from the simulations.Finally, we make a discussion about the stellar tide after the planetary tidal evolution ends up for each system, which is associated with the remaining lifetime of each planet to predict its future. As well-known, the tidal evolution may change the orbit of a planet, as a result, and transit timing variations for a transit planet possibly can be detected by observation. We then introduce the research progress on the transit timing variations in extrasolar planets, and we present a preliminary result.

紫台历年发表论文情况

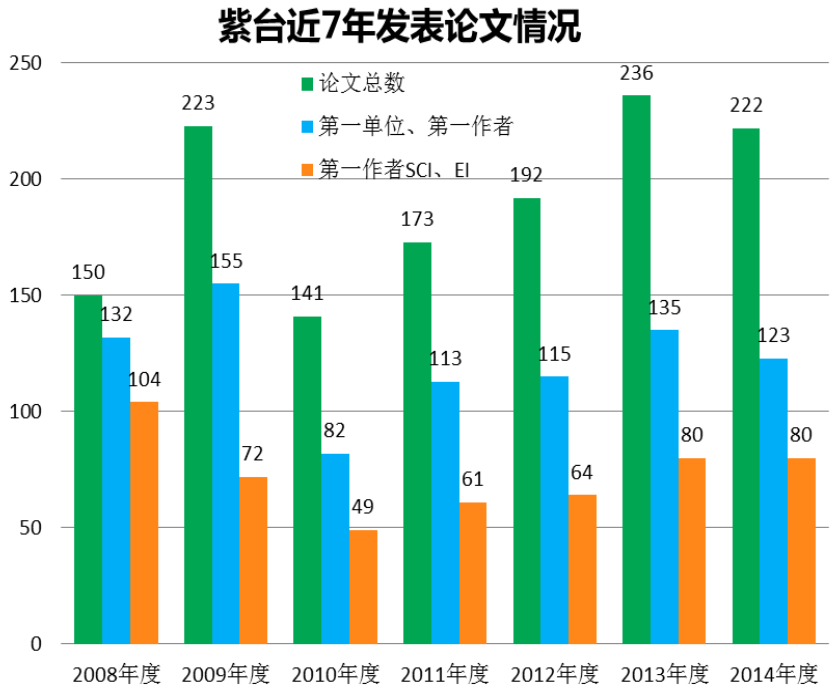
紫台近7年发表论文情况
论文总数
第一单位、第一作者
第一作者SCI、EI
250
200
150
100
50
0
150
132
104
223
155
72
141
82
49
173
113
61
192
115
64
236
135
80
222
123
80
2008年度
2009年度
2010年度
2011年度
2012年度
2013年度
2014年度

专利

序号	类型	名称	发明人	专利号	状态
1	发明专利	新型 C 波段小型化微波隔离器及应用	刘洁，单文磊	201410014285	申请
2	发明专利	双傅立叶变换的太赫兹信号多维图像探测装置及探测方法	史生才，林镇辉，李靖	201410130392	申请
3	发明专利	单接收机太赫兹矢量场形测量装置及其测量方法	娄峥，胡洁，周康敏，林镇辉	201410114486	申请
4	发明专利	用于太赫兹近场测量的准光型探头、探测系统及探测方法	娄峥，胡洁，周康敏，史生才	201410116015	申请
5	发明专利	望远镜圆顶的以太网控制装置	刘伟, 姚大志，华园园	201410255689	申请
6	发明专利	应用于太赫兹频段焦平面阵列的椭球透镜天线优化设计方法	娄峥，史生才，缪巍，刘冬	201410372798	申请
7	发明专利	太赫兹外差阵列接收机本振参考信号功率分配装置及其分配方法	史生才，张文，缪巍，林镇辉	201410538160	申请
8	发明专利	太赫兹量子级联激光器为本振源的超导外差集成接收机	缪巍、娄铮、张文、史生才	201410749633	申请
9	发明专利	一种空间探测仪器加热装置	胡一鸣，张家宇，崔兴柱，常进	201410780652	申请
10	发明专利	天文望远镜实时精确指向的测定方法	张晓祥	ZL201110361868.0	授权
11	发明专利	实时测定天文望远镜指向误差的方法	张晓祥	ZL201110361031.6	授权
12	发明专利	阵列成像系统	张文，缪巍	ZL 201210028016.4	授权
13	发明专利	以固态半导体源谐波为参考源的量子级联激光器锁相系统	缪巍，张文	ZL201210081557.3	授权

2014 年度发表科研论文、专著、专利一览表

团组与学科片	论文总数	第一单位	SCI论文	第一单位SCI	专著	专利申请	专利授权	软件登记
宇宙学、暗物质及高能天体物理研究	5	2	5	2	--	--	--	--
宇宙伽玛暴、中子星及相关物理研究	5	1	5	1	--	--	--	--
太阳高能及相关物理过程研究	10	4	7	2	--	--	--	--
太阳活动的多波段观测研究	13	7	10	5	--	--	--	--
暗物质和空间天文实验室	27	13	22	9	--	1	--	--
暗物质和空间天文	**60**	**27**	**49**	**19**	**0**	**1**	**0**	**0**
恒星结构、演化和脉动研究	2	1	1	0	--	--	--	--
南极天文中心	27	10	19	8	--	--	--	--
星系宇宙学和暗能量研究	5	3	4	2	--	--	--	--
星系中的恒星形成研究	16	5	15	5	--	--	--	--
分子云与恒星形成研究	10	5	9	5	--	--	--	--
毫米波和亚毫米波技术实验室	20	13	12	6	--	7	2	1
青海观测站	14	6	13	5	--	--	--	2
南极天文和射电天文	**94**	**43**	**73**	**31**	**0**	**2**	**2**	**3**
空间目标与碎片观测研究中心	15	15	6	6	--	--	2	--
卫星精密定轨及应用研究	2	2	0	0	--	--	--	--
CCD 相机研制实验室	1	1	0	0	--	1	--	--
应用天体力学和空间目标与碎片	**18**	**18**	**6**	**6**	**0**	**1**	**2**	**0**
近地天体探测和太阳系天体研究	1	1	1	1	--	--	--	--
历算和天文参考系研究	10	9	3	2	--	--	--	--
太阳和太阳系等离子体研究	16	12	14	11	--	--	--	--
天体化学和行星科学实验室	7	4	3	2	--	--	--	--
盱眙天文观测站	6	0	5	0	--	--	--	--
行星科学和深空探测实验室（筹）	10	9	3	3	--	--	--	--
行星科学和深空探测	**50**	**35**	**29**	**19**	**0**	**0**	**0**	**0**
管理和支撑	--	--	--	--	--	--	--	--
其他 汇总	**0**	**0**	**0**	**0**	**0**	**0**	**0**	**0**
总计	**222**	**123**	**157**	**75**	**0**	**9**	**4**	**3**

紫台历年主要科研项目统计

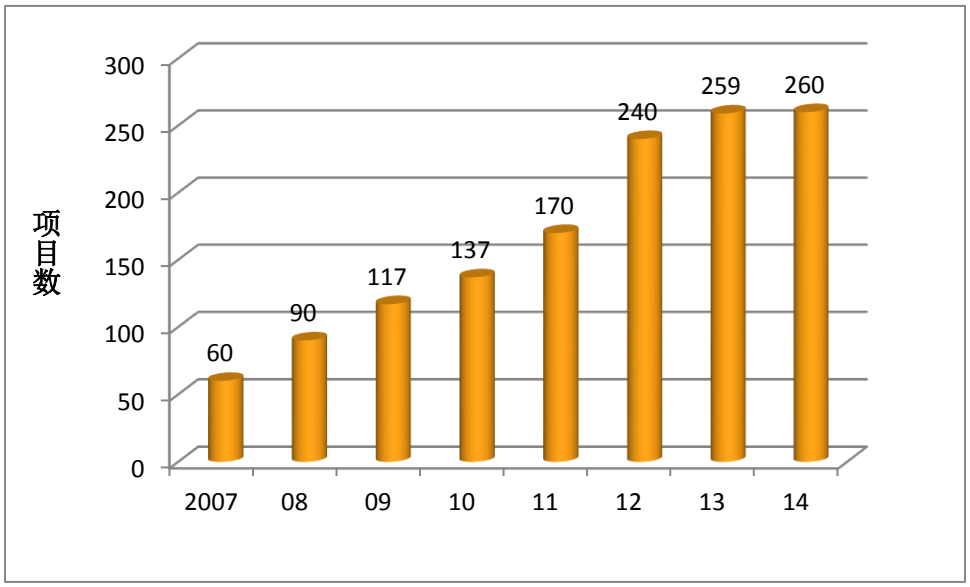

2014 年度在研科研项目

项目类型	在研项目总数	占比	当年新开项目数	在研项目当年到账经费/万
国家任务	140	54%	48	6490
中科院任务	80	31%	40	14029
研究所自选	3	1%	2	35
横向委托	11	4%	5	74
地方任务	25	10%	13	301
其他	1	0%	1	20
总和	**260**	**100%**	**109**	**20949**

学术报告

序号	日期	报告人	单位	职称	题目
1	2014/6/16	Rodolfo Barniol Duran	Racah Institute of Physics, The Hebrew University of Jerusalem	博士	Low luminosity GRBs: A different class, shock breakout and afterglow
2	2014/6/19	侯贤	法国波尔多核物理研究中心天体粒子物理小组	博士	Detections of 7 faint gamma-ray pulsars & constraints on neutron star moments of inertia with the Fermi-LAT
3	2014/6/25	谢克强	美国 Arizona 大学物理系	教授	日球内外能原子的探测
4	2014/7/22	Hui Li	Los Alamos National Laboratory		Relativistic Magnetohydrodynamics and Partice-in-Cell Studies of Magnetically Dominated Outflows
5	2014/10/28	Miroslav Barta	European ALMA Regional Centre - Czech node, Astronomical Institute of Academy of Sciences	博士	Role of plasmoids in energy cascades in magnetic reconnection in solar flares: Modelling and relation to observations
6	2014/11/27	I. Sharykin	俄罗斯科学院空间研究所	博士	Fine Structure of Flare Ribbons & Electric Current
7	2014/11/27	A. Struminsky	俄罗斯科学院空间研究所	博士	Fermi GRO Solar Events
8	2014/12/25	Firoz, K. A.	Space Research Group, Universidad de Alcalá, E-28871 Alcalá de Henares, Spain	博士	Our Recent Studies on High Energy Solar Particle Events
9	2014/5/8	Philip R. Goode	New Jersey Institute of Technology	教授	The 1.6 m Off-Axis New Solar Telescope (NST) in Big Bear
10	2014/6/26	夏茹	鲁汶大学数学系 等离子体天体物理中心 CmPA	博士	Simulating the in-situ condensation process of solar prominences
11	2014/3/5	David Valls-Gabaud	Observatoire de Paris, CNRS, IHEP, NAOC		New views on the Andromeda galaxy M31
12	2014/3/24	Yuanyuan Su	University of California, Irvine	博士	Clusters of Galaxies in X-ray
13	2014/7/2	Irwin, James A.	University of Alabama		The Search for Black Holes in Globular Clusters
14	2014/9/24	陈亮	上海天文台	副研究员	Blazars in the Fermi era
15	2014/10/24	Rene Hudec	Ondrejov Observatory, Czech Republic	教授	Study of high-z Universe and GRBs with Gaia and Photographic Sky Surveys
16	2014/12/25	Hui Dong	IAA-CSIC		Unveiling the Massive Stars in the Galactic Centre
17	2014/7/8	Lister Staveley-Smith	The University of Western Australia	博士	Recent Results from the Australian SKA Site
18	2015/1/9	吕候军	University of Nevada, Las Vegas		The Magnetar central engine in GRBs
19	2014/12/26	马寅哲	英国曼彻斯特大学物理和天文系	博士	Detection of the missing baryons with Planck maps
20	2014/1/3	詹虎	国家天文台	研究员	中国空间站大规模多色成像与无缝光谱巡天的建议

序号	日期	报告人	单位	职称	题目
21	2014/1/17	王慧元	中国科学技术大学	博士	RECONSTRUCTING THE INITIAL DENSITY FIELD OF THE LOCAL UNIVERSE
22	2014/2/27	罗文涛	中科院上海天文台	副研	Galaxy-Galaxy Lensing Data Processing and Filament-Galaxy Lensing
23	2014/2/27	Zhang Jun	上海交通大学	研究员	Accurate Cosmic Shear Measurement Method
24	2014/5/15	Ramin Skibba	University of California, San Diego	博士	Testing Galaxy Formation with Clustering Statistics and Halo Models at 0<z<1
25	2014/5/29	姜方周	耶鲁大学		Comparison of EPS Halo Merger Trees and Statistics of Dark Matter Subhaloes
26	2014/7/10	罗德哲	上海交通大学		The massive satellite population of Milky-Way sized galaxies
27	2014/8/28	Xin Bo	LSST Project office		Simulating the Performance of the Large Synoptic Survey Telescope (LSST)
28	2014/12/17	Darren Croton	Swinburne University of Technology, Australia	教授	How to model the Universe in N easy steps (N>>1)
29	2014/1/10	Sebastien Foucaud	Shanghai JiaoTong University	博士	Evolution of the Dark matter and stellar mass assembly through cosmic time
30	2014/3/20	东苏勃	北京大学 科维理天文与天体物理研究所		Microlensing: Marching Toward a Complete Census of Cold Exoplanet Population
31	2014/7/18	Nanyao Lu	Caltech		Cold, Warm and Hot Molecular Gas in Infrared Galaxies
32	2014/8/27	Jeff Wagg	SKA	博士	From Exoplanets to Cosmic Dawn with the Square Kilometre Array
33	2014/9/12	毛基荣	Kyushu University		Theoretical Investigations of GRB Host Galaxies and Some Hints towards High-z Universe
34	2014/10/21	David Webb	ISR, Boston College		CME and Sunspot Rates for Solar Cycles 21-24
35	2014/10/23	Emanuele Daddi	Commissariat à l'énergie atomique et aux énergies alternatives	博士	Evolution of the star formation and gas content in galaxies through cosmic time
36	2014/11/11	Jonathan Braine	Observatoire de Bordeaux	博士	Star Formation and the Molecular Interstellar Medium of Messier 33
37	2014/11/7	Steven Lord	The SETI Institute (CAS Visiting International Senior Scientist)	教授	The conditions for Star Formation in the Antennae Galaxies: NGC 4038/9 as seen by Herschel PACS.
38	2014/11/5	李江涛	CEA-Saclay, France and Univ. Michigan, USA		Circum-galactic Medium Around Local Spiral Galaxies --- A New Window to Understand Galaxy Evolution
39	2014/11/7	Steven Lord	The SETI Institute (CAS Visiting International Senior Scientist)		Airships as Stratospheric Observatories
40	2014/11/19	罗阿里	国家天文台，LAMOST	研究员	LAMOST 巡天回顾与数据产品的使用

序号	日期	报告人	单位	职称	题目
41	2014/4/23	Qizhou Zhang	Harvard-Smithsonian Center for Astrophysics		How to Make Massive Stars
42	2014/4/29	Shiwei Wu	Max Planck Institute for Astronomy		The Massive Stellar Population of W49: a Spectroscopic Survey
43	2014/4/23	Ke Wang	European Southern Observatory	博士	How to Make Massive Stars: the First Steps
44	2014/5/15	Roy van Boekel	Max Planck Institute for Astronomy	博士	The link between planet formation and planet atmosphere spectra
45	2014/9/19	江治波	紫金山天文台	研究员	访智见闻
46	2014/9/25	彭秋和	南京大学	教授	银河系中心附件发现反常强大磁场的科学意义---磁单极存在的天文观测证据和星系核的黑洞模型失效
47	2014/12/15	Patricio Rojo	Departamento de Astronomia Universidad de Chile	博士	Of Chilean Astronomy, Exoplanets, and a bit of Antarctica
48	2014/12/23	吴元伟	日本国立天文台		Maser Survey towards evolved stars selected from WISE and AKARI data
49	2014/10/21	Wiedner Martina	巴黎天文台		Research interests of LERMA group at the Observatory of Paris
50	2014/11/22	Iwan P. Williams	Queen Mary University of London (QMUL, UK)	教授	Impacts on Earth and what they tell us about the parent bodies
51	2014/6/24	郭政灵	台湾中央大学太空科学研究所	博士	Effects of ion-neutral collisions on Alfven waves: The presence of forbidden zone and heavy damping zone
52	2014/6/27	郭政灵	台湾中央大学太空科学研究所	博士	高空短暂发光事件的介绍以及理论模型
53	2014/6/24	Xianming L. Han	Dept. of Physics and Astronomy, Butler University, Indianapolis, Indiana, USA		Asteroid Observation Techniques
54	2014/1/20	李荐扬	Planetary Science Institute, Tucson, USA		Comet ISON: An interesting comet from the beginning to the end
55	2014/7/14	胡松杰	北京航天飞行控制中心，航天飞行动力学技术重点实验室	博士	深空探测器精密定轨技术及 CE－2 与 Toutatis 联合定轨研究
56	2014/9/19	陈鼎	中国科学院国家空间科学中心，新技术研究室	研究员	High-precision Space Astrometry to Search for Terrestrial Exoplanets
57	2014/12/8	郑晓晨	北京大学		The dynamical fate of planetary systems
58	2014/12/12	Nuno Peixinho	University of Antofagasta, Chile	博士	Kuiper Belt Objects: too much color distracts the spectator

国际合作与台内学术报告统计

团组与学科片	出访人次	占比	来访人次	占比	台内学术报告	占比
宇宙学、暗物质及高能天体物理研究	0	0%	0	0%	0	0%
宇宙伽玛暴、中子星及相关物理研究	3	3%	1	1%	1	2%
太阳高能及相关物理过程研究	12	11%	21	14%	7	12%
太阳活动的多波段观测研究	4	4%	7	5%	2	3%
暗物质和空间天文实验室	34	30%	14	10%	6	10%
暗物质和空间天文	**53**	**46%**	**43**	**29%**	**16**	**28%**
恒星结构、演化和脉动研究	0	0%	0	0%	0	0%
南极天文中心	6	5%	25	17%	3	5%
星系宇宙学和暗能量研究	2	2%	38	26%	9	16%
星系中的恒星形成研究	7	6%	9	6%	12	21%
分子云与恒星形成研究	7	6%	4	3%	8	14%
毫米波和亚毫米波技术实验室	21	18%	17	12%	1	2%
青海观测站	5	4%	4	3%	0	0%
南极天文和射电天文	**48**	**42%**	**97**	**66%**	**33**	**57%**
空间目标与碎片观测研究中心	4	4%	1	1%	0	0%
卫星精密定轨及应用研究	0	0%	0	0%	0	0%
CCD 相机研制实验室	0	0%	0	0%	0	0%
应用天体力学和空间目标与碎片	**4**	**4%**	**1**	**1%**	**0**	**0%**
近地天体探测和太阳系天体研究	3	3%	1	1%	1	2%
历算和天文参考系研究	0	0%	2	1%	2	3%
太阳和太阳系等离子体研究	0	0%	0	0%	0	0%
天体化学和行星科学实验室	1	1%	0	0%	0	0%
盱眙天文观测站	2	2%	1	1%	1	2%
行星科学和深空探测实验室（筹）	3	3%	2	1%	5	9%
行星科学和深空探测	**9**	**8%**	**6**	**4%**	**9**	**16%**
总计	114	**100%**	147	**100%**	58	**100%**

中国 2013 年度“十大天文科技进展”

（紫金山天文台相关部分）

1、DAMPE 完成工程化设计研制并列入欧洲核子中心认可试验名录

DAMPE- Dark Matter Particle Explorer，即“暗物质粒子探测器”,是暗物质粒子探测卫星的科学观测有效载荷。DAMPE 属于中国科学院空间科学先导专项之一，是由我国设计、建造和发射的一颗计划运行于 500 km 高度太阳同步轨道的空间科学实验探测器，其主要科学目标是开展高能正负电子和伽玛射线的观测，进而探寻暗物质存在的证据，并研究其空间分布特性。

暗物质粒子探测器共包括 4 个子探测器：塑闪阵列探测器、硅阵列探测器、BGO 量能器、中子探测器。各载荷协同观测模式下对电子和伽玛光子的观测能段为 5 GeV—10 TeV，能量分辨为 1.5%@800GeV，这些指标属国际先进水平。

2013 年初，暗物质粒子探测器所属各单机完成了初样产品详细设计，并陆续投入研制工作。经历了零部件生产、总装装配、电性能测试、力学环境考核、真空高低温考核、联合调试等关键过程，2013 年底，暗物质粒子探测器完成初样鉴定件的研制，标志着暗物质粒子探测器顺利完成工程化设计及建造。

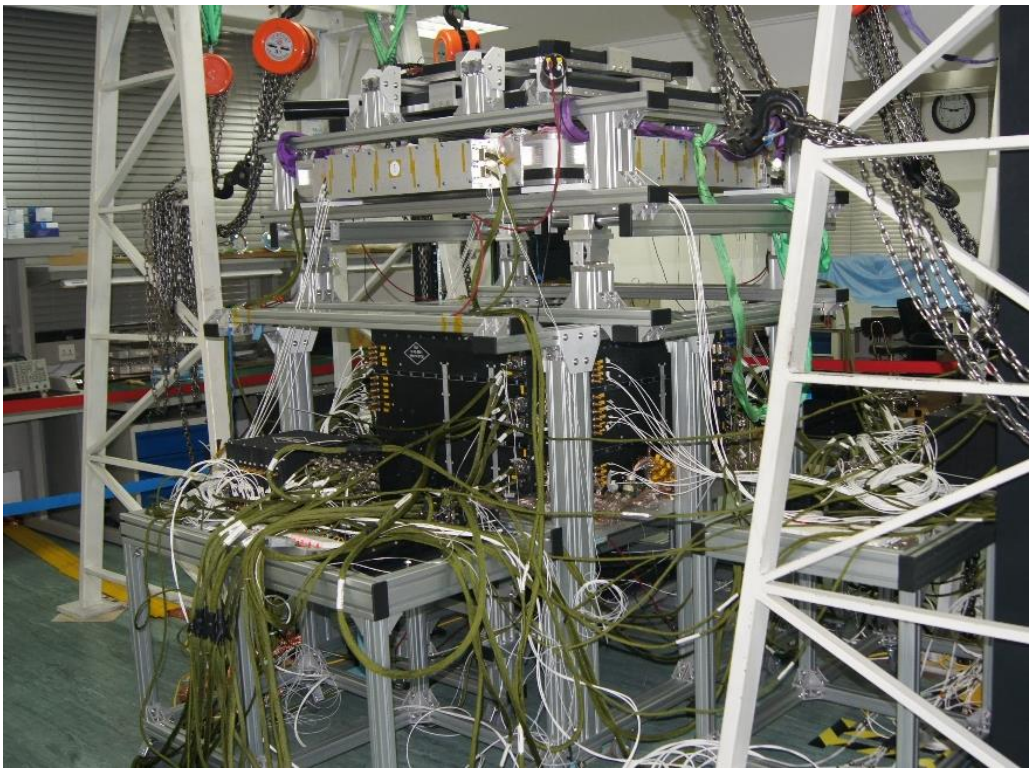

图 1 暗物质粒子探测器联合调试现场

同时，暗物质粒子探测器的载荷配置方案在国内空间应用尚属首次，属于全新设计，其性能指标设计的合理性需要通过地面大型束流试验进行验证。最理想的试验地点为欧洲核子中心，利用其高能粒子（如 50GeV-300GeV 的电子和强子等）对探测器进行标定 验证暗物质粒子探测器的载荷配置方案。经过 2013 年的努力，暗物质粒子探测器 DAMPE 成功列入欧洲核子中心认可试验名录（RE29，http://recognized-experiments.web.cern.ch/recognized-experiments/list.html）。一直以来，有来自 80 个国籍的大约 6500 位科学家和工程师，代表 500 余所大学机构，在欧洲核子中心 CERN 进行试验；这大约占了世界上的粒子物理学圈子的一半，欧洲核子中心已经成为粒子物理学家心目中的圣殿。DAMPE 能够从数十个高能粒子观测项目中脱颖而出，成为首个由中国科学家主导的列入欧洲核子中心认可试验名录的空间高能粒子观测项目，标志着 DAMPE 已经受到国际广泛关注和认可。我们也期待着 2014 年度的束流试验获得圆满成功。

2、利用嫦娥二号数据对图塔蒂斯小行星研究取得重要成果

利用嫦娥二号探测器对 4179 号小行星图塔蒂斯飞越探测获取的光学图像，我们研究了该小行星的物理特性、表面特征、内部结构以及可能的起源等。研究结果表明，嫦娥二号距图塔蒂斯表面最近的距离约为 770 米，获得最高分辨率光学图像优于 3 米/像素。基于所获取的图像，结合探测器的轨道与姿态信息，确定了图塔蒂斯主轴的空间指向。从图像估算了小行星尺寸，新的结果表明图塔蒂斯的长度和宽度不超过 4.75 × 1.95 （±10%） 千米。

从嫦娥二号获取的高分辨率图像中，我们发现图塔蒂斯拥有不规则形状和不平坦表面，其形似一根生姜，由较小的一端“头部”（head）与较大的一端“身体”（body）组成。通过分析获得了图塔蒂斯表面的一些新特征（图 2），这在以往地面雷达观测中未曾发现：在“身体”端部存在一个直径大约 800 米的巨型盆地，在小行星的表面找到了超过 50 处较为明显的、大小不一的陨石坑，其中包括两个先后产生在同一位置附近相互有部分遮盖的陨坑；“颈部”则以近乎垂直角度连接着“头部”和“身体”；其表面存在超过 30 个有巨石特征的区域，通过图像甚至可分辨出尺寸较小的线状结构等特征（图 3）。从这些特征可推断图塔蒂斯很可能是一颗具有碎石堆结构的密近双小行星，可能由两个独立小天体缓慢靠近形成或是约普(YORP)效应作用的结果，抑或是大规模的撞击造成。这些研究对认识太阳系中小行星的形成与演化与近地天体的空间防护具有重要科学价值。

该研究成果在线发表在 Nature 出版集团旗下期刊《Scientific Reports》(《科学报告》) 上，这是探月工程（二期）的重要成果，也是我国在此首次行星际探测活动中，多目标新模式探测、小行星新领域开拓的成功尝试，工程实践与科学研究相融合的成功范例，取得了令人惊叹的结果和国际同行的良好评价。该项成果得益于中科院与多家单位共同合作研究。2013 年 12 月 13 日， Nature 英文网站作为首页头条推介此文，《Nature》中文版推荐为研究亮点-“天文学：与一个近地小行星的近距离接触"(www.natureasia.com/zh-cn/research/highlight/8969/)， 全球多个知名媒体也进行了报道。

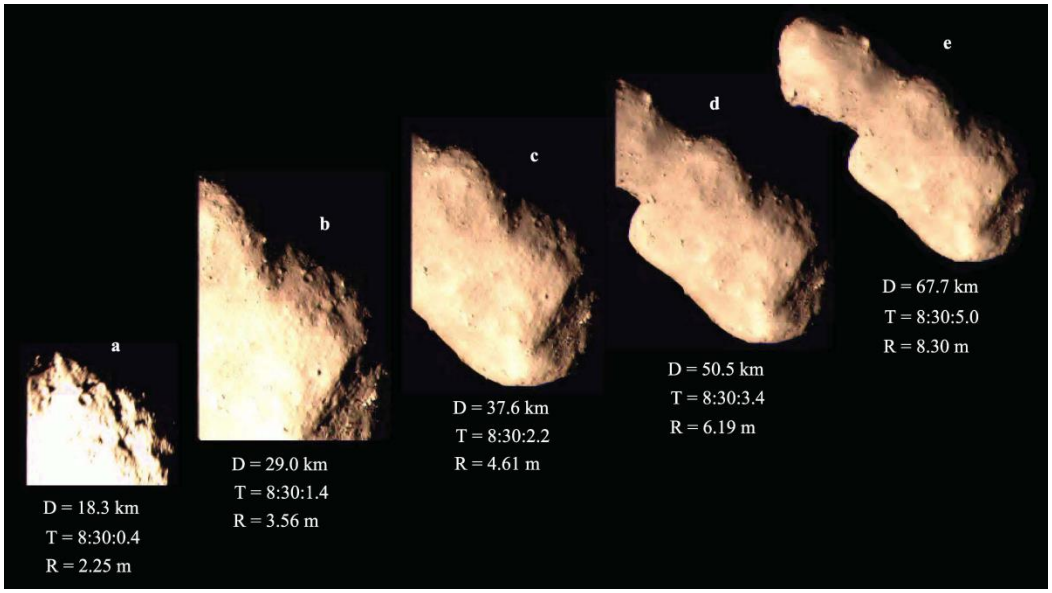

图 2　2012 年 12 月 13 日，嫦娥二号在飞越后对图塔蒂斯小行星成像结果。图 a-e 给出探测器在远离小行星过程中的成像序列。图 a-d 中小行星左侧部分被探测器的太阳帆遮挡。每张图片的成像距离(D)、成像时间(T,UTC)和分辨率（R）在图像下方给出，其中成像距离的误差为 1.1 公里，图像的分辨率与成像距离为线性关系。

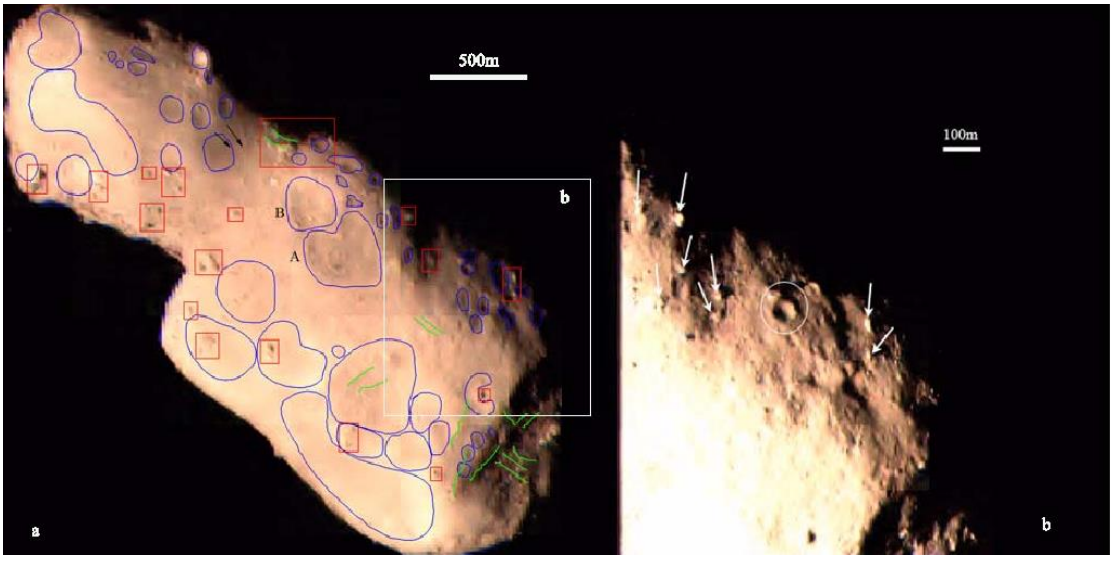

图 3　图塔蒂斯表面的各种地貌特征。(a)在图塔蒂斯的完整图像中标注了坑（蓝色轮廓）和巨石（红色方框）。其中有两个坑的位置非常靠近：较小的坑（B）似乎叠加在较大的坑（A）之上。绿色曲线表征了小行星的线状结构。黑色箭头标出了表面细壤的流向。（b）对图（a）中方框中部分图像的放大。图中给出一个形态完整的坑，其周围随机分布了十余个碎石。

3、成功研制太赫兹超导探测器平台并实现稳定运行

太赫兹波段是继红外和毫米波之后最新发展的、其它波段不可替代的观测窗口，在当代天文学前沿研究领域 - 宇宙生命环境和高红移早期宇宙研究中具有特别重要的作用。在太赫兹波段的宇宙学和天体物理观测研究中，低温超导探测器由于具有无可比拟的超高灵敏度，正发挥越来越重要的作用。位于南极的美国 BICEP2 望远镜正是采用了超导探测器，使探测效率大幅提高，首次实现“大爆炸”引力波探测。

中科院紫金山天文台毫米波和亚毫米波技术实验室于 2012 年成功研制太赫兹超导探测器平台，实现了太赫兹超导探测器芯片的自主制备，进而具备了从太赫兹超导探测器设计、芯片制备到系统集成的完整能力。太赫兹超导探测器平台包括超导及金属薄膜磁控溅射系统、绝缘层磁控溅射系统以及掩膜对准光刻机等核心装置，自 2012 年通过验收以来，优化了超导薄膜及芯片制备工艺，实现了近两年的稳定运行。目前，该平台已能制备高质量的 Nb、Ti、Al 等低温超导薄膜，超导 SIS 混频器、超导 TES 探测器以及超导 MKIDs 探测器等芯片。太赫兹超导探测器平台的成功研制为国家基金委重大科研仪器研制专项、南极天文台太赫兹望远镜计划、以及载人航天工程 2 米多功能光学设施的太赫兹模块等打下关键技术基础。

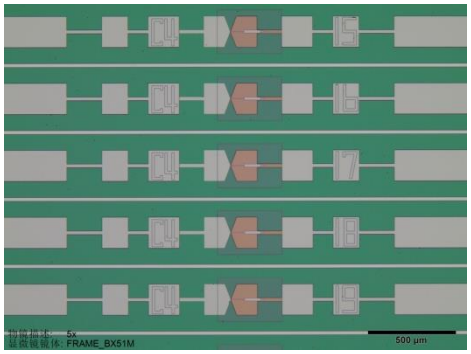

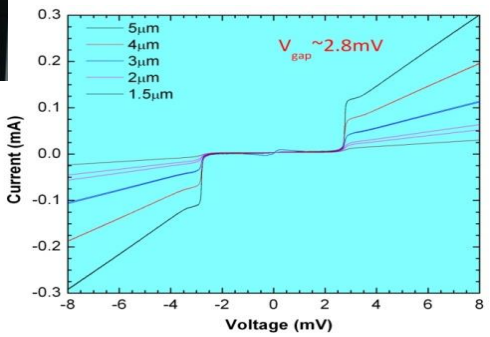

图 5，太赫兹超导探测器平台（左）、制备超导隧道结芯片（右上）和不同面积 Nb 超导隧道结 I-V 特性（右下,与国际同类芯片性能相当）。

4、中国科学家首次精确测定银河系本地臂

银河系旋臂的测量对于研究银河系结构这一天文学和天体物理学中最重要和最基本的问题起着至关重要的作用。自 200 多年前赫歇尔首次提出银河系的尺度、形状和结构起，天文学家们提出了许多的模型，但由于模型所依赖的天体距离的不确定性，

使得银河系结构的研究至今仍停滞不前。因此，精确测定天体的距离是研究银河系结构的重中之重。

以中科院紫金山天文台研究组为主导的BeSSeL国际合作团队在解决了选取合适的目标源、河外背景源、以及地球大气引起的相位延迟误差等一系列挑战性难题以后，通过使用目前世界上分辨率最高的甚长基线干涉阵(VLBA)，通过VLBI相位参考技术，用三角视差直接测量距离的方法精确测定了银河系旋臂中天体的距离，由此确定了距离地球最近的银河系本地臂的形态和运动学性质。该工作所使用的方法使得脉泽和河外背景源之间的相对位置精度达到几个微角秒，将天文视差测量的精度提高了两个量级。

研究结果表明本地臂的一些主要特征都与其他主臂类似，本地臂长5 kpc，宽1 kpc，旋臂中存在着比预期要多的多的大质量恒星形成区。旋臂螺旋角约10度左右，远小于河外星系中主旋臂中凸起的角度，且旋臂的整体运动比银河系转动慢 5 km/s. 该研究成果的重大意义在于：1.这是天文学史上首次精确测定银河系的旋臂结构形态和三维运动，表明精确测量银河系旋臂结构已经从可能变为现实；2.该成果排除了天文学界长期以来认为本地臂是附属于主旋臂的一个凸起的观点，提出其极有可能"升级"为银河系的一条新的主旋臂或主旋臂的一部分(图6)；3.该结果对已经被广泛接受的密度波理论提出了巨大的挑战。详细结果见2013年5月的《天体物理杂志》(Xu et al. 2013, ApJ, 769, 15)。

该工作一经发表就引起了国内外的广泛关注，受到了人民日报，新华社和中央电视台等媒体的相继采访和报道。国际上，《U.S．News and World's Report》，《SPACE》，《Universe Today》和NRAO等多家媒体和网站也都争相报道了这一结果。该工作也成为2013年第222届美国天文学会上的亮点工作并进行了专门报道。

该团队科研人员已经在这个领域进行了 10 多年的探索并取得了突破性进展。他们在2005年首次精确测定了银河系英仙臂的距离(Xu et al.2006,Science,311,54)，标志着精确测量银河系旋臂结构从那时起成为可能，而本次研究结果则将这种可能转变为现实。他们的系列成果被国际专家认为是银河系结构领域的一个里程碑。

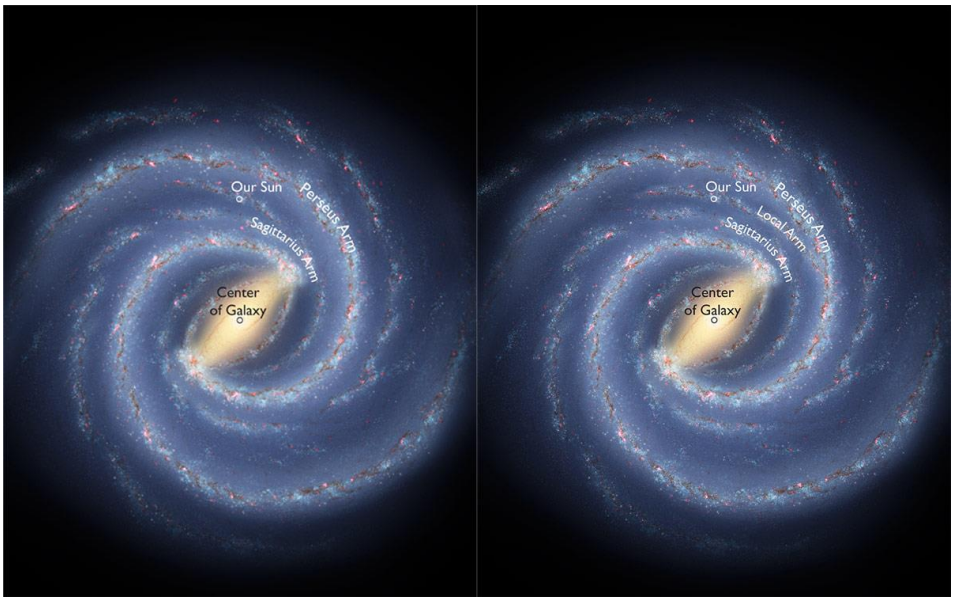

图6. 银河系旋臂结构图：本地臂曾被认为是主臂的一个凸起(左图)，现可能为主臂的一个分支或者主臂的一部分(右图)。

If you are interested in the work of PMO please contact division of Science & Technology Management at

+86-(0)25-83332288, 83332018

pmokjc@pmo.ac.cn